Inhalt

1 Abstract

Determination of pH is an analytical challenge of mayor importance in diagnostics, biotechnology, marine science and many other applications. Luminescence pH sensors facilitate real-time monitoring and are virtually non-invasive. Compared to the well-established electrochemical pH sensors, they offer better sensitivity within their dynamic range and are more easily accessible to miniaturization. The fluorescent pH indicator dye is exceedingly crucial for the performance of every resulting sensor. However, many existing sensors are based on relatively short-wave excitable indicators which often possess limited photostability.

The focus of this work is on the preparation and characterization of novel luminescent pH indicators based on photoinduced electron transfer (PET). That allows originally pH insensitive dyes to become pH indicators and consequently makes new dye classes accessible to pH sensing. In that way, indicators with optimized properties are to be presented. In particular, they are supposed to exhibit long-wave excitability which makes the development of sensors with lower fluorescence and scattering background possible. Other highly important properties are good photostability, high brightness, high sensitivity in the expected pH range of the most important samples (pH 6-9) and good compatibility with useful immobilization matrices. Above all, two classes of PET-modified dyes are presented, rhodamines and perylenes. Both are not intrinsically pH sensitive. The functional rhodamines show outstanding sensitivity in aqueous solution, with dynamic ranges excellently matching physiological pH. They present the spectral properties known for rhodamines, including high brightness, moderate long-wave excitability (~550nm), and good photostability. The presented perylene bisimides feature acid-base sensitivities from moderate to high in organic solvents. Those dyes present good brightness, excitation wavelengths ranging from 510 to 590nm and are known for excellent chemical and photostability. Finally, a pH sensitive perylene applicable in an immobilization matrix useful for pH sensing (polyurethane hydrogel) is presented.

2 Theoretical Background

2.1 Luminescence

This chapter is based on reference [1]. Other references will be cited independently.

Luminescence is the deactivation of electronically excited species by photon emission. A wide diversity of luminescent compounds has been investigated, including organic compounds (most of which are aromatic), inorganic compounds (ions, crystals, glasses) and organometallic complexes. Depending on how excitation of the electronic state has been accomplished, several types of luminescence may be distinguished, the most important of which are shown below:

Table 1: Survey of the most important luminescence types and corresponding excitation pathways.

Mode of excitation	Type of luminescence
photons	photoluminescence
chemical reaction	chemoluminescence
biochemical reaction	bioluminescence
electric field	electroluminescence
thermal energy	thermoluminescence
X-rays, γ-rays or other ionizing radiation	radioluminescence

Photoluminescence, which has been extensively investigated, will be the main subject of this thesis. From now on, the term luminescence will be used representatively for photoluminescence. Of course, it requires photon absorption prior to luminescence.

2.1.1 Light-matter Interactions

Upon absorption, photons are picked up by the species capable of luminescence, creating an excited state (ES) which is superior in energy to the state present prior to absorption (usually the ground state, GS). The energy gap between both states is equal to the energy of the photon absorbed:

$$E_{ES} - E_{GS} = h\nu \qquad \text{Equation 1}$$

E_{ES} Energy of the excited state (J)
E_{GS} Energy of the ground state (J)
ν Frequency of the absorbed photon (s^{-1})
h Planck's constant ($6{,}626069 * 10^{-34}$ Js)

Other types of light-matter interactions can have an impact on absorption and consequently on luminescence. Examples for possibly interfering interactions are scattering, reflection, refrac-

tion or diffraction. In the simplest case, only the propagation velocity of light is reversibly changed when it passes through a sample (transmission).

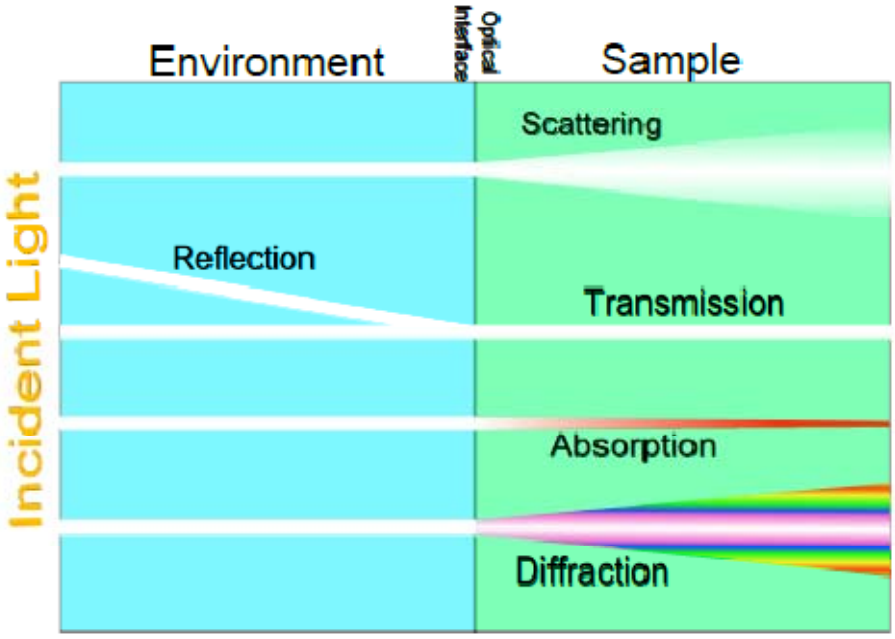

Figure 1: Schematic visualization of light-matter interactions that can occur in the sample bulk or on its surface.

2.1.2 Absorption Characteristics

When a molecule absorbs UV/VIS light, it is promoted from the electronic GS to an ES so that equation 1 is fulfilled. The GS is, according to Boltzmann distribution, by far the most populated state at room temperature. Upon that, most frequently, an electron is moved from the HOMO to the LUMO (although other transitions are possible).
In principle, luminescence corresponds to the reverse transitions, though not all transitions visible in absorption spectra will be observed in luminescence spectra. Transition energies in organic luminophores depend on the type of MOs involved and in general increase in the following order:

$$n \rightarrow \pi^* < \pi \rightarrow \pi^* < n \rightarrow \sigma^* < \sigma \rightarrow \sigma^*$$

$\sigma \rightarrow \sigma^*$ transitions correspond to energies in the deep UV and therefore usually are of little relevancy for spectroscopic applications. $n \rightarrow \pi^*$and $\pi \rightarrow \pi^*$ transitions, on the other hand, are often located in the visible region. $\pi \rightarrow \pi^*$ transitions are of mayor importance in luminescence applications. For $\pi \rightarrow \pi^*$, the presence of unsaturated groups (multiple bonds and aromatic rings) is needed, $n \rightarrow \pi^*$ transitions additionally involve free electron pairs, i.e. functional groups such as C=O, C-OH, C-NH_2. Absorption of a dye at a certain wavelength is quantified by the Lambert-Beer law:

$$A = log\left(\frac{I_0}{I}\right) = \varepsilon_\lambda cd$$ Equation 2

A	Absorption
I_0	Intensity of light entering the sample
I	Light intensity after passing through the sample
ε_λ	Molar absorption coefficient of the dye of interest at a given wavelength λ ($M^{-1}cm^{-1}$)
c	Dye concentration (M)
d	Optical path length of the sample (cm)

ε_λ quantifies the probability that light of a certain wavelength λ is absorbed by a dye. UV/VIS absorption bands are generally rather broad due to vibrational uncertainty of electronic states. Therefore, to quantify the total probability of absorption corresponding to an electronic transition, the oscillator strength f is used:

$$f = \frac{C}{n}\int_{\lambda_L}^{\lambda_R} \varepsilon_\lambda d\lambda$$ Equation 3

f	Oscillator strength
C	Normalization constant
n	Refractive index
λ	Wavelength (nm)
$\lambda_{L,R}$	Left and right edges of the absorption band to be considered (nm)

f is normalized so that its maximum value is 1. π→ π* transitions usually exhibit much higher values of ε and f (as well as higher luminescence quantum yields, 2.1.4) than n→π* transitions. f is proportional to the square of the transition dipole moment, a quantum mechanical term that quantifies the displacement of charges originating from absorption. That means a charge transfer between ES and GS is required for the transition to cause absorption and the latter will be the more intense the more pronounced that charge transfer is. Not all possible transitions are actually visible in UV/VIS spectra, but those which do not fulfil certain selection rules are forbidden. Some are spin-forbidden (section 2.1.3), others are forbidden for symmetry reasons.

2.1.3 Excited State Characteristics

Electronic states are called $S_{0,1,2,...}$ or $T_{0,1,2,...}$ where S stands for singlet, T for triplet and the sub-number refers to the level of electronic excitation (0 stands for the GS, 1 for the first ES, 2 for the second one,…). Most of the following statements will refer to S states, but are equally valid for T states.
The spin multiplicity of an electronic state is related to the number of odd electrons:

$$M = 2|S| + 1$$ Equation 4

M Spin multiplicity of an electronic state
S Sum of electron spins populating that state, paired ones contribute 0, unpaired ones ±1/2

A consequence of equation 4 is that 1 and 3 are the most frequent multiplicities for electronic states, while 2 corresponds to radical species.
A selection rule for electronic transitions is that, due to spin conservation within the system, the spin of the excited electron is preserved. Hence, the ES is a singlet state in most cases because the GS is usually of singlet multiplicity (O_2 is probably the most well-known exception to this rule). In other words, singlet-triplet transitions are spin-forbidden. Excitation in most cases starts from the singlet GS S_0 and can lead to excited singlet states S_1 S_2, S_3,...
Electronic excitation is much faster (10^{-15} s^{-1}) than molecular vibration (10^{-12} s^{-1}-10^{-10} s^{-1}). This means that, according to the Born-Oppenheimer approximation, the distance between the nuclei in the ES will be equal to the one in the GS. Since the bond between two atoms is weaker in the ES and the minimum of the Morse potential is situated at larger bond length, that distance will not be equal to the optimum one. Therefore, the electronically excited state will most likely also be a vibronically excited one (Franck-Condon principle). In other words, the most intense absorption/emission observed will most likely not correspond to the transition between the vibrational GS of the electronic states involved (so-called 0-0 transition) but to higher/lower transition energies.

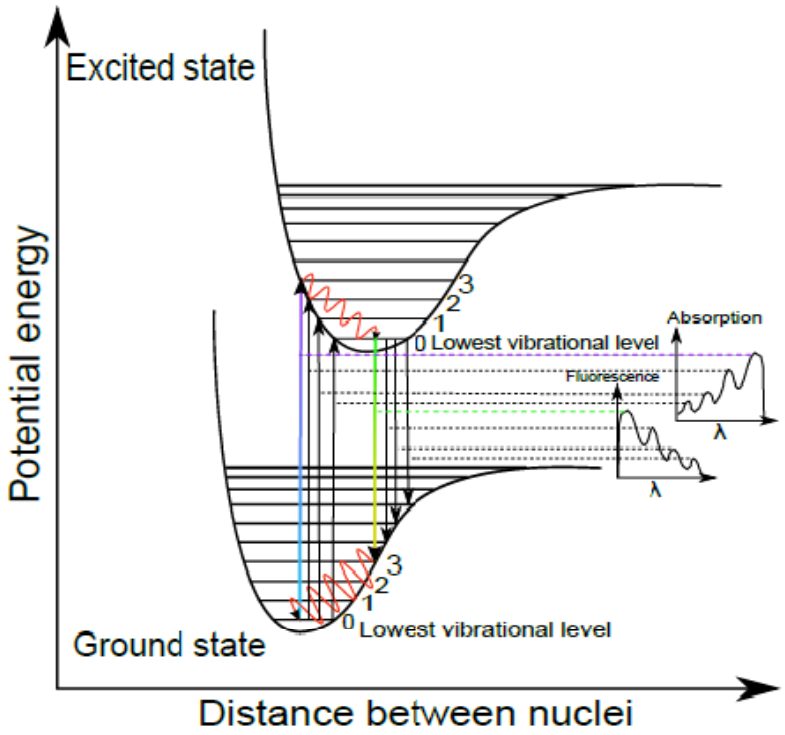

Figure 2: Visualization of the Franck-Condon principle. Electronic excitation also leads to vibronic excitation. Multiple peaks in absorption and luminescence spectra can originate from different vibrational sub-transitions. Rotational sub-transitions are very common, but not indicated here, for the sake of clarity. Vibrational sub-transitions, however, are not always evident as individual peaks but can also cause broadening of the most intense peak.

The shape of absorption and excitation spectra reveals information about the vibrational levels of the ES, the one of emission spectra about the one of the GS.
The energy of vibronic excitation is quickly passed to other molecules or to vibrational and rotational degrees of freedom of the same molecule, i.e. is transformed into heat. This process is called vibrational relaxation and is faster than all activation processes of the electronically ES, including luminescence. Moreover, electrons quickly relaxate from any higher ES to S_1 by internal conversion (2.1.5). Hence, deactivation will depart from the vibrational GS of the first electronically ES.
It has to be emphasized that the ES can have properties totally different to the GS, such as oxidation potential, pK_A values, dipole moment etc. and its reactivity can be very different so that reactions may occur that are impossible in the GS.
$\pi \rightarrow \pi^*$ transitions play a very important role in luminescence dyes. Transitions that go along with pronounced charge transfer are distinguished from "pure" $\pi \rightarrow \pi^*$ transitions (ICT, TICT transitions, 2.1.8). In luminescent complexes including transition metals, d-electrons of the central atom can significantly take part in transitions, so that those may have to be distinguished from "classical" $\pi \rightarrow \pi^*$ transitions in hydrocarbons [2].

2.1.4. Deactivation Kinetics

The following considerations are based on the assumption that a luminophore A forms the excited species A*. Photo-excitation is performed by a light pulse the duration of which is short compared to all deactivation processes of A*.
The deactivation rate of A* is then:

$$-\frac{d[A^*]}{dt} = [A^*] \sum_i k_i \qquad \text{Equation 5}$$

[A*] Concentration of A in the ES (M)
t Time (s)
k_i Time constant of the deactivation process "i" (s^{-1})

k_i is the deactivation rate that i observed if process "i" was the only deactivation mechanism possible.
Integration of differential equation 5, when combined with the following definition of the ES lifetime,

$$\tau_{ES} = 1/\sum_i k_i \qquad \text{Equation 6}$$

yields:

$$[A^*]_t = [A^*]_0 e^{-(t \sum_i k_i)} = [A^*]_0 e^{-(t/\tau_{ES})} \qquad \text{Equation 7}$$

τ_{ES} Lifetime of the ES (s)
$[A^*]_0$ Concentration of A in the ES right after excitation (M)
$[A^*]_t$ Concentration of A in the ES, a time t after excitation (M)

The intensity of light emitted by an excited, luminescent analyte is proportional to $[A^*]_t$:

$$I_{EM} = ck_R[A^*]_t = c\alpha I_0 \Phi_R \qquad \text{Equation 8}$$

I_{EM}	Luminescence emission intensity
k_R	Rate constant of radiative deactivation
c	Constant depending on experimental settings
α	Constant that quantifies the amount of photons absorbed per unit volume
I_0	Intensity of incident light
Φ_R	Quantum yield of radiative deactivation (see below)

The ES lifetime τ_{ES} becomes equal to the lifetime τ_i attributed to the process "i" if no other deactivation pathways are available, or k_i is by far the largest rate constant around.
Provided that photon emission arises solely from deactivation of A*, in the originally ES, and that A* is located in a singlet ES, I_{EM} becomes equal to the observed fluorescence intensity I_F (for definition of fluorescence, see 2.1.5) and Φ_R and k_R become equal to the related terms with fluorescence, Φ_F and k_F. From now on, that will be assumed and fluorescence will be stated representatively for luminescence, unless otherwise stated.
Equation 7 and 8 imply that the fluorescence intensity observed decreases exponentially, once no more excitation takes place. Its decrease obeys a single-exponential decay if ES lifetime is limited by a single process. If various deactivation processes of comparable rate are involved, multi-exponential decay is observed.

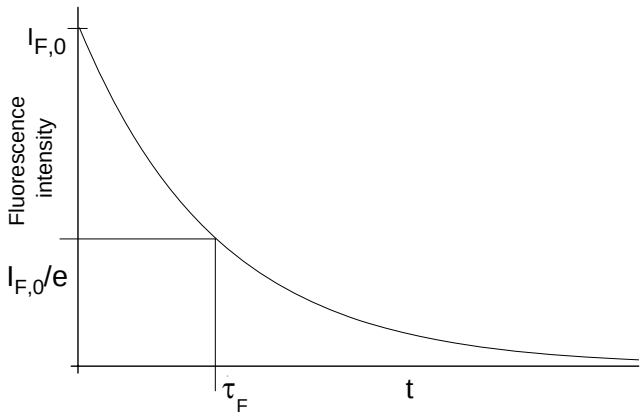

Figure 3: Single-exponential decay of fluorescence intensity I_F over time. Starting from its initial value $I_{F,0}$ it converges to zero. τ_F is the time after which I_F has decreased to I_0/e (37% of its initial value).

ES lifetime is limited by the fastest deactivation process around. If fluorescence is much faster than any other deactivation process, τ of a singlet ES becomes equal to the reciprocal of the fluorescence time constant:

$$\tau_S = 1/k_F \qquad \text{Equation 9}$$

k_F	Fluorescence time constant in (s^{-1})
τ_S	Lifetime of a singlet ES (s)

The quantum yield (QY) Φ of a process is the probability that deactivation of an ES will take place through that process. If a luminescent process is regarded, it is the ratio between the number of photons emitted in the luminescent process and the number of photons absorbed upon excitation:

$$\Phi_i = \frac{k_i}{\sum_i k_i} = k_i \tau_{ES} = \frac{\tau_{ES}}{\tau_i} \qquad \text{Equation 10}$$

Φ_i QY of the process "i"

The decay time of a singlet state is usually referred to as fluorescence decay time. It is longest if fluorescence QY Φ_F is 1 and is shortened when Φ_F decreases since fluorescence has to compete with faster processes then.

2.1.5. Intramolecular Deactivation Processes

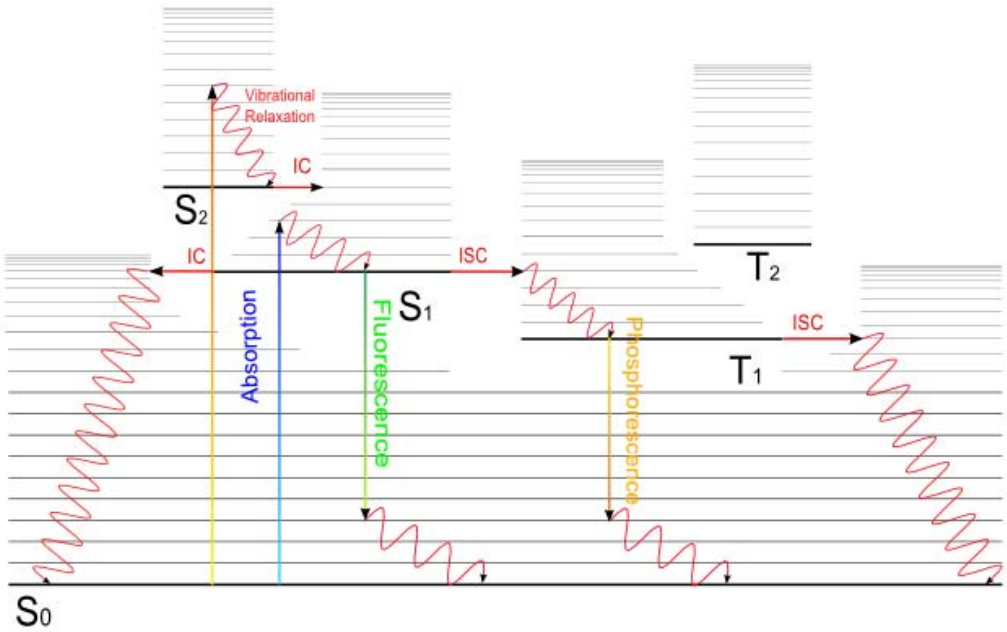

Figure 4: Jablonski diagram, visualizing intramolecular deactivation pathways. A molecule is excited from the singlet GS S_0 to the first singlet ES S_1 and can undergo fluorescence, internal conversion (IC) or intersystem crossing (ISC) to the lowest triplet state T_1.

Fluorescence

Fluorescence is the radiative deactivation of an ES towards a GS of the same spin multiplicity (in most cases $S_1 \rightarrow S_0$). As outlined in figure 2, fluorescence creates vibronically excited S_0 which shows vibrational relaxation immediately. The (average) energy of the emitted photons is inferior to the one of those absorbed upon excitation. Therefore, fluorescence spectra are red-shifted with respect to the corresponding absorption spectra (so-called Stokes shift). The shape of the fluorescence spectra is determined by the population of vibronic states and is thus not influenced by excitation wavelength, but is temperature-dependent.

Fluorescence decay times are usually found within 10^{-10}-10^{-7}s. QY are given by:

$$\Phi_F = k_F / \sum_i k_i = \tau_S k_F \qquad \text{Equation 11}$$

Φ_F Fluorescence QY
k_F Fluorescence rate constant (s^{-1})
τ_S Lifetime of the singlet ES (s^{-1})

Internal Conversion (IC)

IC is a non-radiative transition between two electronic states of the same spin multiplicity. The energy can be distributed over the vibrations and rotations of the excited molecule itself, or it can be passed to the ones of other molecules upon collision. The effectiveness of IC decreases when the energy gap between the states involved increases. As the energy gap between S_0 and S_1 is larger than the gaps between higher ES, other ways of deactivation can be faster there, but all ES higher in energy than S_1 are quickly (10^{-13}-10^{-11}) lowered to S_1 by IC. Since the gap $S_0 \rightarrow S_1$ is directly related to excitation wavelength, IC tends to become more efficient and luminescence tends to become less probable in red-light absorbing dyes. Because rigid structures have less degrees of freedom, IC is less effective with them, that is one of the reasons why many luminophores are quite rigid.

Intersystem Crossing (ISC)

ISC is the transition between two states of the same electronic level but different spin multiplicities (in most cases $S_1 \rightarrow T_1$). This process is in principle spin-forbidden. In some cases, for instance in presence of heavy atoms, it still has a non-zero probability due to spin-orbit coupling and time constants can be 10^{-9}-10^{-7}. All deactivation processes $T_1 \rightarrow S_0$ are spin-forbidden as well and therefore rather slow. According to Hund's law, T_1 is lower in energy than S_1 so that reverse ISC to S_1 is improbable. Thus once ISC has occurred, the lifetime of T_1 can be as long as 10^{-6} – 1s.
ISC quantum yield is given by:

$$\Phi_{ISC} = k_{ISC} / \sum_i k_i = \tau_S k_{ISC} \qquad \text{Equation 12}$$

Φ_{ISC} QY for ISC
k_{ISC} SC rate constant (s^{-1})

Phosphoresence

The radiative deactivation of an ES toward a GS with different spin-multiplicity is called phosphorescence. It is spin-forbidden and therefore slow, but can be rendered possible by ISC as all deactivation processes $T_1 \rightarrow S_0$ are slow. Because the rate constant of phosphorescence is as low as 10^{-6} – 1s, it is seldom observed and its QY is often low. Nevertheless, phosphorescence can be facilitated by using organometallic heavy-metal complexes (those exhibit effec-

tive spin-orbit coupling and hence high Φ_{ISC}) or operating at low temperature and/or in rigid media (both impede IC). Oxygen sensing over phosphorescence quenching of heavy-metal complexes in polymeric matrices at room temperature has been successfully used [3,4]. Due to its much higher lifetime, phosphorescence is easily distinguished from fluorescence by time-resolved methods. It also is observed at higher wavelengths than fluorescence emitted by the same luminophore since T_1 is lower in energy than S_1. Phosphorescence QY is:

$$\Phi_P = k_P \Phi_{ISC} \tau_T \qquad \text{Equation 13}$$

Φ_P Phosphorescence QY
k_P Phosphorescence rate constant (s^{-1})
τ_T Lifetime of the triplet ES (s)

Delayed Fluorescence

E-type and P-type delayed fluorescence can be distinguished. E-type delayed fluorescence is the result of ISC followed by reverse ISC (e.g. $S_1 \rightarrow T_1 \rightarrow S_1$). It shows spectral behaviour equal to common fluorescence but a much lower time constant, comparable to phosphorescence. Although T_1 is lower in energy than S_1, reverse ISC is here possible because of thermal activation of T_1. Therefore, E-type delayed fluorescence shows a characteristic increase with temperature. It is often efficient with fullerenes, but was first observed with eosin.
P-type delayed fluorescence was first observed with pyrene. It is caused by the collision of two molecules in a T state which may allow one of them to return to the corresponding S state (triplet-triplet annihilation). It is more probable concentrated solutions and shows a characteristic dependence on the square of the excitation light intensity.

2.1.6. Intermolecular Deactivation Processes

Models of Quenching Kinetics

Quenching consists in the decrease of luminescence intensity of a given excited luminophore, A*, in presence of another molecule. Several processes involving another molecule can lead to deactivation. As a result, luminescence QY and/or decay time are decreased. The other molecule will be denoted Q (quencher), and any process that decreases luminescence OY (i.e. any process competing with luminescence) is called quenching. It has to be noted that in some quenching processes, new luminescent species can be created, for instance by exciplex formation. However, those processes will still be denoted quenching since that term refers to the originally observed luminescence.
Deactivation by Q requires the excited species A* and Q to be found within a certain maximum distance called encounter distance, which can differ considerably depending on the particular process. Therefore, the kinetics of quenching processes will depend on quencher concentration [Q] and, unlike intramolecular deactivation processes, can depend on molecular transport from Q to A*.

If Q is in large excess with respect to A, one can suppose that there is a non-zero probability that Q will be found within the encounter distance once A* has been formed. If that probability is equal to 1, [Q] can be considered constant (reaction of pseudo-first order: there is no influence of [Q] on the kinetics of the deactivaton process). That is the case when Q is the solvent. If the probability is less than 1, static quenching is present.
If Q is not in large excess, transport of Q towards A* is required within the ES lifetime (diffusion-controlled process). This case is subject to dynamic quenching. The model of collision pair formation has been introduced to describe such a kinetic situation:

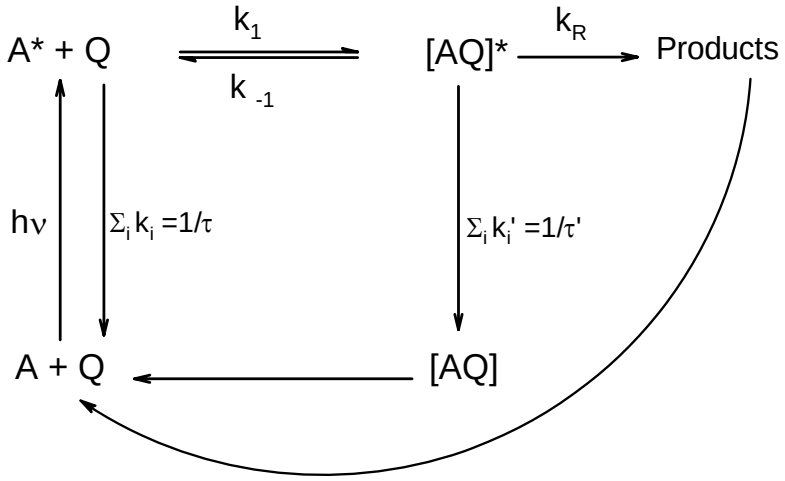

Figure 5: Schematic outline of the kinetic situation for diffusion-controlled quenching. An excited analyte A* interacts with another species, a quencher Q, to form products in one of the processes discussed later in this section. In most cases, those products are equal to or rapidly converted back into A+Q. Collision pair formation between A* and Q is considered an independent kinetic step, with its association rate constant k_1 and its dissociation rate constant k_{-1}. Products are formed from the collision pair [AQ]* with the rate constant k_R. τ and τ' are the fluorescence decay times of A* and the associate [AQ]*. τ is equal to τ' in case of collision quenching, but the fluorescence properties of the associate may also differ from those of the non-associated species (in case of exciplex formation, for instance).

If k_R is the largest rate constant for the deactivation of [AQ]*, quenching is diffusion-limited and the quenching rate constant k_Q becomes equal to k_1 which is a diffusional rate constant. That is usually the case in dynamic quenching by oxygen (2.2.8). On the other hand, if k_R is of the same order of magnitude or smaller, k_Q is proportional to k_R.
In case diffusion is so slow that the probability to form a collision pair within the lifetime of the ES is virtually 0, long-distance energy transfer (radiative EET, discussed in the following) is the only quenching pathway possible.

Dynamic Quenching

If dynamic quenching of a luminescent dye is present, and the quenching rate constant, k_Q, is assumed to be time-independent, luminescence decay time is given by:

$$\frac{\tau_0}{\tau} = 1 + k_Q \tau_0 [Q] \qquad \text{Equation 14}$$

τ_0	Luminescence decay time in the absence of the quencher (s)
τ	Luminescence decay time at variable quencher concentration (s)
k_Q	Quenching rate constant ($M^{-1}s^{-1}$)
[Q]	Quencher concentration (M)

This leads to the Stern-Volmer equation, as k_Q and τ_0 are united to the Stern-Volmer constant:

$$\frac{\Phi_0}{\Phi} = \frac{I_0}{I} = 1 + K_{SV}[Q] = \frac{\tau_0}{\tau} \qquad \text{Equation 15}$$

I_0	Luminescence intensity in the absence of the quencher
I	Luminescence intensity at variable quencher concentration
Φ_0	Luminescence quantum yield in the absence of the quencher
Φ	Luminescence quantum yield at variable quencher concentration
K_{SV}	Stern-Volmer constant (M^{-1})

Both τ_0/τ and I_0/I then show a linear increase over [Q] (figure 6).

Static Quenching

Unlike dynamic quenching, static quenching does not require molecular transport from Q to A* within the ES lifetime.
Static quenching is often associated with the formation of a non-fluorescent GS complex AQ. In rigid or viscous media, where Q cannot approach A^* during the lifetime of the latter, the sphere of effective quenching model has been proposed. It implies that quenching is only effective if Q is found within a certain distance to A^* upon excitation. Both models essentially come down to a decrease in luminophore concentration.
Characteristically, I_0/I vs. [Q] plots are of the same shape as Stern-Volmer plots at low [Q] while they show an upward curvature at higher [Q]. On the other hand, τ_0/τ remains unchanged over [Q].

Simultaneous Static and Dynamic Quenching

Dynamic quenching is often accompanied by static quenching at high [Q] because many quenchers have a certain tendency to act as complexing agents. This results in an upward curvature of the Stern-Volmer plot at high [Q] while equation 15 is obeyed at lower [Q].
A downward curvature is often related to micro-heterogeneity of the surrounding media (2.2.8).

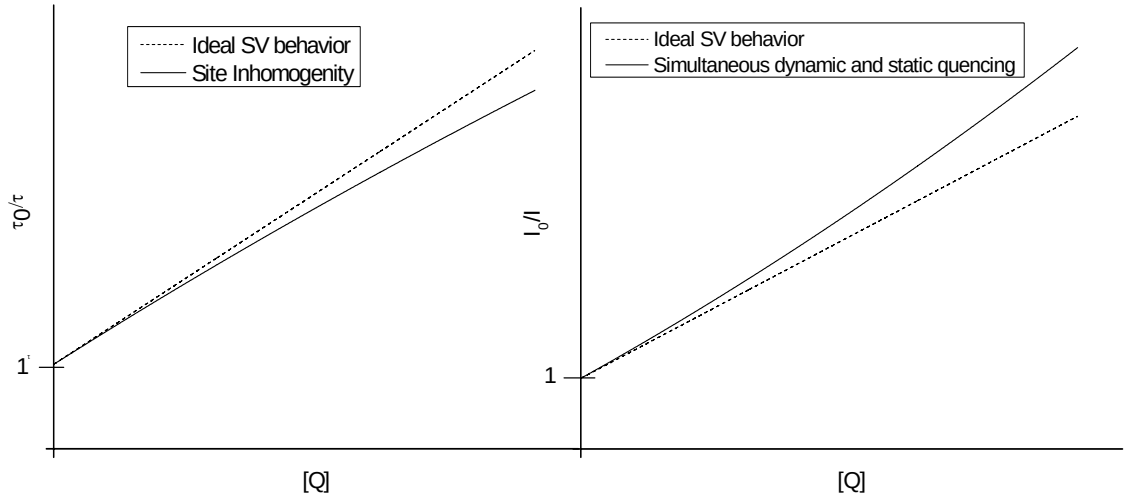

Figure 6: Deviations from the ideal SV behaviour are caused by inhomogeneous microenvironment (left) or by static quenching (right).

Quenching Processes

Photoinduced Electron Transfer (PET)

PET is a redox reaction between an excited fluorophore A* and a quencher. The reaction cannot occur in the GS, but only in the ES as the MO population of the fluorophore is changed (figure 7). Equivalently, redox potentials are remarkably changed with respect to the GS. In this section, the oxidizing agent will be called acceptor A while the reducing one will be called donor D:

Oxidative electron transfer

$$D^*+A \rightarrow D^{\cdot+}+A^{\cdot-} \qquad \text{Equation 16}$$

Reductive electron transfer

$$A^*+D \rightarrow D^{\cdot+}+A^{\cdot-} \qquad \text{Equation 17}$$

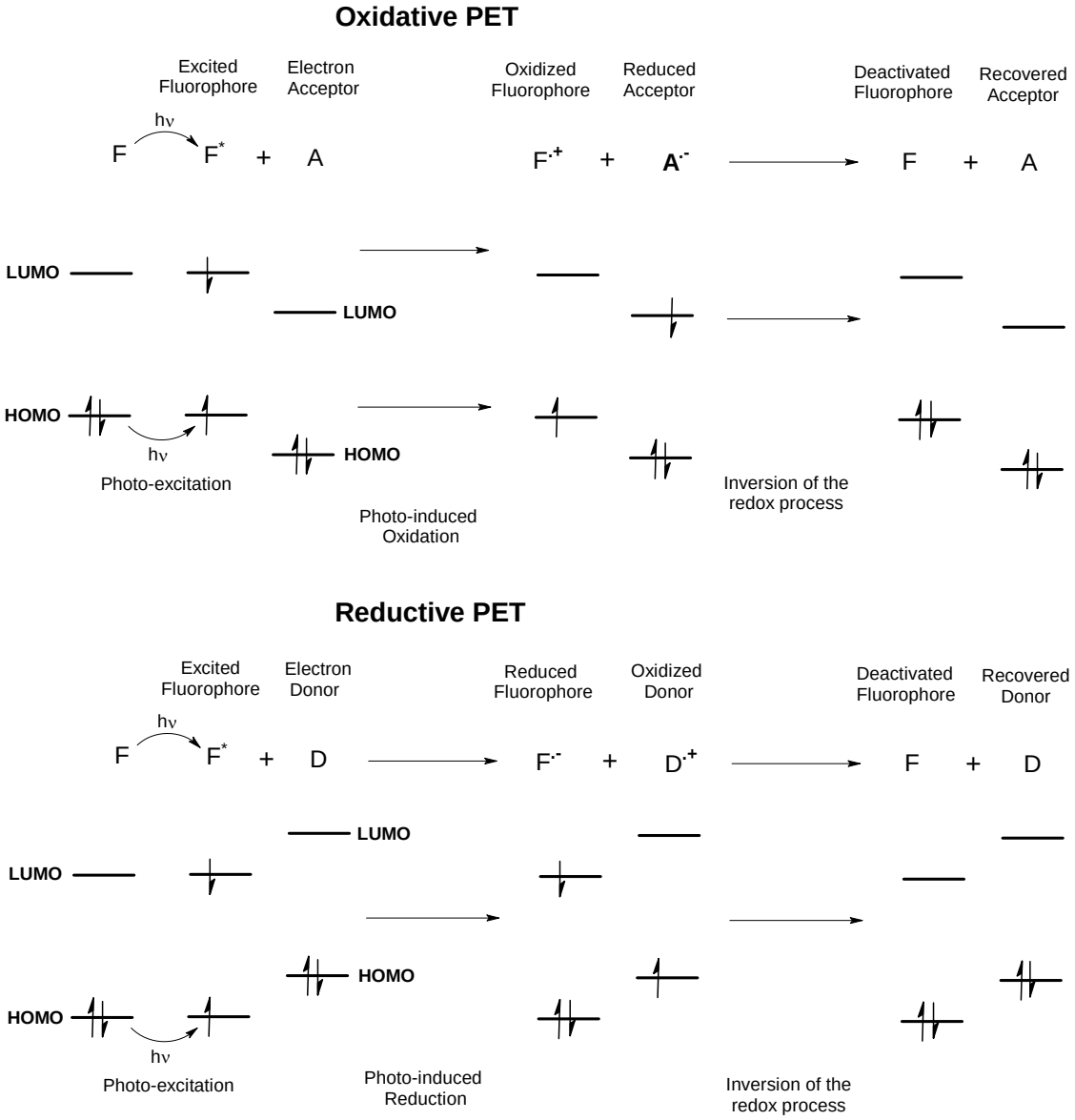

Figure 7: Simplified scheme of the MO populations in PET and the possible consecutive inversion of the redox process. Radicals are created upon PET and the spin multiplicity of the species involved are changed

Once PET has occurred, the oxidized/reduced fluorophore can be re-reduced/-oxidized to form the GS, for instance by the acceptor/donor itself. The only net result of the process is then fluorescence quenching. On the other hand, if the original GS is never recovered, PET makes up the first step in a photo-degradation process.

PET is an example for different reactivity of the ES compared to the GS. Excited molecules can actually be both more strongly oxidizing and reducing agents than the same molecules in the GS.

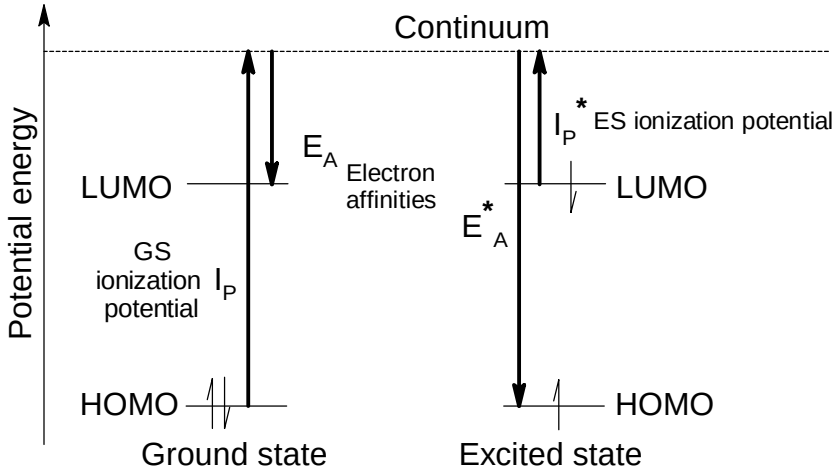

Figure 8: Schematic layout of ionization potentials and electron affinities in the GS and the ES. Because ionization potential in the ES (I_P^*) is lower than in the GS (I_P), the former is more easily oxidized and thus more strongly reducing. On the other hand, electron affinity is more negative in the ES (E_A^*) than in the GS (E_A). Consequently the ES is more easily reduced (more strongly oxidizing). This simplified scheme shows that an excited molecule can be both a more strongly oxidizing and reducing agent than the same molecule in the GS.

PET and its relevance to sensing applications will be discussed in more detail in section 3.1.1.

Excimer Formation

An excimer is a complex formed by an excited fluorophore and another fluorophore molecule in the GS:

$$A^*+A \rightarrow [AA]^* \qquad \text{Equation 18}$$

This is an example of a quenching process upon which a new fluorophore is created. The fluorescence QY of the excimer is not necessarily weaker than the one of the original fuorophore so that fluorescence may undergo a spectral shift rather than disappear. The excimer, which can be considered an extended fluorophore, frequently exhibits more red-shifted and less structured spectra than the original fluorophore. Excimer formation is diffusion-controlled and it gains importance when fluorophore concentration is increased. Fluorescence decay of the excimer obeys a double exponential correlation if excimer formation is reversible and its dissociation rate is comparable to the fluorescence rate constant.
Excimers are one of the reasons why fluorescence intensity does not show a linear response to increasing fluorophore concentration at high values.

Exciplex Formation

Exciplexes differ from excimers by the fact that they are formed with an unlike molecule in the GS and therefore are complexes, not dimers.

$A^*+Q \rightarrow [QA]^*$ Equation 19

Exciplex formation is diffusion-controlled and kinetics frequently are similar to excimer formation. Often they are formed by an electron-rich (donor) and an electro-poor species (acceptor).

Photoinduced Proton Transfer (PPT)

PPT is an acid-base reaction between an excited fluorophore and a proton donor/acceptor which is not thermodynamically favourable in the GS. pK_A values can undergo a shift of several orders of magnitude upon excitation, particularly if the functionality subject to protolysis is part of the chromophore. That is related to excitational charge transfer, which considerably affects the nucleophilic/electrophilic character of certain regions within a molecule. Both acidic and basic properties can be either enhanced or diminished upon excitation. In aqueous media, H_2O can act as both proton donor and acceptor, thus PPT is usually not diffusion-controlled.
Acidic dyes the pK_A value of which is lowered upon excitation have been most extensively investigated. The processes involved are summarized below:

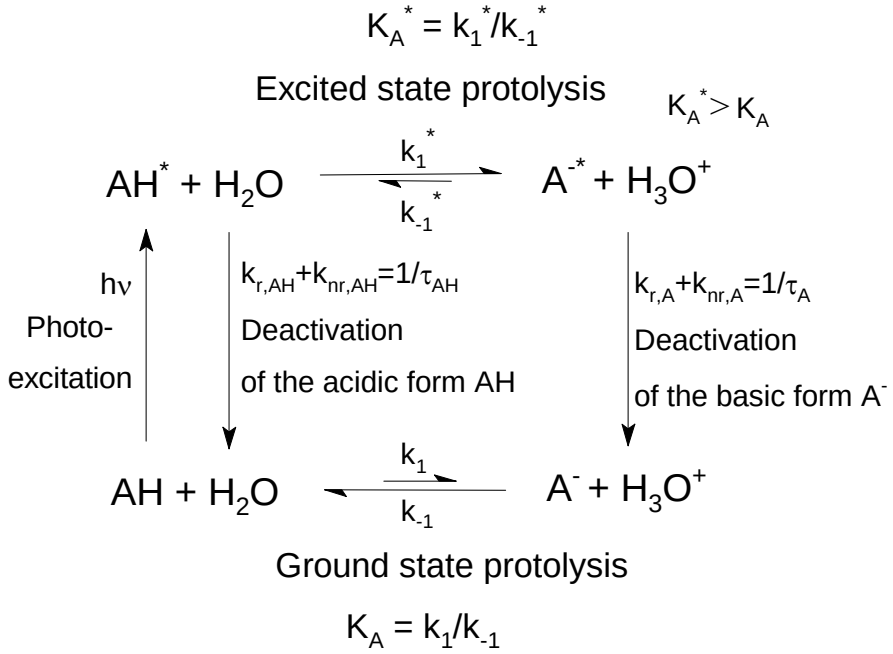

Figure 9: Simplified scheme of the activation, deactivation and protolysis of an acidic fluorescent dye AH subject to PPT. k_R and k_{NR} stand for the radiative and non-radiative deactivation rate constants, τ for the ES lifetimes of the acidic form AH and the basic form A^-. k_1 and k_{-1} represent the protonation and deprotonation rate constants and K the corresponding protolysis equilibrium constants in the GS and the ES (marked with *). The situation shown gives rise to PPT as $K_A^* > K_A$ and deprotonation can be induced by excitation.

A simple method to estimate pK_A^*, the pK_A of the excited state, is through the Förster cycle, a thermodynamic cycle that includes all four species shown in figure 9.

$$pK_A^* - pK_A = C(\nu_{A^-} - \nu_{AH})$$ Equation 20

$pK_A^* - pK_A$	Difference between pK_A values in the ES (*) and the GS
C	Constant of proportionality (s)
$\nu_{A^-} - \nu_{AH}$	Difference between the frequencies corresponding to the 0-0 transitions in the basic (A^-) and acidic (AH) form (s^{-1})

An exact determination of 0-0 transition frequencies may be complicated, but they can be estimated to the average of the frequencies observed in the absorption and the emission maximum.
A consequence of equation 20 is that AH is more acidic in the ES than in the GS if the fluorescence emission spectra of the basic form are red-shifted with respect to the acidic one and vice versa.
The QY of acidic and basic forms are pH-dependent:

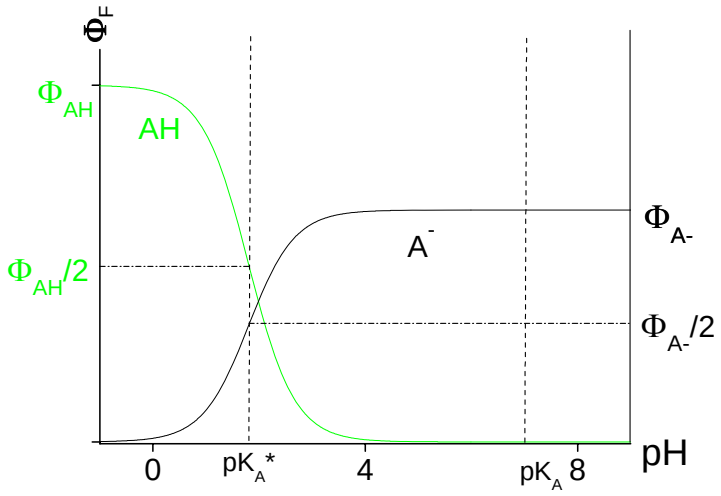

Figure 10: Simplified model for the consequences of PPT on pH-dependent fluorescence QY of an acidic dye AH. It is assumed that pK_A^*=1.8, the ground state pK_A=7 and fluorescence QY for AH is greater than the one of the basic form, A^-. Emission intensity shows the highest alteration at pH close to pK_A^*, which is very different to the pK_A measured in the GS. If pK_A^* is greater than 2, emission of both forms can be observable in the range $pK_A^* \geq pH \geq pK_A$ for kinetic reasons. Figure 10 is also valid for dyes that do not undergo PPT, only then $pK_A = pK_A^*$. Therfore, any dye capable of protolysis shows pH sensitivity at pH close to pK_A or pK_A^*, provided spectral properties of acidic and basic form are significantly different.

Excitation Energy Transfer (EET)

Upon EET, only energy is transferred from an excited donor to an acceptor. Afterwards, the acceptor is found in the ES while the donor has returned to the GS:

$$D^* + A \rightarrow D + A^*$$ Equation 21

EET can take place radiatively and non-radiatively.

Radiative EET is basically the absorption of photons emitted by molecules of the same species as the fluorophore (auto-absorption) or by another species. It can be caused by all molecules that are in at least one wavelength distance from the emitting molecule. The effect is unwanted in analytical applications since it distorts spectra in the area of spectral overlap and provokes errors in calibration curves. It can be avoided by working with low dye concentrations and in a non-absorbing environment.
Non-radiative EET does not involve photon exchange. Equally to radiative ET, energy can be passed from an excited molecule to a not excited one in the same extent as emission spectra of the former and absorption spectra of the latter overlap. Thus, a prerequisite for this transfer mode is that their spectra overlap (they are "in resonance"). Therefore it is frequently called RET (resonance energy transfer). RET is efficient at much smaller interaction distances than radiative EET, though the maximum interaction distance depends on the exact mechanism. Fluorescence spectra are not changed in shape by RET, but their intensity is decreased by a constant factor. Fluorescence decay time is shortened if the RET acceptor is an unlike molecule, otherwise it remains unchanged. There are two RET mechanisms that have been extensively investigated, Förster's and Dexter's mechanism.
Förster's mechanism is most common and investigated (FRET, Förster resonance energy transfer). It is based on coulombic, long-range dipole-dipole interactions and can be effective over a distance up to 10nm. An electron returns from the LUMO to the HOMO of the donor, while in the acceptor another one is promoted from the HOMO to the LUMO.
The rate constant is given by:

$$k_T = \frac{1}{\tau_{D,0}} \left(\frac{R_0}{r}\right)^6 \qquad \text{Equation 22}$$

k_T FRET rate constant (s^{-1})
$\tau_{D,0}$ ES lifetime of the donor in absence of FRET (s)
R_0 Förster critical radius (nm)
r Distance between donor and acceptor (nm)

FRET quantum yield Φ_T is:

$$\Phi_T = \frac{1}{1+(r/R_0)^6} \qquad \text{Equation 23}$$

This shows that FRET efficiency decays by $1 \sim r^6$ and it changes very sharply at distances close to R_0. The Förster critical radius R_0 is the distance at which FRET is equally probable as non-FRET decay of the donor.
Dexter's mechanism takes place at distances ≤1nm and is caused by molecular orbital overlap. An electron is passed from the LUMO of the donor to the one of the acceptor, while simultaneously another one is passed from the HOMO of the acceptor to the one of the donor. As a result, the donor has returned to the GS, the acceptor has been excited. Unlike Förster's mechanism, this involves the actual electron exchange between the donor and the acceptor. However, Förster's mechanism is predominant even at short distances, unless the electronic

transitions it implies are forbidden (if the spin multiplicities of the initial and the final state of donor and/or acceptor are unlike).
FRET has been applied for numerous purposes in optical sensing. FRET systems constitute a powerful tool to quantify distances of about 1-10nm (though for each system, a strong response will only be found when r is close to R_0, according to equation 23). They have been utilized to evaluate processes on a supramolecular level [5,6]. Combining two dyes with appropriate spectral properties so that excitation energy is effectively transferred from a short-wave ("antenna") to a more long-wave absorbing dye has been used in sensors. It is suitable for enhancing brightness - particularly of poorly absorbing dyes - over indirect excitation (light harvesting) or for tuning spectral properties, for instance enlarging Stokes shifts or providing good compatibility with powerful light sources [7].
Other applications of FRET include signal generation on macromolecular receptors such as aptamers [8], polymer analytics and light-harvesting polymers [9], studies of membrane organization and three-dimensional structure investigation in biomolecules [10], to state only a few.

Photoreactions

A wide range of photoreactions involving fluorescent species has been investigated. The ES undergoes a reaction (dissociation, isomerisation, etc.) and the GS is never recovered. Photo-induced reactions originate from different reactivity in the ES, compared to the GS. In fluorescence sensors, they are associated with undesired photodegradation ("bleaching") of the indicator dye which is a mayor issue especially in long-time applications. On the other hand, numerous approaches take advantage of photoreactions in organic [11,13] and inorganic [12] synthesis.

2.1.7 Influence of Functionalities

The relation between structural and spectral features of organic luminophores is complex. Nevertheless, some of the most important trends will be briefly discussed here. They do not claim universal validness, exceptions from the statements given are always possible.
Most organic luminophores are aromatic, though extended conjugated aliphatic π-systems can be luminescent too. $\pi \rightarrow \pi^*$ transitions are most relevant (section 2.1.3). The more extended the conjugated unsaturated π-system of a chromophore becomes, the more red-shifted are both absorption and fluorescence spectra. Both ε and Φ_F tend to increase when the chromophore becomes more extended. Electron-donating groups such as $-NR_2$ and –OR often cause an increase in ε and both absorption and fluorescence spectra can be red-shifted. Electron-withdrawing groups like –CHO or $-NO_2$ can introduce a $n \rightarrow \pi^*$ transition lower in energy than the lowest $\pi \rightarrow \pi^*$ which results in a decrease of ε and low QY. Halogenides do not cause a strong mesomeric effect and usually only induce minor spectral shifts. They can have a considerable impact on redox properties. Considering that photo-oxidation is an important bleaching pathway, they can help to improve photostability of some chromophores (an example is given in [14]). Br and I can favour ISC, though that is not the case in all chromophores, some have triplet states with low accessibility (too different in energy from the singlet states).

Acidic/basic groups (most importantly, -OH) introduce significant spectral changes upon (de)protonation deriving from charge transfer if they are part of the chromophore (acid/base or pH sensitive dyes) but have little or no impact if they are not directly connected. A structural feature particularly meaningful to this thesis is the possibility of PET fluorescence quenching through free amino groups which are not part of the chromophore. Luminescent heavy metal complexes often show high ISC quantum yield and are thus phosphorescent dyes. That is of mayor analytical importance since those are accessible to dynamic quenching by molecular oxygen and consequently O_2-sensitive (2.2.8).

2.1.8 Polarity Effects

Polarity of the surrounding media can affect the spectral location of absorption and fluorescence spectra. These so-called solvatochromic shifts originate from unlike stabilization of GS and ES by their solvate shells. Stabilization corresponds to interactions between permanent and non-permanent dipoles of solute and solvent and to directed interactions such as hydrogen bonds. Polarity cannot be directly quantified, though it is often associated with terms like dipole moment (μ) or dielectric constant (ε). More sophisticated models for polarity, taking into account various parameters, have been discussed in context with spectral properties and may be more universal, but do not allow quantification on a mono-dimensional scale [15]. Both bathochromic and hypsochromic shifts can occur with increasing solvent polarity and have been denominated positive and negative solvatochromism. A redistribution of charges within a molecule frequently takes place upon excitation (photoinduced charge transfer, PCT, or intramolecular charge transfer, ICT). Often, μ is higher in the ES, resulting in higher stabilization by polar solvents with respect to the GS and consequently in positive solvatochromism. Polarity may differently affect absorption and emission maxima and thus have an impact on Stokes shifts.
ICT is often particularly large in aromatic systems where an electron-donating group is conjugated to an electron-withdrawing one (so-called push-pull chromophors). ES are then referred to as ICT excited states, and polarity-induced band shifts are more pronounced. To a certain degree, solvatochromism can be associated with the symmetry of a chromophore, since asymmetric molecules are likely to have a higher dipole moment than symmetric ones of similar structure and polar character of ES and/or GS is a prerequisite for strong solvatchromism [16].
PCT induces a reorientation of the solvate shell of the ES (solvent relaxation) as a result of unlike charge distribution in GS and ES. A relaxed ES can possess different spectral properties to the non-relaxed one present right after excitation. The emission spectra observed may then depend on the rigidity of the surrounding media if reorientation is not much faster than luminescence. Right after excitation, molecular geometry of a chromophore is alike in the GS and the ES, according to the Franck-Condon principle. However, in some ICT dyes, it may change upon solvent relaxation, creating a so-called TICT (twisted intramolecular charge transfer) excited state with distinguishable spectral properties. That has been frequently observed with anilines the amino moiety of which can undergo post-excitational rotation out of the aromatic plane in polar solvents. That results in less conjugation between the aromatic plane and the amino group and consequently in different spectral properties.

2.1.9 Luminescence Measurement

Steady State Measurement

Steady state measurements are carried out under continuous illumination so that the concentration of the excited analyte, [A*], can be considered constant (though in practice, deviations from that may occur, for example due to photo-bleaching).
Fluorescence intensity at a given pair of excitation and emission wavelengths (λ_{EXC} and λ_{EM}) is proportional to the intensiy of excitation light and at low oncentrations also to analyte concentration:

$$I_F = I_{EXC} F_\lambda C(1 - 10^{-A}) = I_{EXC} F_\lambda C\left(1 - 10^{-\varepsilon cd}\right) \sim 2.3\, I_{EXC} F_\lambda C\, \varepsilon cd \qquad \text{Equation 24}$$

I_F	Fluorescence intensity at a given excitation and a given emission wavelength
I_{EXC}	Intensity of excitation light at the excitation wavelength.
C	Constant of proportionality depending on experimental settings
A	Absorption of the analyte at the excitation wavelength
ε	Molar absorption coefficient of the analytet at the excitation wavelength ($M^{-1}cm^{-1}$)
c	Dye concentration (M)
d	Optical path length of the sample (cm)

F_λ is a factor representing the shape of emission spectra. Its integral over the whole spectrum is equal to the fluorescence QY Φ_F. The simplification shown is only valid at low analyte concentrations.

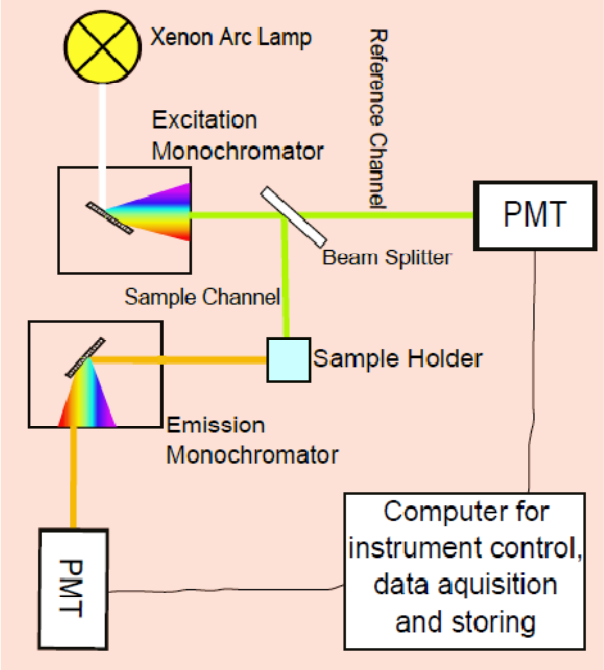

Figure 11:Schematic layout of a steady state fluorescence spectrometer. It is equipped with a xenon arc lamp light source, grating monochromators and PMT detectors. A reference channel is optional and can be also equipped with a quantum counter.

Xenon arc lamps are the most commonly used light sources for spectrofluorimetry, providing good emission intensities from 250nm up to the NIR range. Spectrofluorimeters are equipped with both an excitation and an emission monochromator with tuneable slits. Gratings are almost exclusively used nowadays as they allow a higher resolution than prisms. The emission light coming from the sample is observed perpendicularly to the incident beam to minimize interferences from excitation light. Moreover, monochromator wavelengths and slits are adjusted in a way that excitation and emission wavelengths have no overlap. Photomultplier tubes (PMT) are the most common detectors because of their high sensitivity. Drawbacks are their high price and poor response in the NIR. Photodiodes and avalanche photodiodes are less expensive and less bulky alternatives used in optical sensors.
Excitation spectra are recorded by varying excitation wavelengths at the excitation monochromator while the emission wavelength detected is kept constant. On the other hand, emission spectra are recorded by varying the emission wavelength at the emission monochromator at constant excitation wavelength.
Complications of luminescence measurements can arise from wavelength dependence of the emission intensity of the light source, the transmission of the monochromators or other optical elements and the detector response. Light source and detector response also are inconstant over time which can be (at least partially) corrected by comparison with a reference channel. Background signal can be caused by auto-fluorescence of the sample (polymers, biological samples), scattering or interferences from excitation light (overtones, reflected light etc.). Even in presence of a reference channel, both excitation and fluorescence spectra still require referencing with a reliable fluorescent standard for accurate quantitative intensity measurement.
Fluorescence measurements should be carried out in dilute solutions because of deviations from linearity (equation 24) at higher analyte concentrations. Those are provoked by absorption of both excitation and emission light by the analyte itself (inner filter effects)
and aggregation effects such as excimer formation (2.1.6).
Polarization effects can also distort luminescence measurements because plenty of the processes described in 2.1.5-6 may be affected by the polarization of light and the transmission of monochromators is also dependent on polarization. Those effects can be avoided by using polarizators in front of and behind the sample. Correct fluorescence measurement also requires constant temperature as quantum yields are temperature dependent.
It has to be stated that spectrofluorimetry cannot be used to directly calculate dye concentration from fluorescence intensity because of the uncertainty of experimental conditions (light source emission, monochromator transmission - particularly if slits are adjusted -, PMT response and high voltage, geometry of observation). Calibration helps to overcome that, though it has to be carried out cautiously, maintaining constant experimental conditions.

Time-resolved Measurement

Time-resolved methods not only facilitate monitoring of chemical and physical processes and provide information about kinetic parameters, [17,18] but also allow measurement of luminescence decay time. Luminescence decay time is influenced by far less parameters than intensity, therefore its measurement is subject to far less interferences. Experimental parameters

as described in the previous section have no impact on decay time and it is not even affected by some deactivation processes (like static quenching). That allows more selective monitoring of those processes that do have an impact on it. However, more sophisticated instrumentation is needed, especially for measuring the very short fluorescence lifetimes which requires expensive, non-portable equipment. The longer phosphorescence lifetimes are less difficult to measure and have been used for various sensing applications [3,19,20].
If excitation occurs within an infinitely short time, the luminescent response is in the simplest case given by single exponential decay (section 2.1.4, equations 7,8). The response function is then called δ-pulse response.

Phase Modulation Fluorimetry

In phase modulation fluorimetry, light modulated with a certain modulation frequency is employed for excitation. This results in harmonic response, i.e. the emission of light shows the same modulation frequency but different phase and amplitude.

$$\psi(ex) = A + Bcos(\omega t) \qquad \text{Equation 25a}$$

$$\psi(em) = a + bcos(\omega t - \phi) \qquad \text{Equation25b}$$

Ψ(ex)	Wave function of the excitation light
Ψ(em)	Wave function of the emission light
A,B,a,b	Constants, where A and a make up the average intensity of excitation and emission light, B and b their modulation amplitudes, respectively
ω	Angular modulation frequency (s^{-1})
ϕ	Phase shift of the emission light

With respect to excitation radiation, the emission signal is delayed in time and partially demodulated. B/A and b/a are called modulation depths of excitation and emission radiation because they express the ratio between their modulated and non-modulated fraction. Demodulation is quantified by the demodulation factor M while the phase delay is quantified by ϕ.

$$M = \frac{m}{m_0} = \frac{(b/a)}{(B/A)} \qquad \text{Equation 26}$$

M	Demodulation factor
m	Modulation depth of the emission light
m_0	Modulation depth of the excitation light

Both ϕ and M are characteristics of the harmonic response of the system. They are dependent on the modulation frequency f. When f increases, ϕ approximates to 90° and M approximates to 0, resulting in a totally non-modulated, "flat" emission signal delayed by 90° with respect to excitation radiation when f becomes infinite.

Luminescence decay time and intensity can be calculated from ϕ, M and the amplitude measured by a phase fluorimeter using the following equations:

$$\phi = \arctan(\tau\omega)$$ Equation 27

$$M = \frac{1}{\sqrt{1+(\tau\omega)^2}}$$ Equation 28

$$I = \frac{\alpha}{M}$$ Equation 29

τ Luminescence lifetime (s)
I Luminescence intensity
α Amplitude measured

Pulse Fluorimetry

In pulse fluorimetry, the luminescent response to an excitation pulse is followed over time. The δ-pulse response is given by a sum of exponential decays:

$$I(t) = \sum_i \alpha_i e^{(t/\tau_i)}$$ Equation 30

I(t) δ-pulse response (fluorescence emission intensity as a function of time)
α_i Constant of proportionality to each single exponential i
τ_i Decay time to each single exponential i

If pulse duration is not negligible compared to fluorescence lifetime, deconvolution of the following product has to be performed to determine the δ-pulse response and consequently τ:

$$R(t) = E(t) \times I(t)$$ Equation 31

E(t) Excitation function (intensity of excitation light as a function of time)
R(t) Response function (emission intensity measured over time)

R(t) can be measured with the single-photon timing technique: single photons are detected by a photomultiplier while a large number of subsequent excitations are performed. The time of detection is exactly determined for each photon. The responses to all excitation pulses are summed up to yield the overall response function.
Because the harmonic response to modulated excitation light is the Fourier transform of its δ-pulse response, pulse fluorimetry and phase modulation fluorimetry are equivalent.

2.2 Optical Sensors (Optrodes)

This chapter is based on references [1] and [21]. Other references will be cited independently.
A chemical sensor is a device that detects a chemical or biochemical species (analyte), generating information output in form of an electric signal. In contrast to "conventional" analytic instruments, it aims on monitoring a sample over time, without requiring sampling or manipulation. Several more detailed definitions of chemical sensors have also been given. According to IUPAC definition, a chemical sensor is "...a device that transforms chemical information, ranging from the concentration of a specific sample component to total composition analysis, into to an analytical useful signal. The chemical information, mentioned above, may originate from a chemical reaction of the analyte or from a physical property of the system investigated." [22].
In an optical chemosensor, information about the analyte is provided by detecting binding between the analyte and a fully synthetic receptor (differently to biosensors, in which biomolecules are used) over interaction with electromagnetic radiation. Optical sensing is above all carried out in the UV/VIS range of the spectrum, as cheap and effective optic elements are readily available.
An optical sensor is consisted of a receptor that interacts with the analyte, a transducer that generates a measurable optical signal as a response on the binding event and a data processing unit that converts the optical signal into information output. It can also contain a filter that excludes certain unwanted species from accessing to the receptor. Filters are often polymer layers that prevent, for instance, hydrophilic or charged species from passing. Sensors contain an immobilization matrix for receptor and transducer which can function as a filter or not. Transduction can be based on variation in absorptive, luminescent or refractive properties. Luminescence transduction is most interesting to this thesis and will be discussed in the following section. Absorption transduction is in principle less sensitive while refractometric transduction has been carried out in many differently designed systems and is above all used in biosensors (an example is given in [23]).
Apart from the usual demands to an analytical device such as selectivity, sensitivity, reproducibility of the signal, extended dynamic range etc., sensors are in particular requested to be cheap, small, easy to use and to calibrate, fast in response and robust. Optical sensors have been presented for many analytical purposes including (bio)process monitoring and biological screening [24], toxicologic screening [25], food packaging [26] or clinical monitoring [27], to give only a few examples.

2.2.1 Principles of Luminescence Chemosensors

Luminescence is a powerful analytical tool due to its high sensitivity and selectivity, the possible temporal and spatial (facilitating kinetic studies [17,28] and two- [29,30] or three-dimensional [31,32] imaging) resolution of fluorescent techniques and the possibility of remote sensing. Another advantage lies in the versatility of luminescence techniques, including intensity and decay time measurement, observation at various wavelengths and the additional possibility of polarization measurement. That implies that a large amount of information can be transmitted over electromagnetic radiation.

Because of the great variety of processes that affect luminescence (section 2.1.5-6), information about numerous properties of the micro-environment surrounding a fluorescent probe are accessible to luminescence sensing, opening a wide field of applications. While pH-, O_2- and ion-sensing are well-known and will be discussed individually, some more "exotic" examples for luminescence-based measurement are polymer miscibility [33], accessibility of biomolecules such as nucleic acids [34] or phase transitions in concentrated surfactant solutions [35]. Indeed, that variety also implies a high number of potential cross-sensitivities so that luminescence sensors require very precautious design.

2.2.2 Luminescent Indicators

The indicator dye is the core of a luminescent sensor and perhaps most determing for its performance, even though the matrix and additives (2.2.3) also play an important role and their proper selection is crucial. Requirements to an indicator dye include good sensitivity and linear response in the concentration range focussed, good selectivity, high luminescence brightness, spectral compatibility with optical modules cheaply available (2.2.3), fast and reversible binding to the analyte, good chemical and photostability in the sensing matrix, sufficient synthetic or commercial accessibility in pure form and good compatibility with matrices established for the sensing application focussed. Sensors for main components can require a different design than trace sensors when sensitivity is too high to allow reliable measurement at high analyte concentrations, an example is [36]. Long-wave excitable dyes are particularly advantageous, above all in biological or clinical samples, because there is less fluorescent background from the sample and the sensor itself at longer wavelength and interferences from scattering are less critical. NIR-excitable dyes even facilitate subcutaneous measurement owing to the high transmittance of tissue there [4].
Some analytes show decent fluorescent properties themselves so that they can be measured directly (intrinsic probes), without a luminescent indicator being required. Examples are polycyclic aromatic hydrocarbons [37] or chlorophylls [38]. In most cases, however, the analyte is non-fluorescent and recognition by a receptor becomes necessary.
Sensitivity of the indicator originates from spectral changes (luminescence quenching or enhancement, spectral shift) upon interaction with the analyte. If the analyte binds to the chromophore itself, receptor and transducer are identical (integrated receptor). That is actually a frequent situation in luminescence chemosensors, most oxygen and pH indicators can be classified as such. Oxygen sensing is based on collisional quenching and no actual association occurs. If the receptor is not part of the chromophore, it can be covalently or non-covalently linked to it or embedded into the same matrix. Covalent linkage via a spacer is frequently employed. Examples are fluoroionophores (2.2.7) or PET-based pH sensors which are of mayor importance to this thesis (3.1.1). Although many different indicator dyes with different transduction principles have been designed and employed for sensing, perhaps the most frequently employed principles are dynamic quenching of phosphorescent indicators (oxygen sensors, 2.2.8) and deprotonizable chromophores where spectral properties of acidic and basic form are significantly different (most pH indicators, 2.2.4).
For the design of luminescent indicators it has to be kept in mind that the receptor function is basically responsible for selectivity, reversibility and response time, while spectral properties

and photostability are determined by the chromophore. Therefore, if the receptor is not part of the chromophore, dyes can be designed in a way that properties are optimized, selecting chromophore, receptor and the mode of linkage between them. An example is the design of PET indicators [39]. Dyes with integrated receptors can as well be synthetically modified in order to adjust analyte recognition (modification of the fluorescein chromophore to adjust pK_A value, [40]) and/or spectral and photochemical (more photostable fluorinated benzoporphyrins, [41]) properties. Some modifications may not directly affect the chromophore nor the receptor, but aim on improving applicability in a sensing matrix (lipophilization of fluoresceins to allow non-covalent immobilization in a hydrophilic matrix, [40,42]).

2.2.3 Some Principles of Sensor Design

Sensitive indicators are often not used in solution but immobilized in a (mostly polymer) matrix to yield sensors. Non-covalent immobilization exploits size exclusion or anchoring principles. The latter often consists in attaching a hydrophobic group to a hydrophilic dye so that it is kept within a hydrophobic matrix. Covalent immobilization is more difficult to perform but allows the preparation of fully leaching-free sensors, i.e. the sensitive components are not washed off by the sample. Alternatively, indicators can be bound onto a carrier, performing two-dimensional immobilization. If a luminescent dye is immobilized into a polymeric matrix, the polymer must feature good solubility of the dye to prevent aggregation, good analyte permeability and exclusion of unwanted species (if possible). The properties of the dye must be adequate in the matrix, since upon immobilization, the properties of a dye can be considerably altered, in comparison to solution.
Optrodes are most frequently designed as sensitive layers or fibre optic sensors, though in the recent years sensitive beads have gained importance (2.3).

Instrumentation

Sensing applications call for miniaturized, cheap optical modules. Light emitter diodes (LEDs) are available at low cost, with acceptable performances for most of the VIS spectrum, though there currently is a gap between 535 and 585nm where no LEDs with suitable power have been developed. Emission is relatively broad (peak half width around 50nm [43]). Laser diodes feature more narrow emission and higher emission power but are more expensive and only available for some wavelengths. To separate excitation and emission light, optical filters are employed. Long- and shortpass-filters cut off most of the light under/over a certain cut-off wavelength. Bandpass filters only let a narrow spectral area pass, but decrease the overall intensity more severly. Dyes with a large Stokes shift are advantageous because filters do not cut off as sharply as monochromators which complicates the separation of excitation and emission light. Photodiodes are cheap detectors while avalanche photodiodes are more sensitive but also more expensive. CCD cameras have been used for two-dimensional fluorescence imaging [44].
Waveguides are used to direct light to the sensitive system and from there to the detector. They are based on total reflection of light at the edge to an optically less dense medium.

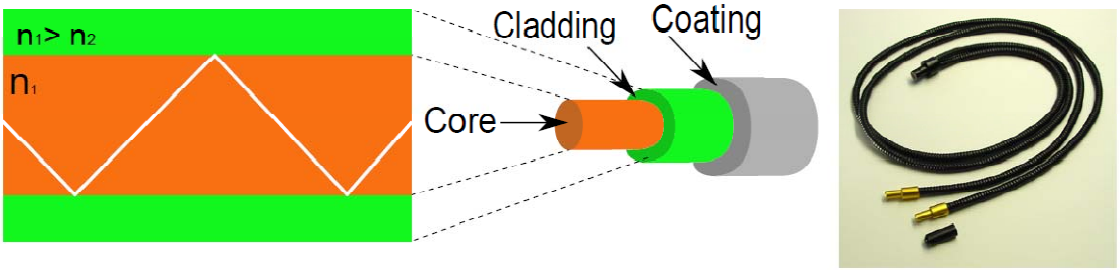

Figure 12: Functional principle of a waveguide. Light is coupled into the core and reflected at the cladding which has a lower refractive index than the core so that total reflection occurs.

Sensor design can involve waveguide fibres (fibre optic sensors, [45]) with the sensitive area incorporated into the fibre itself. Systems with planar waveguides have as well been presented [46,47].

Referencing Techniques

When measuring with luminescent sensors, in principle, the same problems as in spectrofluorimetry (2.1.9) have to be dealt with. Additional complications may arise from insufficient cut-off at optical filters, distortion of the measured signal by the waveguide, bleaching or leaching of the indicator dye. Perturbations by the sample include absorptive or fluorescent background, accompanying species that cause cross-sensitivities or turbidity.
Of course, the first step towards solving those problems is appropriate calibration. However, when fluorescence intensity is measured, additional referencing techniques are necessary. In dual wavelengths referencing, either two excitation or two emission wavelengths are used. The signal is compared to the one of a reference dye which is brought into the sensor together with the indicator. In dual lifetime referencing (DLR), a phosphorescent reference dye is utilized and the signal, which is the sum of the emissions of both dyes, is detected by phase modulation fluorimetry. In that way, the fluorescence of the indicator can be measured indirectly over the more robust lifetime measurement [19,48].

2.2.4 Luminescence pH Sensors

In comparison to electrochemical pH sensors, which are well-established, optical pH sensors are more easily miniaturized, more robust against electromagnetic interferences and allow remote sensing. They offer better sensitivity within their dynamic range, which is indeed narrower (2-3 pH units) than the one of electrochemical sensors. A drawback is their cross-sensitivity to ionic strength which derives from the fact that H^+ concentration instead of activity is measured [40]. Both are related over the Henderson-Haselbach equation:

$$pH = pK_A + log\frac{[B^-]}{[HB]} + log\frac{f_{B^-}}{f_{HB}} - log\, a_{H_2O} \qquad \text{Equation 32}$$

$[B^-],[HB]$	Concentrations of the acidic form HB and the basic one B^- (M)
f_{B^-},f_{HB}	Activity coefficients of the acidic form HB and the basic one B^-
a_{H2O}	Activity of water

Equation 32 shows that the influence of ionic strength on activity coefficients causes cross-sensitivity. High sensitivity is restricted to the range pH=pK_A±1.5.
pK_A refers to the value measured in water. Values measured in different environments (mixtures with organic solvents, immobilization layers) are denominated apparent acidity constants, pK_A'. They are related to pK_A as follows:

$$pK_A = pK'_A + log\frac{f_{B^-}}{f_{HB}} \qquad \text{Equation 33}$$

pK_A' Apparent pK_A value

Activity coefficients not only describe the influence of ionic strength, but the overall interaction of the indicator dye with its microenvironment, compared to the one with water.
According to Janata [49,50], cross-sensitivity to ionic strength can be minimized by using a low-charged indicator dye and immobilizing it into a low-charged microenvironment. For instance, receptors based on fluorescein esters can allow the design of sensors with virtually no sensitivity to ionic strength [40].
Hydrophilic immobilization matrices are needed for pH sensors since they provide good proton permeability. Hydrogels are often utilized. Covalent immobilization may prevent complications. Hydrophilic dyes can suffer from leaching, whereas strictly hydrophobic ones are unlikely to be well soluble in a hydrophilic matrix and aggregation issues may occur. Both is less critical if covalent coupling is carried out. Anyway, sensors based on non-covalent immobilization, which is much easier to perform, have as well been presented [40,42,51,52] as covalent coupling [53-55].
The matrix can have an effect on spectral properties (λ_{MAX} and QY can be influenced) and may cause a shift in pK_A by several orders of magnitude. Deprotonizable dyes with a negatively charged basic form often undergo an increase in pK_A' with respect to pK_A when they are embedded into non-charged immobilization matrices, while protonizable ones with a positively charged acidic form exhibit a decrease. That can be attributed to the more hydrophobic character of those matrices, compared to water so that charged species are destabilized with respect to uncharged ones. In charged matrices, particularly strong (de)stabilization effects and pK_A shifts can be expected.

pH Indicator Dyes

The reception mechanism of fluorescent pH indicator dyes includes reversible binding of the analyte. In other words, the equilibrium between a protonated (acidic) and a non-protonated (basic) form of the dye is shifted in the pH range close to pK_A' which causes an alteration of emission characteristics.
The receptor dye is of mayor importance for the performance of a pH sensor. It should essentially fulfil the requirements given in 2.2.2. Analyte affinity is expressed by pK_A or pK_A' and should match the pH range to be measured. In practice, that is often either physiological pH (7.4), pH in marine systems (7.5-8.5 [42]) or in biotechnological samples (around 6.5) so that a pK_A of 6-8.5 will be suitable for at least one important application. However, lower pK_A can

render the dye suitable to NH_3 sensing (2.2.6). For CO_2 sensing (2.2.5), values of 7-9 are most promising. pK_A values can be adjusted by the introduction of electron-donating (-OR, $-NR_2$) or -withdrawing groups (halogens, CN, carboxyl groups) into the molecule. If the indicator dye is immobilized into a matrix, pK_A is of course also affected by it.
Three indicator classes may be distinguished depending on whether the dye undergoes PPT or PET upon excitation or not (2.1.6). The receptor (functional group capable of protolysis) is not integrated into the chromophore in PET dyes, but it is still bound to it in some way in most cases (3.1.1).

PET-based pH Indicators (class A)

In case of PET, the fluorescence QY of the basic form is usually very low due to intramolecular PET so that fluorescence intensity decreases towards high pH values. In contrast to the other indicator types presented in the following, only QY is affected by analyte binding, while emission spectra maintain their shapes and absorption spectra remain unchanged or change very little. pK_A values measured in pH calibration based on fluorescence measurement are close or equal to those observable in the GS. Fluorescence intensity can virtually decrease to zero (the indicator is "switched off") in basic media, provided background is low and PET efficiency is high. Such a case is presented in 3.3.1.1. That implies potentially higher sensitivity for PET pH indicators than for the other classes yet to be discussed.
In principle, many dyes can be modified to become a PET pH indicator by attaching an amino moiety to them (that comes down to covalent linkage of the receptor). Some examples that can be found in the literature [56,57] are shown below. Indicator dyes based on PET will be discussed in more detail in section 3.1.1.

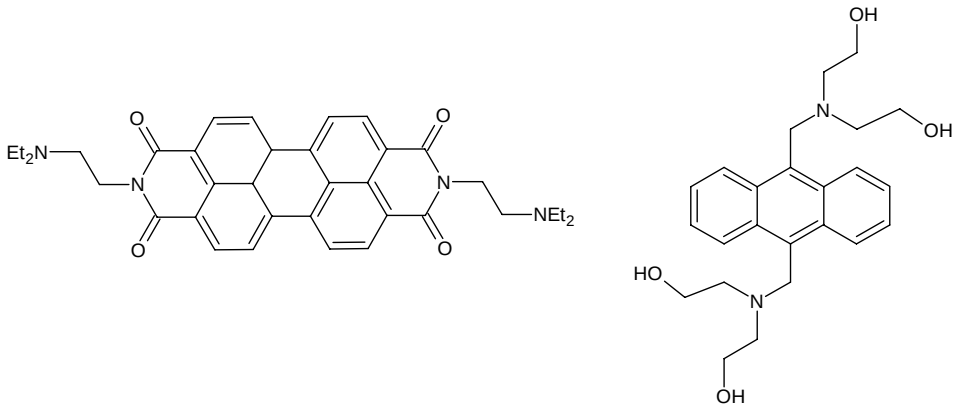

Figure 13: Structures of PET pH indicators presented in the literature, based on perylene (left, [57]) and anthracene (right, [56]) chromophores.

pH Indicators that undergo PPT (class B)

If PPT takes place (but no PET), the ES will be (de)protonated quickly hence only the emission of one form will be observed. In practice, that is mostly the basic form as most dyes that undergo PPT are more acidic in the ES than in the GS. Only excitation spectra are pH dependent, but not the emission spectra. The value of pK_A' measured in fluorescence calibration

can be very different to the pK_A known from the GS since the protonizable group is part of the excited chromophore [2]. Examples are shown below:

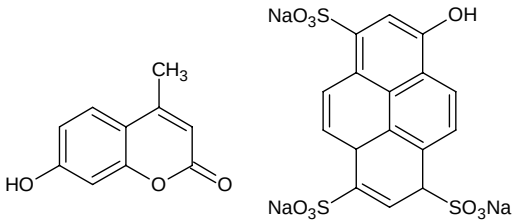

Figure 14: Structures of 7-hydroxy-4-methycoumarine, a.k.a. 4-methylumbelliferone (4-MU) (left) and HPTS, trisodium salt (right), pH sensitive dyes that undergo PPT and have been applied for pH sensing.

HPTS and its derivatives show good photostability and its pK_A of 6.3 is suitable to sensing in biotechnological samples. It has been applied for pH sensing in various materials [58,59].
Drawbacks are low excitation wavelength and high cross-sensitivity to ionic strength [54,60].
4-MU has been applied for intracellular pH sensing [61,62].

pH Indicators that undergo neither PET nor PPT (class C)

If neither PET nor PPT takes place, but acidic and basic form significantly differ in their spectral properties, absorption and both fluorescence emission and excitation spectra of the pH sensitive dye will be shifted depending on the pH. The fluorescence intensity observed can either increase or decrease when pH is increased, depending on fluorescence QY of both forms, excitation and observation wavelengths. Examples are fluorescein dyes, SNARF and SNAFL.
Fluoresceins are xanthenes dyes of long tradition. They are subject to various protolysis and lactonization equilibria, according to figure 15:

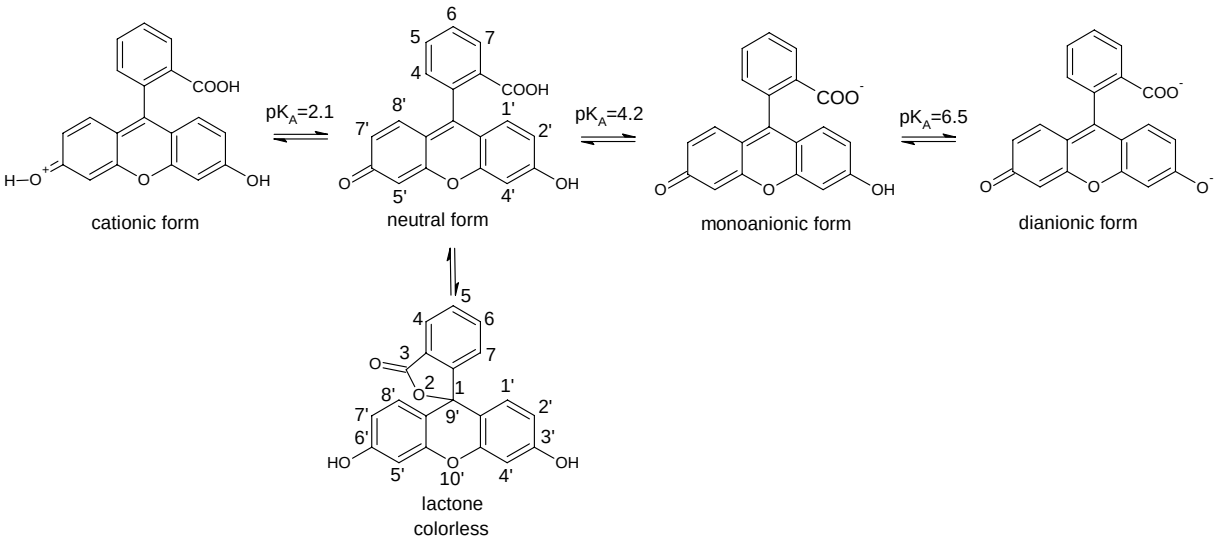

Figure 15: pH dependent protolysis and lactonization equilibria of fluorescein. Numbering is according to [40].

Lactonization mostly affects the neutral form and is often favourable in organic solvents, while it does not normally occur in aqueous solution at pH>5. The equilibrium between the monoanionic and the dianionic form is most relevant to pH sensitivity, although there is some sensitivity at lower pH too, corresponding to the other equilibria. The monoanion shows a hypsochromic and hypochromic shift, together with significantly lower quantum yield (about 0.4) than the dication (>0.9). Emission from the dianion is predominant even at lower pH, but emission is very weak in acidic aqueous solution [63]. In fluorescein derivatives ε is often $>70000 M^{-1}cm^{-1}$ and fluorescence QY is close to or higher than 0.9 for the basic form.
Esterification of the carboxy position prevents lactone formation and has been used for lipophilization. Chloro substituents have been attached to the chromophore to decrease pK_A which has been applied for NH_3 sensing [64]. Alkyl substituents, on the other hand, have been shown to cause an increase [40,42]. Carbonyloxy derivatized fluoresceins show a pK_A increased to the physiological range, allowing intracellular pH sensing [65]. Coupling to other (bio)molecules has been performed through the 5-position (5(6)-carboxyfluorescein, CBF and fluorescein-5-isothiocyanate, FITC), with a wide field of applications [66]. 2',7'-Substituents usually have little impact on spectral properties while 4',5'-substitution results in lower QY [40,58].
SNARF (seminaphtorhodafluor) and SNAFL (seminaphtofluorescein) dyes are more long-wave excitable pH indicators. They are structurally related to fluoresceins and rhodamines. In SNARF the basic form shows stronger fluorescence ($\lambda_{EM,MAX}$ around 630nm), in SNAFL the acidic one does ($\lambda_{EM,MAX}$ around 540nm). Many dyes of these classes feature advantageously higher Stokes shifts (50-90nm) than fluoresceins and pK_A values in aqueous solution are often found in the physiological range. Drawbacks lie in low fluorescence QY and more tedious synthetic routes towards them [67].

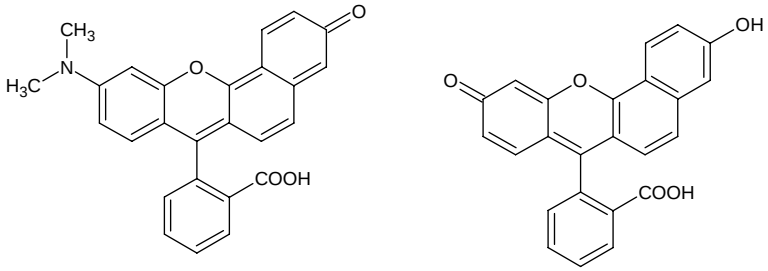

Figure 16: Structues of typical SNARF-1 and SNAFL-1, as denominated by Whitaker et al. [67].

Referencing and Calibration

Indicators of the classes B and C allow sensitivity enhancement by proper selection of excitation and observation wavelengths. That is not possible (and often not required, as sensitivity is high anyway) with class A since the basic form is not spectrally shifted.
Dual wavelength referencing (2.2.3) is frequently employed in pH sensors. In this regard, pH sensors exhibit the advantage that both acidic and basic forms are present at once. Hence one of them can be used for intrinsic dual wavelength referencing and no additional dye has to be used which simplifies sensor design [1,40]. That, as well, is not possible for class A, but extrinsic dual wavelength referencing can be performed. Alternatively, DLR referencing (2.2.3) can be carried out.

Dual wavelength referencing can be carried out in three ways. In double-excitation referencing, both acidic and basic form can be excited in their maxima and emission is detected at a single wavelength. That is possible for dye classes B and C and advantageously independent on dye concentration [40]. On the other hand, double-emission referencing is only possible if emission spectra are shifted (class C only). Double-excitation and double-emission referencing is also possible for class C. It yields higher intensities but is more complicated as it involves four wavelengths, excitation and emission maxima of both forms.
For calibration, fitting to the following equation is universally applicable:

$$pH = pK_A + log\frac{I - I_{HB}}{I_{B-} - I} \qquad \text{Equation 34}$$

I Measured fluorescence intensity as a function of pH
I_{HB}, I_{B-} Converging intensities at low/high pH

That corresponds to a sigmoidal curve with plateau intensities I_{HB} and I_{B-}.
In case of ratiometric measurement, the fit is also sigmoidal, according to the following equation:

$$pH = pK_A + log\frac{R - R_{HB}}{R_{B-} - R} + log\frac{I_{BH}}{I_{B-}} \qquad \text{Equation 35}$$

R Fluorescence intensity ratio $I_{\lambda1}/I_{\lambda2}$ measured at both excitation or at both emission wavelengths selected, depending on the type of ratiometric measurement
R_{HB} Ratio $I_{\lambda1}/I_{\lambda2}$ when only the acidic form is present
R_{B-} Ratio $I_{\lambda1}/I_{\lambda2}$ when only the basic form is present
I_{BH} Intensity $I_{\lambda2}$ when only the acidic form is present
I_{B-} Intensity $I_{\lambda2}$ when only the basic form is present

2.2.5 Luminescence Carbon Dioxide Sensors

The pH sensing concept can be extended to carbon dioxide sensing as CO_2 is an acidic molecule that reacts with H_2O under H^+-release. In a successful concept frequently applied [68,69], the basic, anionic form of the indicator dye is entrapped as an ion pair with a quarternary alkylammonium cation - most frequently tetraoctylammonium, TOA^+ - in an ethylcellulose matrix. TOA^+ stabilizes the charged species in a relatively hydrophobic environment. While H^+ is excluded from the matrix, CO_2 can permeate it, causing protonation of the dye and hence variations in the fluorescence signal. In that way, an essentially pH sensitive layer becomes sensitive to gaseous CO_2 without suffering from pH cross-sensitivity thanks to appropriate selection of matrix and filter. pK_A' of the pH indicator when incorporated into the matrix should be situated between 7 and 9, depending on the analyte concentration range focussed. The dynamic range of a CO_2 sensor is influenced by the indicator dye, the immobilization matrix and the additive (TOA^+ or its tetrabutyl analogue TBA^+). HPTS is an example for a pH indicator that has been employed for CO_2 sensing [68].

$$TOA^+Ind^- + CO_2 + H_2O \rightarrow HInd + TOA^+HCO_3^-$$ Equation 36

Compared to the "Severinghaus" concept [70], where a pH sensitive layer is soaked with bicarbonate buffer, this approach allows better response times and drift stability.

2.2.6 Luminescence Ammonia Sensors

pH indicators can also be adapted to sensing of NH_3 which is a basic gas that reacts with water under proton consumption. Similarly to the concept described in 2.2.5, the indicator is embedded into a gas-permeable membrane and NH_3 is extracted from the aqueous sample into it.

$$NH_3 + HInd \rightarrow NH_4^+ + Ind^-$$ Equation 37

This equilibrium is affected by the protolysis of ammonia (pK_A=9.24) and its distribution between the (usually aqueous) sample and the immobilization matrix. Because sensitivity is governed by the equilibrium constant corresponding to equation 37, indicators with low pK_A' values promise the highest sensitivity. On the other hand, higher pK_A values are desirable in the higher concentration range since too high sensitivity disables indicator response there. Examples for indicator dyes utilized are esters of 2',7'-dichlorofluorescein (pK_A=4.8) and eosin (pK_A=3.8). Cellulose esters have been used as immobilization matrices [64,71].

2.2.7 Luminesence Ion Sensors

Ion sensing is a complex investigative field with a wide variety of applications. Here, only some of the most important concepts will be briefly discussed, with special interest to the application of pH indicators.
Fluorophores carrying chelating/complexing receptors are called fluoroionophores. They can exhibit ion sensitivity owing to variations in luminescence properties over several mechanisms. Some of them are described in the following. If the receptor is properly chosen, high selectivity is possible. Receptors are mostly covalently attached to the fluorophore (with or without a spacer) and can be crowns, cryptands, calixarenes, chelators etc.
Many cation indicators based on PET and employing complexing receptors have been developed. That will be discussed in 3.1.1. Another class of indicators takes advantage of PCT (photoinduced charge transfer, 2.1.8) effects in push-pull chromphores. As with PET indicators, complexing receptors are employed. Often, the electron-donating group is placed near or integrated into them. The electrostatic influence of the cation has a strong influence on the dipole moments in GS and ES and provokes a hypochromic and hypsochromic spectral shift. On the other hand, if the cation is entrapped near the electron-acceptor, a bathochromic shift can be expected. Some concepts that have been presented are Ca^{2+}-sensitive stilbene derivatives with crown receptors [72] and coumarine dyes linked to crown receptors [73]. Fluorescence QY and lifetimes may also be affected in different ways. Fluorescence may be strongly quenched [74] or enhanced [75] upon cation binding. That can, but does not necessarily have to be related to electrostatic effects.

Another approach towards cation sensing includes co-immobilization of a deprotonizable pH indicator and an ionophore into a hydrophobic PVC matrix. When the target cation is extracted into the matrix and bound to the ionophore, the indicator is deprotonated for charge balance reasons. An example employing absorption transduction can be found in [76].
Anion sensors based on dynamic luminescence quenching by halogenide anions have been designed [77]. Other approaches employ anion complexing receptors (ionophores). The anionic, basic form of a lipophilic pH indicator is bound to a lipophilic, cationic or neutral ionophore and both are immobilized in a hydrophobic matrix. When an anion migrates into the matrix, forming an ion pair with the ionophore, H^+ is co-extracted and binds to the indicator [78]. The pH indicator is not required if the ionophore itself is luminescent and sensitive to the anion. This principle can be applied to other anions than halogenides too.

2.2.8 Luminescence Oxygen Sensors

Molecular oxygen is by far the most common dynamic quencher. That is mainly because its GS is of triplet multiplicity and relatively high transition energies ΔE can be passed to oxygen, creating excited singlet oxygen. Dynamic quenching can be caused by any species that features triplet GS, but those are rare. The most important ones apart from oxygen are SO_2 and nitrous oxides such as NO and NO_2. This fact, of course, naturally decreases the number of possible cross-sensitivities and makes is easier to design a selective oxygen optrode.
According to the Stern-Volmer equation (equations 14,15, section 2.1.6), quenching efficiency increases with the ES lifetime (τ) of a luminophore. As a consequence, phosphorescent dyes offer suitable sensitivities. τ is in the μs or ms range for them, compared to ns lifetimes of fluorescent dyes. They also allow measuring luminescence decay time (2.1.9). In practice, phosphorescent oxygen indicators are embedded into (usually hydrophobic) matrices. Sensitivity depends on both τ of the indicator and oxygen permeability of the matrix. The latter is affected by oxygen solubility and its diffusion coefficient. Sensitivity of a sensor can be adjusted over τ of the indicator and over the matrix in order to match the desired range of oxygen concentration.
Oxygen indicator dyes are almost exclusively heavy metal complexes with ligands capable of luminescence which are phosphorescent due to spin-orbit coupling (2.1.5). One of the first dyes investigated was tris(4,7-diphenyl- 1,l0-phenanthroline)ruthenium(II), $[Ru(Ph_2phen)]^{2+}$ [79]. Nowadays, probably the most common dye class are complexes of Pd(II) or Pt(II) with porphyrin derivatives [3,4,41,80]. Those are long-wave excitable and derivatives with different λ_{MAX} and τ can be prepared for different applications, to state only a few features of this interesting dye class. Cyclometallated Ir(III)-coumarin complexes presented recently are mentionable due to their high brightness [81].
The Stern-Volmer model is based upon the simplification that all dye molecules are equally accessible to dynamic quenching. That may be a good approximation for dilute solutions, but if the indicator is immobilized, quenching is affected by the structure of the solid, bulk-surface interactions etc. Therefore, for dynamic quenching in sensors, a downward curvature of the Stern-Volmer calibration plot is frequently observed because there is a distribution of K_{SV} deriving from micro-heterogeneity of the matrix. A model that pays attention to variable

quenching accessibility was proposed by Carraway et al. [82]. It is assumed that two different dyes are present:

$$\frac{\tau_0}{\tau} = \frac{1}{\frac{f_1}{1+[O_2]K_{SV1}} + \frac{1-f_1}{1+[O_2]K_{SV2}}} \qquad \text{Equation 38}$$

τ	Luminescence lifetime as a function of oxygen concentration (s)
τ_0	Luminescence lifetime in the absence of oxygen (s)
$[0_2]$	Oxygen concentration (M) or partial pressure (mbar)
$K_{SV1,2}$	Stern-Volmer constants of both dyes present according to the model (M^{-1} or $mbar^{-1}$)
f_1	Relative fraction of one dye, according to the model

2.3 Magentic Optical Sensor Particles (MOSePs)

The most common sensor design principles are sensitive layers and fibre optical sensors. Although such sensors feature good versatility and robustness, they are subject to limitations in some applications which arise above all from their dimensions. Those include poor applicability in microfluidic systems, in microscopy or for intracellular sensing. Monitoring of fast processes (enzymatic reactions etc.) becomes impossible if response time is too long due to diffusion limitation. Dissolved indicators do not suffer from such limitations, but they often possess low sensitivity and selectivity and are restricted to dyes soluble in the sensing media (mostly water). Also, cross-sensitivities and unspecific interactions are more critical because of the absence of a filter component. Toxicity is problematic in physiological applications.
Optical nano-sensors offer the possibility of combining the advantages of sensors and dissolved indicators, employing a nano-sized immobilization matrix. They are equally flexible to dissolved indicators [83] but still provide a protective layer. Although miniaturization of fibre optic sensors is possible, such miniaturized systems are often expensive and difficult to handle. On the other hand, nano-particles have attracted increasing interest within the recent years.
Some remarkable work was done by Kopelman et al. [84-86]. So-called PEBBLEs (probes encapsulated by biologically localized embedding) were shown to be genuine sensors, i.e. the sensitive component is embedded into an immobilization matrix and thus fully separated from its environment. Their size is negligible compared to a living cell. Acrylamide-based PEBBLEs designed for intracellular sensing of oxygen, pH and Ca^{2+} [85] were presented and several methods for delivery into the cell were proposed [84]. The concept was extended to include other hydrophilic polymer matrices and analytes [86,87].
By now, a large number of novel sensing concepts based on particles have been presented. Some important examples are functionalized gold nano-particles [88], sensors based on quantum dots [89] and multifunctional core-shell systems [90]. While for some applications (intracellular etc.), only nano-particles are useful, others do not require such a high degree of miniaturization and micro-particles can be applied with equal success. Those are more easily collected by sedimentation or magnetic separation (see below). Different synthetic routes are available towards differently sized particles.

In practice, macroscopic sensing devices are often too bulky and expensive for (bio)process monitoring, screening applications and microfluidic or high-throughput systems. Sensor spots with external readout are more convenient, but they have to be pre-immobilized in a defined position and their replacement is usually cumbersome. Nano- and micro-particles can help to provide novel strategies in sensor design. Magnetic optical sensor particles (MOSePs) are particularly interesting in this regard because they are easy to control and manipulate over an external magnetic field. By magnetic collection, they can be moved externally and the sensor does not need to be geometrically designed in advance. Senor spot formation can be carried out at any time and non-invasively (in-situ spot formation). MOSePs can also form a spot in almost any place, are introduced as easily as dissolved indicators, removed by magnetic separation and recycled. An external collection system integrating an optical fibre for data readout has been presented recently [91]. Especially in medical applications, MOSePs could be suitable to several future applications owing to their remote controllability. Examples are drug targeting or photodynamic therapy.

2.4 Polymerization

This chapter is based on references [92,93]. Other references will be cited independently. Polymer chemistry is a very extensive investigative field, and only the aspects of mayor relevance to this thesis will be briefly outlined in this section.

According to IUPAC's definition (1996), a polymer molecule is "A molecule of high relative molecular mass, the structure of which essentially comprises the multiple repetition of units derived, actually or conceptually, from molecules of low relative molecular mass" [94]. It is often associated with the consecutive, uniform iteration of a certain chemical reaction (poly-reaction, polymerization) between monomer units.

Radical poly-addition of C=C double bonds is the only polymerization reaction of great interest to this work, although many other reaction types (cationic, anionic, condensation, metathesis polymerization) or functional groups can undergo polymerization as well. Many monomers of common importance can be classified as derivates of ethylene. This includes acrylates, which are derivatives of acrylic acid or 2-methylacrylic acid. Most acrylates readily undergo radical polymerization.

Homopolymerization of one monomer is distinguished from copolymerization whereupon various different monomers are polymerized to form a polymer that consists of different subunits. Polymers formed by polymerization of monofunctional monomers are mostly linear or somewhat branched, while copolymerization with a di- or polyfunctional monomer yields more or less cross-linked polymers, depending on the cross-linker ratio. Cross-linked polymers are known to become increasingly insoluble in any solvent as the degree of cross-inking increases. Moderately cross-linked ones may be swellable, while highly cross-linked ones are not even capable of swelling.

2.4.1 Course of a Radical Chain Polymerization

A radical polymerization is started by the generation of radicals. Most frequently, chemical initiators are added. They are thermally decayed to form radicals (initiation reaction) so that polymerization is started by heat. α,α'-azoisobutyronitrile, AIBN, is often used in organic solvents, while $K_2S_2O_8$ is useful for aqueous systems. The initiator radical adds to a C=C double bond to form a monomer radical. That radical can add to other C=C units so that a radical chain reaction is initiated (propagation reaction). The propagation reaction is in concurrence to termination reactions with other polymer radicals, initiator or solvent radicals. Reactions with other polymer radicals include radical recombination, by which the molecular weight of the chain formed is doubled, and disproportion, where molecular weight remains constant. Chain transfer reactions, upon which the radical functionality is transferred to another species (solvent, another polymer chain or another part of the growing polymer chain itself), are also possible. The molecular weight of the polymer obtained depends on the probability of chain transfer and termination reactions. Therefore it will be higher if polymerization is carried out in a solvent that hardly undergoes chain transfer reactions. On the other hand, substances that easily form radicals (like thiols, RSH) can be added to keep the polymer chain short. Also, low initiator concentration leads to longer polymer chains. Because O_2 quickly destroys radicals oxidatively, radical polymerizations have to be carried out in deoxygenated systems.

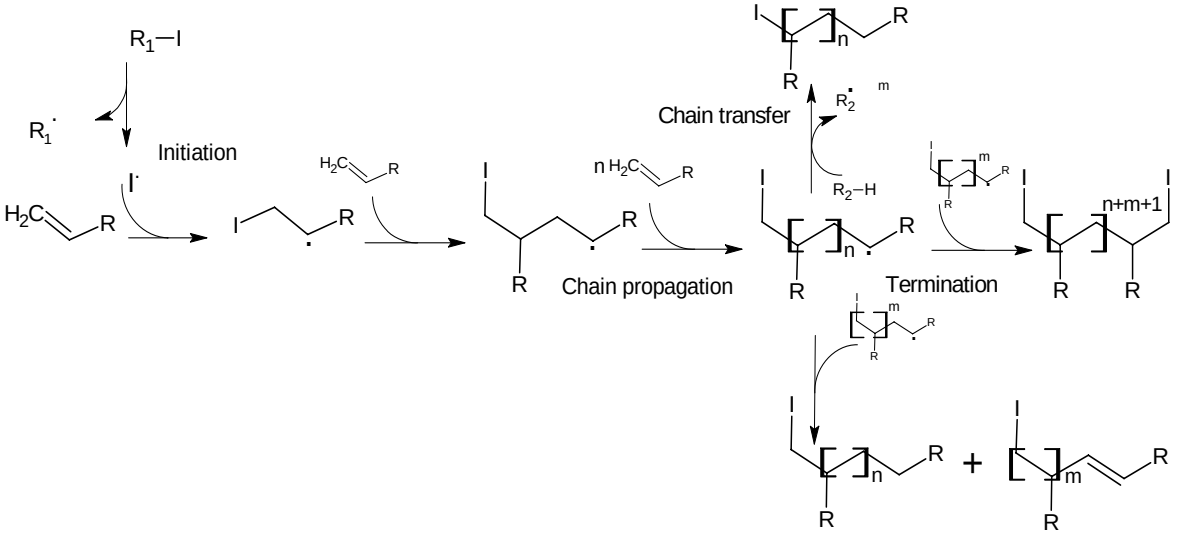

Figure 17: Simplified outline of the course of a radical chain polymerization.

Polymerization velocity in terms of polymerization rate r_P can be expressed by:

$$r_P = -\frac{d[M]}{dt} = k_P[M]\left(\frac{r_i}{2k_T}\right)^{1/2} \qquad \text{Equation 39}$$

r_P	Rate constant of polymerization (Ms^{-1})
[M]	Monomer concentration (M)
t	Time (s)
k_P	Rate constant for propagation
r_i	Rate of initiation reaction
k_T	Rate constant for termination

Because the initiation reaction is usually monomolecular, one consequence of equation 39 is that polymerization rate will increase with the square root of initiator concentration.

2.4.2 Polymerization Media

Polymerization can be carried out in solution, in substance, in suspension or in emulsion. Polymerization in solution is simple, but the molecular weight obtained is limited by chain-transfer reactions involving the solvent. If the polymer is insoluble, precipitation polymerization is present. On the other hand, polymerization in substance can yield higher molecular weight, but problems may arise from increasing viscosity at high conversions, as monomers are immobilized. That limits polymerization yield and causes monomer impurities. Moreover, the reaction heat is hard to be dissipated. Suspension polymerization takes place in monomer droplets stabilized by colloids ($CaSO_4$, $BaSO_4$ etc.). In emulsion polymerization, smaller droplets (1-100µm, compared to 50-500µm for suspension polymerization) are stabilized by a surfactant such as sodium dodecyl sulfate. In both suspension and emulsion polymerization, water is most frequently employed as the continuous phase. Hydrophilic monomers can also be dispersed - with or without being dissolved in water - in a hydrophobic organic solvent ("inverse" or "water in oil" suspension/emulsion polymerization).

2.4.3 Copolymerization

When a mixture of monomers is polymerized, the composition of the resulting copolymer is determined by polymerization kinetics. Kinetics cannot be compared to those of each monomer alone (homopolymerization), but every copolymerization system has its own kinetics. In the simplest case, copolymerization involves two monomers M_1 and M_2. Then, four propagation reactions of the polymer chain P are possible:

R_{11}:	$P\text{-}M_1 + M_1 \rightarrow P\text{-}M_1\text{-}M_1$	with the rate constant k_{11}	Equation 40a
R_{12}:	$P\text{-}M_1 + M_2 \rightarrow P\text{-}M_1\text{-}M_2$	with the rate constant k_{12}	Equation 40b
R_{11}:	$P\text{-}M_2 + M_1 \rightarrow P\text{-}M_2\text{-}M_1$	with the rate constant k_{21}	Equation 40c
R_{11}:	$P\text{-}M_2 + M_2 \rightarrow P\text{-}M_2\text{-}M_2$	with the rate constant k_{22}	Equation 40d

The following monomer reactivity ratios are then of great importance:

$$r_1 = k_{11}/k_{12} \qquad \text{Equation 41a}$$

$$r_2 = k_{22}/k_{21} \qquad \text{Equation 41b}$$

r_1 and r_2 quantify the probability that a polymeric chain terminated by a monomer M_1 or M_2 will react with a like monomer, rather than with an unlike one.
If one supposes that $k_{12}=k_{21}$ (both cross reactions are equally probable), the ratio of the rates at which both monomers enter the copolymer, which is equal to the relative composition of the polymer, is:

$$\frac{d[M_1]}{d[M_2]} = \frac{[M_1](r_1[M_1]+[M_2])}{[M_2](r_2[M_2]+[M_1])}$$ Equation 42

$d[M_1]/d[M_1]$	Relative composition of the polymer formed
$[M_1]$, $[M_2]$	Concentrations of the monomers M_1 and M_2 (M)
r_1, r_2	Monomer reactivity ratios of M_1 and M_2

or equivalently:

$$F_1 = \frac{r_1 f_1^2 + f_1 f_2}{r_1 f_1^2 + 2 f_1 f_2 + r_2 f_2^2}$$ Equation 43

Where f_1 and f_2 are the relative ratios of M_1 and M_2 in the reaction mixture:

$$f_1 = 1 - f_2 = 1 - \xi_1 = \frac{[M_1]}{[M_1]+[M_2]}$$ Equation 44

F_1	Ratio of M_1 in the polymer formed
$f_{1,2}$	Relative ratios of M_1 and M_2 in the reaction mixture
ξ_1	Conversion in M_1

Equation 42 and 43 also indicate the composition of a polymer formed in a continuous reactor if monomer concentrations are kept constant at all time. In a batch reactor, polymer composition depends on conversion since the reaction mixture will enrich in the component consumed more slowly. The evolution of polymer composition with conversion is then of great interest. Integration of monomer balance equations yields the following relation:

$$\xi = 1 - \left[\frac{f_1}{(f_1)_0}\right]^{\frac{r_2}{1-r_2}} \left[\frac{f_2}{(f_2)_0}\right]^{\frac{r_1}{1-r_1}} \left[\frac{(f_1)_0 - \left((1-r_2)/(2-r_1-r_2)\right)}{f_1 - \left((1-r_2)/(2-r_1-r_2)\right)}\right]^{\frac{1-r_1 r_2}{(1-r_1)(1-r_2)}}$$ Equation 45

ξ	Overall conversion
$f_{1,2}$	Relative ratios of M_1 and M_2 in the reaction mixture
$(f_{1,2})_0$	Initial relative ratios of M_1 and M_2 in the reaction mixture (when ξ=0)
r_1, r_2	Monomer reactivity ratios of M_1 and M_2

Semiquantitatively, it can be stated that the polymer formed under batch conditions will be richer in M_1 than the feed at low conversions if $r_1 > r_2$ and vice versa. At higher conversions, the reactor will enrich in M_2 and so will the polymer formed then.
The parameters k_1 and k_2, and consequently, the polymer composition calculated from them, are normally more or less independent on the composition of the environment (concentration of species like solvent, initiator, etc.). Parameters taken from the literature can thus be used to estimate the composition of many copolymers. However, stronger deviations might occur if, for instance, polymerization is carried out in dispersion since kinetics depend on the distribution of the monomers between the continuous and the disperse phase. If r-values are un-

known, they can be determined in accordance with equation 43 by investigating the tion of copolymers formed in a batch reactor at low conversion.
Depending on the values of r_1 and r_2, several copolymerization systems can be distinguished:

Ideal Copolymerization ($r_1r_2 = 1$)

In this case, the relative probability of chain propagation with M_1 is always the same, regardless of which monomer is at the end of the growing polymer chain (ideal behaviour). If $r_1 = r_2 = 1$, the copolymerization is perfectly statistic. If $r_1 > 1$ and $r_2 < 1$, the ratio of M_2 in the polymer is smaller than the one in the monomer mixture. A polymer rich in M_2 can only be obtained with a large excess. If $r_1 \gg r_2$ (extreme ideal behaviour) it might even be difficult to insert M_2 into the polymer at all. Copolymerization behaviour is often visualized in copolymerization diagrams where the composition of the polymer is correlated to the one of the monomer mixture it is prepared from:

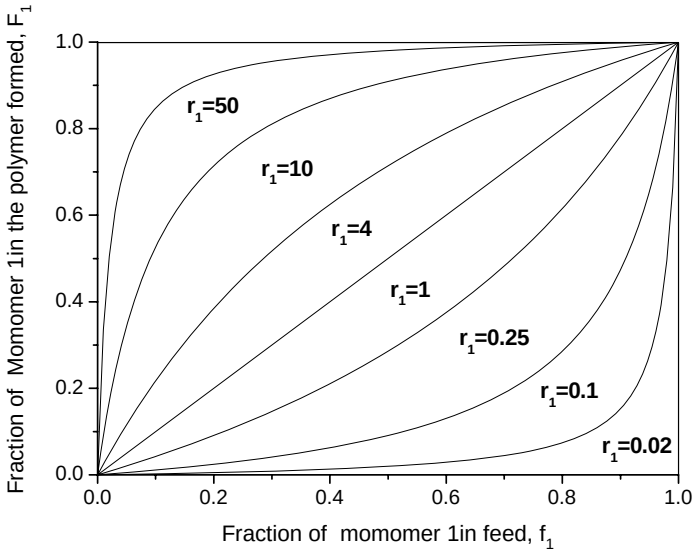

Figure 18: Copolymerization diagram for ideal copolymerizations ($r_1r_2 = 1$). The polymer is richer in M_1 than the monomer mixture (feed) if $r_1>r_2$ and vice versa.

In batch polymerization, where f_1 depends on conversion, diagrams of this type only indicate the composition of the polymer initially formed. Time-dependent behaviour of batch polymerizations can be predicted employing equation 45. An example is shown in 3.3.2.1.

Alternating Copolymerization ($r_1, r_2 < 1$, $r_1r_2 \sim 0$)

This involves a tendency towards an alternating monomer sequence, such as $M_1M_2M_1M_2M_1M_2$…. Alternation becomes the stricter the smaller r-values are. If $r_1 = 0$, M_1 might even be impossible to homo-polymerize. If $r_1 = r_2 = 0$ (extreme alternating behviour), chain propagation is strictly alternating, while short blocks can be formed if $r_1 \neq 0$ and/or $r_2 \neq 0$ (moderate alternating behviour). An example for this behaviour is the polymerization of

styrene and maleic anhydride (MA) to yield PSMA. In that case, r_2 is close to 0 (for MA = M_2) and it is very difficult to obtain a polymer richer in MA than 50%.

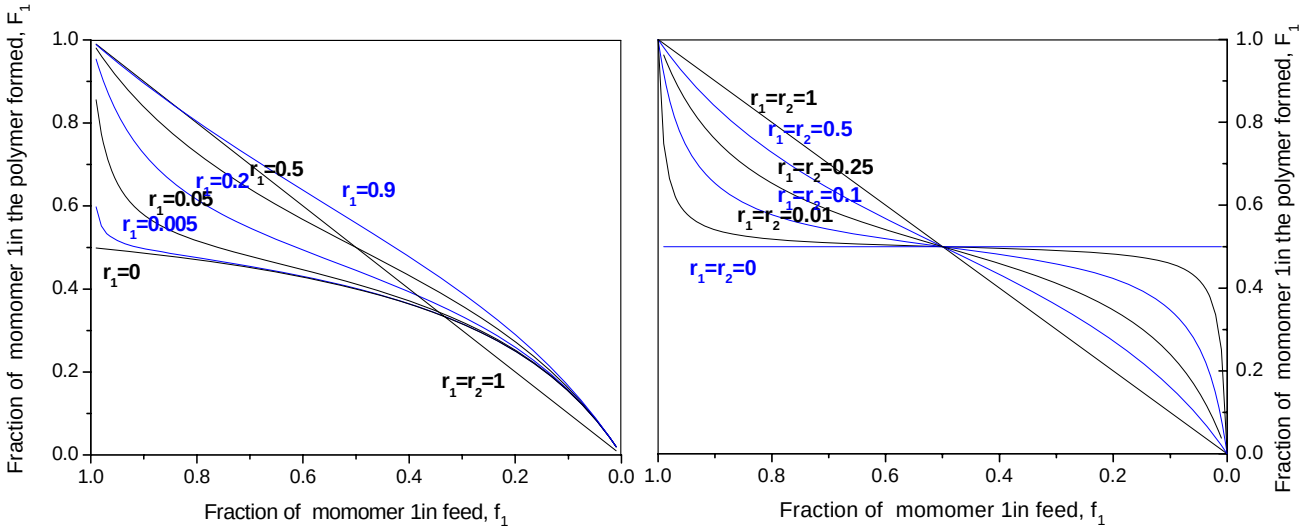

Figure 19: Copolymerization diagram for alternating copolymerizations (r_1, r_2 < 1, r_1r_2 ~ 0) where r_2 = 0.5 (left) and r_2 = r_1 (right). It is shown that those systems tend to an alternating monomer sequence and thus stick to the line F_1=F_2=0.5 which corresponds to a strictly alternating sequence, above all when and r_1 and/or r_2 become very small.

An interesting situation is available in the intersection of any plot in figure 19 with the curve $r_1 = r_2 = 1$. Then, the composition of the polymer formed is equal to the monomer ratio present in the reaction mixture, and in a batch reactor, polymer composition is independent on conversion. This is called azeotropic copolymerization.

.

Block Copolymerization Case 1 ($r_1 > 1 > r_2$ but $r_1r_2 \neq 1$)

This entails the formation of a polymer rich in M_1. In batch systems, the M_2 ratio in the polymer will increase towards the end of polymerization. In extreme cases, a block-copolymer of M_1 is formed and another one of M_2 is attached to it once all M_1 has been consumed (though in practice, the M_2 copolymer might not be formed if k_{22} is very low). These systems are in principle adequate for the synthesis of block copolymers with two blocks, but they are not found very frequently.

Block Copolymerization case 2 (r_1, r_2 > 1)

For this situation, which is actually rare, a sequence of homopolymer blocks within the polymer chain is typical, such as $M_1M_1M_1M_2M_2M_2M_1M_1M_1$. Blocks become longer as r_1 and r_2 become higher and if both are very high, a mixture of homopolymerized macromolecules or a polymer with two blocks (case 1) will be formed.

Experimental data with ideal and alternating copolymerization diagrams have been published by Mayo and Walling [95].

If more than two monomers are involved, copolymerization obeys the same principles, but its mathematical treatment is more complicated. As a conclusion, it should be emphasized that not all monomers can be copolymerized and copolymer composition can vary considerably depending on relative reactivity ratios of the system and conversion of a batch reactor. Kinetic data from the literature cannot perfectly predict the behaviour of a "real" system, but it helps to estimate possible trends and results.

2.4.4 Miniemulsion and Microemulsion Polymerization

Dispersion polymerization can yield polymeric particles the size distribution of which is determined by (but not necessarily equal to) the one of the dispersed droplets in polymerization. Emulsion polymerization has been shown to be valuable for the preparation of fluorescent nansensors [84].
While common emulsion polymerization yields micro-particles, nano-sized polymer particles can be obtained by means of miniemulsion polymerization. Monomer droplets of such small size (30-200nm when ionic surfactants are used) are created by high shear which in laboratory scale processes is usually performed employing an ultrasonic unit. In that way a miniemulsion is prepared from a continuous and a disperse component together with a surfactant, such as sodium dodecyl sulfate (SDS). The continuous phase is water, or a highly hydrophobic organic solvent in the case of inverse miniemulsion. Once the miniemulsion has been prepared, it can be used to perform polymerization within the nano-droplets so that polymerization directly yields nano-particles, but also to prepare particles from a bulk polymer solution.
Microemulsion requires higher surfactant concentrations (in the range of 5-10%) and the employment of a co-surfactant of lower molecular weight, for example SDS with PeOH as co-surfactant. Microemulsion in principle can be used for the same purposes as miniemulsion without requiring any shear, but practical realization can be difficult.

2.4.5 Hydrogels

Hydrogel is a general term for hydrophilic, but water-insoluble polymers. They are swellable with water and can take up as much as 90% of it, but cross-linking prevents them from being dissolved. Synthetic hydrogels are based on poly(meth)acrylic acid, poly(meth)acrylamide, polyvinylpyrrolidone, polyurethanes or polyvinyl alcohol. Cross-linked polyacrylates are useful in bioscience (gels for electrophoresis). Hydrogels have been used as hydrophilic immobilization matrices in luminescence pH sensors [40,53,96].

2.5 Dynamic Light Scattering (DLS)

Size and size distribution of nano-particles and macromolecules in suspension, emulsion and solution can be studied by DLS. Essentially, the velocity of the Brownian motion is measured and correlated to particle size. That random, diffusive motion is caused by collisions of the particle with solvent molecules. As its velocity also depends on temperature and viscosity of the media, they need to be known and kept constant.

$$d = \frac{kT}{3\pi\eta D}$$ Equation 46

d Hydrodynamic diameter of the object to be measured (m)
η Dynamic viscosity of the media ($kgm^{-1}s^{-1}$)
D Translational diffusion coefficient of the object to be measured (m^2s^{-1})
k Boltzmann constant ($1{,}38065*10^{-23}$ JK^{-1})
T. Temperature (K)

DLS is an indirect method providing information about the hydrodynamic radius of a particle which can be associated with the diameter of a sphere that would diffuse at the same speed as the particle to be measured. The hydrodynamic radius of a particle is not only affected by its total volume but also by its shape, surface properties and by the surrounding medium.
Light emitted by a He/Ne-Laser is scattered by the particles in the sample. The measured intensity depends on the observation angle as scattering on various objects can result in constructive or destructive interference, depending on size and position of scattering objects. Because of the Brownian motion, intensity will also change over time and the rate of intensity change will depend on diffusion rate of the particles.
Time dependence of the measured intensity is converted into a correlation function G(τ) by a digital correlator, a device which automatically evaluates intensity data. G(τ) compares two points in time with a delay time τ, yielding a value of 1 when both signals are identical and 0 when there is absolutely no relation between them. When τ increases, the measured intensities become less similar until there is no similarity left and the relative intensities have become totally random. This corresponds to a decrease in the value of G(τ). The bigger the measured particles are, the longer will be the time τ at which the similarity between two compared signals begins to decrease. On the other hand, the more monodisperse the sample is, the steeper is the decrease in G(τ). Consequently, information about both average size and size distribution are available from the correlation function.
An example for a correlation function is:

$$G(\tau) = A[1 + Be^{-2\Gamma\tau}]$$ Equation47a

where

$$\Gamma = D\left(\frac{4\pi n}{\lambda_0} sin\left(\frac{\theta}{2}\right)\right)^2$$ Equation47b

A Baseline of the correlation function
B Intercept of the correlation function
τ Time between two measurement points compared (s)
D Translational diffusion coefficient of the object to be measured (m^2s^{-1})
n Refractive index of the dispersant
λ_0 Wavelength emitted by the light source (m)
θ Scattering angle

Equation 47 is valid for perfectly monodisperse samples; the correlation function for polydisperse samples can be calculated as follows:

$$G(\tau) = A[1 + B[g(\tau)]^2] \qquad \text{Equation48}$$

where g(τ) is the sum of the individual correlation functions for all particle sizes involved.

Determination of Particle Size Distribution

A typical correlation function is shown below:

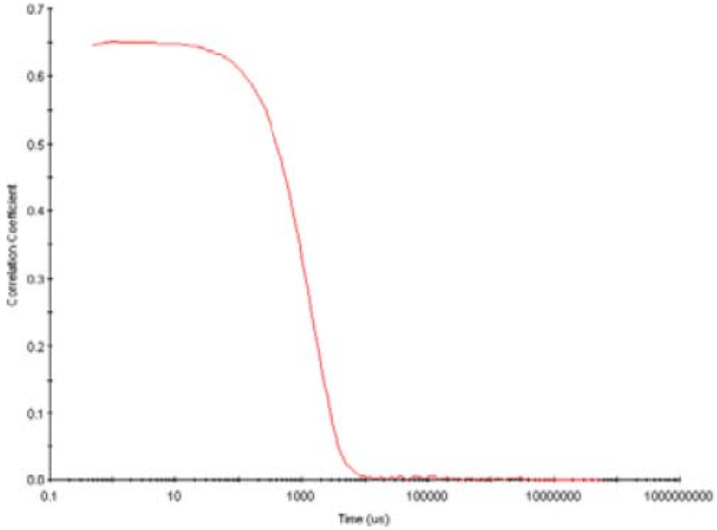

Figure 20: Typical correlation function in DLS, taken from [97].

The diffusion coefficient D is then calculated by approximation of the correlation function and leads to the particle diameter d, according to equation 46. Intensity distribution over time has now been converted to intensity distribution over particle diameter. Such a distribution is illustrated in figures 74 and 76. Polydispersity indices (PDIs) are calculated over a linear approximation of the inflection area and will increase as the slope of the obtained line decreases.

Determination of Zeta Potential

Particles in suspension usually develop a certain surface charge, either due to the presence of charged functional groups or by adsorption of charged species. As a result, an electrical double layer with opposite charge is formed. The charge density of that layer will decrease from the particle surface to the bulk of the dispersant until its potential is equal to the one of bulk. The zeta potential is the potential at the slipping plane, the spherical layer that separates fluid attached to the surface from freely mobile fluid. This is visualized below:

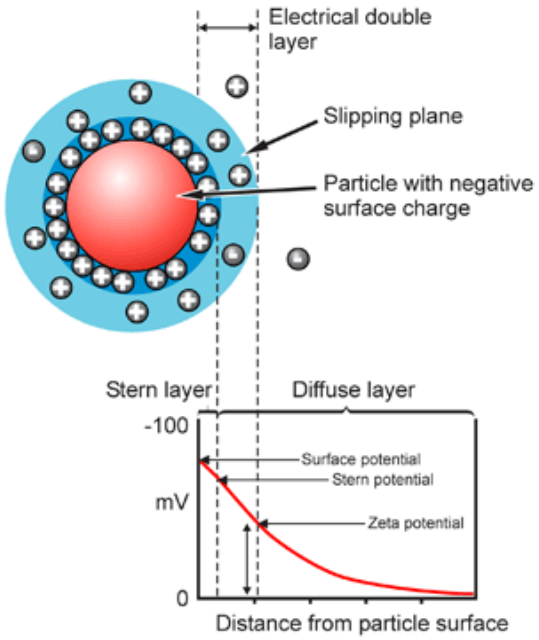

Figure 21: Schematic illustration of the zeta potential, taken from [97].

A high zeta potential correlates to a high surface charge of the same sign. That also implies high aggregation stability since particles of high, equal charge will repulse each other. Zeta potential can be measured by DLS, correlating it to the migration rate in an electric field. In practice, that is performed by placing a sample into a cuvette equipped with electric poles and applying AC voltage. The zeta potential of the particles is proportional to their migration rate. The latter can be determined by means of the so-called laser Doppler anemometry technique. An incident beam of laser light is subject to a phase shift which is measured and correlated to particle migration rate using Smoluchowski or Huckel theory.

3 Practical Part

3.1 Introduction

Aim of this thesis is the preparation new pH indicator dyes with the following properties:

- Feature pH sensitivity through PET effect, which is to be accomplished by introducing an amino moiety into a fluorescent molecule. That molecule should preferably not be intrinsically pH sensitive as various protonation steps complicate calibration.
- Long-wave excitation and emission.
- Contain a functionality through which covalent coupling can be accomplished (like. COOH, NH_2 etc.), or alternatively, be sufficiently lipophilic for the preparation of leaching-free sensors by physical entrapment.

Although the presence of the PET quenching mechanism is not necessarily a prerequisite to all approaches focussed in this work, the goal is here to prepare novel pH indicators based on chromophores that have not been extensively applied for pH sensing (like those shown in classes B and C, section 2.2.4) but feature advantages over pH indicators already well-known. Obviously, PET is a very promising route towards that because it offers modularity (3.1.1). Figure 22 below visualizes how an indicator dye can be designed, assembling different modules.

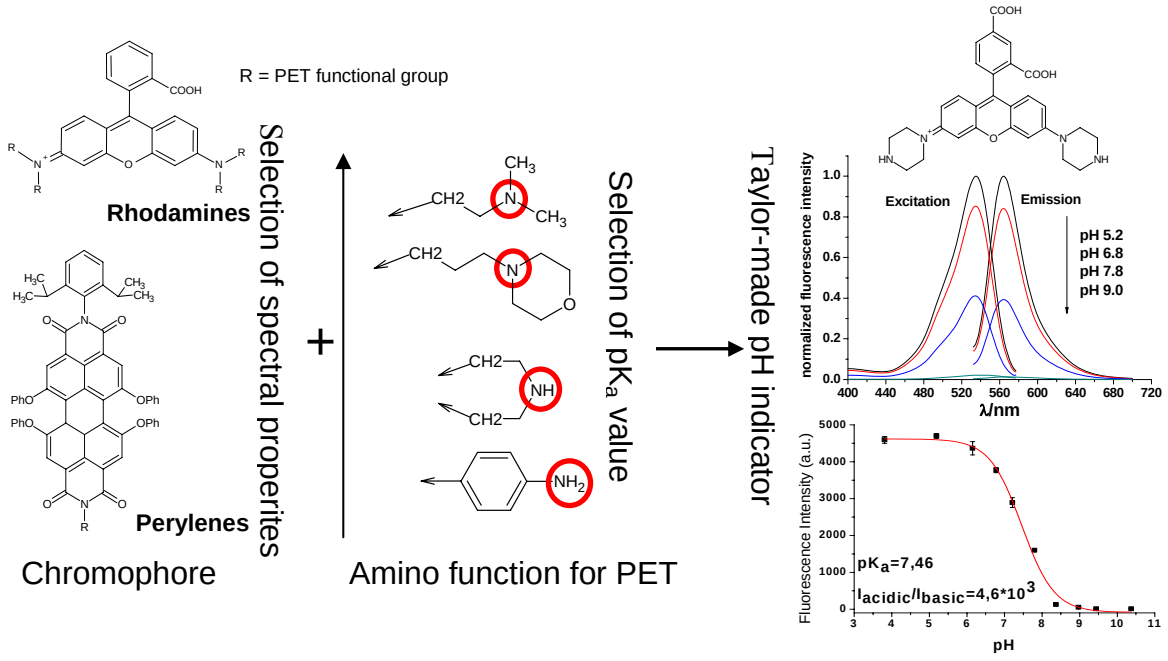

Figure 22: Schematic visualization of how a novel pH indicator is designed and its properties are tuned by assembling different, selected modules

Of course, the indicators should also match the requirements to indicator dyes stated in 2.2.2 and 2.2.4, most importantly good brightness, (photo)stability and an appropriate pK_A in solution or a matrix useful for pH sensing. For the preparation of pH sensors, physical entrapment in polyurethane-based hydrogel matrices has been chosen as a straightforward concept. Secondly, covalent coupling to magnetic optical sensor particles is tackled. For that, dyes are planned to be functionalized with a carboxy group for coupling. Magnetic particles are amino-functionalized by covering them with a cross-linked acrylate shell including a monomer carrying amino groups. Coupling is performed with EDC/sulfo-NHS, a system established for coupling of biomolecules [66]. This process explained in more detail in 3.1.5.

3.1.1 PET-based Fluorescence Indicators

Electron transfer involving excited fluorophores has already been reported by A.Weller in the 1960s [98], there also considering association between the products of equation 16 or 17 (2.1.6). Such an exciplex formation results in bathochromic emission shifts of aromatic hydrocarbons and is observed in particular in apolar solvents.
The thermodynamic driving force is for reductive PET (without exciplex formation):

$$\Delta G_{Q,PET} = E(D/D^+) - E(A^-/A) - \Delta E(A) - \frac{e_0^2}{\varepsilon a} \qquad \text{Equation 49}$$

$\Delta G_{Q,PET}$	Free enthalpy of PET (eV)
$E(D/D^+)$	Oxidation potential of the donor (eV)
$E(A^-/A)$	Reduction potential of the acceptor (eV)
$\Delta E(A)$	Singlet excitation energy of the acceptor (in oxidative PET, for the donor) (eV)
e_0	Elementary charge ($1.602176*10^{-19}$C)
ε	Dielectric constant of the surrounding media
a	Encounter distance of D and A radicals for pair formation (m)

The latter term is called ion pairing energy.
Many systems have been reported in the literature of reductive PET being exploited for the design of sensitive fluorophores where the donor is an amino moiety and its oxidation potential is extensively changed upon binding of protons or metal cations. In such systems, the amino function acts as receptor, while the fluorophore makes up the transducer. In this case, Weller's equation can be written as follows:

$$\Delta G_{Q,PET} = E_{Ox,Rec} - E_{Red,Flu} - \Delta E_{Exc,Flu} - E_{IP} \qquad \text{Equation 50}$$

$\Delta G_{Q,PET}$	Free enthalpy of the PET process (eV)
$E_{Ox,Rec}$	Oxidation potential of the receptor (eV)
$E_{Red,Flu}$	Reduction potential of the fluorophore (eV)
$\Delta E_{Exc,Flu}$	Singlet excitation energy of the fluorophore (eV)
E_{IP}	Ion pairing energy (eV)

PET is of superior or comparable rate to fluorescence if $\Delta G_{Q,PET}$ is exergonic or slightly endergonic [2]. Often, it is so exergonic that fluorescence is, in the absence of the analyte, almost completely quenched by it. In some cases, PET does not occur due to kinetic barriers [99,100]. Quenching over PET is prevented when the receptor has been protonated or associated with a cation, as electron density is dramatically reduced. As a result, fluorescence is switched "on" in the presence of the analyte, while it is frequently completely switched "off" in its absence. That allows the design of highly sensitive sensors and molecular switches [101].

As also stated in section 2.2.4, PET essentially constitutes a quenching mechanism, decreasing fluorescence QY but leaving all other spectral properties unaltered. However, in many practical systems with a short or no spacer absorption spectra are somewhat shifted because of electrostatic interactions between the positively charged protonated or associated receptor and the chromophore. That shift is in general much smaller than those observed with integrated receptors (non-PET pH indicators, classes B and C, section 2.2.4).

Equation 50 shows that PET efficiency will increase with reducibility and excitation energy of the chromophore (thus short-wave excitable, electron-poor ones being more accessible to it), with oxidability of the amino component (electron-rich, highly basic amines favouring it the most) and with solvent polarity. As a result of the latter, cross-sensitivity to environment polarity can occur in PET sensors, and in some systems, PET may only occur in polar media. This effect is a drawback in some applications, though it has been taken advantage of for polarity sensing [102,103].

Receptor and transducer are often covalently connected by a spacer, but PET systems without any spacer (integrated systems [104] or non-conjugated, orthogonal systems connected by a virtual C_0 spacer [105,106]) as well as non-covalently connected ones [107] can also be found in the literature. Aliphatic amines are the most common receptors, but aromatic ones and carboxylate groups have as well been employed. Introduction of different receptors allows tuning of the pK_A value and systems already investigated cover a broad pH range. The design of reverse PET systems, where an electron is passed from the fluorphore to the receptor, has also been investigated [2].

A mayor advantage of PET sensing systems lies in the fact that they are composed of various elements that can be assembled in many ways and thus considered modules [39] (figure 22). The most basic modules are fluorophore and receptor which can be varied to select spectral properties, and affinity to the analyte, respectively. More complex signalling devices can be designed by assembling a larger number of modules [102]. For pH sensing, affinity to the analyte is essentially given by the pK_A value. Consequently, by adequate selection of the receptor, dyes with selected spectral properties can be adapted to various applications that require different pK_A and used in various sensing materials, bouncing off effects the matrix may have on pK_A. The possibility of independently combining different features is not possible with dyes of integrated character. Not every combination of modules will yield a sensitive dye, but a prior estimation if PET is favourable can be based on Weller's equation, provided that redox potentials of fluorophore and receptor or of adequate models for those are known.

PET pH sensors have been designed, for instance, with anthracene [56], naphtalene, perylene [57], and diaryl pyrazoline [108] fluorophores. In most cases, aliphatic or aromatic amines are covalently connected via a short spacer. Most of the dyes mentioned, however, exhibit low

excitation wavelengths and poor to moderate brightness, mostly due to relatively low absorption coefficients. Sensing performance could be significantly improved by introducing more intensely and more long-waved absorbing and emitting dyes.
For ion sensing, additional interest has to be taken in the receptor and its affinity to the particular analyte. PET cation sensors can be based on the same principle as PET pH sensors, using chelating receptors which simultaneously act as PET electron donors. Once the cation has been bound, its electron-withdrawing effect makes PET unfavourble and fluorescence is enhanced. PET cation receptors have been designed, for instance, with receptors based on coronands (e.g. amine coronands bound to fluoresceine for Zn^{2+}-recognition [109]), cryptands (an example for K^+ recognition by a cryptand very closely bound to a coumarine fluorophore was presented by Golchini et al. [110]) and calixarenes (Na^+ sensing with a calixarene-derivatized pyrene, [111]). Bound to anthracene chromophores, coronand receptors have also been employed for sensing Na^+ with negligible cross-sensitivity to protons [112]. Ca^{2+} sensing by attaching a previously established receptor [113] to various chromophores has been reported, achieving excellent sensitivity. In that case, the electron-withdrawing effect induced upon analyte binding to the receptor is accompanied by a conformational change which further elevates the reduction potential of the receptor, enhancing sensitivity [114]. A different PET mechanism, involving electron transfer between the fluorophore and the metal cation, has been employed for recognition of transition metal ions. The receptor is then only required for complexation but not for electron release. An example is Ni^{2+} and Cu^{2+}-recognition with a chelating receptor bound to anthracene [115].
PET cation receptors can also involve excimer formation [116] and energy transfer.

3.1.2 Rhodamine Dyes

Rhodamines are xanthenes dyes represented by the structure shown in figure 24. They usually exhibit high absorption coefficients ε of around $100000 M^{-1}cm^{-1}$ and fluorescence QY Φ_F are close to unity for various derivatives. That implies rather bright emission, and consequently, high sensitivity can be accomplished with PET functionalities when fluorescence is completely extinguished in basic media. Absorption maxima range from 500 to 580nm and Stokes shifts are small (around 20-30nm) [117,118].

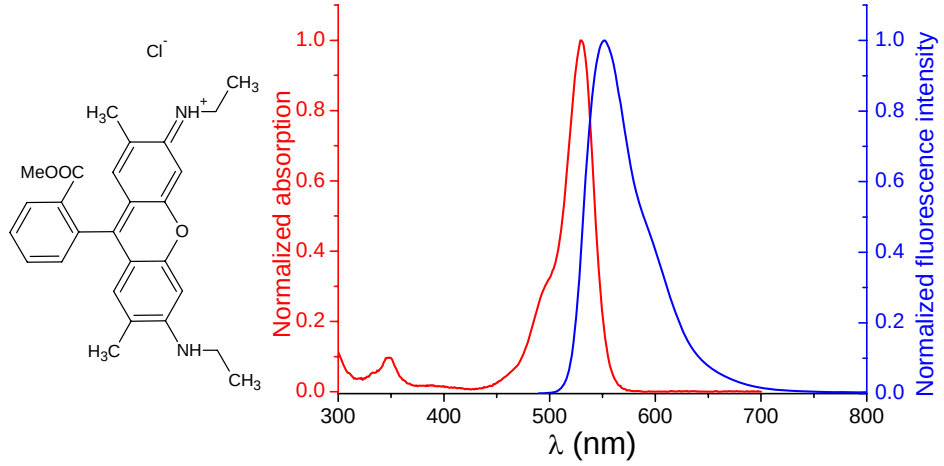

Figure 23: Absorption and fluorescence emission spectra of rhodamine 6G, representatively for rhodamine dyes.

Due to the spectral properties mentioned, together with generally good photostability, rhodamines have been utilized as laser dyes [119], fluorescence standards [120], for fluorescence microscopy, imaging of single molecules [121], fluorescent labelling and measurement inside living cells [122] or in energy transfer (FRET) systems [5], to state only a few applications.
Rhodamines are subject to the following equilibria:

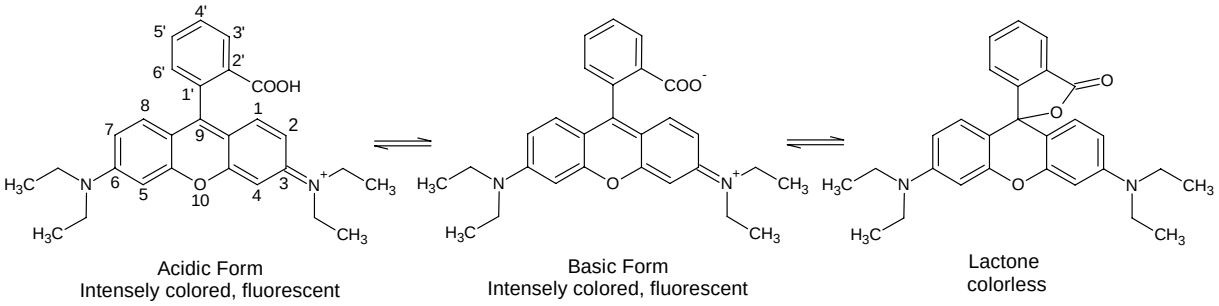

Figure 24: Protolysis and lactonization equilbria of rhodamines, demonstrated with rhodamine B. Numbering is according to [118].

The protolysis equilibrium has little effect on spectral properties, though the QY of acidic and basic form usually differ a little [118]. As a consequence, rhodamines show, in contrast to fluoresceines, no (or very poor) intrinsic pH sensitivity. Lactonization is an issue with rhodamine dyes. It is a fast and reversible reaction, often favourable in apolar, aprotic environments and provokes almost complete disappearance of fluorescence emission.
Some commercially available and frequently used rhodamine dyes are shown below:

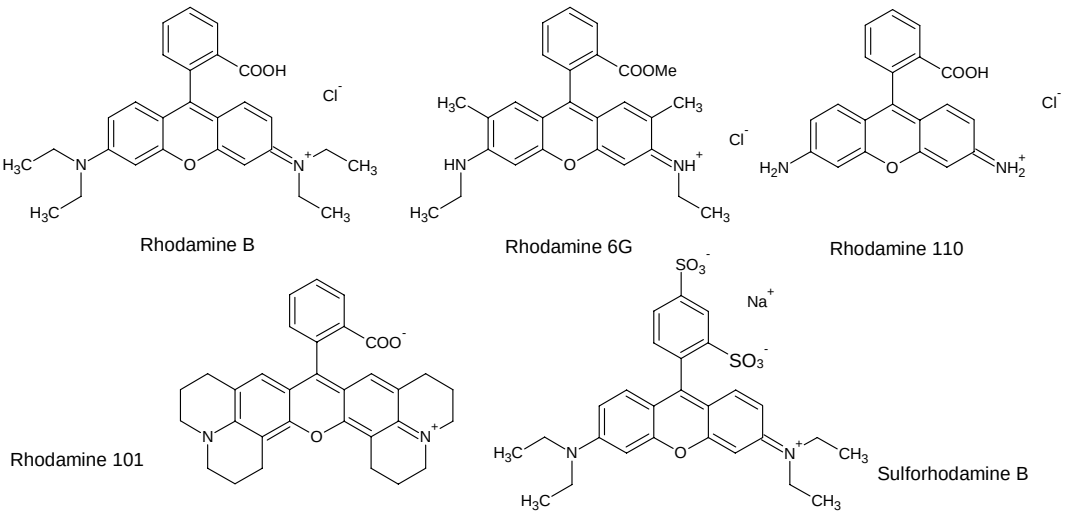

Figure 25: Structures of some commercially available rhodamines.

Rhodamine B and rhodamine 6G are available at low cost. Modification of the xanthenes nitrogen atoms can have a big impact on spectral properties. Alkylation of amino functions causes a bathochromic shift. Absorption maxima are 545nm for rhodamine B, 528nm for rhodamine 6G and 497nm for rhodamine 110 in MeOH [117]. Φ_F is decreased particularly by long-chained substituents, unless the alkyl groups are rigidised. For instance, Φ_F is 0.98 for rhodamine 101 in basic EtOH but only 0.70 for rhodamine B [118]. On the other hand, modifications in the 4' or 5' position affect spectral properties little and are thus ideal for coupling to biomolecules etc. Apart from vibrational quenching (IC), a non-fluorescent TICT (2.1.8) excited state is assumed to play a role in non-radiative deactivation [118,123].
Sulforhodamine B is an example for sulforhodamines, a dye class that differ from "conventional" rhodamines only by 2',4'-disulfate instead of 2'-carboxy substitution. They feature much better solubility in water, exhibiting similar spectral properties with slightly higher absorption and emission wavelengths than comparable rhodamines.
Rhodamines are most frequently prepared as follows:

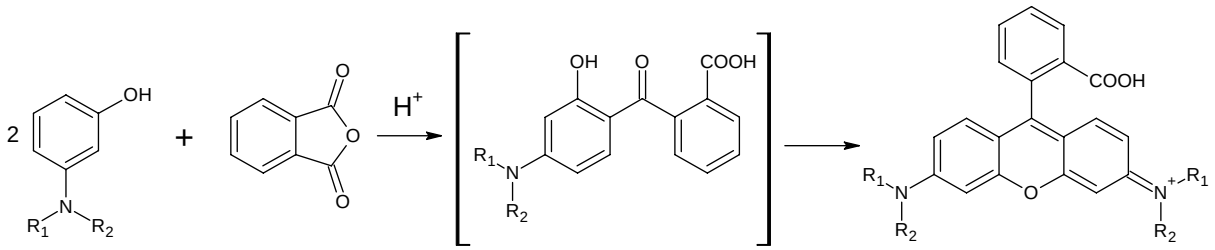

Scheme 1: The most common synthetic pathway towards rhodamines, condensation of a m-aminophenol and a phtalic anhydride derivative in the presence of an acidic catalyst. The intermediate shown is irreversibly formed, but it can be recuperated from the final product under strongly basic conditions.

A traditionally employed catalyst for this reaction is $ZnCl_2$. Nevertheless, in this work $MeSO_3H$ is used which has been successfully employed in corresponding fluorescein synthe-

sis [124,125]. Alternatively to scheme 1, the m-aminophenol can be condensed with an aromatic aldehyde. That has been employed for the preparation of sulforhodamines [126].
In this work, synthesis of a rhodamine functionalized with a free amino group is tackled. In that way, rhodamine is transformed into a pH sensitive PET dye. That indicator can be suggested to feature high sensitivity and the advantageous spectral properties of rhodamines mentioned earlier. Rhodamines are more long-wave excitable than many other pH indicators of common use (fluorescein derivatives or HPTS, 2.2.4). The synthetic approach chosen first is shown in scheme 3 (section 3.2.2.1) and would attach piperazinyl functions very close to the xanthene core. The product also contains a (4',5')-carboxy group making it suitable for covalent coupling. The pK_A of the product can be expected to be lower than the one of common organic amines (10-11 is most common [127]) due to the presence of another, electron-withdrawing nitrogen and is therefore likely to match the pH range of important applications (2.2.4). Furthermore, all components are available at low cost.

3.1.3 Squaraines

Squaraines have been named after squaric acid which was first synthesized by Cohen et al. in 1959 [128]. They are obtained by condensation of the acid with N-substituted anilines (many examples are available in [129]). Synthesis can be carried out easily by azeotropic distillation.

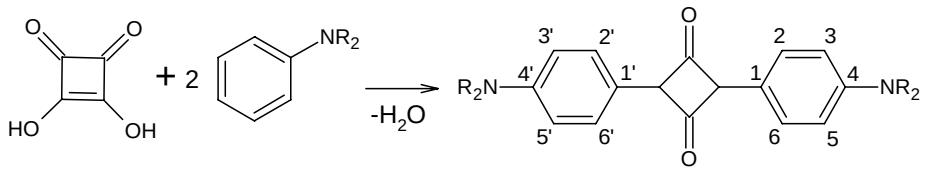

Scheme 2: Numbering (according to [131]) and general synthesis of squaraines.

While they usually exhibit panchromic absorption in the solid state [130], maxima in solution are sharp, located around 650nm and feature extraordinarily high absorption coefficients of more than $300000 M^{-1}cm^{-1}$. Fluorescence QY has been reported to be around 0.7 in unsubstituted and even higher in 2,2'-hydroxylated derivatives, which implies extraordinate brightness [131]. Despite their small Stokes shifts (20-30nm is most commonly observed), squaraines are thus interesting, bright, long-wave excitable dyes. Most squaraines have been reported to be poorly soluble in EtOH or $CHCl_3$ but better in polar, aprotic solvents like DMSO and DMF [129].
Based on their photoconductivity already recognized in the 1970s [132] and semiconductivity, applications in electrophotographic photoreceptors [133] and organic solar cells [134] have been reported. 2,2'-dihydroxysquaraines have been found to be pH sensitive and applicable for pH sensing in aqueous solution [135]. However, utilization in solid matrices has, to my knowledge, not been reported.
Therefore, the suitability of 2,2'-dihydroxysquaraines, accessible for instance by condensation of squaric acid with m-dibutylaminophenol (scheme 12, section 3.2.2.10), as luminescent pH indicator dyes was to be tested. A pH indicator with the excellent brightness and high excitation wavelength featured by squaraines is indeed very promising. pK_A of such a system has

been reported to be around 9 [135] which could be suitable for measuring marine samples or CO_2.

3.1.4 Perylene Dyes

Perylene dyes are derived from perylene-3,4,9,10-tetracarboxylic bisanhydride (structure is shown in figure 27). They feature characteristic, vibrationally dissolved absorption spectra:

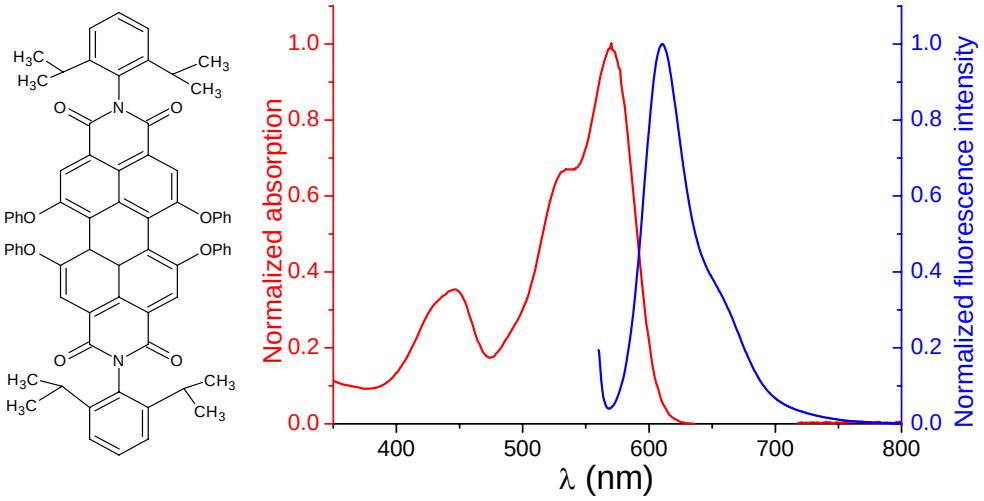

Figure 26:Absorption and fluorescence emission spectra of lumogen red, representatively for perylene dyes.

In particular, the corresponding perylene bisimide dyes (PBIs) have been found useful for a wide variety of purposes and applications, including OLEDs [136], OFETs [137], photovoltaic cells [138], fluorescent solar collectors [139], electrophotographic devices [140], dye lasers [141] and molecular switches [142].
Though spectral properties can greatly vary depending on substituents introduced, ε in PBIs are usually found between 30000 and 90000$M^{-1}cm^{-1}$, Stokes shifts around 40nm and fluorescence QY are close to unity for many derivatives [139]. Apart from good brightness, PBIs offer outstanding chemical, thermal and photochemical stability [143]. Another advantage is their good versatility with respect to synthetic modification for tuning spectral and sensing properties and to extension of the chromophore for the synthesis of dyes excitable at remarkably longer wavelengths [144,145].

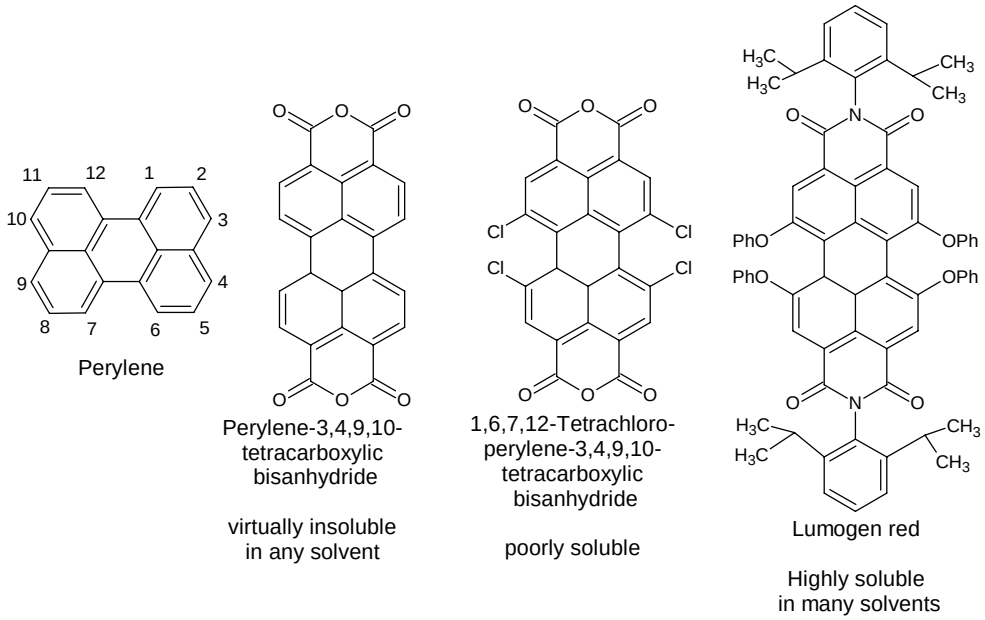

Figure 27: General structure of perylene and structures of selected perylene dyes

Starting from perylene-3,4,9,10-tetracarboxylic bisanhydride, the system can be modified in two ways. Reaction with primary amines leads to the corresponding perylene bisimides (PBIs), and the 1,6,7 and 12 positions ("bay region") can be halogenated. Tetrachlorination [146,147], dibromination [148] and tetrabromination [149] have been reported. The halogenides formed can be considered intermediates that can undergo nucleophilic aromatic substitution. Though introduction of various substituents including cyano and amino groups has been reported, [148,149], phenol and its derivatives are inserted most frequently. Tetrasubstitution with phenol not only causes a red-shift by about 70nm (the most intense absorption maximum is shifted from around 510nm in the tetrachlorinated dye to around 580nm, [150]), but also helps to overcome aggregation which is a severe problem with perylene dyes. The flat, polycondensed aromatic system shows extensive aggregation tendency as molecules are kept on top of each other by charge-transfer type π-π interactions („stacking"). If the 1,6,7 and 12 positions are halogenated, the system becomes twisted [148] so that solubility improves a little. Substitution with more bulky aromatic substituents improves it much more remarkably. Those are forced to localize orthogonally with respect to the aromatic plane and complicate stacking. The *N*-substituents in the imide position usually have little effect on spectral properties due to nodes in HOMO and LUMO situated at the nitrogen atoms [148], but particularly branched substituents increase solubility, with respect to the virtually insoluble bisanhydride. In lumogen red, a commercially available perylene dye (figure 27), all positions mentioned carry bulky substituents. The aromatic plane is no longer sterically accessible to stacking, as a result, much better solubility in a variety of organic solvents is achieved [151]. This is visualized in the following 3D model:

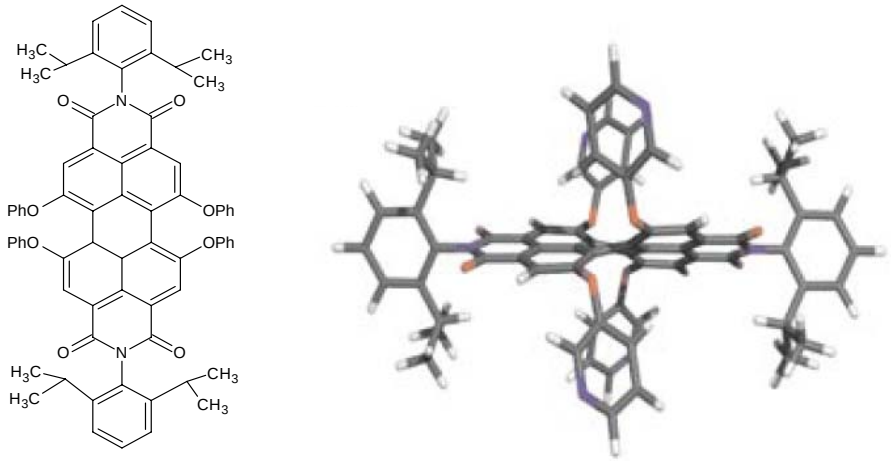

Figure 28: Three-dimensional model of lumogen red. Both in the imide and the bay region, bulky substituents are forced to align perpendicularly to the aromatic plane. That keeps other molecules from approaching and stacking is complicated.

Imide formation can be reversed by saponification under strongly basic conditions, and also partial saponification has been reported [148]. Hence, imides may be employed as protective groups for anhydrides. That makes indirect substitution of a halogen with a nucleophile in perylene bisanhydrides (PBAs) possible since PBIs are more stable against nucleophilic attack [152].

The synthetic concept tackled in this work starts from 1,6,7,12-tetrachloroperylene-3,4,9,10-tetracarboxylic bisanhydride, which is commercially available. There are two ways to attach a PET functionality, either introducing it with the N-substituents upon imide formation, or by substitution of chlorine. The former was chosen as appropriate coupling reagents are available at low cost and substitution of chlorine would have to be stopped at the monosubstituted intermediate, complicating the synthetic approach. Multiple substitution might worsen fluorescence brightness of the acidic form as well and complicate calibration of the sensitive dye since multiple deprotonation steps would be involved. 3-(1-morhpholino)propylamine was chosen as the amino component whereat the hydrophilic morpholino group was supposed to improve solubility in the hydrophilic environment required for pH sensing. That reaction is shown in scheme 13 (section 3.2.2.11) and attaches a morpholino function as PET group to each anhydride, linked via a C_3 spacer. In case the presence of two PET functions causes undesirable effects, mixed condensation with 2,6-diisopropylaniline can be attempted, expectedly improving solubility at the same time. For the synthesis of unsymmetrical PBIs, simple mixed condensation [153] has been presented in the literature as well consecutive condensation [154]. A more sophisticated approach involves partial hydrolysis of symmetrical PBIs and condensation of the monoanhydride monoimide obtained with the second amino component [155].

PET has already been observed in PBIs unsubstituted in the bay region, caused by amino groups attached to the imide substituent. Good sensitivity with tertiary amines and moderate sensitivity with primary ones (because of their lower oxidation potential) has been reported. [57]. According to Weller's equation 50, PET efficiency depends on oxidation potentials of both chromophore and amino group. Electron-withdrawing chloro substituents can be expected to enhance reducibility of the chromophore, the introduction of relatively weakly nucleophilic morpholine should thus be justified.

A PET pH indicator obtained in that way, with the advantageous properties of perylenes mentioned earlier would also be more long-wave excitable than many pH-indicators known. However, longer excitation wavelengths (510-520nm can be expected for the product presented) are still very desirable and a significant red-shift is already available by substitution of Cl with phenoxy. For even longer excitation wavelengths, extension of the chromophore [144,145] can be attempted.

3.1.5 Physical Entrapment into Sensor Matrices

Layer Coating

Coating is a simple, straightforward concept for the production of sensitive layers. In the simplest case, indicator dye and a matrix polymer are dissolved in a volatile solvent and formed to a layer which dries as the solvent evaporates. Coating is affected by few parameters, and if it is performed from homogeneous mixtures, the composition of the layer is equally homogenous and its composition is the same as the one of the original cocktail. It has been successfully used in lab scale as well as in industrial scale. Prerequisites to the technique are sufficient solubility of the dye in both polymer and solvent and low solubility in the sensing media (mostly water, so for pH sensors).
In this work, D4, a polyurethane-based hydrogel is used as polymeric matrix for pH sensors. It is a block copolymer, consisting of more hydrophilic and more hydrophobic domains [40].

PS/PVP Particles

PS/PVP particles consist of a block copolymer with hydrophobic polystyrene and hydrophilic polyvinylpyrrolidone units which form a hydrophobic core and a hydrophilic shell. Luminescent dyes can be immobilized into both domains, depending on the solvent used for staining. In THF/H_2O, the core is swollen, so that lipophilic dyes diffuse into it and are trapped inside once the solvent has been evaporated. More hydrophilic dyes can be brought into the the shell in 70% aqueous EtOH by which only the shell is swollen. Staining in both core (oxygen and temperature indicators, lipophilic pH indicators) and shell (hydrophilic ion and pH indicators) of PS/PVP particles has been reported [60]. They have been successfully applied in pH sensing [51] and make up an alternative to the more frequently utilized hydrogel matrices.

RL100 Particles

RL 100 particles are prepared from a commercial bulk polymer consisted of poly-(methylmethacrylate) bearing positively charged quaternary ammonium groups. It is soluble in organic solvents of intermediate polarity such as acetone or THF, but can be precipitated with water, forming nano-particles (30nm regime) of low optical density. This matrix offers the advantage of high affinity to negatively charged dyes so that leaching of those may be prevented. Due to its charge, on the other hand, it is likely to cause higher cross sensitivity to ionic strength in pH sensors, compared to non-charged matrices. It may also have a strong effect on the pK_A value of the system (2.2.4).

3.1.6 Coupling to Magnetic Particles

Preparation of magnetic nanosensors for pH is another objective focussed in this work. The concept towards that is shown below:

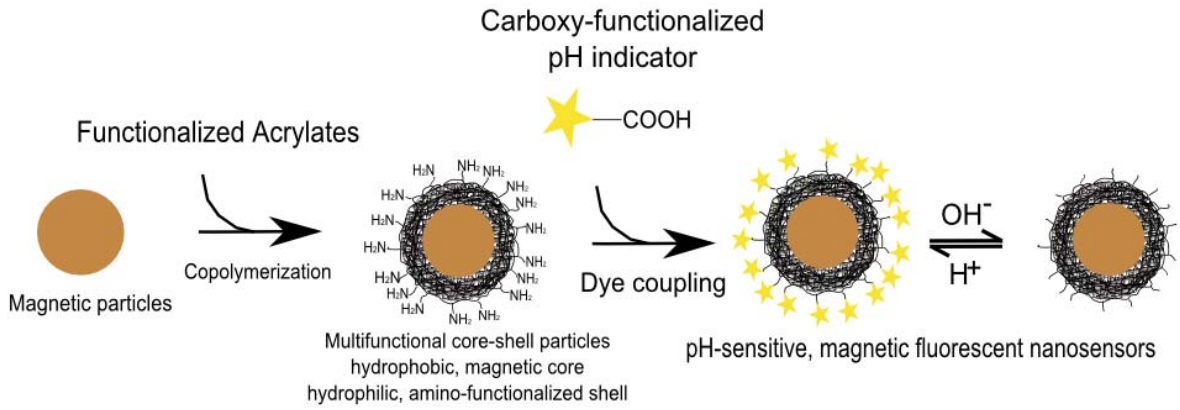

Figure 29: Schematic overview of the concept towards pH sensitive magnetic particles. Amino-functionalized magnetic particles are obtained by emulsifier-assisted core-shell polymerization of functional acrylates in presence of magnetic core particles. A carboxy-functionalized fluorescence pH indicator is bound to the shell in a subsequent coupling step.

Preparation of magnetic nano-particles dispersible in water by precipitation has been reported by Mistlberger et al. [156]. Those particles are co-precipitated from bulk polystyrene-co-maleic anhydride (PSMA) and lipophilized Fe_3O_4 nano-particles. In aqueous solution, they undergo hydrolysis and then carry negatively charged carboxylate groups on their surface, allowing the formation of stable aqueous dispersions and derivatization. In order to obtain amino-functionalized magnetic particles, they were to be covered with a cross-linked acrylamide-based hydrogel shell containing amino groups. That was to be accomplished with emulsifier-assisted radical core-shell co-polymerization in aqueous suspension. In the approach presented, acrylamide was chosen as the bulk component of the hydrogel shell and co-polymerized with acrylates bearing amino groups in the presence of an acrylate cross-linker.
Coupling between the carboxy and the amino function in aqueous solutions can be performed with EDC/sulfo-NHS as coupling agents, as described in the literature [66]. That has been extensively employed, in particular with macromolecular biomolecules such as proteins [157] but also with small molecules [158]. In that way, a pH sensitive indicator dye carrying a carboxy function can be covalently bound into a hydrophilic matrix that can be expected to feature excellent proton-permeability. Acrylamide-based matrices can take up over 90% of water [159] and have been successfully employed as matrices for pH sensing [53,84].

3.2 Experimental

3.2.1 Instrumental

Absorption spectra were recorded with fully automatic baseline correction on a Cary50 UV-VIS spectrophotometer, Varian, Palo Alto, United States. Samples with a noticeable scattering background were corrected for the baseline with Origin Pro 7.5 software, Origin Lab Cooperation, Northampton, United States.
Fluorescence spectra were recorded on a Hitachi F-7000 spectrofluorimeter, Hitachi, Krefeld, Germany. All spectra were corrected for detector response.
NMR spectra were recorded on a 300MHz instrument (Bruker).
DLS measurements were performed with a Zetasizer instrument (Malvern Instruments, Malvern, UK). All correlation analyses were performed with the manufacturer-supplied software. Disposable capillary cuvettes equipped with electric contacts for zeta potential measurement were also obtained from the supplier.
N_2 and Ar, both of 99,999% purity, were supplied by Air Liquide, Graz, Austria. Hydromed D4 hydrogel was purchased from CardioTech International Inc., Wilmington, United States.
Support for sensitive layers was supplied by Puedz, Vienna, Austria.
A list of all chemicals used can be found in the appendix.

3.2.2 Dye Synthesis

3.2.2.1 *N,N'*-Bis-(3-azapentmethylene)-(4',5')-carboxyrhodamine ("BPCR")

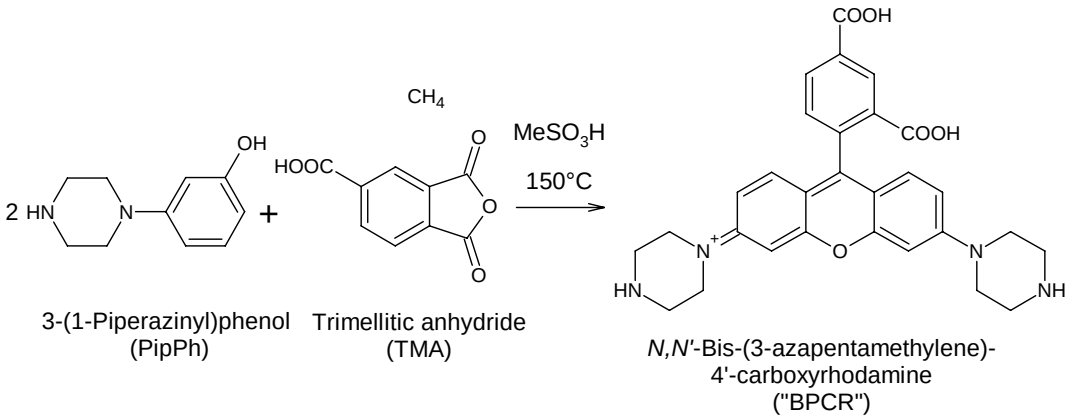

Scheme 3: Synthesis of *N,N'*-bis-(3-azapentamethylene)-(4',5')-carboxyrhodamine ("BPCR").

In this preparation, not only the 4'-carboxy isomer shown, but a mixture with the 5'-carboxy one is formed. For the sake of clarity, only the 4'-carboxy isomer will be drawn in reaction schemes of condensations involving TMA, representing the mixture formed in reality.
TMA (1.62g, 8.42mmol) and PipPh (3g, 16.83mmol) were powdered together in a mortar and suspended in $MeSO_3H$ (25ml). The suspension was heated to 150°C and stirred until the absorption of the deep red reaction mixture was constant (A=0.45 at λ_{MAX}=528nm when diluted by 20000) after 3.5h, showing absorption spectra expected for a rhodamine dye, equal in shape to figure 23. The mixture was poured onto THF (30ml), the sticky black precipitate was

isolated by centrifugation and purified by repeated recrystallisation from MeOH. The product (1.89g, 44%) was identified by NMR spectroscopy:

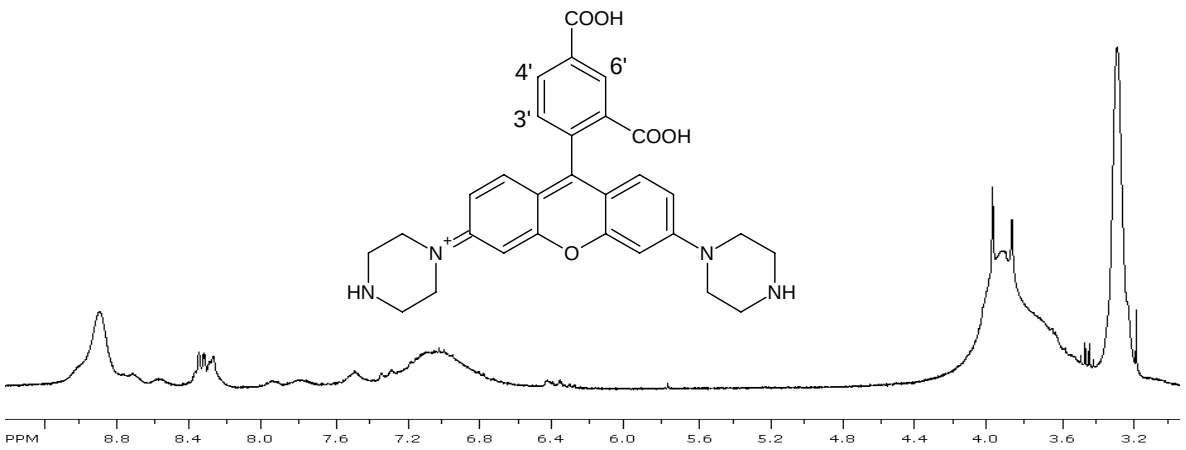

Figure 30: ^{1}H-NMR spectrum of BPCR, 300MHz, DMSO-d6.

δ=8.69-8.80 (1H, s, $Ar_{6'}H$); 8.35 (1H, d, $Ar_{4'}H$, J=7.1Hz); 8.29 (1H, d, $Ar_{3'}H$); 6.76-7.36 (6H, m, ArH), 3.80-4.09 (8H, m, $ArNCH_2$-); 3.16-3.34 (8H, m, -C<u>H</u>$_2$NH).

3.2.2.2 Alkylation of *N,N'*-Bis-(3-azapentamethylene)-(4',5')-carboxyrhodamine ("BPCR")

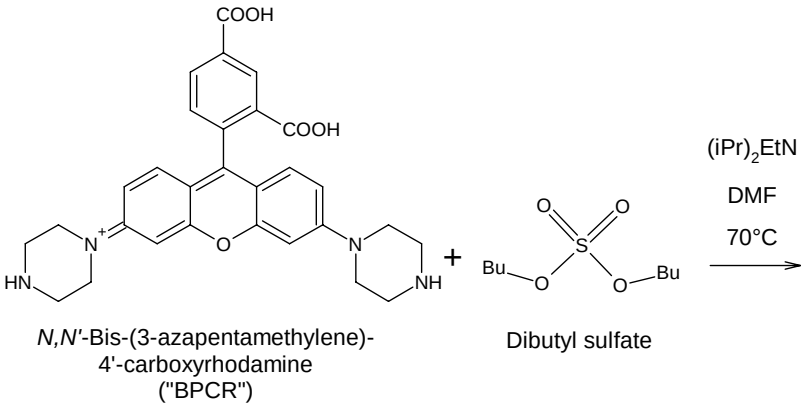

Scheme 4: Alkylation of *N,N'*-bis-(3-azapentamethylene)-(4',5')carboxyrhodamine ("BPCR").

BPCR (100mg, 0.188mmol) and Bu_2SO_4 (149µl, 0.784mmol) were dissolved in DMF(10ml), the resulting deep violet solution was heated to 70°C and ethyldiisopropylamine (EDIPA; 526µl, 3.02mmol) was added in portions. After stirring for 2h, TLC revealed the formation of multiple products:

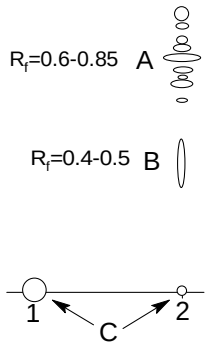

Eluent: MeOH:$CHCl_3$:NH_3(25% in H_2O) 66:33:1

1: Starting material, BPCR, in MeOH
2: Reaction mixture after stirring for 2h

A,B: Series of spots (products formed)
C: Starting material, BPCR

All spots are of purple colour and fluorescent when excited at 366nm

Figure 31: Sketch of TLC taken to monitor the alkylation of BPCR.

3.2.2.3 Alkylation of 3-(1-Piperazinyl)phenol

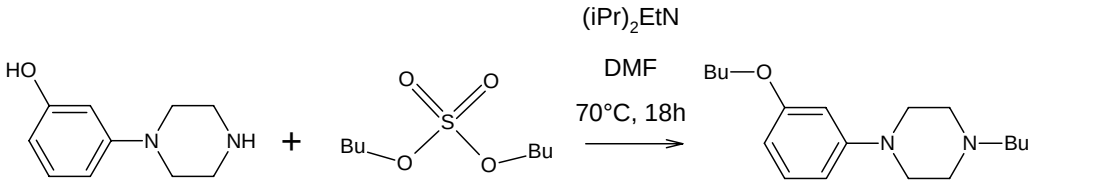

3-(1-Piperazinyl)phenol (PipPh) | Dibutyl sulfate | m-Butyloxy-(4-butylpiperazinyl)benzene

Scheme 5: Alkylation of 3-(1-piperazinyl)phenol.

To PipPh (2g, 11.2mmol) and ethyldiisopropylamine (EDIPA; 3.14ml, 18mmol) was added anhydrous DMF (80ml) to yield a dark brown suspension. After stirring at RT for 1h, Bu_2SO_4 (2.22ml, 11.2mmol) was added and the mixture was heated to 70°C for 3h. Reaction progress was surveyed by TLC.

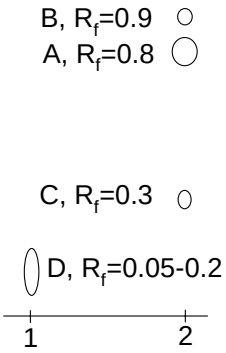

Eluent: MeOH:$CHCl_3$ 25:75

1: Reaction mixture right before Bu_2SO_4 was added
2: Reaction mixture after stirring for 3h

A: Main product
B,C: Side products
D: Starting material, 3-(1-piperazinyl)phenol

All spots are of brown colour and fluorescent when excited at 254nm (but not at 366nm)

Figure 32: Sketch of TLC taken to monitor the alkylation of PipPh.

DMF was evaporated in a vacuum and the main product, represented by spot A, was isolated by column chromatography with silica gel (0.04-0.063mm) as stationary and $CHCl_3$/MeOH/ NH_3(25% in H_2O) 85/14/1 as mobile phase to yield 1.64g (51%) of a dark brown solid.

Spot A was identified as m-butyloxy-(4-butylpiperazinyl)benzene by NMR spectroscopy:

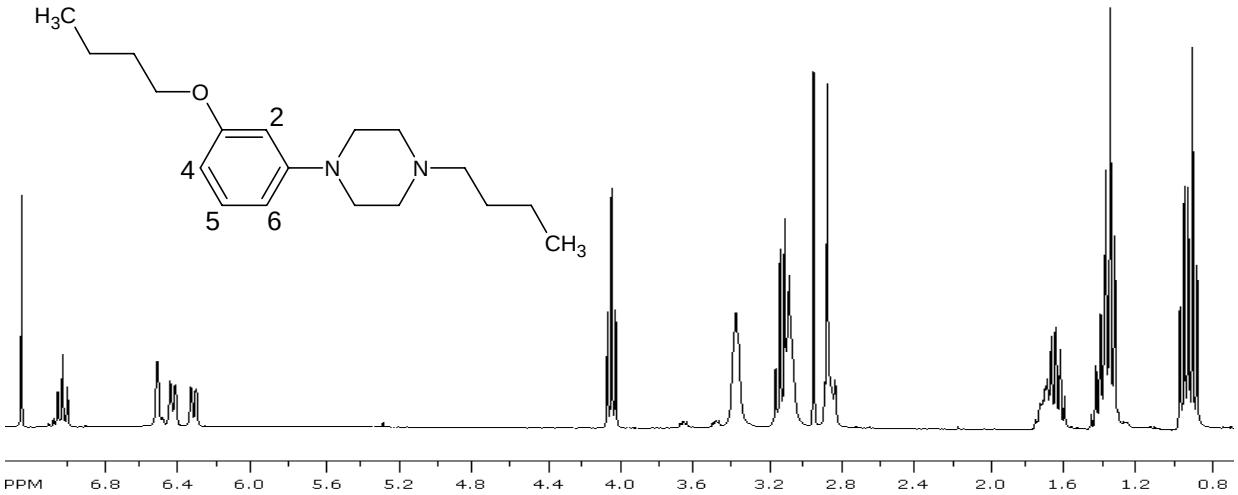

Figure 33: ^{1}H-NMR spectrum of m-butyloxy-(4-butylpiperazinyl)benzene, 300MHz, $CDCl_3$.

δ=7.04 (1H, dd, Ar_5H, J_{Ar45}=8.1Hz, J_{Ar56}=9.6Hz,); 6.52 (1H, s, Ar_2H); 6.44 (1H, dd, Ar_4H, J_{Ar46}=1.2Hz,); 6.32 (1H, dd, Ar_6H); 4.05 (2H, t, OCH_2-, J=6.6Hz); 3.33-3.41 (4H, m, $ArNCH_2$-); 3.07-3.19 (4H, m, $BuNCH_2$-); 2.87 (2H, t, $NC\underline{H}_2C_3H_7$); 1.59-1.71 (4H, m, -$C\underline{H}_2C_2H_5$); 1.31-1.42 (4H, m, -$C\underline{H}_2CH_3$); 0.87-0.96 (6H, m, -CH_3).

The spectrum is in good agreement with the product structure proposed.

3.2.2.4 *N,N'*-Bis-(3-aza-3-butylpentamethylene)-(4',5')-carboxyrhodamine ("BuPCR")

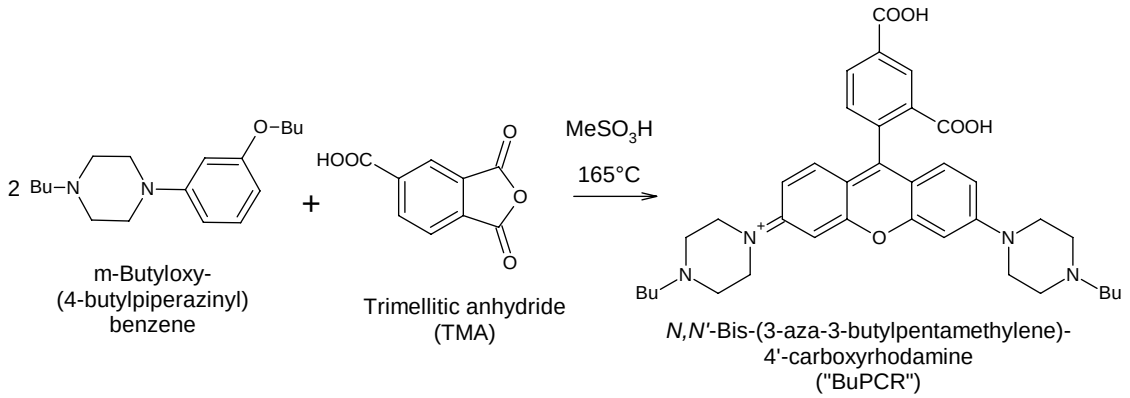

Scheme 6: Synthesis of *N,N'*-bis-(3-aza-3-butylpentamethylene)-(4',5')-carboxyrhodamine ("BuPCR").

m-Butyloxy-(4-butylpiperazinyl)benzene (0.8g, 2.75mmol) and TMA (0.55g, 2.86mmol) were added to $MeSO_3H$ (10ml) and the resulting brown suspension was refluxed until absorption of the reaction mixture was constant (A=0.18 at 531nm when diluted by 10000) after 3.5h, showing absorption spectra expected for a rhodamine dye, equal in shape to figure 23. The reaction mixture was poured onto saturated aqueous NaCl (500ml), the black precipitate

was separated by centrifugation, washed with saturated NaCl, dried and purified by column chromatography with silica gel (0.04-0.063mm) as stationary and $CHCl_3$/MeOH 80/20 as mobile phase. The deep purple solid obtained was redissolved in MeOH, filtered and dried to yield N,N'-Bis-(3-aza-3-butylpentamethylene)-(4',5')-carboxyrhodamine (58mg, 7%).

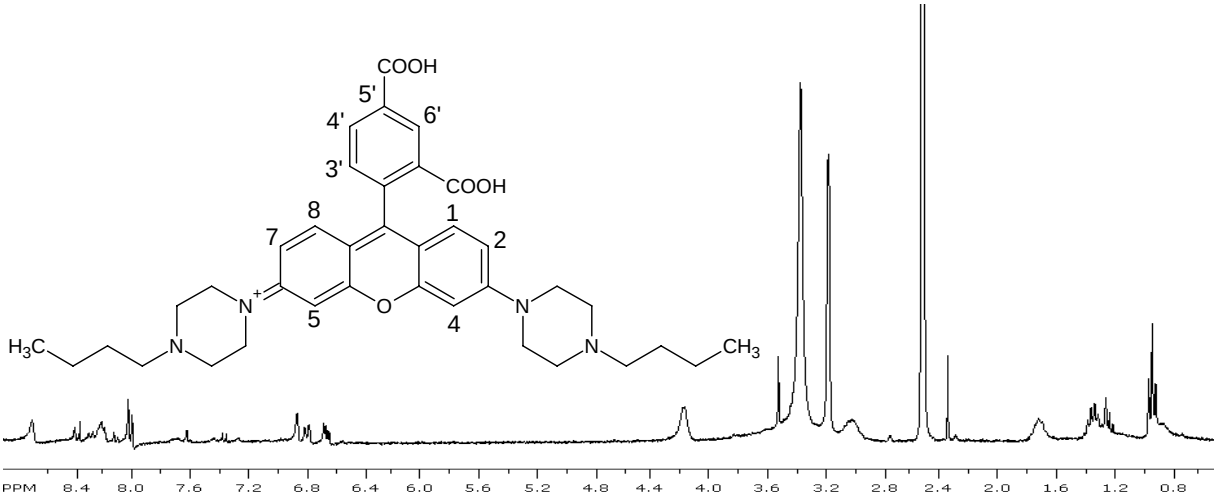

Figure 34: ^{1}H-NMR spectrum of BuPCR, 300MHz, DMSO-d6.

δ=8.72 (1H, s, $Ar_{6'}H$); 8.23 (1H, dd, $Ar_{4'/5'}H$, $J_{Ar3'4'}$=7.9Hz, $J_{Ar5'6'}$=5.1Hz*); 8.03 (1H, d, $Ar_{3'}H$); 6.87 (2H, m, $Ar_{4,5}H$); 6.79 (2H, dd, $Ar_{1,8}H$, J_{Ar12}=8.7Hz, J_{Ar14}=2.6Hz); 6.66 (2H, dd, $Ar_{2,7}H$, J_{Ar24}=3.7Hz); 4.12-4.26 (8H, m, $ArNCH_2$-); 3.52 (1H, s, COO-H_1); 2.96-3.08 (12H, m, NCH_2-); 2.34 (1H, s, COO-H_2); 1.63-1.79 (4H, m, -C<u>H</u>$_2C_2H_5$); 1.21-1.37 (4H, m, -C<u>H</u>$_2CH_3$); 0.92 (6H, t, -CH_3, J=7.2Hz).

*The doublet-doublet character of this resonance could originate from the fact that the product is a mixture of 4'-and 5'-carboxyisomer (only the latter is shown).

This spectrum is complicated by large signals derived from DMSO (only 99% D) and water (2.54 and 3.30ppm), as well as by poor signal-to-noise ratio. Nevertheless, it is in agreement with product structure, clearly indicating the presence of two butyl substituents.

3.2.2.5 *N,N'*-Bis-(3-aza-3-butylpentamethylene)-(4',5')-octadecylaminocarboxyrhodamine ("RhODA").

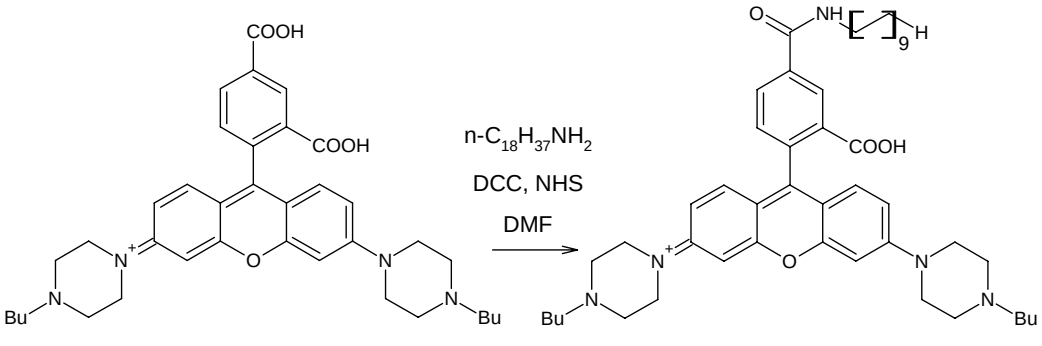

N,N'-Bis-(3-aza-3-butylpentamethylene)-4'-carboxyrhodamine ("BuPCR")

N,N'-Bis-(3-aza-3-butylpentamethylene)-4'-octadecylaminocarboxyrhodamine ("RhODA")

Scheme7: Synthesis of *N,N'*-bis-(3-aza-3-butylpentamethylene)-(4',5')-octadecylaminocarboxyrhodamine ("RhODA").

BuPCR (30mg, 0.047mmol), DCC (50mg, 0.242mmol) and NHS (50mg, 0.434mmol) were dissolved in DMF (5ml) and the resulting red solution was stirred for 2h at RT. EDIPA (100µl, 0.574mmol) and octadecylamine (ODA; 100mg, 0.371mmol) in DMF (5ml), pre-heated to 50°C, were added and the purple reaction mixture was again stirred for 48h. TLC indicated the formation of a lipophilic product:

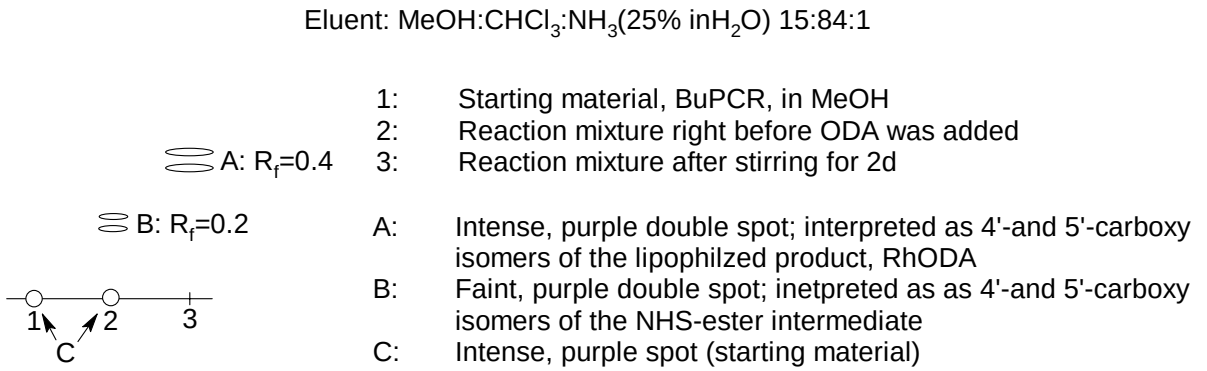

Figure 35: Sketch of TLC taken to monitor the synthetis of RhODA.

The reaction mixture was concentrated to dryness, the crude product was dissolved in $CHCl_3$, filtered, concentrated in a vacuum and purified by column chromatography with silica gel (0.04-0.063mm) as stationary and $CHCl_3$/MeOH/NH_3(25% in H_2O) 90/9.5/0.5 as mobile phase.

The product obtained was obviously contaminated with colourless substance and ε was determined as low as ε = 10000$M^{-1}cm^{-1}$. However, absorption spectra showed now signs of spectrally relevant pollutants (figure 49) and TLC displayed only spot A. It was therefore concluded that impurities are mostly derived from silica. Though the low purity of the product does not allow definite verification of its structure, it can be assumed to be the one claimed, as it exhibits pronounced lipophility (soluble in $CHCl_3$ where BuPCR is completely insoluble in and not extractible into water), combined with spectral properties very similar to BuPCR.

28mg of substance were obtained the product content of which can be estimated to 2.8mg (7%) when assumed that ε of the pure product is 100000$M^{-1}cm^{-1}$ (based on [118]).

3.2.2.6 Amidation of Rhodamine 101

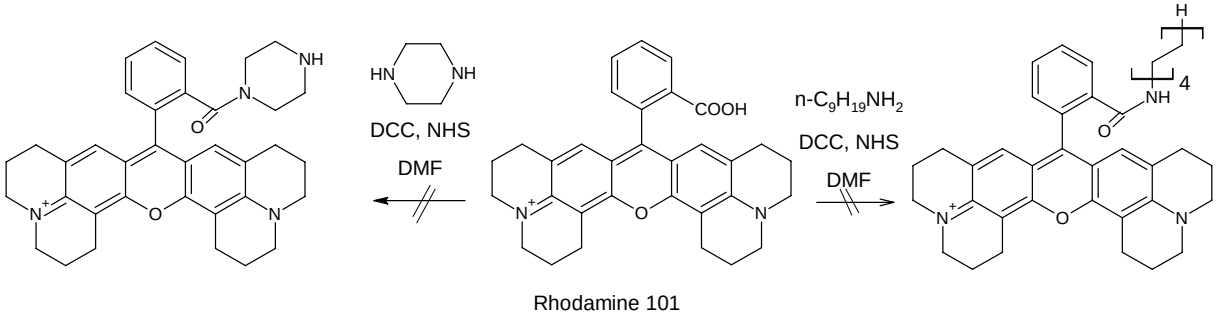

Scheme 8: Amidation of rhodamine 101.

Amidation of rhodamine 101 was attempted with piperazine and octylamine (OAM). For this reaction, the amidation protocol reported by Schröder et al. [160] was adapted, employing an excess in amine component because of the expected low carbonyl reactivity of the 2'-carboxy moiety in rhodamine 101 due to steric hindrance.
For the octylamide, rhodamine 101 (20mg, 0.041mmol) was dissolved in DMF abs. (2ml) and subsequently NHS (7.5mg, 0.065mmol) and one drop of Et_3N were added. The resulting deep purple solution was left to stir at RT for 2.5h, DCC (12mg, 0.058mmol) and OAM (10 µl, 0.099mmol) were added and the reaction mixture was again stirred for 2d at RT. With piperazine, the reaction was carried out in the same way, but 15mg (0.130mmol) of NHS, 25mg (0.121mmol) of DCC and 50mg (0.580mmol) of piperazine (instead of OAM) were used.
TLC gave no indication of any product formed. The reaction mixture with piperazine remained equally fluorescent when diluted with water and acid or base (1M aqueous HCl, or NaOH, respectively) was added, without any signs of pH sensitivity. The one with OAM was diluted with a tenfold excess of water and extraction with an equal volume of EE was performed. The absorption of the slightly pink coloured organic phase was measured and found to be similar to the one of a reference (2mg of rhodamine 101 in 2ml of H_2O/DMF 9:1, extracted with 2ml of EE). Consequently, no signs of lipophilization were found. Hence it was concluded that amidation of the 2'-carboxy moiety is not effective with the protocol cited which has been shown to be effective with the 5-carboxy position in fluorescein [160].

3.2.2.7 Lissamine rhodamine B 4'-piperazinyl amide ("LiPA")

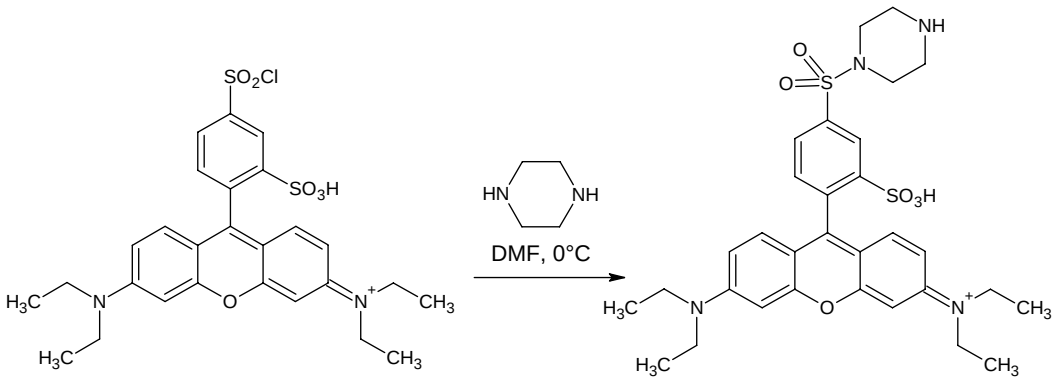

Lissamine rhodamine B

Lissamine rhodamine B piperazyl amide ("LiPA")

Scheme 9: Synthesis of lissamine rhodamine B-4'-piperazinyl amide ("LiPA").

For the preparation of this sulfamide, the protocol proposed by Nudelman et al. was employed [161]. Lissamine rhodamine B sulfonyl chloride (50mg, 0.087mmol; a.k.a. sulforhodamine B acid chloride) was added into a flask containing piperazine (38mg, 0.441mmol), filled with N_2 and precooled to 0°C. DMF abs. (15ml) was added and the deep purple reaction mixture was stirred overnight. DMF was removed under reduced pressure, the oily residue was redissolved in EE (100ml) and extracted with an equal volume of saturated aqueous $NaHCO_3$. The organic phase was concentrated to dryness and the products detectable by TLC (see below) were separated from each other by column chromatography with silica gel (0.04-0.063mm) as stationary and CH_3CN:MeOH/NH_3 (25% in H_2O) 80/19/1 as mobile phase.

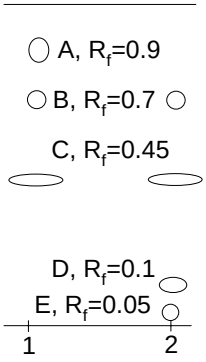

Eluent: CH_3CN:MeOH:NH_3 (25% in H_2O) 80:19:1

1: Starting material, lissamine rhodamine B
2: Reaction mixture after stirring overnight

A: Faint spot, interpreted as staring material
B: Faint, interpreted as starting material (minor isomer)
C: Most intensely coloured, interpreted as hydolyzed starting material
D: Spot of intermediate intensity, interpreted as product
E: Faint, interpreted as product (minor isomer)

All spots are purple and show orange fluorescence

Figure 36: Sketch of TLC taken to monitor the synthesis of LiPA.

Possible products fractions are "D" (11mg, 12%, ε = 88000 $M^{-1}cm^{-1}$) and "E" (3mg, 5%, ε = 103000 $M^{-1}cm^{-1}$). "D"&"E" and "A"&"B" could be stereoisomers, since lissamine rhodamine B sulfonyl chloride is a mixture of 4'- (mayor component) and 2'- sulfonyl chloride.
Spot "D" was identified by NMR spectroscopy:

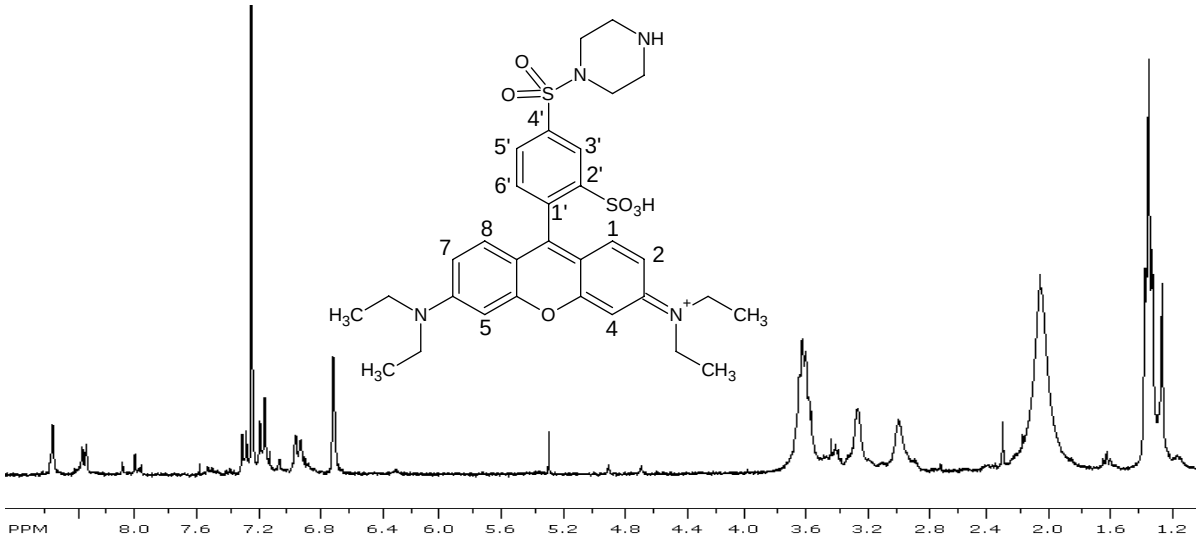

Figure 37: ^{1}H-NMR spectrum of LiPA, 300MHz, $CDCl_3$.

δ=8.58 (1H, s, $Ar_{3'}H$); 8.37 (1H, d, $Ar_{5'}H$, $J_{Ar5',6'}$=8.1Hz); 7.31 (1H, d, $Ar_{6'}H$); 7.19 (2H, d, $Ar_{1,8}H$, J_{Ar12}=9.4Hz); 6.95 (2H, dd, $Ar_{2,7}H$, J_{Ar24}=1.2Hz); 6.72 (2H, d, $Ar_{4,5}H$); 3.62 (8H, q, $NC\underline{H_2}CH_3$, J=6.3Hz); 3.21-3.30 (4H, m, $SO_2NC\underline{H_2}$-); 2.93-3.03 (4H, m, $SO_2NCH_2C\underline{H_2}$-); 1.30 (12H, t, $-CH_3$, J=6.9Hz).

This spectrum is in agreement with the product spectrum reported by Nudelman et al. [161]. Additional resonances originate from the solvent ($CHCl_3$, δ=7.26) and from eluent residues (CH_3CN, δ=2.06, EtOH, δ=1.25; δ~3.6).

3.2.2.8 *N*-(3-Azapentamethylene)-*N'*,*N'*-dibutylrhodamine ("SemiPR")

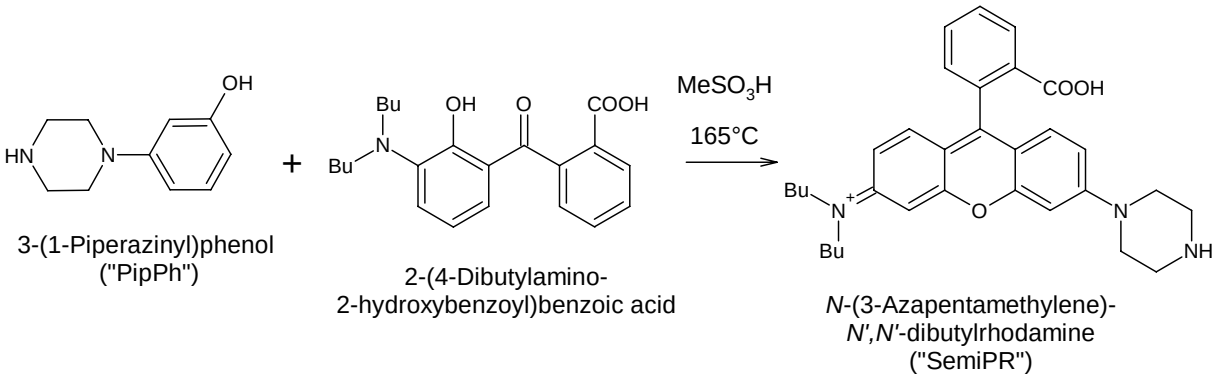

Scheme 10: Synthesis of *N*-(3-azapentamethylene)-*N'N'*-dibutylrhodamine ("SemiPR").

2-(4-Dibutylamino-2-hydroxybenzoyl)benzoic acid (1.51g, 4.09mmol) and PipPh (0.72g, 4.04mmol) were added to $MeSO_3H$ (25ml) and the resulting suspension was refluxed until absorption of the deep red reaction mixture was constant (A=0.34 at 544nm when diluted by 40000) after 1.5h, showing absorption spectra expected for a rhodamine dye, equal in shape to figure 23. After cooling to RT, 10M NaOH (10ml) was added dropwise to the mixture and it was poured onto vigorously stirred, saturated aqueous $NaHCO_3$ (100ml). The black precipitate was separated by centrifugation, washed with saturated $NaHCO_3$, dried and purified by column chromatography with silica gel (0.04-0.063mm) as stationary and EtOH/THF/NH_3 (25% in H_2O) 49/50/1 as mobile phase. The product was again dissolved in MeOH, filtered over cellite and dried to yield 1.48g (69%) of a purple solid.

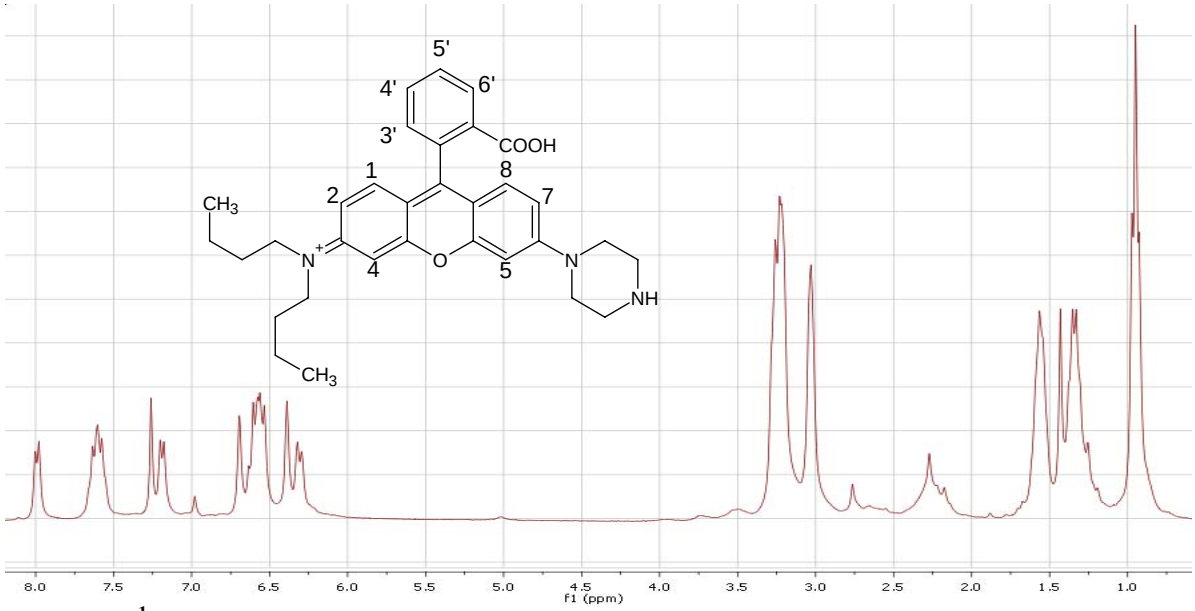

Figure 38: ^{1}H-NMR spectrum of SemiPR, 300MHz, $CDCl_3$.

δ=7.99 (1H, s, $Ar_{6'}H$, J=6.8Hz); 7.54-7.67 (2H, m, $Ar_{4'}H$,$Ar_{5'}H$); 7.19 (1H, d, $Ar_{3'}H$, J=7.2Hz); 6.69 (1H, s, Ar_5H); 6.51-6.64 (3H, m, Ar_1H,Ar_7H, Ar_8H); 6.39 (1H, s, Ar_4H); 6.31 (1H, d, Ar_2H, J=8.0Hz); 3.16-3.30 (8H, m, $ArNCH_2$-); 2.98-3.05 (4H, m, $HNC\underline{H}_2$-); 1.51-1.63 (4H, m, $NCH_2C\underline{H}_2$-); 1.34 (4H, q, -$C\underline{H}_2CH_3$, J=6.9Hz); 0.95 (6H, t, -CH_3, 6.6Hz).

3.2.2.9 Alkylation of *N*-(3-azapentamethylene)-*N'*,*N'*-dibutylrhodamine

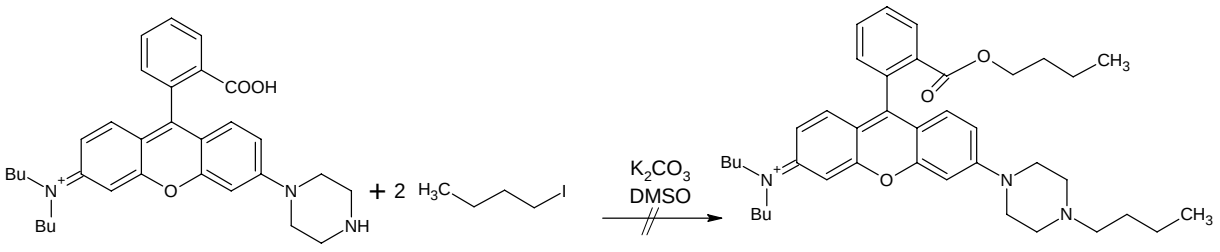

N-(3-Azapentamethylene)-*N'*,*N'*-dibutylrhodamine ("SemiPR")

n-Butyl iodide

Scheme 11: Alkylation of *N*-(3-azapentamethylene)-*N'*,*N'*-dibutylrhodamine.

For this reaction, the protocol proposed by Schröder [160] was employed. SemiPip (50mg, 0.092mmol), n-BuI (21µl, 0.180mmol) and finely powdered K_2CO_3 (60mg, 0.326mmol) were added to DMSO (5ml). Upon heating to 80°C, the deep violet reaction mixture changed its colour to faint brown. After 15h, the reaction mixture showed no pH sensitivity any more when diluted with H_2O, EtOH or any other solvent. On the other hand, its colour disappeared completely when diluted with acetone, indicating that lactonization is still possible. TLC showed almost complete formation of a single product.

3.2.2.10 Bis[4-dibutylamino-2-hydroxyphenyl]squaraine

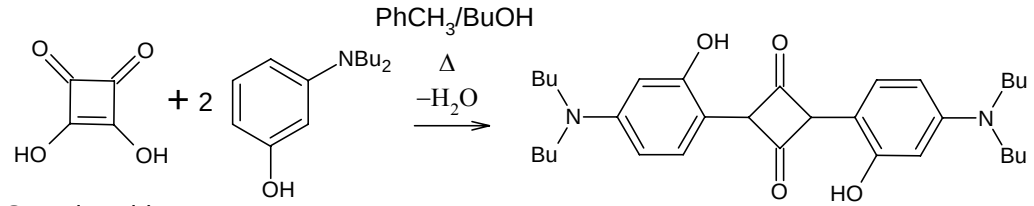

Squaric acid

m-(Dibutylamino)phenol

Bis[4-(dibutylamino)-2-hydroxyphenyl]squaraine

Scheme 12: Synthesis of bis[4-dibutylamino-2-hydroxyphenyl]squaraine.

Squaric acid (100mg, 0.877mmol) was suspended in BuOH (60ml) in an open flask and dissolved by heating to 50°C. m-Dibutylaminophenol (388mg, 1.754mmol) in toluene (40ml) was added and the mixture was heated to 140°C until absorption of the deep blue-green reaction mixture was constant (A=0.6 at λ_{MAX} = 544nm when diluted by 10000) after 2.5h. The mixture was allowed to cool to RT and left overnight. The dark green precipitate formed was filtered, washed with hexane, dissolved in hot EtOH and again filtered. EtOH was evaporated and the crude product was purified by recrystallisation from acetone to yield a green, fine-grained powder (363mg, ε = 284000 $M^{-1}cm^{-1}$, 58%).

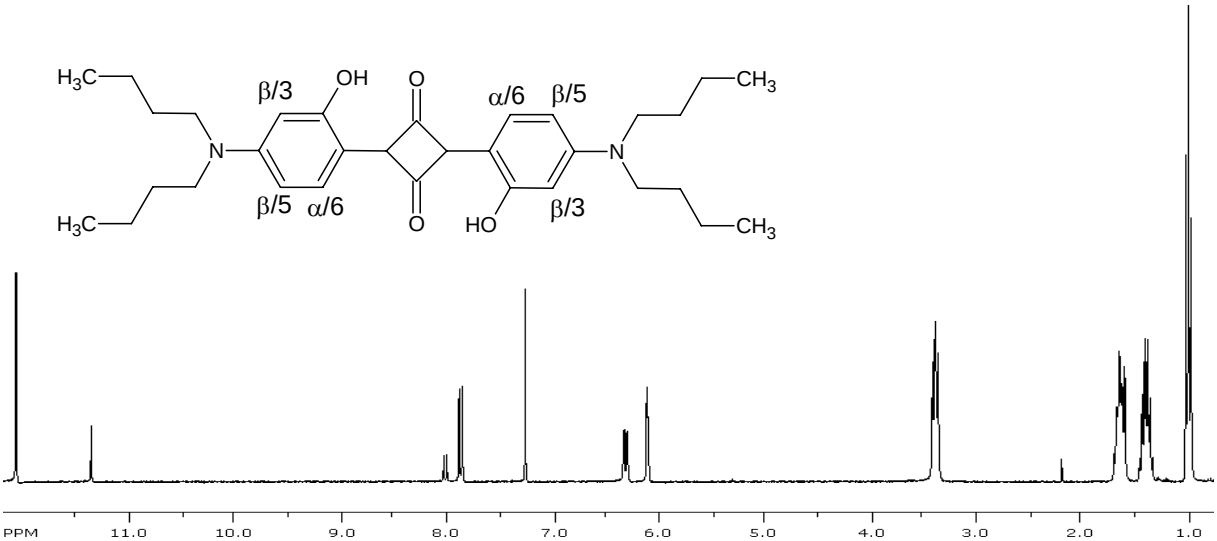

Figure 39: ^{1}H-NMR spectrum of bis[4-dibutylamino-2-hydroxyphenyl]squaraine, 300MHz, $CDCl_3$.

δ=12.09 (2H, s, OH); 7.87 (2H, d, ArH_{α}, $J_{Ar\alpha\beta5}$ =9.3Hz); 6.31 (2H, dd, $ArH_{\beta5}$, $J_{Ar\beta\beta}$ =2.8Hz); 6.10 (2H, d, $ArH_{\beta6}$); 3.37 (8H, t, NCH_2-, J=7.8Hz); 1.57-1.68 (8H, m, -C$\underline{H_2}C_2H_5$); 1.37 (8H, h, C$\underline{H_2}CH_3$, J=7,3Hz); 0.97 (12H, t, -CH_3).

The resonances observed are in agreement with the chemical shifts reported for squaraines (8.5ppm for aromatic α- and 7ppm for β-protons, [162]), considering that the electron-pushing effect of the hydroxyl groups can cause a shift towards lower magnetic field. Additional resonances at 11.38 and 8.02ppm are interesting since those are of the same relative intensity with respect to 12.09 and 7.87ppm and may indicate the presence of cis/trans- isomers.

3.2.2.11 1,6,7,12-Tetrachloro-*N,N'*-di(3-(1-morpholino)propyl)perylene-3,4,9,10-tetracarboxylic bisimide ("Cl-DMPBI")

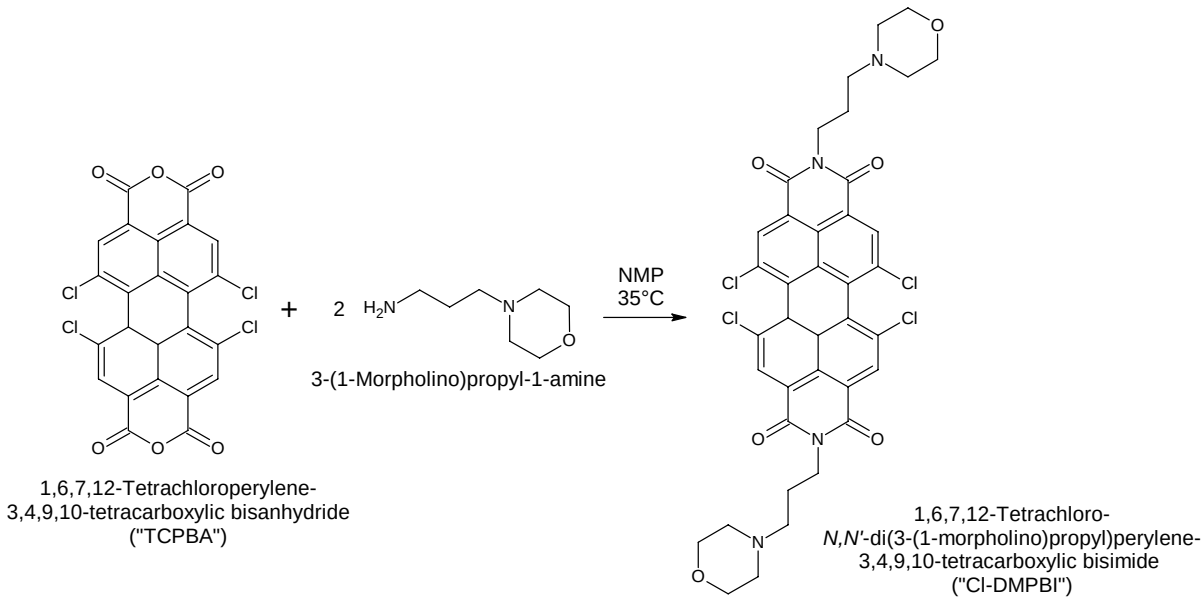

Scheme 13: Synthesis of 1,6,7,12-tetrachloro-*N,N'*-di(3-(1-morpholino)propyl)perylene-3,4,9,10-tetracarboxylic bisimide ("Cl-DMPBI").

TCPBA (1g, 1.89mmol) was dissolved in NMP (100ml), warmed to 35°C in a N_2 atmosphere and 3-morpholinopopyl-1-amine (578µl, 4.25mmol) in NMP (5ml) was added dropwise. After stirring for 2h, the reaction mixture showed extensive pH sensitivity. It was added in portions onto 400ml of saturated aqueous NaCl, containing 50mM HCl. The orange precipitate was separated by centrifugation, washed, redissolved in CH_2Cl_2, dried with Na_2SO_4 and purified by column chromatography with silica gel (0.04-0.063mm) as stationary and THF/$CHCl_3$ 30/70 as mobile phase, followed by recrystallization from CH_2Cl_2/EtOH. Cl-DMPBI was obtained as an orange powder, 1.14g (77%).

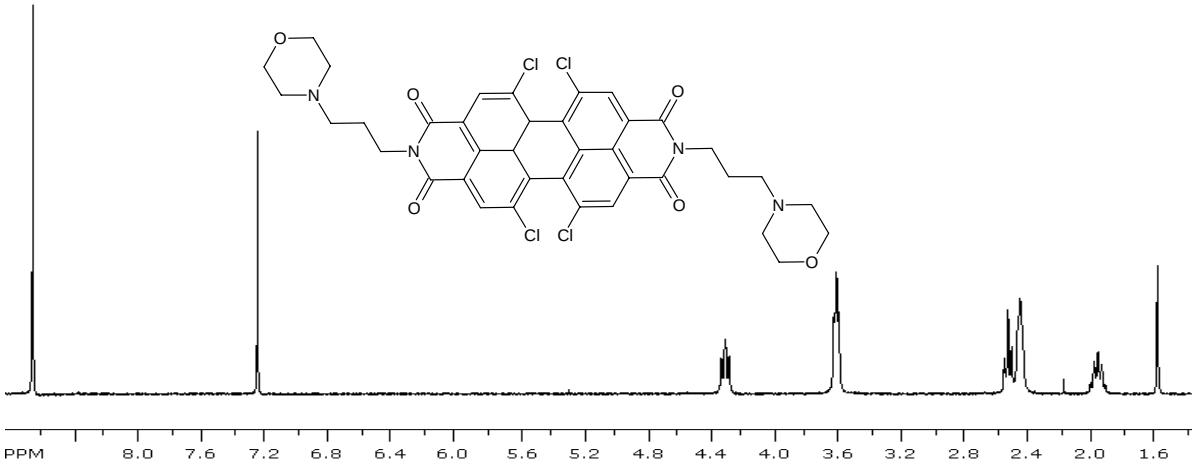

Figure 40: ^{1}H-NMR spectrum of Cl-DMPBI, 300MHz, $CDCl_3$.

δ=8.68 (4H, s, ArH); 4.31 (4H, t, $(CO)_2NCH_2$-, J=7.3Hz); 3.61 (8H, t, OCH_2-, J=4.4Hz); 2.52 (4H, t, $NC\underline{H}_2C_2H_5N(CO)_2$, J=6.8Hz); 2.45 (8H, t, $NC\underline{H}_2CH_2O$, J=3.9Hz); 1.86 (4H, p, $NCH_2C\underline{H}_2CH_2N$).

3.2.2.12 1,6,7,12-Tetraphenoxy-*N,N'*-di(3-(1-morpholino)propyl)perylene-3,4,9,10-tetracarboxylic bisimide ("PhO-DMPBI")

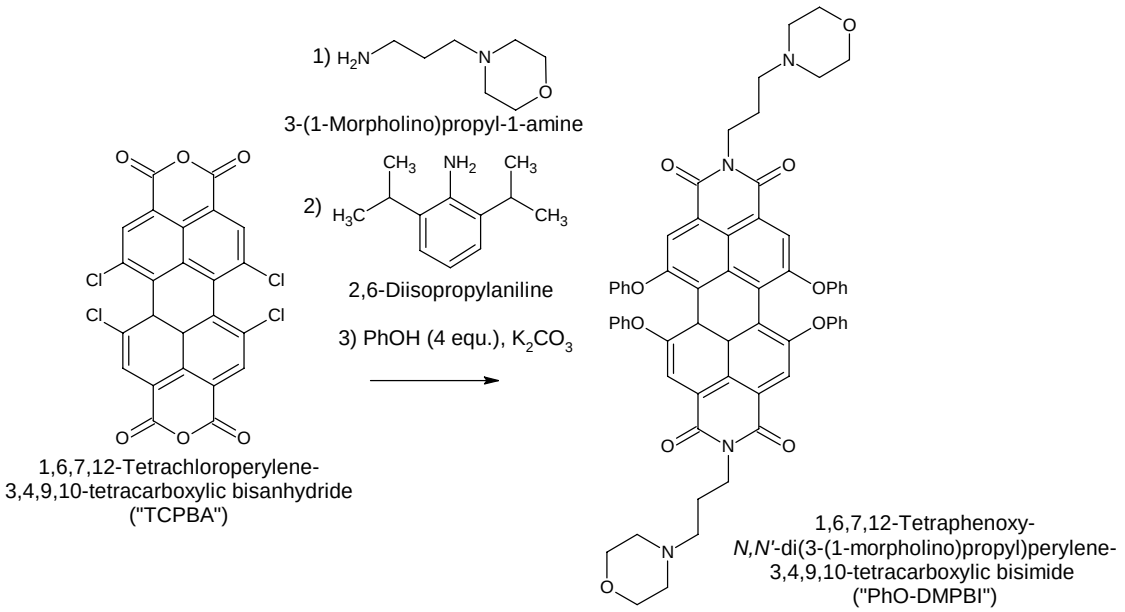

Scheme 14: Synthesis of 1,6,7,12-tetraphenoxy-*N,N'*-di(3-(1-morpholino)propyl)perylene-3,4,9,10-tetracarboxylic bisimide ("PhO-DMPBI").

This reaction was initially planned to provide the mixed imide with one 3-(1-morpholino)propyl and one 2,6-diisopropylphenyl substituent bound to the imide nitrogen atoms. Instead, PhO-DMPBI shown beyond was formed under the reaction conditions applied.

TCPBA (250mg, 0.47mmol) was added to NMP (20ml), heated to 50°C and 3-(1-morpholino)propyl-1-amine (69µl, 0.47mmol) in NMP (5ml) was added dropwise. The deep orange mixture was further heated to 75°C and 2,6-diispropylaniline (106µl, 0.56mmol) in NMP (5ml) was added dropwise. The reaction mixture now showed pH sensitivity, fluorescence being observable only in acidic solution. It was flushed with Ar for 15 minutes, phenol (450mg, 4.78mmol) and K_2CO_3 (750mg, 5.43mol) were added while the mixture was heated to 110°C. After stirring for 24h in a nitrogen atmosphere, absorption spectra of the reaction mixture indicated a red-shift to about 575nm. The mixture was carefully neutralized with $MeSO_3H$ and precipitated into a mixture of 10% aqueous NaCl/EtOH/acetone (85:10:5). The black precipitate obtained was separated by centrifugation, washed, redissolved in CH_2Cl_2 1:1, dried with $NaSO_4$ and purified by column chromatography with silica gel (0.04-0.063mm) as stationary and THF/$CHCl_3$ 50/50 as mobile phase, followed by recrystallization from CH_2Cl_2/EtOH. PhO-DMPBI was provided as a deep violet solid, 41mg (18%).

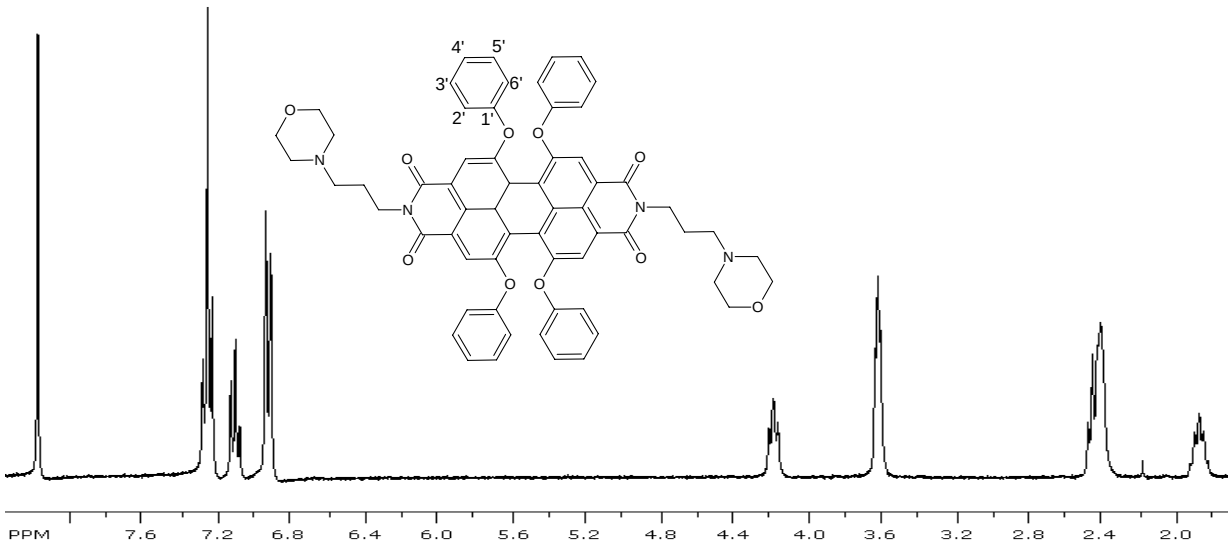

Figure 41: ^{1}H-NMR spectrum of PhO-DMPBI, 300MHz, $CDCl_3$.

δ=8.19 (4H, s, PhO-C-CH); 7.26 (8H, t, $Ar_{3'}H$, $J_{Ar2'3'}=J_{Ar3'4'}=7.6$Hz); 7.11 (4H, t, $Ar_{4'}H$); 6.93 (8H, t, $Ar_{2'}H$); 4.18 (4H, t, $(CO)_2NCH_2$-, J=7.2Hz); 3.61 (8H, t, OCH_2-, J=4.4Hz); 2.32-2.48 (12H, m, NCH_2-); 1.86 (4H, p, $NCH_2C\underline{H}_2CH_2N$, J=7.2Hz).

3.2.2.13 1,6,7,12-Tetra-(4-*tert*-butylphenoxy)-*N,N'*-di(3-(1-morpholino)propyl) perylene-3,4,9,10-tetracarboxylic bisimide ("tBuP-DMPBI")

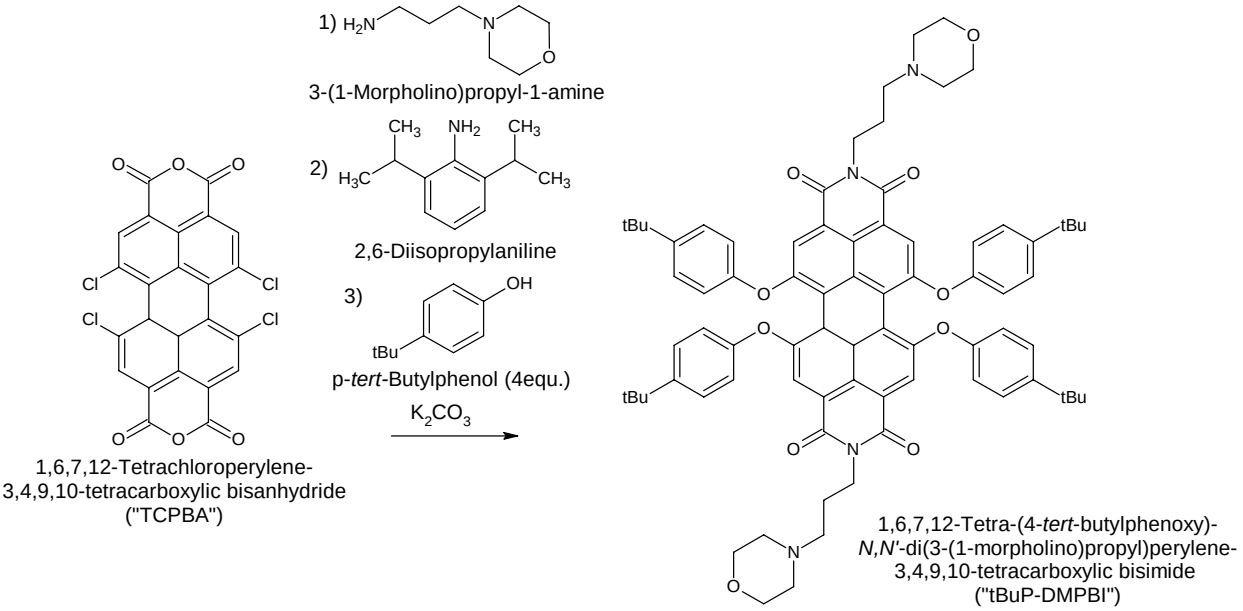

Scheme 15: Synthesis of 1,6,7,12-tetra-(4-*tert*-butylphenoxy-*N,N'*-di(3-(1-morpholino)propyl)perylene-3,4,9,10-tetracarboxylic bisimide ("tBuP-DMPBI").

This reaction was initially planned to provide the mixed imide with one 3-(1-morpholino)propyl and one 2,6-diisopropylphenyl substituent bound to the imide nitrogen atoms. Instead, tBuP-DMPBI shown beyond was formed under the reaction conditions applied.

TCPBA (250mg, 0.47mmol) was added to NMP (20ml), heated to 70°C and 3-(1-morpholino)propyl-1-amine (69µl, 0.47mmol) in NMP (5ml) was added dropwise. The deep orange mixture was further heated to 90°C and 2,6-diispropylaniline (106µl, 0.56mmol) in NMP (5ml) was added dropwise. The reaction mixture now showed pH sensitivity, fluorescence being observable only in acidic solution. It was flushed with Ar for 10 minutes, p-*tert*-butylphenol (750mg, 4.99mmol) was added and K_2CO_3 (810mg, 5.86mol) was added in portions while the mixture was heated to 120°C. After stirring for 24h in an Ar atmosphere, when absorption spectra of the reaction mixture indicated a red-shift to about 580nm, it was carefully neutralized with $MeSO_3H$ and precipitated into a mixture of 10% aqueous NaCl/EtOH/acetone (85:10:5). The black oil obtained was separated by centrifugation, washed, redissolved in acetone/CH_2Cl_2 1:1, dried with $NaSO_4$ and purified by column chromatography with silica gel (0.04-0.063mm) as stationary and THF/CH_2Cl_2 40/60 as mobile phase, followed by recrystallization from CH_2Cl_2/EtOH. tBuP-DMPBI was provided as a deep violet solid, 62mg (23%).

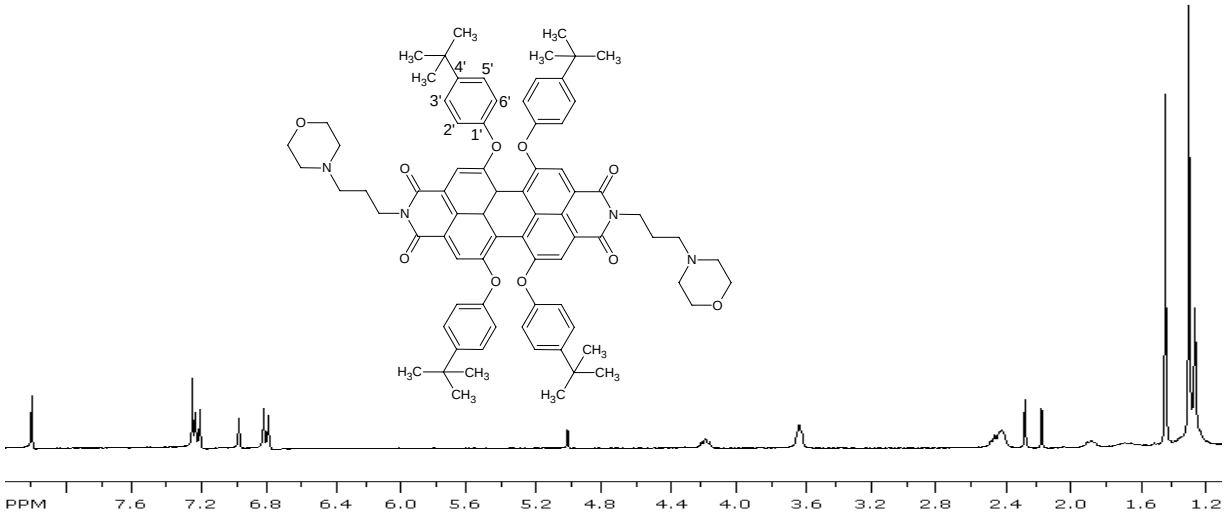

Figure 42: ^{1}H-NMR spectrum of tBuP-DMPBI, 300MHz, $CDCl_3$.

δ=8.22 (4H, s, *t*BuPhO-C-CH-); 7.23 (8H, d, Ar_3'H, J_{Ar}=8.7Hz); 6.82 (8H, d, Ar_2'H); 4.18 (4H, t, $(CO)_2NCH_2$-, J=7.3Hz); 3.62 (8H, t, OCH_2-, J=3.6Hz); 2.35-2.50 (12H, m, NCH_2-); 1.88 (4H, p, $NCH_2C\underline{H}_2CH_2N$, J=6.9Hz); 1.29 (36H, s, $-CH_3$).

Additional signals in this spectrum (δ=6.98; 5.01; 2.27; 1.43) are due to BHT which is contained in THF (eluent in chromatography) as a stabilizer.

3.2.2.14 1,6,7,12-Tetrachloro-*N*-(2,6-diisopropylphenyl)-*N'*-(3-(1-morpholino)propyl) perylene-3,4,9,10-tetracarboxylic bisimide ("Cl-AMPBI")

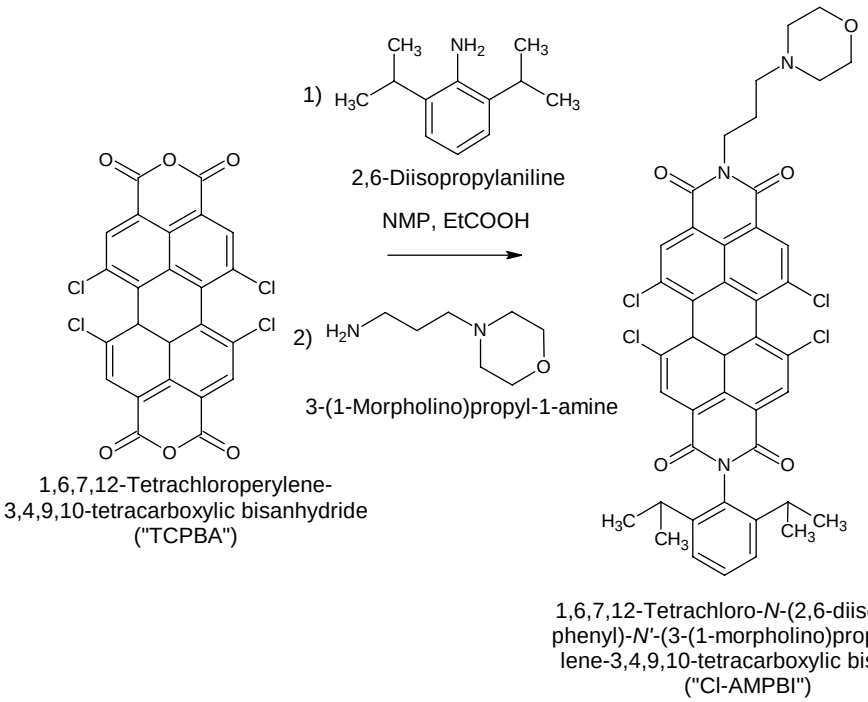

Scheme 16: Synthesis of 1,6,7,12-tetrachloro-*N*-(2,6-diisopropylphenyl)-*N'*-(3-(1-morpholino)propyl) perylene-3,4,9,10-tetracarboxylic bisimide ("Cl-AMPBI")

TCPBA (177mg, 0.33mmol) was dissolved in NMP (20ml) preheated to 60°C. Propionic acid (5ml) and 2,6-diisopropylaniline (68µl, 0.36mmol) were added and the mixture was heated to

110°C for 18h. After cooling to RT, 3-(1-morpholino)propyl-1-amine (52µl, 0.36mmol) in NMP (5ml) were added dropwise and the mixture was again stirred for 2h. TLC showed the formation of a new product:

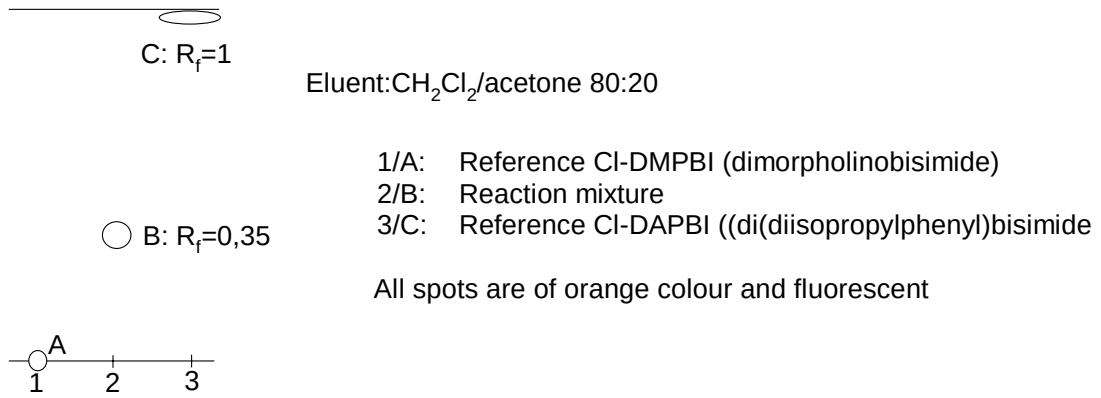

Figure 43: Sketch of TLC taken to monitor the synthesis of Cl-AMPBI

The mixture was added to 250ml of 100mM aqueous HCl, extracted with $CHCl_3$, the united organic phases were dried with Na_2SO_4 and the crude product was purified by column chromatography with silica gel (0.04-0.063mm) as stationary and CH_2Cl_2/acetone 80/20 as mobile phase. 28mg (10%) of Cl-AMPBI were obtained as orange crystals.

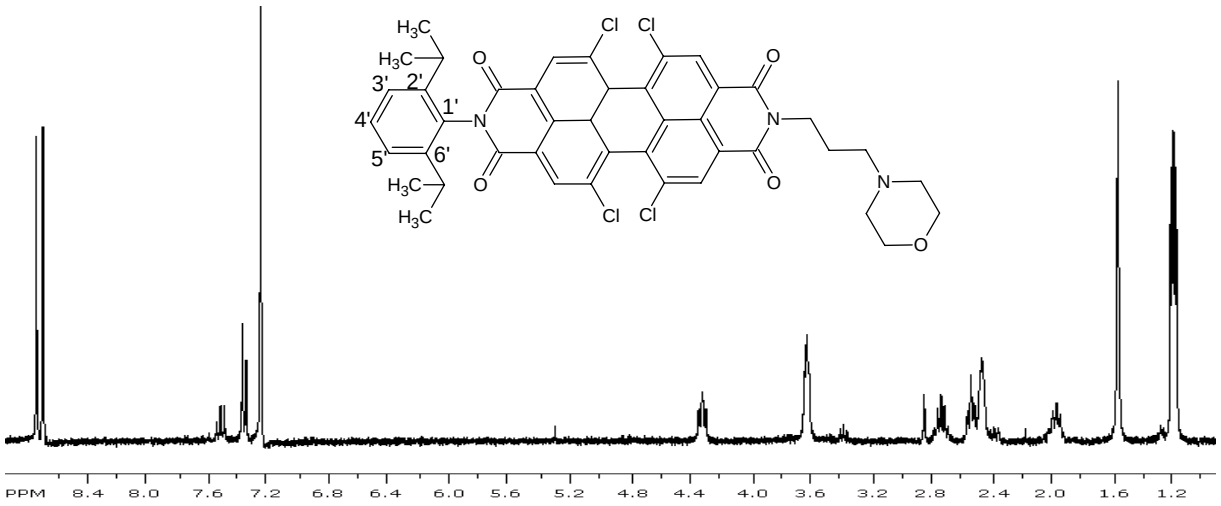

Figure 44: ^{1}H-NMR spectrum of Cl-AMPBI, 300MHz, $CDCl_3$

δ=8.75 (2H, s, Cl-C-CH-(1)); 8.71 (2H, s, Cl-C-CH-(2)); 7.53 (1H, t, $Ar_{4'}H$, J_{Ar}=7.6Hz); 7.37 (2H, d, $Ar_{3',5'}H$); 4.32 ($(CO)_2NCH_2$-, J=7.3Hz); 3.63 (4H, t, OCH_2-, J=4.5Hz); 2.73 (2H, m, -$C\underline{H}(CH_3)_2$, J=6.8Hz); 2.53 (2H, t, $NC\underline{H}_2C_2H_5N(CO)_2$, J=6.9Hz); 2.46 (4H, t, $NC\underline{H}_2CH_2O$ J=3.9Hz); 1.96 (2H, p, $NCH_2C\underline{H}_2CH_2N$, J=7.3Hz); 1.19 (12H, dd, -CH_3, J_1=6.7Hz, J_2=4.1Hz*).

*The two different couplings found for the methyl groups are most likely due to a rotational barrier between two methyl groups in the same isopropyl group. While the larger coupling constant can be clearly attributed to the vicinal carbon (δ=2.73, J is almost equal there), the smaller one is found for neither of the aromatic hydrogen atoms which only exhibit coupling between them.

The identity of Cl-AMPBI is clearly confirmed by this spectrum.

3.2.3 Dye Characterization

3.2.3.1 pH Calibration

For pH calibration, a concentrated solution of the dye to be investigated was prepared and diluted by such a ratio that absorption was between 0.05-0.2. That was achieved by adding 100mM aqueous buffer (phosphate, carbonate or citrate, depending on pH) corresponding to each pH to be measured and, to maintain constant ionic strength, 100mM aqueous NaCl in a ratio of 1:20 (V/V).
Sensitive layers on mylar support were affixed into a cuvette which was filled with the appropriate buffer/NaCl mixture. Prior to each measurement, the layer was washed three times with the buffer to be measured next.
pK_A values were determined from fluorescence emission spectra as those show much stronger acid/base dependence than absorption spectra. Anyway, pK values determined from absorption spectra are also stated in the corresponding calibration plots and denominated pK_A[a]. If possible, the isobestic point wavelength determined from absorption calibration was used for excitation. Since that was not well suitable for rhodamine dyes because of their small Stokes shifts, those were excited at shorter wavelengths. PET efficiency, here defined as acid/base induced change in fluorescence brightness when excitation is performed equally effective, was then corrected for absorption using the following equation:

$$E_{PET} = \frac{I_{acidic}}{I_{basic}} * \frac{I_{A,basic}}{I_{A,acidic}} = \frac{I_{acidic}}{I_{basic}} * \frac{\left(1-10^{-A_{basic}}\right)}{\left(1-10^{-A_{acidic}}\right)} \qquad \text{Equation 51}$$

E_{PET}	PET efficiency
I_{acidic}/I_{basic}	Sensitivity measured in pH calibration (ratio of converging emission intensities in acidic and basic solution)
$I_{A,basic}/I_{A,acidic}$	Ratio of light intensity absorbed in basic and in acidic solution
A_{acidic}	Converging value of absorption at the excitation wavelength in acidic solution
A_{basic}	Converging value of absorption at the excitation wavelength in basic solution

On the other hand, the more broad absorption range of perylenes (figure 26), together with their very weak acid/base induced shift of absorption spectra in polar environment, allows direct determination of PET efficiency from fluorescence calibration.

3.2.3.2 Surveying Acid/base Sensitivity in Organic Solvents

A concentrated dye solution was diluted with a large excess of solvent to be tested so that absorption was about 0.15. To samples of equal concentration was added either acidic or basic component, according to table 2 below, in small portions until fluorescence remained constant. The intersection of absorption spectra in acidic and basic media was used for excitation with a narrow excitation slit (2.5nm) in fluorescence measurement. For perylene dyes with various intersections, the one closest to the central absorption maximum of the acidic form (figure 26, for example) was chosen. Fluorescence spectra of acidic and basic form were re-

corded instantaneously and with equal spectrometer settings, intensities of acidic and basic sample, observed in the maximum of the acidic form, were divided.

Table 2: Acidic/basic reagents employed for surveying acid/base sensitivity in organic solvents. They were diluted by 100 with THF and added in small portions.

Solvent	Acid	Base
cyclohexene	CF_3COOH	TBAOH 1M in MeOH
toluene	CF_3COOH	TBAOH 1M in MeOH
$CHCl_3$	CF_3COOH	TBAOH 1M in MeOH
THF	$MeSO_3H$	TBAOH 1M in MeOH
acetone	$MeSO_3H$	1M aqueous NaOH
EtOH	$MeSO_3H$	1M aqueous NaOH

3.2.3.3 Determination of Fluorescence Quantum Yields

A suitable fluorescence standard with accurately known QY was chosen. Dye and standard were diluted to an absorption of about 0.05 at the excitation wavelength and excited at equal wavelength with a narrow slit (1nm) at the excitation monochromator. For acid/base sensitive dyes, dilute acid/base (according to table 2) were added in small portions until fluorescence was constant in order to determine QY of both forms. QY was calculated using the following equation:

$$\Phi_D = \Phi_S \frac{\int I_{F,D} d\lambda}{\int I_{F,S} d\lambda} \frac{1-10^{A_{S,Exc}}}{1-10^{A_{D,Exc}}} \frac{n_D^2}{n_S^2} \qquad \text{Equation 52}$$

Φ_D	Quantum yield of the dye to be measured
Φ_S	Quantum yield of the fluorescence standard
$I_{F\ D/S}$	Fluorescence intensity of the dye/standard
λ	Observation wavelength (nm)
$A_{D/S,\ Exc}$	Absorption of the dye/standard at the excitation wavelength
$n_{D/S}$	Refractive index of the solvent used for the dye/standard

Table 3: Solvents, acidic/basic reagents and standards used for the determination of fluorescence quantum yields.

Dye	Solvent	Refractive index[f]	Acid/base added	Standard
BPCR	H_2O[d]	1.330	aqueous HCl/NaOH	rhodamine B (EtOH)[a]
BuPCR	MeOH	1.329	aqueous HCl/NaOH	rhodamine B (EtOH)[a]
LiPA	EtOH	1.3600	-	rhodamine 101 (EtOH)[b]
SemiPR	EtOH	1.3600	aqueous HCl/NaOH	rhodamine 101 (EtOH)[b]
Squ[g]	acetone	1.359	aqueous HCl/TBAOH[e]	nile blue (EtOH)[c]
Cl-DMPBI	$CHCl_3$	1.445	CF_3COOH/TBAOH[e]	rhodamine B (EtOH)[a]
PhO-DMPBI	acetone	1.359	$MeSO_3H$/TBAOH[e]	rhodamine 101 (EtOH)[b]
tBuP-DMPBI	acetone	1.359	$MeSO_3H$/TBAOH[e]	rhodamine 101 (EtOH)[b]
Cl-AMPBI	$CHCl_3$	1.445	CF_3COOH/TBAOH[e]	rhodamine B (EtOH)[a]

[a] $\Phi_F = 0.70$ [117,118]
[b] $\Phi_F = 0.98$ [118]

[c] Φ_F = 0.27 [163]
[d] QY of the basic form was measured in MeOH
[e] 1M methanolic solution
[f] according to [164]
[g] bis[4-dibutylamino-2-hydroxyphenyl]squaraine

3.2.3.4 Photobleaching Experiments

Dye solutions with an absorption of 0.5 in the maximum were prepared and illuminated with a red LED (643nm). The cuvette containing the sample was placed in the focus of a curved mirror and its absorption was followed over time. Every measurement point was compared with a reference, an equal sample which had been stored in the dark over the entire illumination time.

3.2.4 Physical Entrapment into Polymeric Matrices

3.2.4.1 Fabrication of sensitive Layers

Polymer, dye and solvent were mixed in the amounts stated in table 4 below and the resulting cocktail was homogenized under vigorous stirring. Using a Pasteur pipette, it was put onto a mylar support as a smooth stripe and quickly coated with a coating knife to form a thin layer which was left to dry.

Table 4: Compositions of all cocktails for the preparation of the sensitive layers investigated, from left to right: Dye content with respect to the polymer, dye weight used, polymer fraction in the cocktail, polymer weight used, solvent, thickness of the coating knife used, absorption of the layer in the most intense maximum. Amounts are those required for the preparation of 2ml cocktail.

Dye	c_{Dye} (w/w)	m_{Dye} (mg)	f_{Poly} (w/w)	m_{Poly} (mg)	Solvent	Coating knife	A_{MAX}
RhODA	-	-	10%D4	165	EtOH/H_2O 9:1	75µm	0.05
Squ[a]	0.25%	0.6	10%D4	230	THF/$CHCl_3$ 1:1	25µm	0.82
PhO-DMPBI	0.25%	0.5	10%D4	190	THF	75µm	0.10
tBuP-DMPBI	0.25%	0.5	10%D4	190	THF	75µm	0.16
Cl-AMPBI	0.25%	0.5	10%D4	190	THF	75µm	0.20

3.2.4.2 Fabrication of sensitive PS/PVP Particles

PS/PVP particles (547µl of a 38% aqueous suspension, ρ=1.04g/ml, containing 200mg of particles) were added to a mixture of EtOH (80ml) and H_2O (40ml) and subsequently, bis[4-dibutylamino-2-hydroxyphenyl]squaraine (1mg, 2µmol), dissolved in EtOH (20ml), was added dropwise. The mixture was concentrated under reduced pressure to 10% of its original volume, H_2O (100ml) was added and the mixture was again concentrated to 20ml.

3.2.4.3 Fabrication of sensitive RL100 Particles

RL100 polymer (250mg) and bis[4-dibutylamino-2-hydroxyphenyl]squaraine (0.63mg, 1µmol) were dissolved in acetone (80ml) in a 400ml beaker and under agitation, a fourfold excess of H_2O was added. Acetone was evaporated under reduced pressure, and the resulting aqueous suspension was concentrated to 20ml.

3.2.5 Production and Characterization of Magnetic Particles

3.2.5.1 Production of Magnetic Core-particles

Polymer concentrate containing 10% (w/w) PSMA EF80 (Sartomere) in THF was mixed with commercial lipophilized magnetite EMG1300 (Ferrotec), 4% (w/w) suspension in anhydrous THF, to yield cocktails with the compositions listed in table 5 below. Using a sampler, the cocktail was added onto an excess of water within 1-2s while agitation was provided by a vortex mixer (1200min^{-1}). THF was removed in a stream of air and the brown suspensions were filtered through a syringe filter (Micropore, 400µm) to remove large aggregates (if present). Average sizes Z_{av} and polydspersity indices PDI of the particles were determined by DLS.

Table 5: Compositions of mixtures used for precipitation of magnetic core particles, from left to right: Total cocktail volumes, fraction of PSMA EF80 polymer in the cocktail, fraction of EMG 1300 magnetite particles, volume of water used for precipitation; Z_{av} and PDI of the magnetic particles obtained.

Name	V_C (ml)	f_{Poly} (%w/w)	f_{Mag} (%w/w)	V_{H2O}(ml)	Z_{av} (nm)	PDI
C1	4	1.0	0.2%	11	135.5	0.081
C2	4	1.0	0.2%	11	136.8	0.136
C3	4	1.0	0.2%	11	132.6	0.089
C4	4	1.0	0.2%	11	134.5	0.076
C5	4	1.0	0.2%	11	123.3	0.059
C6	4	1.0	0.2%	11	124.8	0.065
C7	4	0.6	0.12%	11	103.3	0.068
C8	4	0.6	0.12%	11	104.5	0.088
C9	4	1.0	0.2%	11	120.8	0.085
C10	4	1.0	0.2%	11	123.0	0.093
C11	4	1.0	0.2%	11	122.0	0.072
C12	4	1.0	0.2%	11	120.1	0.078
C13	5	0.5	0.1%	10	112.0	0.079
C14	4	1.0	0.2%	11	130.5	0.065

3.2.5.2 Core-shell Polymerization

All components were added to the core particles in form of aqueous solutions the concentrations of which are stated in % w/w in the following. AAM refers to acrylamide (bulk component), “Amine 1” to 2-aminoethylmethacrylate hydrochloride and “Amine 2” to *N*-(3-aminopropyl)methacrylamide hydrochloride (amino-functionalized monomers, AFMO), “Bis” to *N,N’*-methylenebisacrylamide (crosslinker), KPD to potassium peroxodisulfate and SDS to

sodium dodecylsulfate. Amine 1, Bis and SDS solutions were filtered through a syringe filter prior to use. KPD solutions were freshly prepared for each polymerization and all monomer solutions were stored at 4°C and used for no longer than 2 weeks.
AAM (10% solution) and Bis (2.5% solution) were added to core particle suspension (type and amount are stated in table 6 below) to achieve the amounts detailed in table 6. Water was added to reach the total volume stated. For polymerizations in basic media, 100µl of 1M NaOH per ml total volume were added. The resulting suspension was flushed with nitrogen. SDS (10% solution) was added to reach a concentration of 1.25mM and under stirring, the mixture was heated to 85°C, again flushed with N_2 and KPD (5% solution) was added to achieve a concentration of 1.2g/l. Either Amine 1 or Amine 2 (both 10% solutions) as AFMO was added afterwards. Unless otherwise stated, the AFMO was added 20min after KPD and polymerization was quenched after 1.5h with an excess of oxygen-saturated water. The core-shell particles obtained were washed at least three times by magnetic separation.

Table 6: Amounts and conditions employed for core-shell polymerization, from left to right: Amounts and type of core-particle suspension used (table 5), absolute amount of acrylamide (AAM), molar ratio of amino-functionalized monomer (AFMO; Amine 1 or Amine 2) with respect to AAM, molar ratio of crosslinker (Bis) with respect to AAM, total volume of the polymerization mixture; further deviations from the protocol given beyond are detailed in the rightmost column.

Name	Core particles	AAM	AFMO (%n/n)	Bis (%n/n)	V_{Total}	Remarks
CS1	5ml C1	68mg	-	2.5	10ml	a,5h
CS2	3ml C2	40mg	10Amine1	5.0	12ml	
CS3	5ml C3	68mg	10Amine2	5.0	10ml	a,3h
CS4	5ml C2	68mg	5Amine1	5.0	10ml	
CS5	1ml C4	14mg	-	2.5	2ml	
CS6	1ml C4	14mg	-	5	2ml	
CS7	1ml C4	14mg	-	7.5	2ml	
CS8	1ml C4	14mg	-	10.0	2ml	
CS9	1ml C4	14mg	-	12.5	2ml	
CS10	1mlC5	14mg	5Amine2	2.5	2ml	b
CS11	1mlC5	14mg	10Amine2	2.5	2ml	b
CS12	1mlC5	14mg	20Amine2	2.5	2ml	b
CS13	1mlC5	14mg	5Amine2	10	2ml	b
CS14	1mlC5	14mg	10Amine2	10	2ml	b
CS15	1mlC5	14mg	20Amine2	10	2ml	b
CS16	1mlC5	14mg	0Amine2	5	2ml	
CS17	1mlC5	14mg	2.5Amine2	5	2ml	
CS18	1mlC6	14mg	5Amine2	5	2ml	
CS19	1mlC6	14mg	7.5Amine2	5	2ml	
CS20	1mlC6	14mg	10Amine2	5	2ml	
CS21	1mlC6	14mg	5Amine2	2.5	2ml	
CS22	1mlC6	14mg	7.5Amine2	2.5	2ml	
CS23	1mlC6	14mg	10Amine2	2.5	2ml	
CS24	1mlC6	14mg	2.5Amine2	10	2ml	

CS25	1mlC6	14mg	7.5Amine2	10	2ml	
CS26	20mlC11+C12	271mg	-	5	25ml	
CS27	20mlC9+C10	270mg	0.5Amine2	5	25ml	
CS28	20mlC7+C8	258mg	5Amine2	5	25ml	
CS29	1mlC14	13.4mg	1Amine2	5	2ml	c
CS30	1mlC14	13.3mg	2Amine2	5	2ml	c
CS31	1mlC14	12.9mg	5Amine2	5	2ml	c
CS32	1mlC14	12.2mg	10Amine2	5	2ml	c
CS33	1mlC14	11.5mg	15Amine2	5	2ml	c
CS34	1mlC14	109mg	20Amine2	5	2ml	c
CS35	1mlC14	81mg	40Amine2	5	2ml	c
CS36	1mlC14	54mg	60Amine2	5	2ml	c
CS37	1mlC14	13.4mg	-	5	2ml	

[a] polymerization was quenched after time stated
[b] polymerization was carried out in basic media
[c] relative ratio in "Bis" is stated with respect to the total amount of monofunctional monomers

3.2.5.3 Aggregation Stability Testing

Stability in salt solutions was tested by diluting the original particle suspension by 30 with salt solution and storing it for 18h prior to DLS measurement. As salt solutions, 100mM NaCl/10mM phosphate buffer, pH7.4 (mimicking physiological conditions), 1M NaCl and 100mM phosphate buffer, pH 7.4 and 12, were employed.
To evaluate stability against magnetic concentration, particles were collected three times and resuspended. Afterwards, they were treated with sonication for 30min.

3.2.5.4 Covalent Dye Coupling

For labelling with CBF assisted by EDC/Sulfo-NHS, a protocol proposed for protein coupling was adapted [165,166]. Molar amounts of CBF (carboxy component) and CS particles (amino component) were calculated from the protein amounts proposed, under consideration of the average relative abundances of lysine, aspartic acid and glutamic acid [167,168] and the average molar mass of a protein per amino acid unit [169]. Because the ratio in amino groups per CS particle weight is unknown, for the calculation it was supposed that all AFMO introduced had been bound to the hydrogel shell and was accessible to coupling. Particle amount with respect to the dye was then varied according to table 7 below.
CBF (4.0mg, 10.8µmol) was dissolved in 100mM carbonate buffer (400µl), pH9.9, and added to a freshly prepared solution of EDC hydrochloride (3.8mg, 20µmol) and sulfo-NHS (10.9mg, 50µmol) in 100mM MES buffer (10ml), pH 5.45. The solution was stirred at RT for 20min and 2-mercaptoethanol (14µl, 0.16mmol) was added. After additional 10min, this activated CBF-NHS ester solution was added to a CS particle solution and the mixture was diluted with an excess of 250mM phosphate buffer, pH7.47, so that pH in the resulting mixture was in the range 7.03-7.29. The reaction mixture was left under continuous stirring for 2d,

then the CS particles were washed by magnetic separation with aqueous phosphate buffer, pH9.8, until no fluorescence was detectable in the washing buffer.
Amounts employed in all labelling experiments are listed below, in which each one was carried out three times.

Table 7: Amounts applied for fluorescent labelling with CBF, from left to right: Type of core-shell particles used (table 6), AFMO ratio upon core-shell polymerization, relative molar ratio of CBF to the amino functions in CS particles (if all AFMO is available in form of amino-functions), volumes of activated CBF solution added, volume of phosphate buffer (pH 7.47) added, volume of CS particle suspension used.

Name	CS Particles	AFMO (%n/n)	CBF:Amine n:n	V_{CBF}	V_{Buffer}	V_{Part}
LC1	CS28	5	2:1	926µl	2ml	0.06ml
LC2	CS28	5	1:5	926µl	2ml	0.6ml
LC3	CS28	5	1:100	46µl	1ml	0.6ml
LC4	CS27	0.5	2:1	926µl	2ml	0.6ml
LC5	CS27	0.5	1:5	93µl	1ml	0.6ml
LC6	CS27	0.5	1:100	46µl	1ml	0.6ml
LC7	CS26	0	-	93µl	1ml	0.6ml

For coupling with BuPCR, the exact same protocol was employed, with equal molar amounts of all components.

3.2.6 Zeta Potential Measurement

Concentrated particle suspensions were diluted with 100mM aqueous NaCl to give only slightly turbid samples. pH was adjusted using 100mM phosphate buffer, in a ratio not higher than 1:20 (V/V) with respect to NaCl. Zeta potential was measured by DLS.

3.3 Results and Discussion

3.3.1 Dye Synthesis and Characterization

3.3.1.1 *N,N'*-Bis-(3-azapentmethylene)-(4',5')carboxyrhodamine ("BPCR")

BPCR was obtained as a deep purple powder, highly water-soluble, showing bright orange luminescence only in acidic, but not in basic solution.

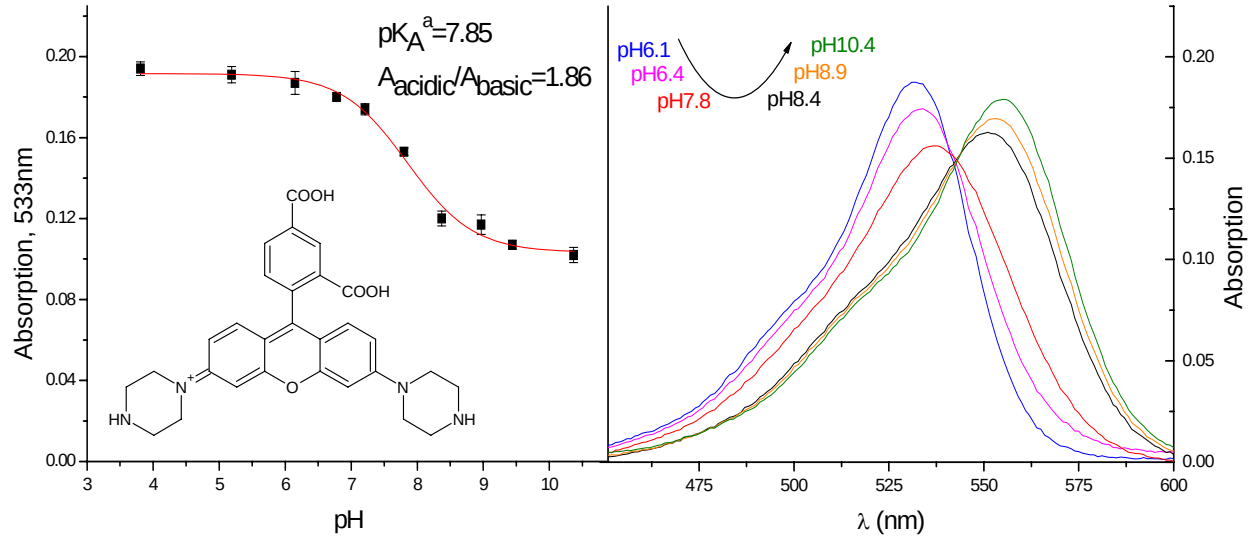

Figure 45: Absorption pH calibration of BPCR in H_2O shows a bathochromic shift for the basic form (λ_{MAX}=555nm) by over 20nm with respect to the acidic one (λ_{MAX}=532nm) with an isobestic point of 542nm. From that derives pH sensitivity when absorption is observed in the maximum of the acidic form.

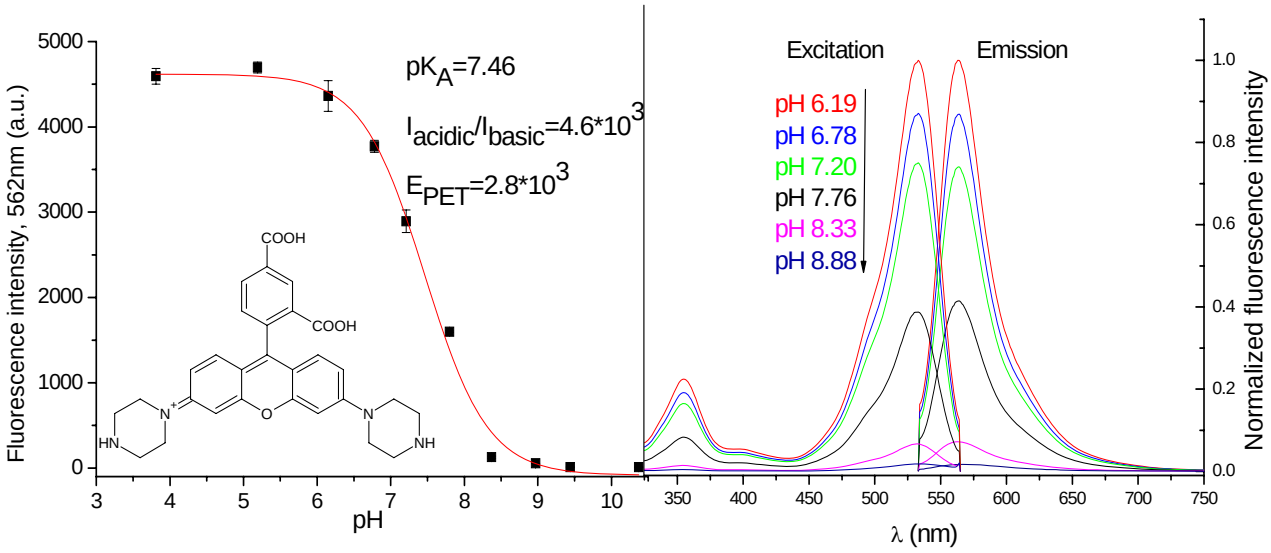

Figure 46: Fluorescence pH calibration of BPCR in H_2O, based on fluorescence emission measurement, λ_{EXC}=518nm, and the corresponding fluorescence emission and excitation (λ_{EM}=570nm) spectra. PET efficiency is so high that the dye comes down to an on-off switch. The pK_A value also matches the physiological range very well.

The spectral properties shown above meet those expected for a PET system (2.2.4), showing very pronounced changes in fluorescence intensity, unchanged shapes of fluorescence spectra and only minor variations in absorption spectra. The changes are fully reversible, as far as that is ascertainable without carrying out long-time studies.
The absorption maximum of the acidic form is at lower wavelength than the one of rhodamine B (545nm in MeOH) the substitution pattern of which is similar. Taking into account that a red-shift is observed in the order rhodamine 123, rhodamine 6G, rhodamine B (507,528, 545nm in MeOH, [117]) as the aromatic nitrogen atoms become substituted and their electron-pushing effect is increased, that may be related to the presence of the strongly electron-withdrawing protonated second nitrogen atoms in the piperazinyl groups. On the other hand, the maximum of the basic form is located between rhodamine B and rhodamine 101 (563nm in EtOH, [118]). That can be attributed to the weaker electron-withdrawing effect of the uncharged second nitrogen and the fact that the substituents are rigidised to a certain degree, similarly to rhodamine 101. The spectral shift between acidic and basic form is surprisingly large. That could derive from the strong inductive effect of two charged groups located close to the chromophore. Rhodamines are known to undergo certain changes in spectral properties related to the protolysis of the 2'-carboxy group and its inductive effect [118]. No such behaviour was detected at lower pH, corresponding to the pK_A of carboxy groups. Perhaps that effect is overcompensated for by interactions involving the piperazinyl groups. Fluorescence of the basic form is too weak to allow reliable determination of its maximum.
The pK_A value of 7.46 corresponds to the deprotonation equilibrium of the 4-position in the piperazine ring and is higher that $pK_{A,1}$ (5.68) in piperazine, which corresponds to deprotonation of a dication, but lower than $pK_{A,2}$ (9.82, [170]). The electron-withdrawing effect of the nitrogen in 1-position is, with respect to free piperazine, intensified by its conjugation with the aromatic system. Though two piperazine rings are present, only one transition is effective for pH calibration. As both groups are widely separated by a rigid system, the pK_A can be expected to differ only by the statistical value of 0.3 [171]. However, $pK_{A,2}$ may not be recognizable at all as the first protolysis step already causes PET so efficiently that its probability is not affected by the presence of a second free amino group.
Fluorescence QY (0.79) is higher than the one of rhodamine B (0.70) but lower than the one of rhodamine 101 (0.98, both in EtOH). That may correspond to the less extensive rigidization of the amino substituents, with respect to rhodamine 101, the high QY of which can be attributed to hindrance of IC by rigidization of the alkyl substituents [118].
BPCR is so hydrophilic that physical entrapment in a hydrogel is impossible as it is completely washed off the polymer instantaneously. For immobilization, it needs to be derivatized with a long-chained alkyl group (anchoring principle, 2.2.3) or covalently coupled. The anchoring group ought to be attached to the (4',5')-carboxy group, as such extensive lipophilization close to the amino moiety of the piperazine ring, which is responsible for PET, might cause that area of the dye to migrate into a hydrophobic part of the hydrogel where PET does not occur or is less effective. Because the secondary amino group in the piperazinyl function causes complication of the lipophilization reaction and most likely also would complicate covalent coupling with DCC (scheme 7), alkylation is necessary.

BPCR shows high brightness and excellent sensitivity in the physiological range, together with spectral properties typical for a rhodamine. It is therefore, in principle, well suited for applications in solution such as intracellular measurement, microscopy or three-dimensional imaging. For the preparation of sensors, derivatization is necessary and will be best carried out in the (4',5')-position.

3.3.1.2 Alkylation of *N,N'*-Bis-(3-azapentamethylene)-(4',5')carboxyrhodamine ("BPCR")

In this reaction a large number of products were formed, as displayed by figure 31. Those were not isolated, since chromatographic separation of such highly charged rhodamines turned out to be very complicated. Instead, alkylation of PipPh was tackled.

3.3.1.3 Alkylation of 3-(1-Piperazinyl)phenol ("PipPh")

Alkylation of PipPh with Bu_2SO_4 yielded the *N,O*-dibutyl derivative as main product. The *N*-alkylated product desired in the first place might have been formed as a side product (e.g. spot B, figure 32). However, attempts to carry out the reaction in the same way as described in 3.2.2.3 but with a smaller amount of Bu_2SO_4 and at lower temperature were shown by TLC to yield the same main product. Anyway, the product obtained here is also suitable for dye synthesis, as detailed in the following. Fortunately, no dialkylation of nitrogen was detected since that would make preparation of a PET dye impossible.

3.3.1.4 *N,N'*-Bis-(3-aza-3-butylpentamethylene)-(4',5')-carboxyrhodamine ("BuPCR")

Rhodamine synthesis was possible with the *O*-alkylated product obtained, probably because the ether group is cleaved by hot $MeSO_3H$ to in-situ form the free phenol. Indeed, the low yield of this step may have been caused by the fact that the ether has to be cleaved prior to dye formation. However, adapting protocol 3.2.2.4 by adding TMA to the reaction mixture after heating for 2h resulted in no dye formation at all, but smelly reduction products of $MeSO_3H$ were formed.
Despite the drawback of low yield, the synthetic approach via alkylation of PipPh can be rated superior to the alkylation of BPCR, because all components are cheaply available, and by alkylation of BPCR it is difficult to obtain a pure product.
BuPCR is deep purple, and, in comparison to BPCR, less soluble in water, but better soluble in MeOH and EtOH. Orange luminescence is observed only in acidic solution. Spectral and pH dependent properties are rather similar to BPCR (figures 45,46):

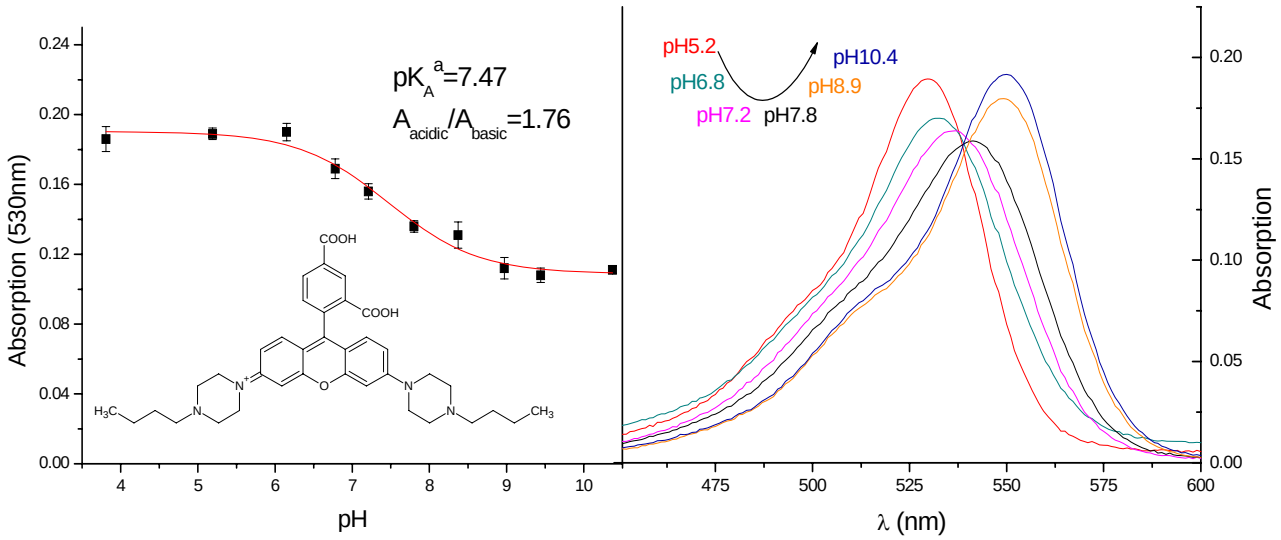

Figure 47: Absorption pH calibration of BuPCR in H_2O shows a bathochromic shift for the basic form (λ_{MAX}=550nm) by 20nm with respect to the acidic one (λ_{MAX}=530nm) with an isobestic point of 539nm. From that derives pH sensitivity when absorption is observed in the maximum of the acidic form.

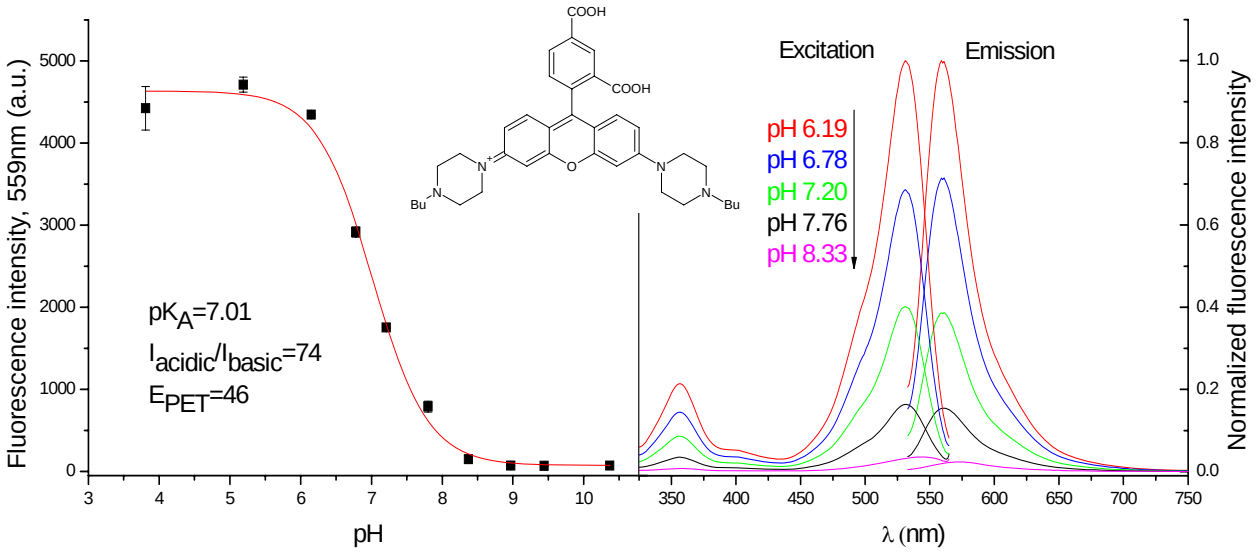

Figure 48: Fluorescence pH calibration of BuPCR in H_2O, based on fluorescence emission measurement, λ_{EXC}=515nm, and the corresponding fluorescence emission and excitation spectra (λ_{EM}=570nm). PET efficiency is so high that the dye comes down to an on-off switch. The pK_A value also matches the physiological range very well. Fluorescence emission is red-shifted by 20nm from 559nm (acidic) to 579nm in basic solution, an equal shift as observed with absorption.

Although both dyes are of on-off switch character, PET efficiency is by almost two orders of magnitude lower than the one of BPCR. That is surprising since a tertiary amino group can be expected to be of higher electron-density and therefore more oxidizable than a secondary one. The pK_A of BuPCR (7.01) is a little lower than the one of BPCR (7.46). It is not uncommon for secondary amines to be more basic than tertiary ones for steric reasons [172]. BuPCR also matches physiological range well. As with BPCR, pK_A^a determined from absorption is higher

than pK_A calculated from fluorescence. pK_A is more reliable here because of the much stronger pH dependence of fluorescence intensity.
Fluorescence QY (0.88) is higher than the one of BCPR (0.79). That is a little surprising since one can expect the butyl chains to enhance IC. However, non-radiative deactivation can involve other processes as well (3.1.2).

BuPCR shows similar properties to BPCR. Its pK_A is a little lower (7.01 compared to 7.46) and therefore it is better suited for applications at lower pH than BPCR. Its preparation is more laborious, but it constitutes an intermediate for the derivatization of the (4',5')-carboxy group.

3.3.1.5 *N,N'*-Bis-(3-aza-3-butylpentamethylene)-(4',5')-octadecylaminocarboxyrhodamine ("RhODA")

As stated in 3.2.2.5, RhODA shows spectral properties very similar to BPCR and BuPCR, but is much more lipophilc.

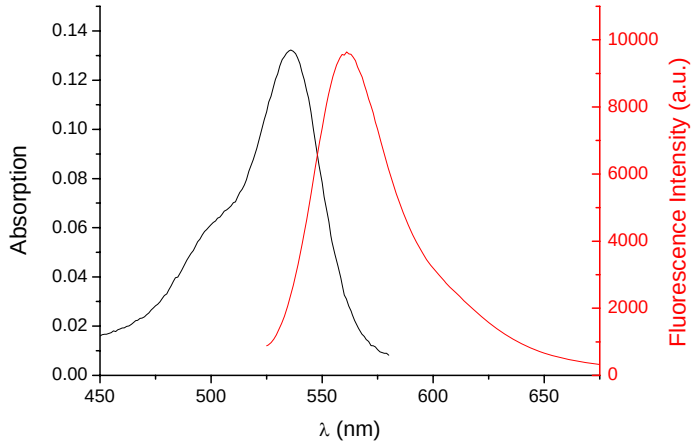

Figure 49:Absorption and fluorescence emission, λ_{EXC}=510nm, spectra of RhODA in $CHCl_3$ acidified with CF_3COOH. The spectra are similar in shape and spectral location ($\lambda_{ABS,MAX}$=536nm; $\lambda_{EM,MAX}$=561nm) to BuPCR (figure 48). Absorption is essentially absent in neutral or basic solution, probably due to lactonization.

Embedded into a hydrogel layer, RhODA showed no signs of significant leaching (when stored in aqueous buffer for 12h, the buffer showed no fluorescence while the absorption of the layer remained constant). pH calibration in a hydrogel layer is shown in the following:

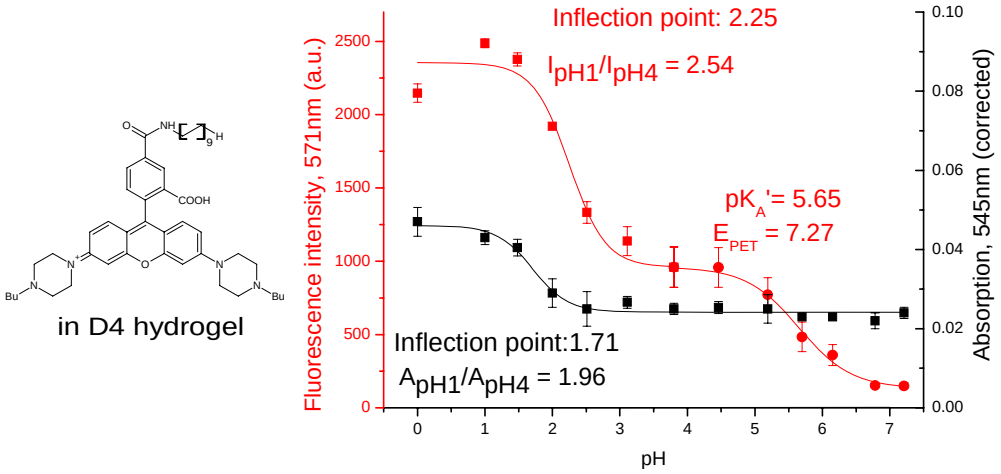

Figure 50: pH calibration of RhODA in D4 hydrogel derived from absorption and fluorescence emission spectra, λ_{EXC}=515nm. A PET related transition at pH = 5.6 and a lactonization related one at pH=2.5 can be observed.

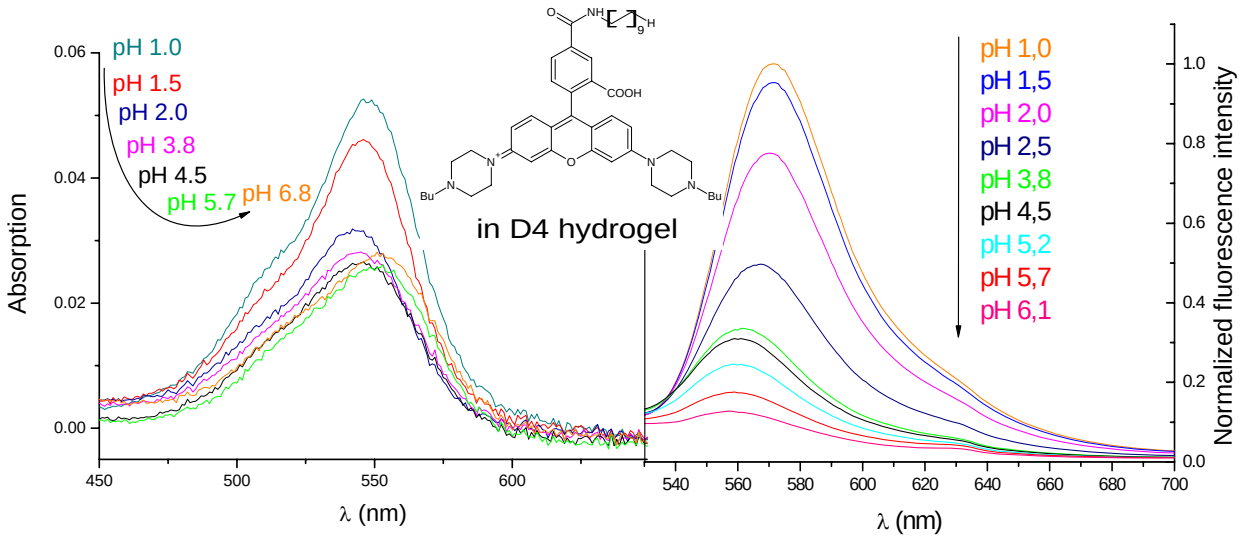

Figure 51: Absorption and fluorescence emission spectra of RhODA in D4 hydrogel, corresponding to figure 50. Absorption at increasing pH shows a hypochromic shift between pH1-4 and a bathochromic one (546nm to 551nm) between pH 4-7. Fluorescence there undergoes a two step-decrease in intensity and a hypsochromic shift (571 to 558nm).

In figure 50, the equilibrium at pH=5.65 has been identified as PET related since fluorescence intensity is altered while absorption remains essentially unchanged. An apparent pK_A' of 5.65 can allow sensing in biotechnological samples where pH~6 is not uncommon. PET efficiency is not as high as in solution (sevenfold, compared to the on-off switch character of BuPCR in aqueous solution) but still enables good sensitivity. Some dye molecules might be located in hydrophobic areas inside the hydrogel where PET does not occur, still causing some fluorescence at basic pH. Compared to BuPCR in aqueous solution, the apparent pK_A' value is shifted by about 1.5 units to the acidic, in agreement to the behaviour outlined in 2.2.4. Interestingly, the fluorescence maximum is considerably blue-shifted with increasing pH which is

in contrast to absorption spectra as well as to the behaviour of BPCR and BuPCR. There is a red-shift in absorption spectra at basic pH, but it is much less pronounced than for BPCR and BuPCR (5nm compared to around 20nm), corresponding to a more long-wave absorbing acidic (546nm compared to 530nm for BuPCR in solution), but not basic (551nm, 550nm for BuPCR) form.
However, a second equilibrium is clearly recognizable at lower pH. The decrease in fluorescence intensity is there accompanied by a decrease in absorption. This transition is most likely caused by lactonization of the dye (3.1.2). The lactonization equilibrium could be associated with the protolysis of a carboxy group, although that would be supposed to correspond to higher pH. Lactonization is only partial, some dye molecules do not suffer from it, possibly because they are located in more hydrophilic areas of the hydrogel where lactonization is not favourable. At around pH=2, about 50% of the dye molecules undergo lactonization and are not available to the PET related transition at higher pH. In practice, that will not only cause a loss in sensitivity of the layer, but also further complications (irreproducibility of sensor preparation, unstable signals, complication of calibration by additional, lactonization related equilibria). For application in polymer matrices, esterification of the 2'-carboxy group, which prevents lactonization, would therefore be desirable.

RhODA is in principle pH-sensitive in a hydrogel matrix, though its pK_A (5.65) is a little low for most applications. Unfortunately, it undergoes lactonization in a hydrogel matrix. That decreases sensitivity and is likely to complicate measurement. The preparation of 2'-esterified rhodamines was therefore tackled.

3.3.1.6 Amidation of Rhodamine 101

This experiment was carried out in order to test if amidation of the (sterically hindered) 2'-carboxy function in a rhodamine is possible. That would facilitate a straightforward synthetic strategy since derivatization prevents lactonization at the same time, and commercially available starting material (rhodamine B or 101) could be used. Furhter modification could be achieved, for instance, in the following way:

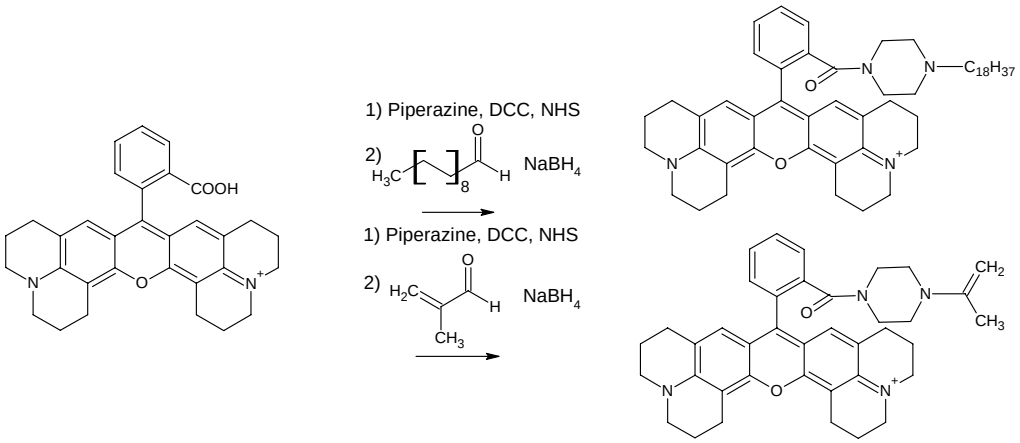

Scheme 17: Possible synthetic routes towards PET rhodamines starting from rhodamine 101, assuming that amidation of the 2'-carboxy function is possible. The octadecyl group would make the dye lipophilic (top, right), while with methacroleine a polymerizable dye could be available (bottom, right).

Equivalent modification with sulforhodamines has been reported by Zenkl [173]. As reported in 3.2.2.6, piperazine and octylamine were used as amino components. Those were chosen because it should be easy to detect if the reaction was successful, as piperazine is supposed to yield a pH sensitive dye while octylamine should make it much more lipophilic. However, none of both was detected. It was therefore concluded that direct amindation of the 2'-position in rhodamines with DCC is not possible due to steric hindrance.

3.3.1.7 Lissamine rhodamine B-4'-piperazinyl amide ("LiPA")

The strategy outlined in the previous section can be adapted attaching the piperazinyl function to the (4',5')-position.

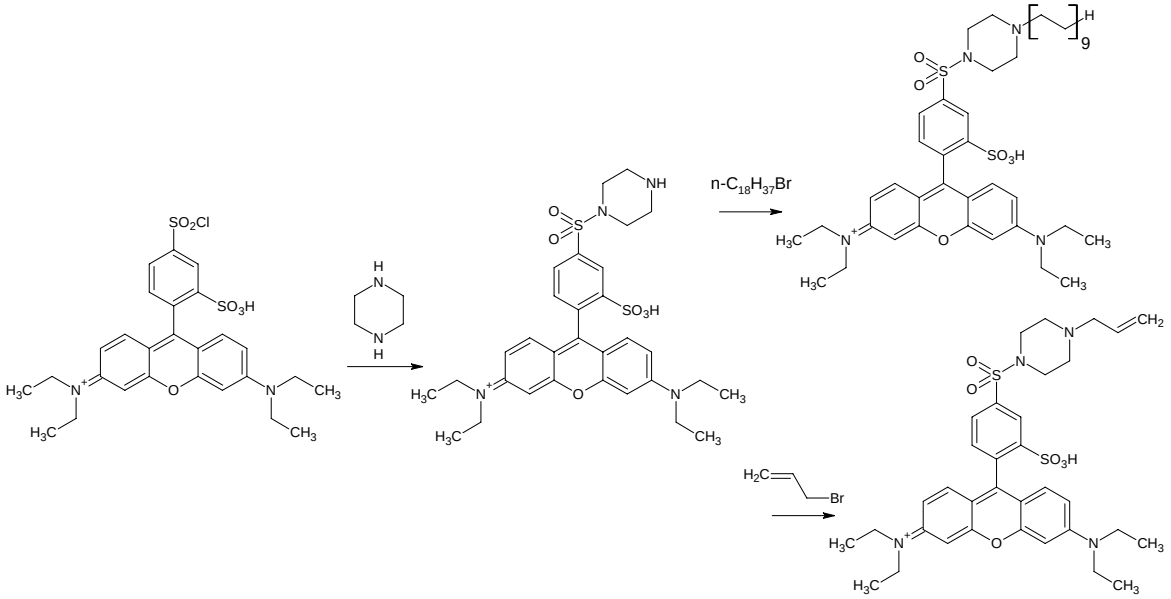

Scheme 18: Examples for possible synthetic routes towards PET rhodamines starting from lissamine rhodamine B, assuming that amidation of the (4',5')-position with piperazine yields a pH sensitive dye. The octadecyl group would make the dye lipophilic (top, right), while with allyl bromide a polymerizable dye would be available (bottom, right).

Attachment of a piperazinyl group to the 4'-position was successful and spectral properties of the product are similar to sulforhodamine B (table 8) though fluorescence QY is significantly lower (0.48, compared with 0.91 reported for sulforhodamine B, [174]). Unfortunately, none of the product fractions obtained shows any pH sensitivity at all.

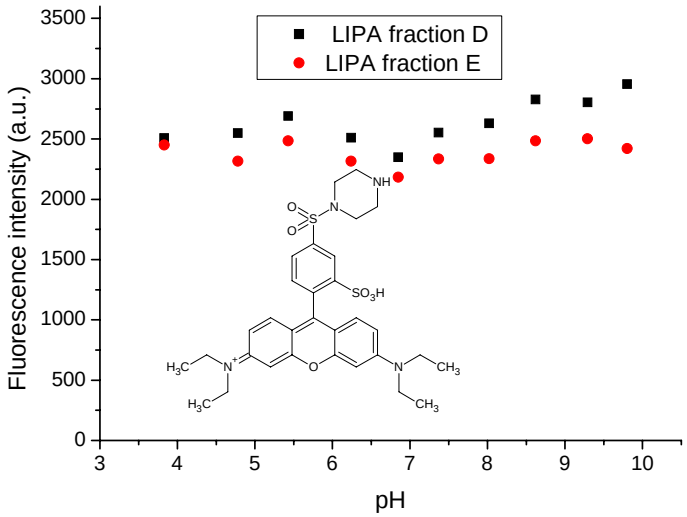

Figure 52: pH calibration of the product fractions obtained according to 3.2.2.7 where fraction D is the main product identified by NMR spectroscopy and E is the side product. Neither shows any signs of PET effect at all.

It was concluded that amidation of the 4'-carboxy position in rhodamines is not a suitable route towards PET rhodamines. The lack of sensitivity could be cause by the larger distance between PET functionality and chromophore, compared to B(u)PCR.

3.3.1.8 *N*-(3-Azapentamethylene)-*N'*,*N'*-dibutylrhodamine ("SemiPR")

Synthesis of SemiPR was enhanced in order to realize the following synthetic strategy:

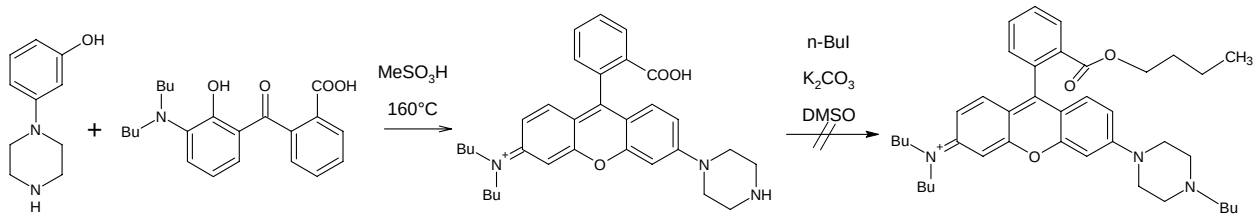

Scheme 19: Concept for the preparation of a PET rhodamine that cannot undergo lactonization for application in polymer matrices.

SemiPR is a violet solid of significantly less hydrophilic character than BPCR or BuPCR, being poorly soluble and weakly fluorescent in water. Solubility in H_2O/EtOH mixtures is much better and orange luminescence is stronger in acidic than in basic solution. SemiPR is also soluble in organic solvents such as THF or EE, but the solution is only weakly coloured, particularly under basic conditions. That is most likely caused by lactonization.
Acid/base sensitivity of SemiPR in H_2O/EtOH mixtures increases with EtOH content. pH calibration was performed in EtOH/H_2O 1:1 and in pure H_2O.

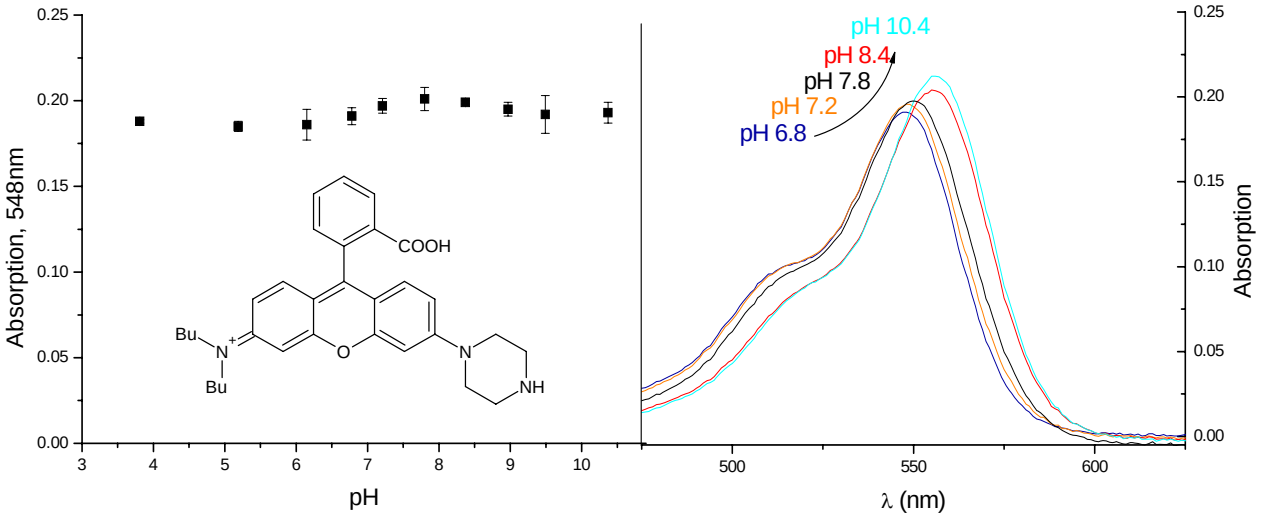

Figure 53:Absorption pH calibration of SemiPR in EtOH/H_2O 1:1 shows a small hyperchromic and bathochromic (λ_{MAX}=555nm, compared to λ_{MAX}=548nm in acidic solution) shift in basic media. Absorption in the maximum of the acidic form is virtually independent on pH.

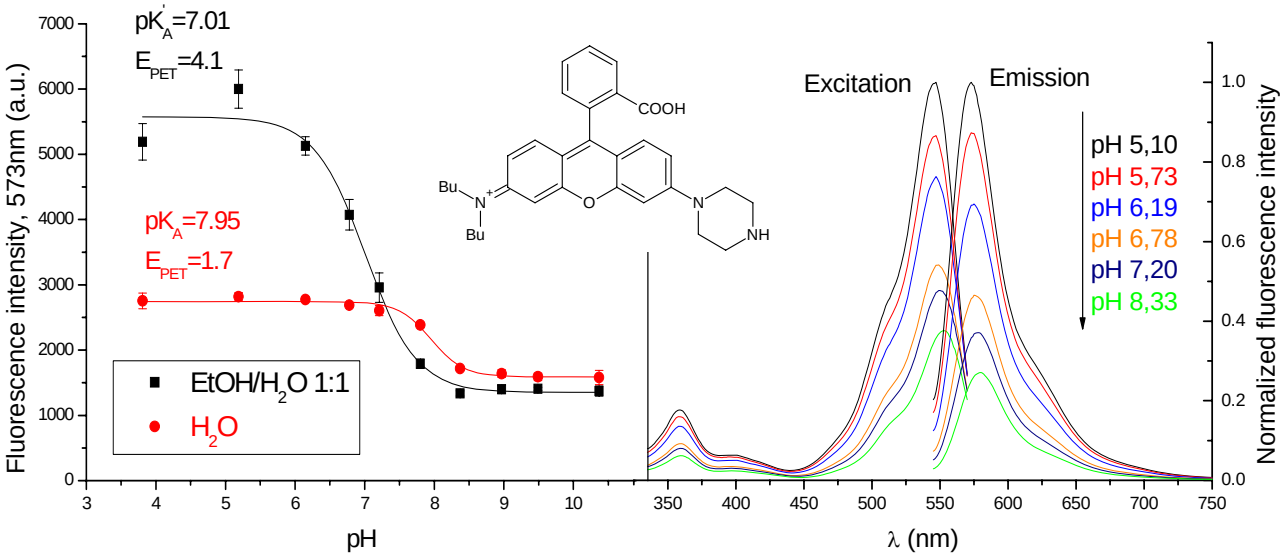

Figure 54: Fluorescence pH calibration of SemiPR, based on fluorescence emission measurement, λ_{EXC}=545nm, carried out in water and in EtOH/H_2O 1:1. Corresponding fluorescence emission and excitation spectra (λ_{EM}=580nm) were recorded in EtOH/H_2O 1:1. Fluorescence emission is red-shifted by 8nm to 581nm in basic solution, similarly to absorption. PET efficiency is strongly dependent on the solvent, moderate in EtOH/H_2O 1:1 and poor in water. Both pK_A in water and pK_A' in EtOH/H_2O 1:1 match the physiological range.

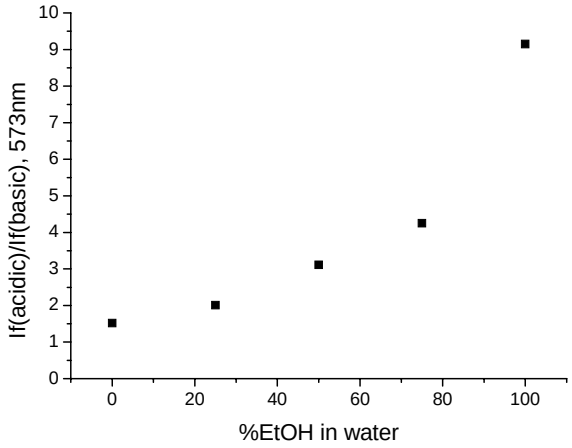

Figure 55: Comparison of acid/base sensitivity of SemiPR (2.4µM) in different EtOH/H_2O mixtures, displayed as ratio between fluorescence intensity measured in the emission maximum (λ_{EXC} = 533nm) in 16mM HCl and 16mM NaOH.

PET efficiency is much lower than for the rhodamines carrying two piperazinyl functions, BPCR and BuPCR (table 8). That is remarkable, apparently the excited chromophore is not efficiently reduced by one piperazinyl function. Furthermore, it is uncommon that PET is enhanced in apolar media. That could be related to the dependence of fluorescence QY of the acidic form on the solvent. Fluorescence is actually very weak in acidic aqueous solution, and though it is obviously enhanced as EtOH is added, QY still is as low as 0.18 in EtOH. Such a low value may be caused by the longer butyl chains which are expected to enhance IC. However, the even worse brightness in water seems likely to be related to the low water-solubility of the dye even in acidic solution. Because rhodamines are known to undergo lactonization in basic media, acid-base sensitivity (and its enhancement with increasing EtOH content) might be partially caused by lactonization of the basic form, although absorption spectra in EtOH/H_2O 1:1 did not point towards that (absorption was actually more intense in basic media). Still, the basic form shows much stronger fluorescence (even visible with the naked eye) than the ones of BPCR and BuPCR so that the high PET efficiency of those appears to be introduced by the second piperazinyl group.

Compared to BPCR and BuPCR, the absorption of the acidic form is red-shifted and the bathochromic shift of the basic one is less pronounced so that the basic forms of all three dyes show similar absorption maxima (table 8). That can be explained with the weaker overall electron-withdrawing effect of only one charged piperazinyl group in the acidic form.

Compared to BPCR, the pK_A value observed in water is lower and differs from it by 0.45 which is not far from the statistical value of 0.3 for deprotonation probability of two independent acidic groups [171]. The lower apparent pK_A' in 50% ethanolic solution can be attributed to the lower polarity of the solvent.

Consequently, SemiPR is much less suitable for pH sensing in solution because it is much less sensitive and sensitivity in water is very poor. SemiPR cannot be characterized in a hydrogel layer since it is washed off within a few minutes. Anyway, if such a layer is prepared, it turns almost white as the solvent evaporates (the same behaviour was observed with RhODA). That indicates that lactonization still is likely to be an issue and esterification of the 2-carboxy

function (scheme 19) is required. However, based on the observations described in 3.2.2.9, it was concluded that SemiPR undergoes double alkylation before the carboxy group is esterified. That makes prevention of lactonization rather complicated as insertion of protective groups would be required.

SemiPR is only weakly fluorescent in aqueous solution, probably due to limited solubility. Its pK_A value is not very different from BPCR, but sensitivity is much lower and the dye is not of on-off switch character. One piperazinyl group is thus not sufficient to allow high PET efficiency. Furthermore, attempted esterification of the 2'-carboxy position leads to double alkylation of the piperazinyl group and therefore results in total loss of sensitivity. That complicates the preparation of any PET rhodamine as an amino function always will be present. Rhodamines also offer only limited accessibility to extension of the chromophore for the preparation of more long-wave excitable dyes. Therefore, no further effort was taken to obtain a PET rhodamine for application in immobilization matrices.

The properties of all prepared rhodamines are summarized below:

Table 8: Properties of rhodamines in acidic/basic form, from left to right: Top: fluorescence quantum yields, absorption maxima wavelengths. Bottom: molar absorption coefficients in the maximum, emission maxima wavelengths, pK_A values determined from fluorescence emission spectra, pK_A[a] values determined from absorption spectra, PET efficiency. Unless otherwise stated, all parameters were determined in water.

Dye	Φ_F	$\lambda_{ABS,\ MAX}$ (nm)
BPCR	0.79±0.02 /(8±1)*10^{-4}(H_2O/MeOH)	532/555
BuPCR	0.88±0.01/(13±3)*10^{-3}(MeOH)	530/550
RhODA	-	546/551[a]
LiPA	0.48±0.01(EtOH)	567[c]
SemiPR	0.18±0.02/0.073±0.01(EtOH)	548/555[b]

Dye	ε_{max} ($M^{-1}cm^{-1}$)	$\lambda_{EM.\ MAX}$ (nm)	pK_A	pK_A[a]	E_{PET}
BPCR	8.13*10^4/7.36*10^4	562/-	7.46	7.85	2.8*10^3
BuPCR	8.69*10^4/8.51*10^4	559/579	7.01	7.47	46
RhODA	-	571/558[a]	7.27[a]	-	7.3[a]
LiPA	9.32*10^4	591[c]	-	–	-
SemiPR	8.43*10^4/9.14*10^4 [b]	573/581[b]	7.01[b]	7.95[b]	4.1[b]

[a] in D4 hydrogel layer
[b] in EtOH/H_2O 1:1
[c] in EtOH

3.3.1.9 Bis[4-dibutylamino-2-hydroxyphenyl]squaraine

An intensely absorbing, very bright long-wave excitable dye has been synthesized in an astonishingly simple way. It presents intermediate solubility in organic solvents (more than 1% in THF) and is in low concentrations also soluble in EtOH/H_2O. Acidic solutions are bright blue, while basic solutions are violet in organic solvents and dark blue in EtOH/H_2O.

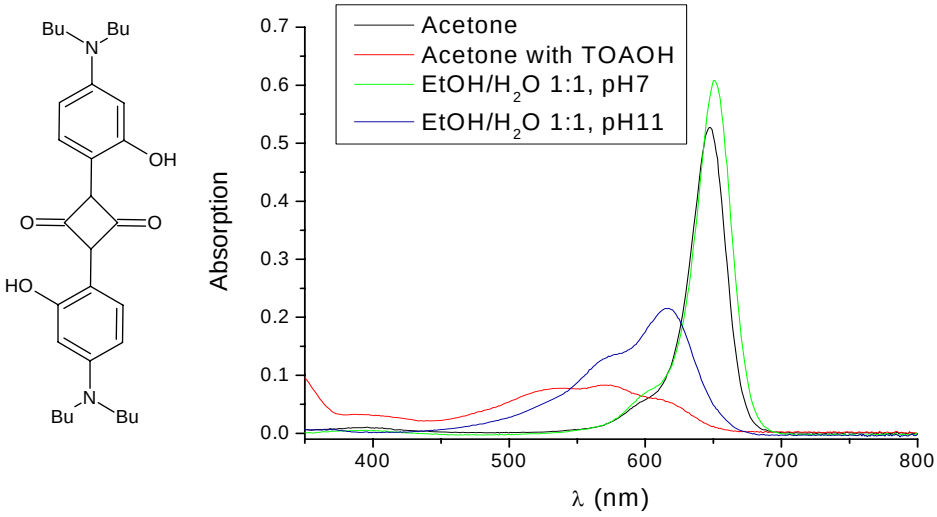

Figure 56: Absorption spectra of bis[4-dibutylamino-2-hydroxyphenyl]squaraine, 1.7µM in acetone/acetone 0.03%TOAOH/EtOH:H_2O 1:1, 3mM phosphate buffer pH7/pH11.

The broad, distorted shape of the spectrum in basic acetone could originate from aggregation. Bis[4-dibutylamino-2-hydroxyphenyl]squaraine also features excellent pH sensitivity, as the basic form is virtually non-fluorescent.

Fluorescence brightness is roughly 2 times lower in EtOH/H_2O than in acetone. That still implies good brightness, as ε is very high and Φ_F as high as 0.81 in acetone.

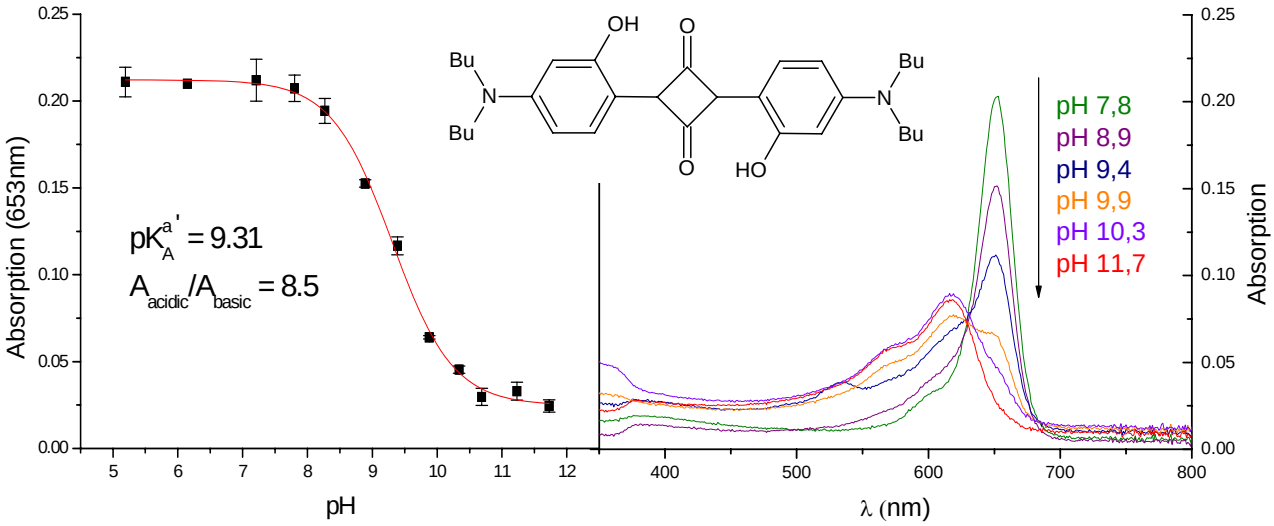

Figure 57: Absorption pH calibration of bis[4-dibutylamino-2-hydroxyphenyl]squaraine in EtOH/H2O 1:1 shows a hypsochromic shift for the basic form (λ_{MAX}=652nm) with respect to the acidic one (λ_{MAX}=618nm). Absorption in the maximum of the acidic form is strongly dependent on pH while there is a clear isobestic point at 631nm.

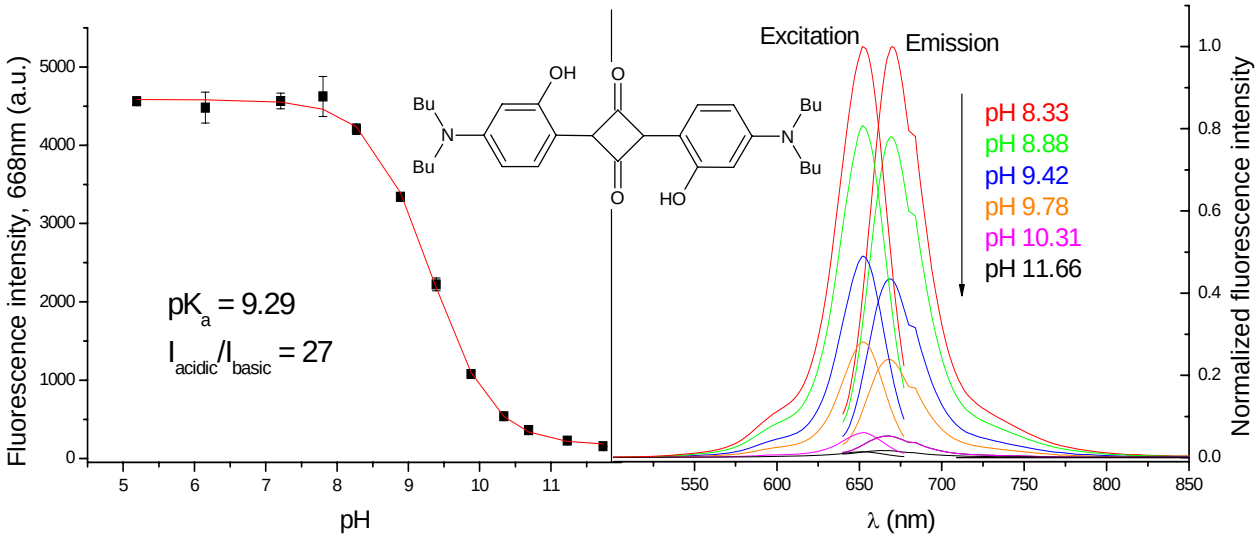

Figure 58: Fluorescence pH calibration of bis[4-dibutylamino-2-hydroxyphenyl]squaraine in EtOH/H2O 1:1, based on fluorescence emission measurement, excited in the isobestic point (λ_{EXC}=631nm) and corresponding fluorescence emission and excitation spectra (λ_{EM}=690nm) show high acid/base sensitivity in an elevated pH area.

This dye is a typical example for a pH indicator that undergoes neither PET nor PPT (class C, section 2.2.4), all spectra being strongly pH dependent. The apparent pK_A' measured in principle enables sensing in marines systems as the pH of seawater and marine sediment is within 7,2-9,2 [43]. 9.31 is a common pK_A value for a phenolic system and is similar to values published for a comparable system [135]. The presence of an isobestic point indicates that the basic form is soluble in the calibration medium. All acid-base induced spectral changes are reversible in solution. In contrast to absorption spectra, emission spectra only show a very small bathochromic shift in basic media and no converging value that would correspond to the emission maximum of the basic form can be found. The shoulder in emission spectra is also typical for squaraines, those can have multiple emission bands due to exciplex formation with the solvent [131].

For immobilization, bis[4-dibutylamino-2-hydroxyphenyl]squaraine was incorporated into D4 layers, PS/PVP particles and RL100 particles. Fluorescence and absorption spectra in those matrices are shown below, where those in PS/PVP particles are left out because luminescence turned out to be very weak in that material. Fluorescence spectra were recorded subsequently with equal spectrometer settings and samples of equal absorption to get a coarse estimation of relative brightness in distinct materials.

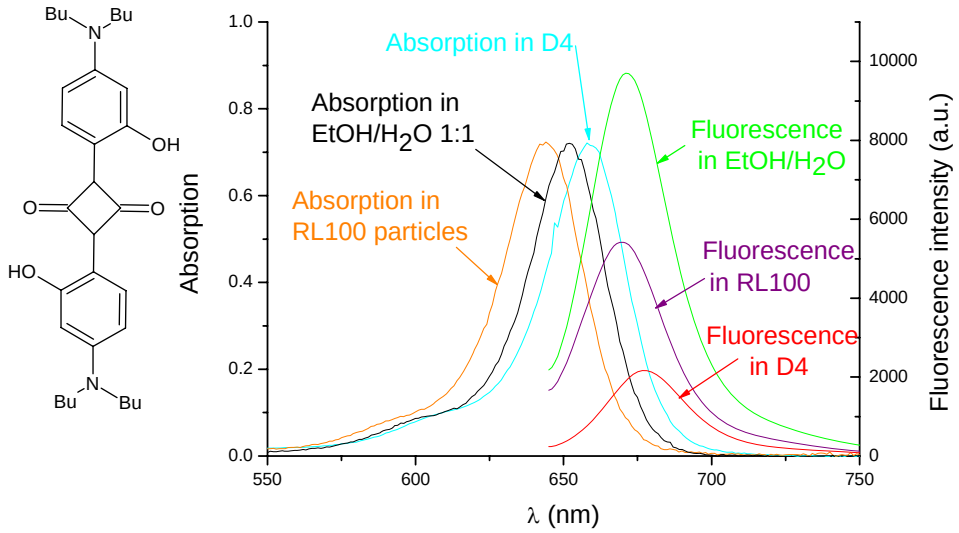

Figure 59: Absorption and emission spectra of bis[4-dibutylamino-2-hydroxyphenyl]squaraine in different immobilization matrices. All spectra are similar in shape, but there is a batho-chromic shift in D4 and a hypsochromic one in RL100 particles, compared to solution. Maxima are listed in table 9. Emission intensities differ, but are remarkably lower than in solution of equal solution.

In addition to poor brightness, sensing behaviour is significantly worse in the polymer matrix than in solution:

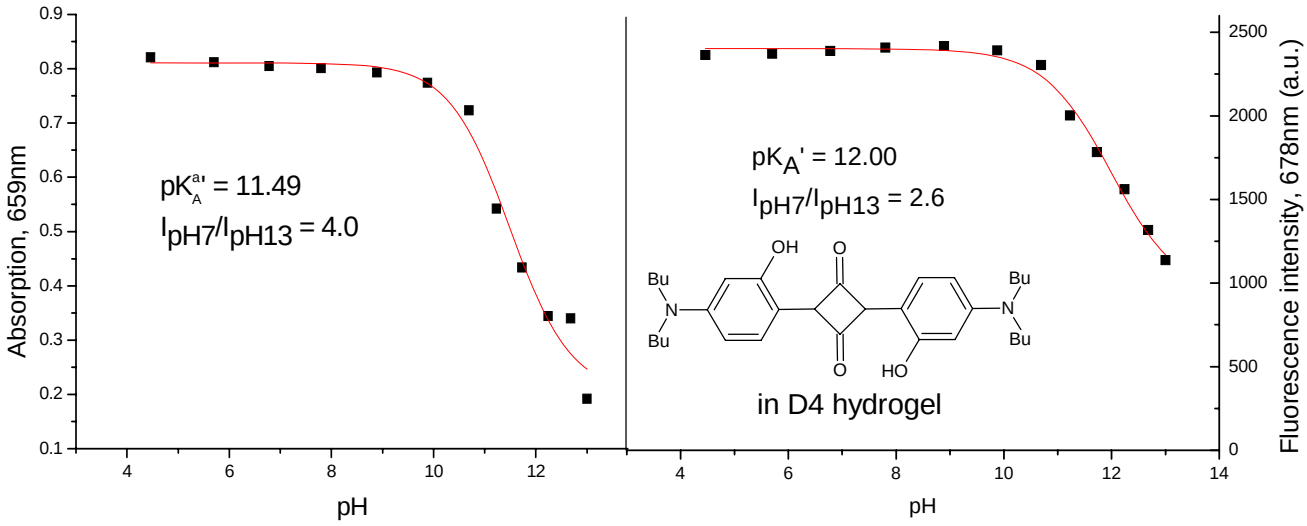

Figure 60: pH calibration of bis[4-dibutylamino-2-hydroxyphenyl]squaraine, 0.25% in D4. A strong shift in pK_A towards highly basic values is observed so that there is no converging value for the basic form recognizable. Sensitivity is also much lower than in solution.

The shift in the apparent pK_A' towards higher values, compared to the one in solution, is not unexpected for a species that is deprotonated to form a negatively charged basic form (2.2.4). In this matrix, indeed, it is so large that it will not match any common applications. Also criti-

cal is the poor sensitivity and brightness. Furthermore, the transition shows poor reversibility, as indicated below:

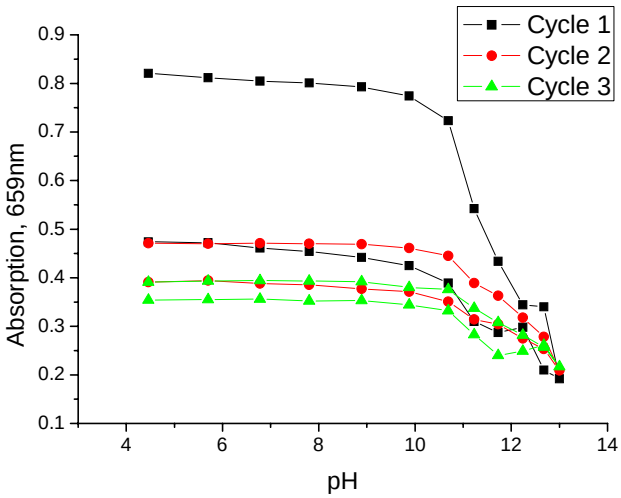

Figure 61: pH calibration cycles of bis[4-dibutylamino-2-hydroxyphenyl]squaraine, 0.25% in D4, monitored over absorption in the maximum. Each cycle was started at pH 4,5 and increased up to 13.0 to go back to 4.5

The poor reversibility observed is most likely related to low stability of the dye in the hydrogel matrix. That is in fact rather obvious as freshly prepared layers show the same bright blue colour observable in solution, but turn to pale violet over time. With some layers, that process is so fast that it can be followed with absorption spectra and even with the eye. Other layers remain stable over some hours or days, but all of them change colour and absorption spectra eventually.

Irreversibility could be related to aggregation or decomposition of the dye under basic conditions (squarates have been reported to be unstable in basic environment due to hydrolysis [129]). Therefore, bis[4-dibutylamino-2-hydroxyphenyl]squaraine was incorporated into RL100 particles, as the positively charged environment provided by those can be expected to decrease pK_A'.

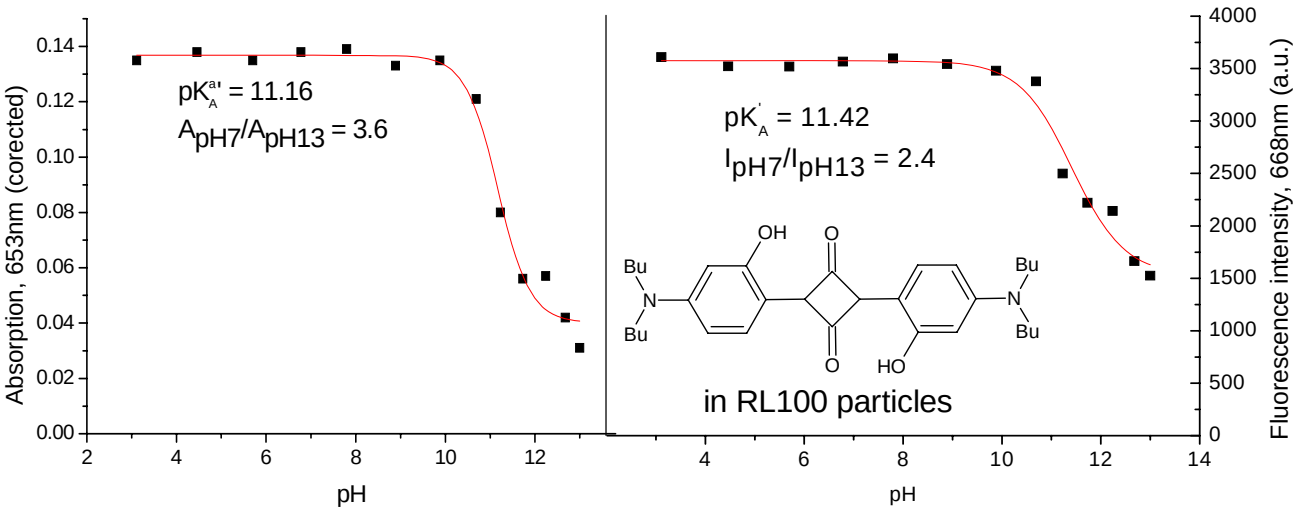

Figure 62: pH calibration of bis[4-dibutylamino-2-hydroxyphenyl]squaraine, 0.25% in RL100 particles. A strong shift in pK_A towards highly basic values is observed so that there is no converging value for the basic form recognizable. Sensitivity is also much lower than in solution.

Surprisingly, the behaviour observed in RL100 is about the same as in D4, showing a higher apparent pK_A' value than in solution and limited sensitivity. Reversibility is poor too, similarly to the D4 matrix. That could indicate that the pH sensitivity derives from (partially) irreversible processes (aggregation, chemical or photochemical degradation) rather than from protolysis.

Consequently, bis[4-dibutylamino-2-hydroxyphenyl]squaraine has been shown to be inapplicable to pH sensing in any immobilization matrix investigated. To critically evaluate dye properties (regardless of the immobilization matrix), photostability of the dye was investigated:

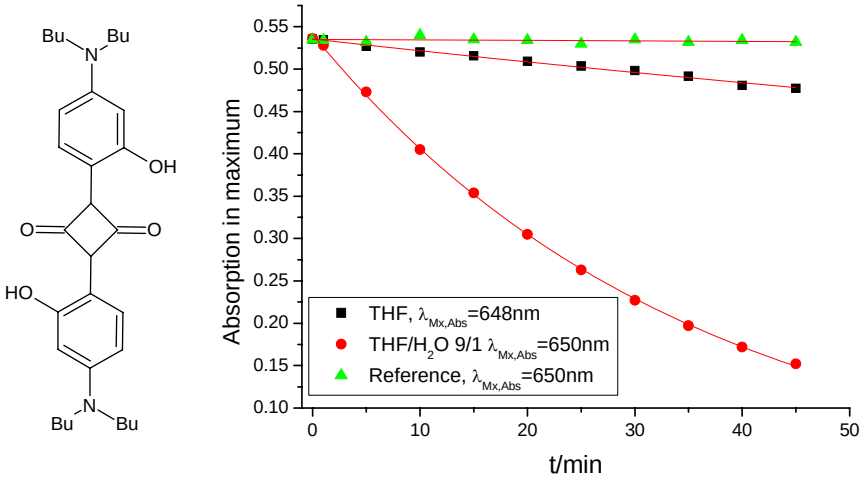

Figure 63: Monitoring of photobleaching of bis[4-dibutylamino-2-hydroxyphenyl]squaraine, illuminating with a red LED (643nm). In pure THF, compared to a mixture with 10% H_2O, bleaching is severe and enhanced by the presence of water. As a reference, bis[4-dibutylamino-2-hydroxyphenyl]squaraine was shown to suffer from no degradation by water in an equal sample (THF, 10% H_2O) when stored in the dark

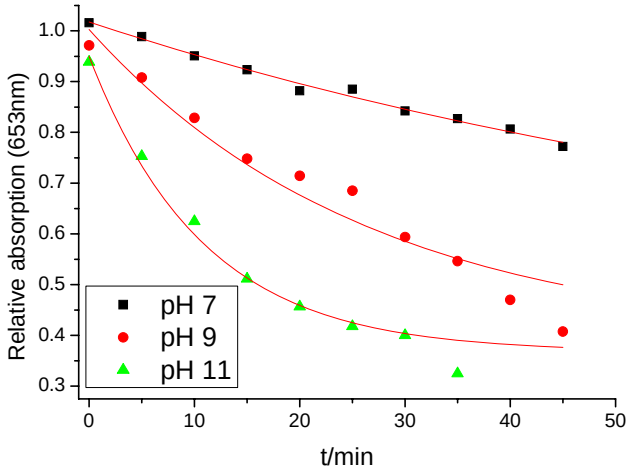

Figure 64: Monitoring of photobleaching of bis[4-dibutylamino-2-hydroxyphenyl]squaraine in EtOH/H_2O 1:1, illuminating with a red LED (643nm) at different pH. All data points are referenced to an equally composed solution stored in the dark. Samples were of equal absorption at 643nm and absorption was observed at 653nm, the maximum of the acidic form, regardless of the shape of absorption spectra at different pH.

Figure 63 proves that the dye is rapidly photo-degraded in the presence of water. Bleaching is very significant not only in basic, but also in acidic solution (figure 64). The spectra corresponding to figures 63 and 64 are not shown here, but exhibit the same pH dependent shapes as shown in figure 57. Bleaching leads to a decrease of the entire spectrum by a constant factor, without any changes in shape or formation of any new observable emissions.
It has to be concluded that bis[4-dibutylamino-2-hydroxyphenyl]squaraine is not suitable for pH sensing because it is photo-degraded in the presence of water.

Properties of bis[4-dibutylamino-2-hydroxyphenyl]squaraine are summarized below:

Table 9: Properties of bis[4-dibutylamino-2-hydroxyphenyl]squaraine in different solvents and immobilization matrices in acidic/basic form, from left to right: Top: fluorescence quantum yields, absorption maxima wavelengths, molar absorption coefficient in the maximum. Bottom: fluorescence emission maxima, pK_A values determined from fluorescence emission spectra, pK_A[a] values determined from absorption spectra, acid base sensitivity factors (ABSF) determined in fluorescence calibration.

Solvent/material	Φ_F	$\lambda_{ABS,\ MAX}$ (nm)	ε_{max} ($M^{-1}cm^{-1}$)
EtOH/H_2O 1:1	-	652/618	$2.94*10^5/1.30*10^5$
Acetone	$0.81\pm0.08/(10\pm3)*10^{-4}$	646/536	
D4 hydrogel	-	658/624	
RL100 particles	-	644/622	

Solvent/material	$\lambda_{EM.\ MAX}$ (nm)	pK_A	pK_A[a]	ABSF
EtOH/H_2O 1:1	671/-	9.29	9.31	27
Acetone	666/-	-	-	-
D4 hydrogel	677/672	12.00	11.49	2.6
RL100 particles	670/663	11.42	11.16	2.4

Bis[4-dibutylamino-2-hydroxyphenyl]squaraine is highly pH-sensitive in the elevated pH range (pK_A=9.31), extraordinarily bright and long-wave excitable (640nm). Unfortunately, its properties are much worse in immobilization matrices. Moreover, its low photostability in the presence of water renders it practically useless for pH sensing.

3.3.1.10 1,6,7,12-Tetrachloro-*N,N'*-di(3-morpholinopropyl)perylene-3,4,9,10-tetracarboxylic bisimide (Cl-DMPBI)

Cl-DMPBI was obtained as an orange solid the fluorescence of which is essentially turned off in basic solution. The reaction involves formation of a more short-wave absorbing species. That was interpreted as opening of the anhydride ring(s) which leads to acyclic di- or tetracarboxylates. Similar compounds have been reported to show more short-wave absorption than PBAs [139].

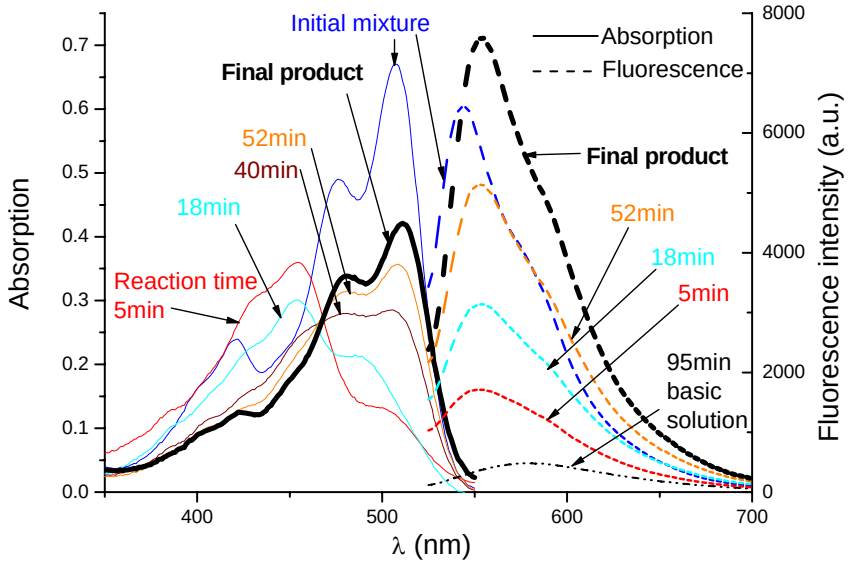

Figure 65: Monitoring of the reaction mixture in the preparation of Cl-DMPBI over absorption and fluorescence emission (λ_{EXC}=510nm) spectra. Samples are equally concentrated and were diluted by 1000 with acetone and acidified with $MeSO_3H$, unless otherwise stated. Spectra of the final product are represented by bold lines. A more short-wave absorbing species (454nm) is formed almost instantaneously and may result from opening of the cyclic anhydrides. That species is more slowly converted into the product which shows absorption spectra similar in shape but weakly bathochromically (from 509 to 513nm) and more strongly hypochromically shifted, compared to the starting material. The intermediate shows reduced brightness. The product exhibits strong fluorescence only in acidic solution and emission spectra are bathochromically (from 544 to 554nm) and hyperchromically shifted compared to the staring material.

Imidation of TCPBA turned out to take place very quickly. The intermediate mentioned is formed within several minutes at 35°C, and after 2h, the reaction is complete. The high reactivity observed is interesting, taking into consideration that many protocols in the literature suggest much longer reaction times and higher temperatures with both aromatic and aliphatic

amines [150,153,175]. However, if such conditions are applied, extensive formation of side-products is observed. Also, an excess of amine was found to be disadvantageous, resulting in formation of side products that feature very long-waved (up to 800nm) absorption and no or little fluorescence. Possible interpretations are substitution of chlorine with OH^- or with excess amino component.

Cl-DMPBI is - in neutral media - poorly to moderately soluble in organic solvents and insoluble in water. Solubility in more polar solvents such as acetone or EtOH is remarkably increased upon acidification. That is easily explained by the dicationic character of the acidic form which increases polarity and complicates stacking.

A survey of acid-base sensitivity in various organic solvents showed a strong response in any environment tested:

Table 10: Acid-base dependent properties of Cl-DMPBI, from left to right: Solvent used, dielectric constant of the solvent ε_S, absorption maximum wavelengths in acidic/basic solution, emission maximum wavelengths in acidic/basic solution, ratio of fluorescence intensity in acidic and basic media when equal samples are excited in a wavelength of equal absorption (i.e. acid-base sensitivity).

Solvent	ε_S	$\lambda_{ABS,MAX}$ (nm)	$\lambda_{EM,MAX}$ (nm)	I_{acidic}/I_{basic}
Cyclohexene	2.1	522/516	564/556	32±1.7
Toluene	2.4	525/523	556/548	43±3.1
$CHCl_3$	4.8	523/521	556/551	67±4.4
THF	7.5	517/515	551/549	105±3.9
Acetone	21.0	515/513	551/547	99±5.2
EtOH	34.3	515/514	552/550	50±2.6

Cl-DMPBI shows a tendency towards negative solvatochromism, especially in emission maxima. Also, there is a slight hypsochromic shift of the basic form with respect to the acidic one which tends to decrease with increasing solvent polarity. Such an influence of acidity/basicity of the environment on spectral properties can be attributed to interactions between the chromophore and the positively charged group of the acidic form. In a similar way, for instance, spectral properties in rhodamines are slightly changed upon (de)protonation of the 2'-carboxy group, even though it is not directly part of the chromophore [118].

Cl-DMPBI has been shown to be highly pH sensitive both in polar and apolar media. Decreasing sensitivity in apolar solvents can originate from decreasing PET efficiency according to Weller's equation (equation 50). The lower value in EtOH may be related to the reductive properties of EtOH.

PET and solubility effects cannot be fully distinguished with a dye of such moderate solubility, but it seems very unlikely that sensitivity is exclusively caused by solubility effects, as sensitivity is present and of the same direction in any solvent tested and fluorescence is switched on/off instantaneously and regardless of dye concentration. Thus, Cl-DMPBI can be considered a PET dye.

pH calibration in EtOH/H_2O 1:1 shows no variation in absorption spectra over pH up to pH=9, while at higher pH a long-waved (>700nm) maximum is formed at the expense of the spectrum of Cl-DMPBI (similar to figure 72). That spectral variation is only partially reversible and could be caused by degradation of the dye (substitution of chlorine with OH^-).

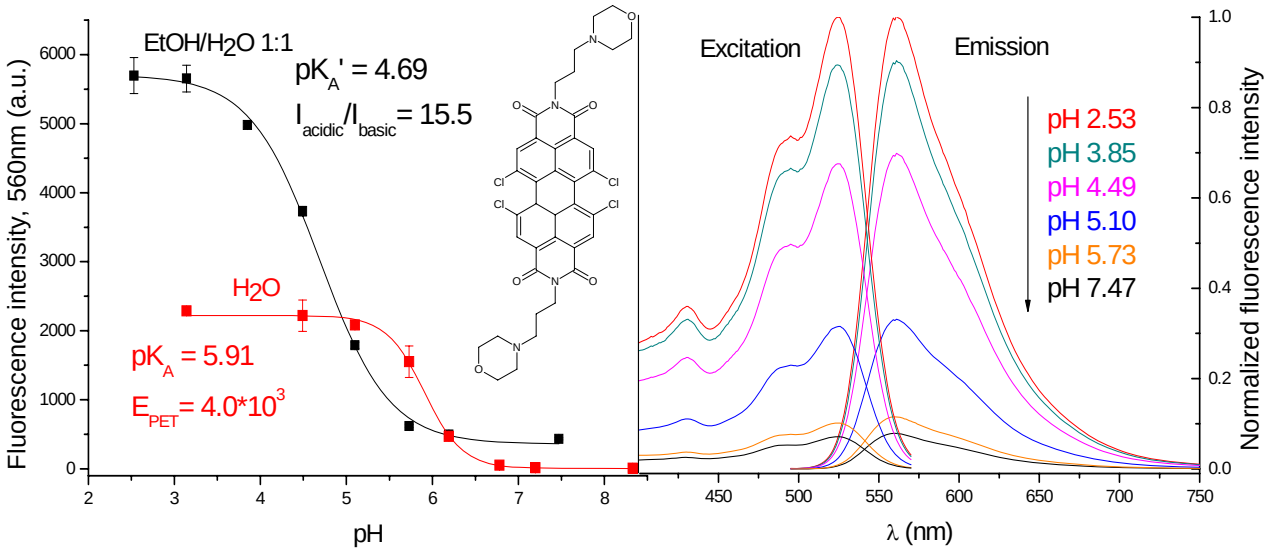

Figure 66: Fluorescence pH calibration of Cl-DMPBI, based on fluorescence emission measurement, λ_{EXC}=486nm, carried out in water and in EtOH/H_2O 1:1. Corresponding fluorescence emission and excitation spectra (λ_{EM}=580nm) were recorded in EtOH/H_2O 1:1. In both environments high pH sensitivity is observed while there is no wavelength shift ($\lambda_{ABS,MAX}$=524nm, $\lambda_{EM,MAX}$=561nm in EtOH/H_2O 1:1).

Absorption and fluorescence spectra are in good agreement with the behaviour expected for a PET dye. Acid-base sensitivity in EtOH/H_2O is lower than all values obtained in non-aqueous media but still very satisfying. The very high value detected in H_2O is partially caused by the very low solubility of the basic form. The pH induced changes in fluorescence spectra are fully reversible.

The pK_A detected in H_2O is lower than the one of *N*-methylmorpholine (7.38; [176]). That can be explained with the presence of an electron-withdrawing imide-nitrogen. pK_A' in EtOH is even lower due to the more hydrophobic environment, destabilizing the charged acidic form.Fluorescence QY is satisfying (0.88) and in agreement with the high QY known for (both chlorinated and non-chlorinated) PBIs [139].

When incorporated into D4 hydrogel, Cl-DMPBI suffers from strong leaching (complete in <5min) in acidic media, whereas in neutral media no signs of leaching are detectable. That is not surprising since the dye is well soluble in acidic aqueous solution. In contrast to that, the basic form is completely insoluble even in EtOH.

Cl-DMPBI is highly acid-base sensitive in organic solvents and virtually of on-off switch character. Its pK_A was determined to 5.9 in aqueous solution, but virtual insolubility of the basic form might distort that value. On the other hand, the dicationic character of the acidic form causes its leaching from hydrogel matrices. Lipophilization is thus required to allow application in sensors. Substitution of chlorine with aryloxy is promising as it simultaneously makes the dye more long-wave excitable.

3.3.1.11 1,6,7,12-Tetraphenoxy-*N*,*N'*-di(3-morpholinopropyl)perylene-3,4,9,10-tetracarboxylic bisimide (PhO-DMPBI)

This reaction was carried out to improve solubility of the PET perylene dye Cl-DMPBI, simultaneously achieving a bathochromic shift by about 60nm by introducing phenoxy groups.
The originally intended synthesis of a mixed bisimide with one 3-(1-morpholino)propyl and one 2,6-diisopropylphenyl substituent at the imide nitrogens was not successful, probably due to low reactivity of 2,6-diisopropylaniline. In the literature, longer reaction times are often employed to obtain an imide with 2,6-diisopropylaniline, and propionic acid is a frequently used solvent [150,175], so acidic catalysis might be crucial. Instead, 3-(1-morpholino)propyl-1-amine has formed a symmetric bisimide with part of the TCPBA inserted. Anyway, the bathochromic shift has been accomplished. The modest yield is easily explained by the use of only one equivalent of 3-(1-morpholino)propyl-1-amine and the fact that all reaction steps were carried out without purification in this one-pot approach, naturally favouring side reactions. Nevertheless, a sufficient amount of PhO-DMPBI was obtained to characterize it without requiring laborious purification of the intermediate. Of course, yield could be increased by inserting a sufficient amount of amino component and carrying out two-step synthesis. Indeed, for the preparation of asymmetric bisimide a more sophisticated approach is required (3.1.4).
PhO-DMPBI is of red colour in solution and shows orange fluorescence. Solubility turned out to be worse than expected, being significantly better than the one of Cl-DMPBI in apolar solvents such as $CHCl_3$ but not better or even worse in more polar solvents such as THF or EtOH. While Cl-DMPBI is well soluble in acidic polar solvents, solubility of PhO-DMPBI is improved less upon acidification in such solvents. This emphasizes the less polar character of the dye, caused by the introduction of apolar phenoxy groups.
pH sensitivity turned out to be significantly lower than the one of Cl-DMPBI in more polar organic solvents and essentially absent in apolar ones. That is evident in the following table:

Table 11: Acid-base dependent properties of PhO-DMPBI, from left to right: Solvent used, dielectric constant of the solvent ε_S, absorption maximum wavelengths in acidic/basic solution, emission maximum wavelengths in acidic/basic solution, ratio of fluorescence intensity in acidic and basic media when equal samples are excited in a wavelength of equal absorption (i.e. acid-base sensitivity).

Solvent	ε_S	$\lambda_{ABS,MAX}$ (nm)	$\lambda_{EM,MAX}$ (nm)	I_{acidic}/I_{basic}
Cyclohexene	2.1	571/563	605/595	0.49±0.02
Toluene	2.4	575/568	609/603	1.7±0.06
$CHCl_3$	4.8	583/577	619/614	1.5±0.06
THF	7.5	566/564	603/600	2.7±0.10
Acetone	21.0	566/563	606/600	4.1±0.12
EtOH	34.3	571/569	613/610	2.9±0.09

Spectral properties of PhO-DMPBI in different acidic/basic solvents are not very different from those observed with Cl-DMPBI and discussed there, of course all spectra being red-shifted by about 60nm. The pronounced bathochromic shift in $CHCl_3$ is remarkable. Fluorescence QY of the acidic form (0.88, acetone) is equally high to Cl-DMPBI, implying good brightness. Spectral shifts depending on solvent polarity are more pronounced than with Cl-

DMPBI. That may be explained with the stronger electron-withdrawing character of the phenoxy group, increasing the push-pull character of the dye (2.1.8).
The significant decrease in acid-base sensitivity is obviously related to the substitution of chlorine with phenoxy. By replacing an electron-withdrawing group with an electron-donor, reduction potential of the chromophore is likely to be diminished. Moreover, its excitation energy is decreased by the bathochromic shift. Both effects weaken the thermodynamic driving force of PET (equation 50). As a result, PET is only favourable in polar environments, showing moderate probability even there, in contrast to Cl-DMPBI, where it is highly favourable, regardless of the environment. Here again, solubility effects have to be taken into account. The inversed pH sensitivity in cyclohexene may correspond to lower solubility of the acidic form. Increasing sensitivity in polar media might be caused by better solubility of the acidic form there, the basic one generally being less soluble as stacking is more favourable with uncharged molecules. Consequently, PhO-DMPBI cannot be definitely verified to be a PET dye. Still, pH sensitivity in solvents such as THF or acetone is present regardless of dye concentration. That argues for PET causing at least part of the sensitivity (for solubility effects, a pronounced concentration effect can be expected).

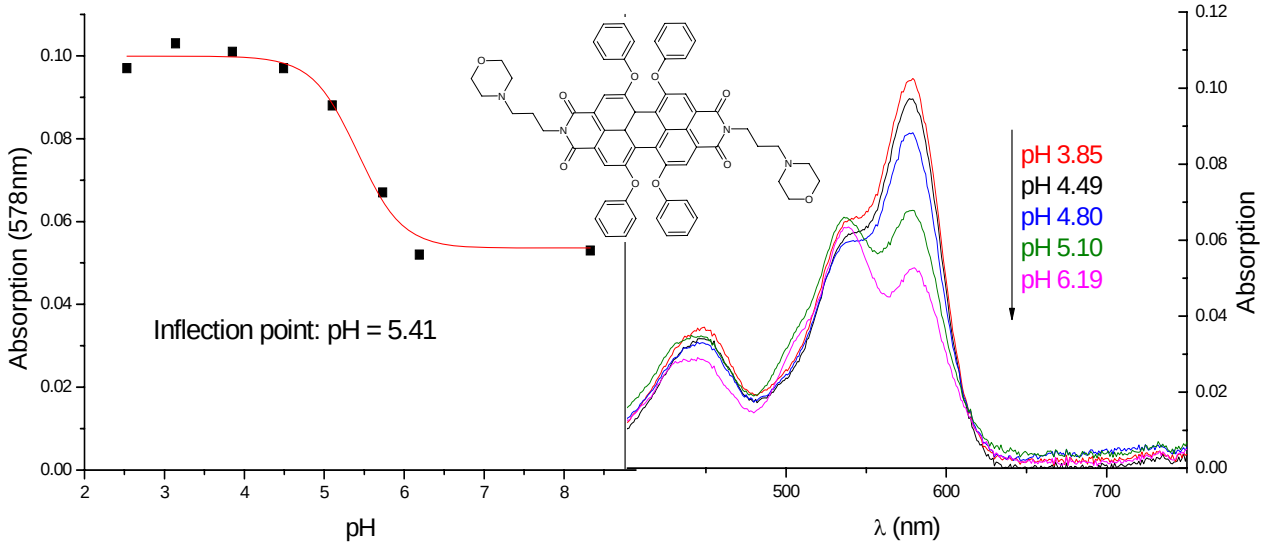

Figure 67: Absorption pH calibration of PhO-DMPBI in EtOH/H_2O 1:1, observed in the most long-wave maximum (578nm), shows increasing distortion of the spectra, while the location of the maxima remains unchanged. Absorption in the central maximum (537nm) is essentially pH-independent. The distortion is most likely caused by aggregation.

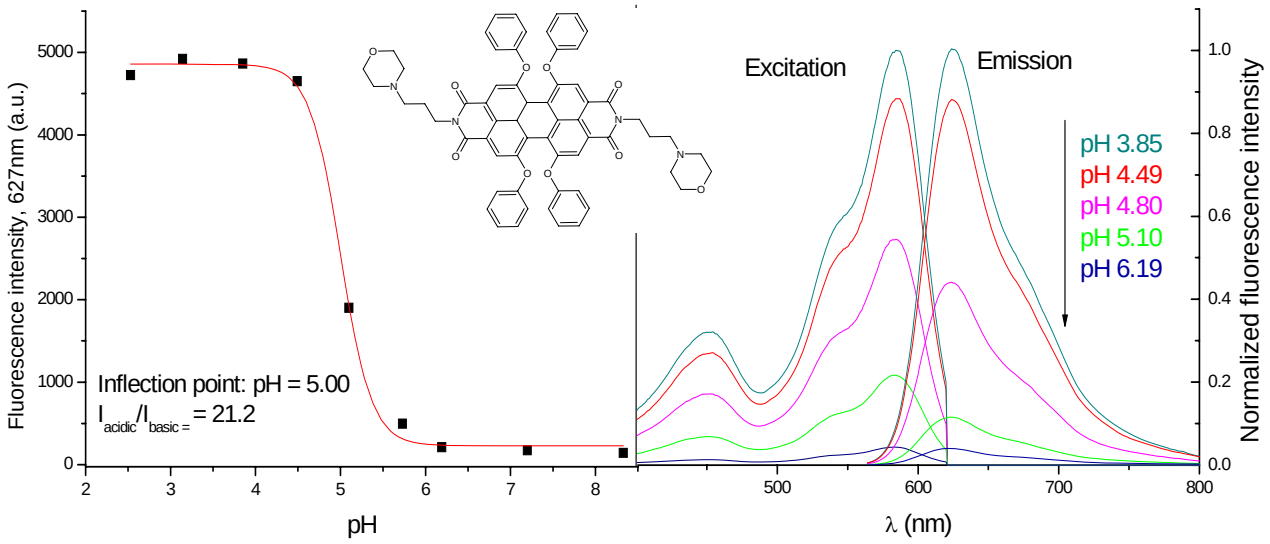

Figure 68: Fluorescence pH calibration of PhO-DMPBI in EtOH/H_2O 1:1 based on fluorescence emission measurement (λ_{EXC}=540nm), observed in the emission maximum (627nm) and corresponding fluorescence emission and excitation spectra (λ_{EM}=620nm). The high sensitivity is at least partially caused by aggregation which is indicated by the distortion of absorption spectra (figure 67) which corresponds to similar pH values of 5-6. Also, fluorescence is weak even in acidic solution. There is no noticeable pH-induced shift in emission maximum.

Aggregation issues in EtOH/H_2O become evident after some hours as dye precipitate is formed in basic solution, leaving behind a colourless solution. The pH dependent behaviour of fluorescence spectra can therefore as well be caused by decrease in dye concentration due to aggregation as by PET. The system was found to be reversible and even the precipitate is re-dissolved upon acidification of a basic sample. The high pH sensitivity observed cannot be exclusively attributed to PET and PET efficiency cannot be determined. The inflection point may also originate from aggregation and even though that may be closely related to protolysis it cannot be denominated a pK_A value. It is not too different form the pK_A' of Cl-DMPBI in the same media, but the dynamic range is narrower. While in a sample of Cl-DMPBI in acidic EtOH/H_2O, fluorescence is obvious even when it is exposed to daylight, the one of PhO-DMPBI is hardly visible even when UV-illuminated in a dark room. Consequently, the principally high QY is diminished in polar media due to poor solubility.

When PhO-DMPBI is embedded into D4 hydrogel, the properties of the sensitive layers vary from one to another and over time. Some layers are equal in colour to solutions and show very similar spectra when freshly prepared. However, within a short time the colour may (irreversibly) change to faint violet. Then, distorted absorption spectra similar the ones shown in figure 67 are observed. The layers may be pH sensitive (dynamic range roughly pH 4-6) first, but sensitivity may decrease and the dynamic range may be shifted over time. Other layers are not pH sensitive, or they turn faint violet instantaneously as the cocktail solvent vaporizes, show hardly any fluorescence at all and distorted absorption spectra. These observations are most likely related to aggregation processes. The dye may be soluble and sensitive in some areas of the hydrogel (which consists of more polar and less polar areas), but it will eventually migrate into areas where it undergoes irreversible aggregation.

Since PhO-DMPBI shows poor sensing performance in EtOH/H_2O and in hydrogels, a more soluble derivative has to be obtained. Sensing efficiency is not great even in better solvents, although a sensitivity factor of 4 (present in acetone) may still be satisfying for many applications. Low sensitivity is, of course, disadvantageous for a PET pH sensor. The on-off switch character is lost, and excitation/observation wavelengths cannot be tuned to increase sensitivity for obvious reasons. Furthermore, polarity cross-sensitivity is likely to be an issue with dyes like PhO-DMPBI. Introduction of a more oxidizable amino function may help to overcome this problem.

PhO-DMPBI can be prepared from commercially available TCPBA in a one-pot approach. It is more long-wave excitable, but its acid-base sensitivity, compared to Cl-DMPBI, is significantly reduced (factor 3-4) and only present in polar solvents. That can be attributed to the electron-pushing character of the phenoxy substituents. Due to its low solubility, it is not applicable in a hydrogel matrix. Replacement of phenoxy by *tert*-butylphenoxy was tackled to improve solubility.

3.3.1.12 1,6,7,12-Tetra(4-*tert*-butylphenoxy)-*N,N'*-di(3-morpholinopropyl)perylene-3,4,9,10-tetracarboxylic bisimide (tBuP-DMPBI)

From the synthetic point of view the same statements are valid as outlined in 3.3.1.11. Here again, the symmetric bisimide with 3-(1-morpholino)propyl-1-amine was formed. *tert*-Butylphenol was used instead of phenol because even higher solubility was expected due to the presence of the bulky tBu substituent. A similar structure (carrying aromatic p-aminophenyl as imide substituent) had been reported to be subject to PET [177].
tBuP-DMPBI is of red colour in solution and shows orange fluorescence. Solubility in organic solvents is significantly better than the one of PhO-DMPBI, in particular in solvents of medium polarity like THF. It is still poorly soluble in polar solvents such as EtOH, and solubility is much lower than the one of lumogen red, which carries diisopropylphenyl substituents at the imide nitrogens. Substituents in the imide region still seem to play a more important role for the prevention of aggregation processes than those in the bay region.

Table 12: Acid-base dependent properties of tBuP-DMPBI, from left to right: Solvent used, dielectric constant of the solvent ε_S, absorption maximum wavelengths in acidic/basic solution, emission maximum wavelengths in acidic/basic solution, ratio of fluorescence intensity in acidic and basic media when equal samples are excited in a wavelength of equal absorption (i.e. acid-base sensitivity).

Solvent	ε_S	$\lambda_{ABS,MAX}$ (nm)	$\lambda_{EM,MAX}$ (nm)	I_{acidic}/I_{basic}
Cyclohexene	2.1	577/569	611/603	0.80±0.09
Toluene	2.4	581/574	616/609	1.2±0.06
$CHCl_3$	4.8	591/586	626/621	1.1±0.11
THF	7.5	572/571	608/605	2.5±0.13
Acetone	21.0	572/568	611/606	3.0±0.07
EtOH	34.3	577/575	620/617	2.1±0.10

Spectral properties of tBuP-DMPBI are similar to those of PhO-DMPBI which have been discussed earlier. Slightly more bathocromically shifted spectra can be attributed to the

stronger electron-pushing effect of the alkylphenol compared to the unsubstituted one. Acid-base sensitivity shows a similar dependence on solvent polarity as in PhO-DMPBI, but is generally a little lower. That could originate from the electron-pushing tBu-group which increases electron density in the chromophore and elevates excitation wavelength.
Fluorescence QY of the acidic form is lower (0.66) than the one of PhO-DMPBI (0.88) but still satisfying.

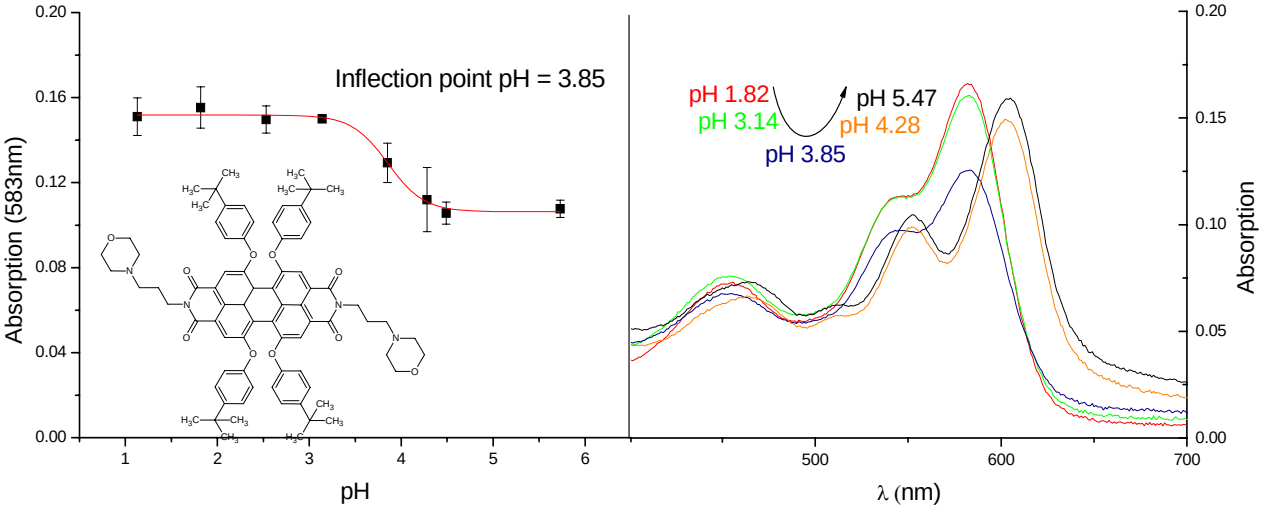

Figure 69: Absorption pH calibration of tBuP-DMPBI in EtOH/H_2O 1:1, observed in the most long-wave maximum of the acidic form (583nm), shows a remarkable bathochromic shift in basic media (λ_{MAX}=603nm) while the shape shows only minor pH dependence. The shift is most likely caused y aggregation.

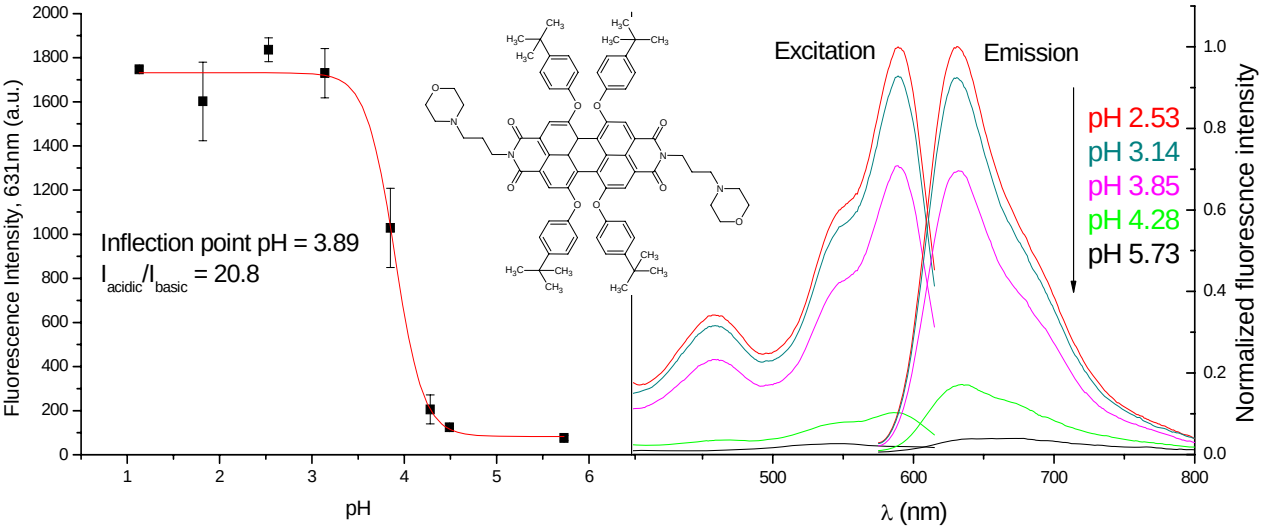

Figure 70: Fluorescence pH calibration of tBuP-DMPBI in EtOH/H2O 1:1 based on fluorescence emission measurement (λ_{EXC}=550nm), observed in the emission maximum in acidic media (631nm) and corresponding fluorescence emission and excitation spectra (λ_{EM}=620nm). There is pH-induced red-shift in the emission maximum ($\lambda_{MAX,BAS}$=639nm), though it is less pronounced than in absorption spectra ($\Delta\lambda$=20nm there). The high sensitivity is at least partially caused by aggregation which is indicated by the bathochromic shift of absorption spectra (figure 69) which corresponds to similar pH values of 3-4. Also, fluorescence is weak even in acidic solution.

The red-shift of the absorption spectra in EtOH/H_2O, accompanied with an increase of long-wave absorbing background, can be attributed to aggregation, not only because such a shift is typical for aggregates, but also because dye precipitation is observed after some time. The high sensitivity found in EtOH/H_2O 1:1 is at least partially caused by the low solubility of the basic form, as emphasized by precipitation. Here again, the inflection point cannot be directly attributed to protolysis, though the latter may be closely related to aggregation. Similarly to PhO-DMPBI, fluorescence of tBuP-DMPBI is very weak in this environment.
When tBuP-DMPBI is embedded into D4 hydrogel, the colour of the layer turns from red to faint violet immediately as the solvent vaporizes. It is then very weakly fluorescent and virtually non-sensitive. Absorption spectra are red-shifted, similarly to those in basic EtOH/H_2O. Regarding pH sensitivity, a slight decrease in absorption is observable at pH 4-5, which is accompanied by a hypsochromic shift in emission spectra and emission intensity is only slightly decreased (by about 10%). All spectral changes are reversible. They are best explained by formation of an aggregate which can undergo protolysis. Both forms are similarly weakly fluorescent and spectral properties are slightly different.
The properties of the hydrogel layer, including essential absence of useful pH sensitivity, are not representative to tBuP-DMPBI, but to the aggregate. In the same way, the pH sensitivity observable in solution cannot be directly related to PET as aggregation also plays an important role there. Although tBuP-DMPI may be better soluble in media of low or medium polarity, solubility in polar environment is not noticeably better, probably because of the hydrophobic character of the *tert*-butyl groups.
Consequently, although tBuP-DMPBI shows acid-base sensitivity, it is not suitable fot pH sensing in aqueous solution or in a hydrogel matrix due to poor solubility. The design of derivatives with better solubility is required. That can involve the introduction of bulky substituents to the imide nitrogen (such as the one in lumogen red, figure 27) as apparently that region plays a mayor role for solubility.

tBuP-DMPBI shows similar properties to PhO-DMPBI. Its solubility is better but still too low for application in immobilization matrices. Acid-base sensitivity in organic solvents is a little lower than the one of PhO-DMPBI (factor 2-3). Preparation of an asymmetric PBI, carrying one PET group and one solubilising diisopropylphenyl substituent in the imide positions, was tackled at this point.

3.3.1.13 1,6,7,12-Tetrachloro-*N*-(2,6-diisopropylanilino)-*N'*-(3-(1-morpholino) propyl) perylene-3,4,9,10-tetracarboxylic bisimide (Cl-AMPBI)

It is remarkable that this asymmetric PBI could be prepared in a one-pot approach since most protocols in the literature suggest multi-step synthesis [153-155]. Although those methods would probably allow a better yield, Cl-AMPBI was here obtained in a straightforward way, starting from not too pricey compounds and avoiding tedious purification of the intermediates. Cl-AMPBI shows better (indeed still limited) solubility than the other perylene dyes presented in solvents of medium polarity like THF or acetone. It is also soluble in EtOH to some extent, unlike Cl-DMPBI. The solubilising effect of the one diisopropylanilino group seems to be equal or superior even to the one of four *tert*-butylphenoxy groups. Acid/base sensitivity lies between the one of PhO-DMPBI and Cl-DMPBI and is still high, regardless of the solvent.

Table 13: Acid-base dependent properties of Cl-AMPBI, from left to right: Solvent used, dielectric constant of the solvent ε_S, absorption maximum wavelengths in acidic/basic solution, emission maximum wavelengths in acidic/basic solution, ratio of fluorescence intensity in acidic and basic media when equal samples are excited in a wavelength of equal absorption (i.e. acid-base sensitivity).

Solvent	ε_S	$\lambda_{ABS,MAX}$ (nm)	$\lambda_{EM,MAX}$ (nm)	I_{acidic}/I_{basic}
Cyclohexene	2.1	518/517	548/546	13.0±0.6
Toluene	2.4	524/523	553/553	19.1±1.3
$CHCl_3$	4.8	523/522	552/551	18.9±0.7
THF	7.5	517/516	548/548	17.9±0.3
Acetone	21.0	515/515	548/547	22.8±1.9
EtOH	34.3	516/516	551/551	12.4±1.1

Although acid-base sensitivity is significantly lower than for Cl-DMPBI, where two morpholino groups are present, one PET-group is still sufficient to allow high acid-base sensitivity. That is in contrast to the investigated rhodamines, where one piperazinyl group enables only poor acid-base sensitivity (3.3.1.8). The influence of solvent polarity on absorption/emission maxima of the neutral form is similar to the one for Cl-DMPBI and less pronounced than the one of the aryloxy-substituted dyes which fits into the concept presented earlier (stronger push-pull character of the aryloxy substituents causes stronger sensitivity to polarity, 3.3.1.11). The maxima of acidic and basic forms are much more similar than for any of the other perylene dyes. That can be explained with the less polar character of the monocationic acidic form. Fluorescence QY is high (0.95 which is the highest of all synthesized perylenes).
Unlike the other perylene dyes investigated, Cl-AMPBI can be immobilized to form stable pH sensitive layers. Those layers do not show any spectral variations over several days.

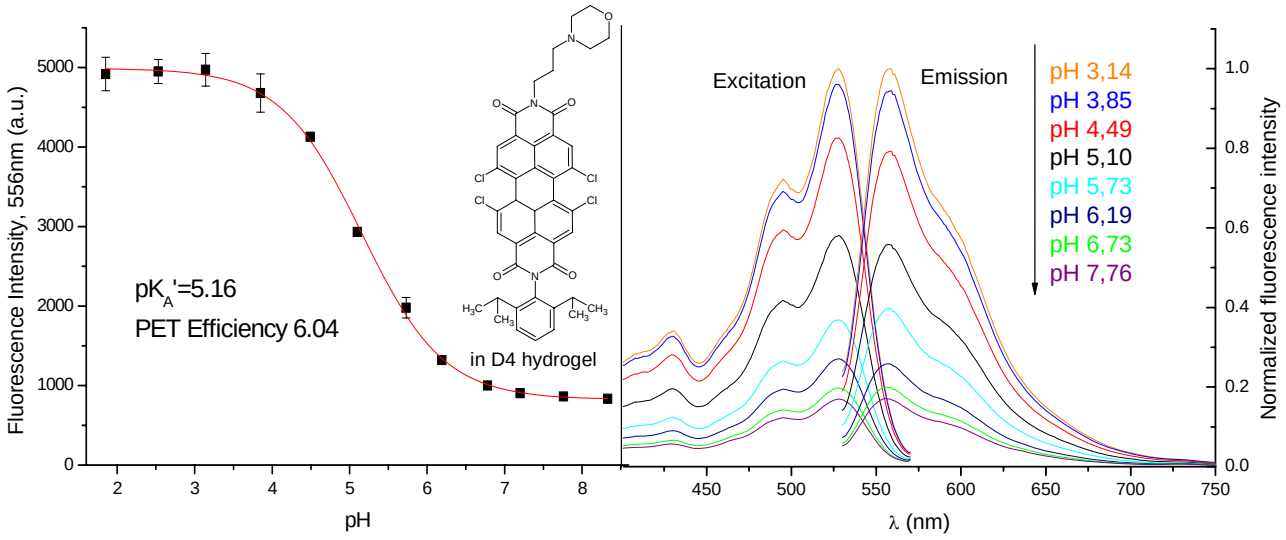

Figure 71: Fluorescence pH calibration of Cl-AMPBI, 0,25% in D4 hydrogel, based on fluorescence emission measurement (λ_{EXC}=526nm), observed in the emission maximum (556nm) and corresponding fluorescence emission and excitation spectra (λ_{EM}=580nm). Sensitivity is good though pK_A' is not ideal for the most common sensing applications. There is no wavelength shift in excitation and only a very small hypsochromic one (558 to 556nm) in emission spectra with increasing pH.

Ideally for a PET indicator dye, Cl-AMPBI shows unchanged absorption spectra over a wide pH range. The formation of a long-waved maximum at the expense of product absorption occurs only at high pH (>10, which is far outside the sensitive range), is partially reversible and can be attributed to dye decomposition:

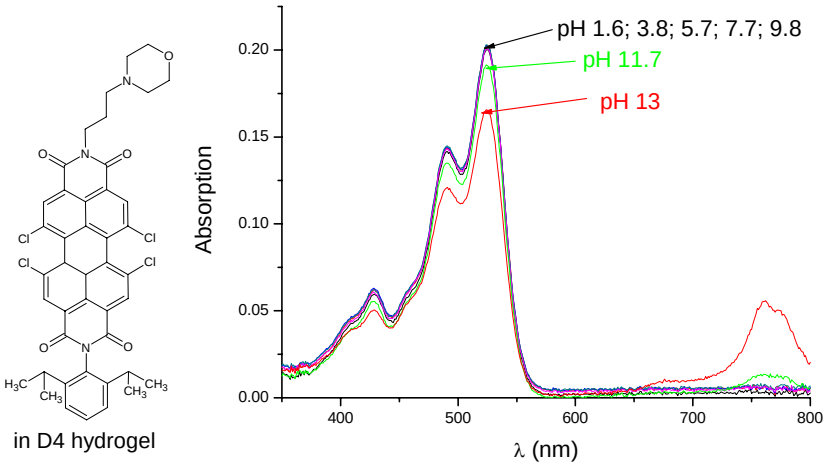

Figure 72: Absorption spectra of Cl-DMPBI, 0.25% in D4 hydrogel, are constant over a wide pH range and throughout the sensitive pH area. Only at elevated pH, decomposition products are formed.

Although acid/base sensitivity is less pronounced in the sensitive layer than in organic solvents, it still allows effective sensing. The pK_A value (5.16) is too low for the sensitive range to match physiological range, but there still is some sensitivity around pH~6 which is relevant to biotechnological samples. Although Cl-AMPBI suffers from much less leaching than Cl-

DMPBI, it is not completely leaching-free, as indicated by the pH calibration cycles shown below. Those were recorded with the same piece of layer and in each cycle it was washed with buffer about 100 times.

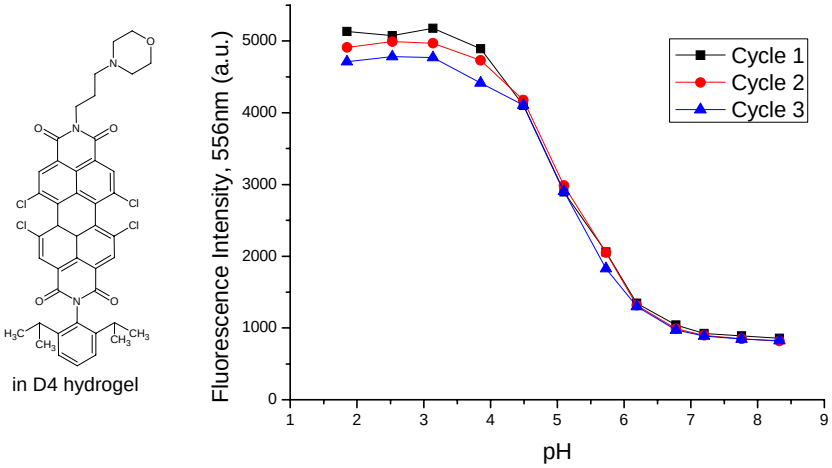

Figure 73: pH calibration cycles of Cl-DMPBI, 0.25% in D4 hydrogel. In each cycle, the layer was washed with buffer about 100 times. A signal decrease by about 1% per cycle is observed.

Leaching to that extent does not constitute a problem for reliable pH calibration, but definitely is an issue for long-term measurement. Although signal drifts due to leaching can be overcome by ratiometric measurement, design of a less hydrophilic pH indicator is desirable. The introduction of different amino groups is promising for extending the pH range available for sensing. Substitution of chlorine by phenoxy/aryloxy is the most obvious way to obtain more long-wave excitable pH indicators. Indeed, the sensitivity of such dyes which contain electron-pushing substituents but only one PET group still is to be investigated.

Cl-AMPBI, an asymmetric PBI, could be prepared from commercial TCPBA in a simple one-pot approach. Its sensitivity in organic solvents is between the one of Cl-DMPBI (two PET groups) and PhO-DMPBI (two PET groups, phenoxy-substituted) but still high. Its solubility is remarkably better and it is applicable in a hydrogel matrix. There, it shows an acid-base sensitivity factor of 6 where pK_A'=5.2. It still suffers from some leaching. Replacement of the morpholino group with another amino could lessen leaching and enhance sensitivity. Substitution of chlorine with aryloxy would yield a more long-wave excitable and probably leaching-free dye, but sensitivity is yet to be tested. Alternatives can involve extended chromophores related to perylene.

The most important properties of the synthesized perylenes are summarized below:

Table 14: Properties of perylenes in acidic/basic form, from left to right: Top: fluorescence quantum yields, absorption maxima wavelengths, molar absorption coefficients in the maximum. Bottom: emission maxima wavelengths, pK_A values determined from fluorescence emission spectra, acid-base sensitivity factors (ABSF) in organic solvents determined according to 3.2.3.2, PET efficiency. Unless otherwise stated, λ and ε were determined in $CHCl_3$, pK_A in water.

Dye	Φ_F	$\lambda_{ABS,\ MAX}$ (nm)	ε_{max} ($M^{-1}cm^{-1}$)
Cl-DMPBI	$0.88\pm0.10/0.017\pm4*10^{-4}$ ($CHCl_3$)	523/521	$3.91*10^4/4.11*10^4$
PhO-DMPBI	$0.88\pm0.02/0.19\pm4*10^{-3}$ (Acetone)	566/564[b]	$4.45*10^4/4.51*10^4$ [b]
tBuP-DMPBI	0.66±0.03/0.18±0.03 (Acetone)	572/571[b]	$4.23*10^4/4.31*10^4$ [b]
Cl-AMPBI	$0.95\pm0.04/0.03\pm3*10^{-3}$($CHCl_3$)	523/522	$3.88*10^4/3.85*10^4$

Dye	$\lambda_{EM.\ MAX}$ (nm)	pK_A	ABSF	E_{PET}
Cl-DMPBI	561/561	5.9	>30[a]	
PhO-DMPBI	603/600[b]	5.9[c.d]	≤4.1[a]	
tBuP-DMPBI	608/605[b]	3.9[c.d]	≤3.0[a]	
Cl-AMPBI	552/551	5.16[e]	>12[a]	6.04[e]

[a] in various organic solvents
[b] in THF
[c] in EtOH/H_2O 1:1
[d] pK_A determined correspond to aggregation, rather than protolysis
[e] in D4 hydrogel

3.3.2 Particle preparation and Characterization

Magnetic core-particles were to be covered with a cross-linked acrylate hydrogel shell by emulsifier-assisted radical core-shell co-polymerization in aqueous suspension. Components are acrylamide (AAM, bulk component), 2-aminoethylmethacrylate hydrochloride ("Amine 1") or *N*-(3-aminopropyl)methacrylamide hydrochloride ("Amine 2"; amino-functionalized monomers, AFMO), "Bis" (*N,N'*-methylenebisacrylamide, crosslinker), KPD (potassium peroxodisulfate, initiator) and SDS (sodium dodecylsulfate, emulsifier).

3.3.2.1 Copolymerization Characteristics

Core-shell polymerization exclusively with AAM and Bis (CS1, table 6) was shown to be effective by monitoring Z_{av} of the particles over polymerization time by means of DLS. Z_{av} increased irreversibly during the polymerization. Irreversibility is confirmed by the fact that there are no signs of decrease in Z_{av} when the particles obtained are washed (table 15). The increase in Z_{av} is unlikely to correspond to aggregation since PDI of the particles remains more or less unchanged throughout the polymerization, indicating constant monodispersity, and a smooth distribution of Z_{av} is observed (figure 74). That has been observed in various core-shell polymerizations without amino-functionalized monomer and is shown with CS1 as a typical one:

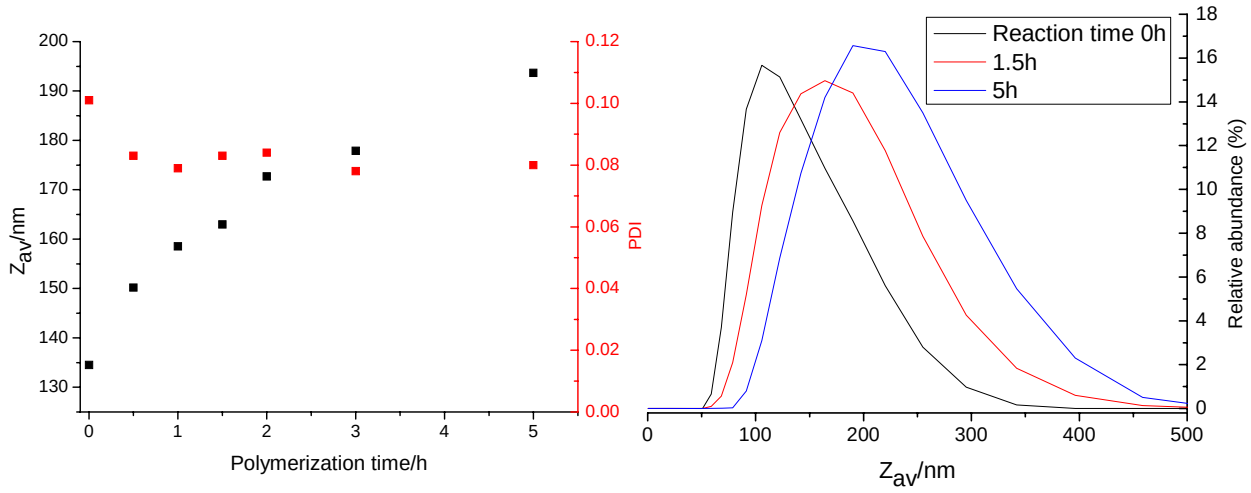

Figure 74: Z_{av} (left, black), PDI (left, red) and distribution of particle size (right) in polymerization CS1 followed over polymerization time. An increase in Z_{av} with more or less constant PDI is observed, size distribution remains single-peaked and of comparable peak-width. That indicates that average particle size increases due to shell formation, not aggregation.

Table 15: Z_{av} and PDI of CS1 when washed several times by magnetic separation

Washing Steps	Z_{av}/nm	PDI
0	193.7	0.080
1	194.9	0.092
2	195.2	0.087
3	196.6	0.086

Z_{av} shows no temperature dependence in the range 16-45°C.

The impact of relative crosslinker concentration on the size of the particles formed was studied (polymerizations CS5-9):

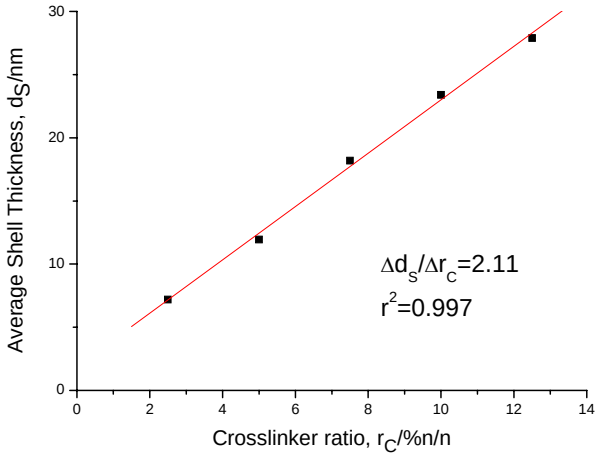

Figure 75: Influence of crosslinker ratio, with respect to AAM, on the average thickness of the hydrogel shell formed (d_s) in polymerizations CS5-9. Shell thickness d_S can be adjusted varying the amount of crosslinker when the other parameters are kept constant.

The shell thickness d_S was calculated as follows:

$$d_S = (Z_{av} - Z_{av,Core})/2 \qquad \text{Equation 53}$$

d_S	Average thickness of the hydrogel shell formed
Z_{av}	Average size of the CS particles formed
$Z_{av,Core}$	Average size of the core particles, right before KPD was added

As visualized in figure 75, the thickness of the hydrogel shell can be adjusted by varying the crosslinker concentration. The relation found actually exhibits good linearity. Increasing d_S with crosslinker ratio may be interpreted as a shift in the equilibrium between polymer in solution and polymer bound to the core-particles. More crosslinked polymer is less soluble and more probable to form a network around the core-particles.
While without any amino component, the core-shell particles form stable dispersions in water the Z_{av} of which remained within ±10% over six weeks, severe precipitation occurred upon polymerization if Amine 1 was added. That was attributed to ion pair formation of the ammonium hydrochloride moiety with the negatively charged carboxy groups on the surface of the core particles. Their zeta potential is decreased which results in aggregation. If the amino component was added after the polymerization has been started, no aggregation was observed. Though it was added to most polymerizations 20min later than the initiator, aggregation is prevented too if it is added as fast as 5min later. In that way, CS particles could be obtained with both Amine1 and Amine2, with no signs of aggregation upon polymerization:

Table 16: Z_{av} and PDI of CS2 and CS3 (table 6), compared to those of the core-particles they were prepared from. Z_{av} is increased and since PDI is even reduced that is due to enlargement, not aggregation.

Name	Specification	Z_{av}/nm	PDI
CS2	10% Amine1	183.2	0.074
C2	Core to CS2	136.8	0.136
CS3	10% Amine2	222.5	0.032
C3	Core to CS3	132.6	0.089

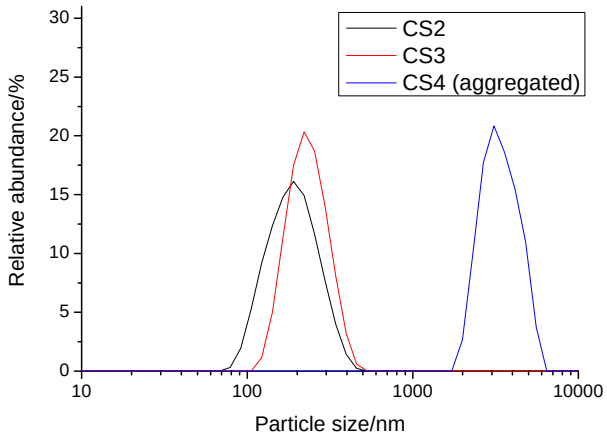

Figure 76: Particle size distribution of non-aggregated CS 2 and CS 3 obtained by copolymerization involving Amine 1 and Amine 2, respectively. They are compared with CS4 which showed severe aggregation.

These CS particles are of homogeneously distributed nanometre-size, as indicated by the low PDI and the relatively narrow and single-peaked size distribution.
On the other hand, aggregation also occurs in basic media (pH12) if the AFMO is added together with or prior to KPD, although amino groups should not be cationic there. Still, the growing polymer shell seems to protect the core-particles and prevent them from aggregating. Aggregation is fully avoided if the AFMO is added only 5 minutes later than KPD. If phosphate or citrate buffer is present during polymerization, aggregation is inevitable, no matter when the AFMO is added. Once prepared, CS particles can be stored in dilute phosphate buffer, but not in citrate buffer where they aggregate within a few hours.
Still, a high AFMO ratio leads to worsened aggregation stability, and ratios of 10% or higher will not yield stable nano-particles:

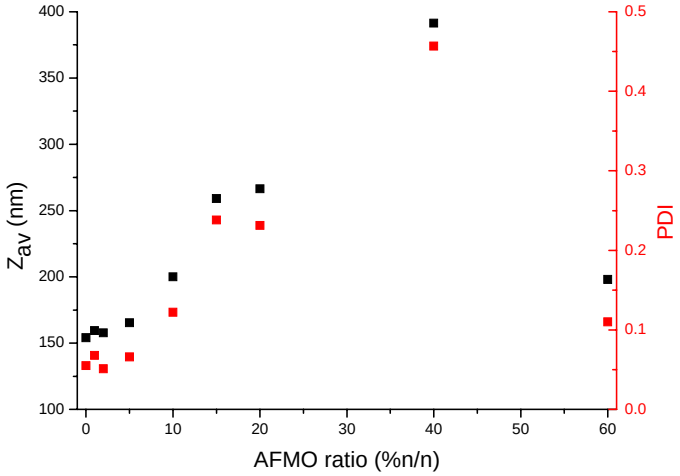

Figure 77: Z_{av} and PDI of polymerizations CS29-37 where the amount of Amine 2 was the only parameter varied. Z_{av} and PDI show a steady increase with the amount of Amine 2 introduced into polymerization up to high values, indicating increasing aggregation tendency. Very high AFMO ratios seem to reverse the trend.

For the interpretation of copolymerization behaviour, copolymerization diagrams, displaying the composition of the copolymer as a function of monomer ratio in the polymerization mixture and conversion, were calculated using equations 43 and 45 (section 2.4.3). Monomer reactivity ratios for the monomers (or for acrylates with a substitution pattern as similar as possible) were taken from the literature [178]. Since those reactivities have been determined under different conditions, the calculation will not be perfectly valid for the system investigated here which is more complicated and influenced by the heterogeneous character of the polymerization mixture. Nevertheless, it helps to estimate the polymerization behaviour.

Table 17: Monomers chosen for the calculation of copolymerization diagrams and corresponding monomer reactivity ratios (equations 43,45). Those diagrams predict the copolymerization behaviour of Amine 1 and Amine 2 (figures 78 and 79). Monomers were selected by the most similar substitution pattern to the acrylates experimentally used.

	Prediction for Amine 1			
	Monomer 1	**Monomer 2**	**r_1**	**r_2**
Calculation	2-hydroxyethyl methacrylate	acrylamide	1.89	0.05
Experiment	2-aminoethyl methacrylate	acrylamide		
	Prediction for Amine 2			
	Monomer 1	**Monomer 2**	**r_1**	**r_2**
Calculation	*N*-(2-hydroxypropyl) methacrylamide	*N*-2-(4-hydroxyphenyl)ethyl acrylamide	1.01	0.09
Experiment	*N*-(3-aminopropyl) methacrylamide hydrochloride	acrylamide		

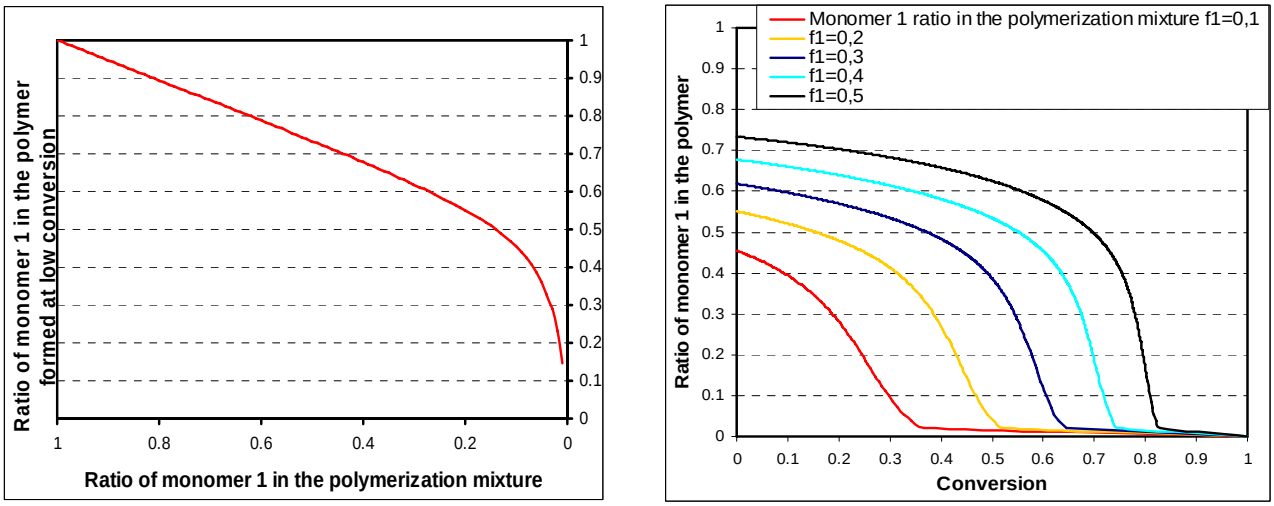

Figure 78: Copolymerization diagram calculated for Amine 1, according to table 17. The AFMO is more reactive and joins the polymer faster than the bulk component (AAM).

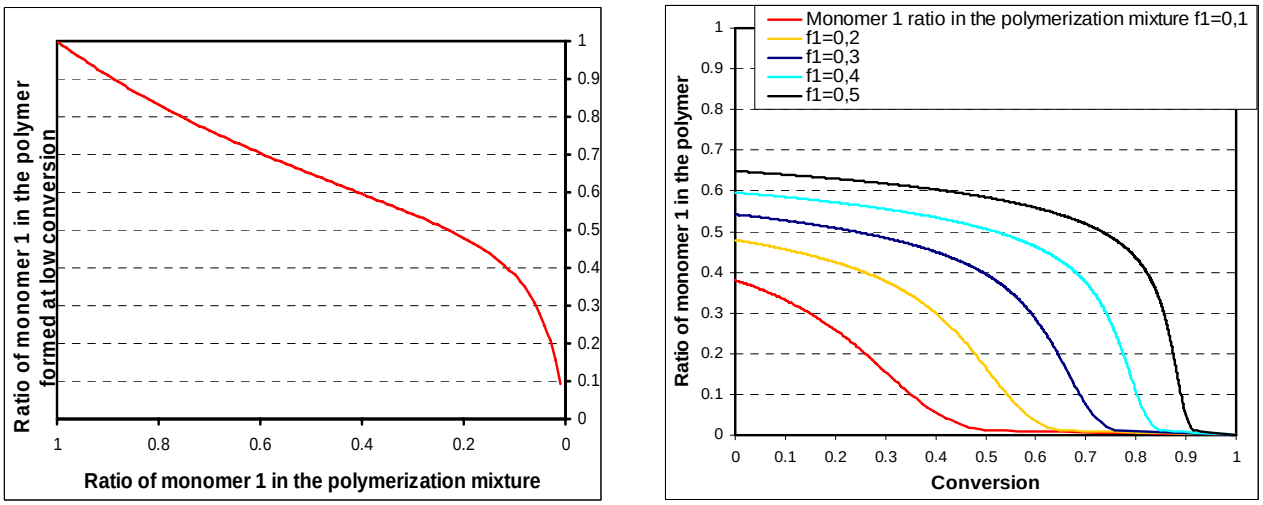

Figure 79: Copolymerization diagram calculated for Amine 2, according to table 17. The AFMO is more reactive and joins the polymer faster than the bulk component (AAM).

For both Amine 1 and Amine 2, similar behaviour can be expected. Due to higher reactivity of the methacryltes, the polymer formed is expected to be richer in AFMO than the current mixture of unreacted monomers. The AFMO content decreases over the course of polymerization as it is consumed more quickly than the bulk component. Consequently, the AFMO is not distributed homogeneously over the acrylate shell, but it is concentrated in the areas that are formed right after the AFMO has been added. Furthermore, it is likely to form AFMO blocks, which is not evident in the diagrams, but can be expected because both systems are examples of "Block copolymerization case 2" (2.4.3).

3.3.2.2 Zeta Potential Measurement

The zeta potential of core particles and core-shell particles was measured as a function of pH:

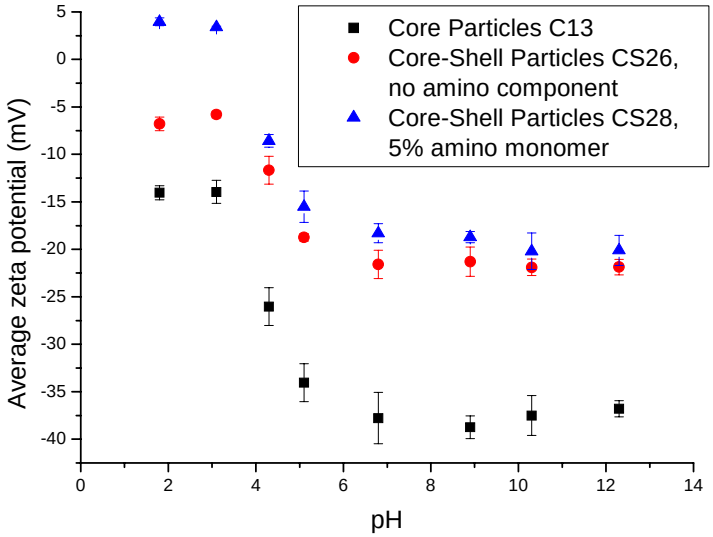

Figure 80: Zeta potential of core particles and core-shell particles with and without AFMO as a function of pH. All exhibit a strong decrease of the negative value at pH 4-5 which is typical for the protonation of a negatively charged carboxy group on the surface.

Like the core particles, the core-shell particles also show a strong increase in zeta potential at pH 4-5 which can be associated with the (second) pK_A of the maleic acid unit. The values at low pH may be less trustworthy since obvious aggregation of the core particles occurs at pH<4. Core-shell particles aggregate as well, but at lower pH. The uncharged acrylamide shell induces a significant overall increase in zeta potential, but the effect of the carboxy groups is still distinct. A possible explanation is only partial covering of the particles. On the other hand, if the acrylamide shell is loose and very permeable, the core which is compact and not swollen by water may still play an important role in the surface chemistry of the CS particles. The expected decrease in zeta potential due to amino protolysis (pH 9-11) is visible but within the uncertainty range. Obviously, the carboxy groups contribute to the zeta potential of the CS particles.

3.3.2.3 Aggregation Stability Testing

It turned out that even if aggregation can be avoided during polymerization, the nano CS particles aggregate upon magnetic collection. In many cases, aggregation is so severe that millimetre-sized lumps are formed and no nano-particles can be separated. Filtration through a syringe filter (400µm) yields completely transparent solutions, without any particles detectable by DLS. Eventually, most dispersions turn colourless, which indicates that not even micro-particles are left. Aggregation of this severity is a problem that needs to be overcome since it prohibits surface access of an indicator during coupling.due to diminished specific surface area. Therefore, several polymerization parameters (ratio of AFMO and crosslinker; basicity of polymerization media) were varied and aggregation stability of the resulting CS particles was tested:

Table 18: Aggregation stability of CS particles in NaCl solution. Z_{av} and PDI of different CS particles when freshly prepared, stored in 100mM NaCl/20mM phosphate buffer and stored in 1M NaCl are compared. Specification of preparation conditions is effected as "ratio in AFMO (Amine2)/ratio in crosslinker (Bis)", both %(n/n); B stands for basic polymerization media; further details can be found in table 6.

Name	Specification	Freshly prepared		100mMNaCl/buffer		1M NaCl	
		Z_{av}/nm	PDI	Z_{av}/nm	PDI	Z_{av}/nm	PDI
CS10	5%/2.5%;B	151.1	0.070	156	0.051	214.8	0.048
CS11	10%/2.5%;B	155.3	0.058	168.8	0.054	271.4	0.116
CS12	20%/2.5%;B	144.8	0.084	2747	0.085	1545.9	0.653
CS13	5%/10%;B	160.3	0.083	162.4	0.043	178.3	0.059
CS14	10%/10%;B	149.3	0.071	185.2	0.054	178.5	0.073
CS15	20%/10%;B	152.5	0.074	177.3	0.056	165.7	0.048
CS16	0%/5%	154.2	0.058	159.8	0.041	158.5	0.057
CS17	2.5%/5%	175.8	0.068	176.9	0.049	177.5	0.050
CS18	5%/5%	182.8	0.069	188.8	0.056	189.0	0.066
CS19	7.5%/5%	193.1	0.054	194.9	0.064	196.4	0.054
CS20	10%/5%	187.9	0.069	192.1	0.050	189.8	0.054
CS21	5%/2.5%	251.9	0.068	291.9	0.124	292.3	0.120
CS22	7.5%/2.5%	195.8	0.062	210.7	0.056	213.7	0.047
CS23	10%/2.5%	327.4	0.180	338.4	0.185	335.0	0.185
CS24	2.5%/10%	176.5	0.066	188.6	0.054	188.7	0.068
CS25	7.5%/10%	162.5	0.047	163.8	0.064	165.1	0.048

An increase in Z_{av}, compared to freshly prepared particles, is considered a sign of aggregation. Size distributions are not shown here, but PDI < 0.100 usually correspond to smooth, single-peaked ones. If PDI is around 0.150, a second peak at >1µm, caused by aggregates, is often observed, and if PDI > 0.200, only a small amount of nano-particles are detectable by DLS and millimetre-sized lumps are usually observable in the sample.

Many samples (CS10, 13, 16-20,24,25) offer reasonable stability at physiological salt concentration and several (16-20,24,25) even in 1M NaCl. In general, aggregation stability is better when crosslinker ratio is higher and it is poor when the ratio is <5% (CS11,12,21-23). There is no well-defined trend concerning AFMO concentration, but if the ratio is too high, severe aggregation occurs even at low salt concentrations (CS12,21,23). If one supposes that aggre-

gation is caused by interactions between amino groups, low crosslinker content may result in more flexible polymer chains within the hydrogel network which can interloop more easily.

Table 19: Aggregation stability of CS particles upon magnetic collection in water, followed by sonication. Z_{av} and PDI of different CS particles when freshly prepared, magnetically collected and sonicated afterwards are compared. Specification of preparation conditions is effected as "ratio in AFMO (Amine2)/ratio in crosslinker (Bis)", both %(n/n); B stands for basic polymerization media; further details can be found in table 6.

Name	Specification	Freshly prepared		Magnetically collected		Sonicated	
		Z_{av}(nm)	PDI	Z_{av}(nm)	PDI	Z_{av}(nm)	PDI
CS10	5%/2.5%;B	151.1	0.070	175.6	0.115	172.3	0.136
CS11	10%/2.5%;B	155.3	0.058	172.9	0.092	250.5	0.357
CS12	20%/2.5%;B	144.8	0.084	1433	0.092	596.1	0.494
CS13	5%/10%;B	160.3	0.083	195.5	0.155	182.8	0.134
CS14	10%/10%;B	149.3	0.071	181.2	0.083	172.2	0.107
CS15	20%/10%;B	152.5	0.074	457.6	0.440	636.6	0.667
CS16	0%/5%	154.2	0.058	187.4	0.080	187.9	0.135
CS17	2.5%/5%	175.8	0.068	625.0	0.343	758.6	0.339
CS18	5%/5%	182.8	0.069	1239	0.577	296.2	0.200
CS19	7.5%/5%	193.1	0.054	625.1	0.601	281.3	0.207
CS20	10%/5%	187.9	0.069	536.3	0.448	320.4	0.307
CS21	5%/2.5%	251.9	0.068	1463	0.576	367.6	0.196
CS22	7.5%/2.5%	195.8	0.062	1610	0.541	435.2	0.297
CS23	10%/2.5%	327.4	0.180	1614	0.583	519.0	0.577
CS24	2.5%/10%	176.5	0.066	336.1	0.303	304.9	0.213
CS25	7.5%/10%	162.5	0.047	642.1	0.566	248.1	0.246

Particles prepared in basic media (CS10-15) exhibit reasonable stability against magnetic collection (unless AFMO content is too high, CS12,15) while the others are subject to aggregation (CS17-25; it does not occur with CS16 as those do not contain any AFMO). In CS12,15,17-25, millimetre-sized aggregates are formed. Sonication in many cases leads to a decrease in Z_{av} (though it even increases with some samples), and large aggregates, if present, dissolve, leaving an optically homogeneous suspension. However, sonication never allows complete regeneration of a nano-suspension once it has aggregated and its success sometimes only lasts for a short time. After several hours, large aggregates are again formed in some samples (that was observed with CS21,25, for instance).

If aggregation is caused by hydrogen bond interactions, it is supposed to be influenced by the pH of the surrounding media. Magnetic collection was thus attempted in basic media (pH12) where, in contrast to neutral water, all amino groups are supposed to be deprotonated, and aggregation was found to be far less critical. That is outlined with some samples in the following:

Table 20: Aggregation stability of CS particles upon magnetic collection in water at different pH. Z_{av} and PDI of different CS particles when freshly prepared and magnetically collected in 100mM phosphate buffer, pH 12 and 7.4, are compared. Specification of preparation conditions is effected as "ratio in AFMO (Amine2)/ratio in crosslinker (Bis)", both %(n/n); B stands for basic polymerization media; further details can be found in table 6.

Name	Specification	Freshly prepared		Collected at pH12		Collected at pH7,4	
		Z_{av}(nm)	PDI	Z_{av}(nm)	PDI	Z_{av}(nm)	PDI
CS10	5%/2.5%;B	151.1	0.070	152.3	0.063	202.3	0.097
CS13	5%/10%;B	160.3	0.083	164.5	0.086	180.8	0.114
CS15	20%/10%;B	152.5	0.074	237.4	0.196	836.5	0.388
CS17	2.5%/5%	175.8	0.068	184.9	0.112	655.7	0.454
CS19	7.5%/5%	193.1	0.054	276.1	0.177	949.0	0.317
CS24	2.5%/10%	176.5	0.066	202.6	0.098	378.1	0.205

Consequently, aggregation of the CS particles investigated can be minimized by using a low AFMO ratio (not higher than 10%, better <5%) and not too low crosslinker ratio (around 10%, not <5%). If copolymerization is carried out in basic media, more stable CS particles can be obtained. Aggregation upon purification by magnetic separation can be suppressed by performing it in basic media. However, certain stability against collection in neutral media has to be achieved, because purification after coupling of a luminescent dye in strongly basic media is not recommended due to low stability of some dyes. Most sensing applications involve pH6-9 (section 2.2.4), thus stability in that pH range should be at least good enough to allow formation of a homogeneous sensor spot. For the system presented, the best approach is to adapt polymerization conditions (as described initially in this paragraph) and purify the CS particles provided by magnetic separation in basic media so that fluorescent labelling can be carried out with nano-particles. After the coupling step, purification can be carried out in neutral or weakly basic media, only limited aggregation will occur, which is not a drawback (aggregated micro-particles are collected faster than nano-particles) as long as no large aggregates (lumps) are formed and formation of a homogeneous spot is still possible.

Attachment of an acrylate shell to magnetic core particles made of PSMA is possible, but introduction of amino-functionalized monomers significantly worsens aggregation stability. By adapting polymerization conditions, particles can be obtained that are stable at physiological pH and salt concentration for a time sufficient for many applications (several days to weeks) and can be magnetically collected.

3.3.3 Covalent Dye Coupling

Dye coupling was attempted with commercial 5(6)-carboxyfluorescein as a model substrate and with synthesized BuPCR.

The amount of labelling dye bound to the particles is a very critical parameter. Too dense charging will result in self-quenching and the fluorescence signal can be very weak or totally absent. On the other hand, if coupling efficiency is poor, and the content of accessible amino groups in the polymeric shell is low, very little dye is bound and the resulting signal is too weak to be detectable in a sample that shows a scattering background and self-absorption by magnetite. CBF was chosen as a pH sensitive model dye because its carboxy function is at-

tached in the same way as the one of BuPCR, spectral properties, pK_A and water solubility are also comparable and it is commercially available. CS particles were prepared for labelling with a high amount (5%), a low amount (0.5%) and without AFMO, as a reference to exclude errors from non-covalent bonding background. As detailed in table 7, CBF amounts range from 10% to 0.005% with respect to the AAM amount introduced into polymerization.
Unfortunately, all particles coupled with CBF and BuPCR were virtually non-fluorescent after a sufficient number of washing steps. Though some of those coupled with CBF showed weak fluorescence enhanced in basic media, the signal was weaker than raman/scattering signals and non-reproducible, i.e. of three samples coupled in the same way never more than one showed any mentionable signal.
Possible reasons for the failure in coupling are manifold. Firstly, there is no definite prove for the presence of amino groups, although the particles obtained by copolymerization with AFMO show different behaviour (above all, regarding aggregation) than those with AAM only, even after the monomers have been washed off. Zeta potential curves (figure 80) indeed do not imply the presence of many amino functions. Poor coupling efficiency may be an additional reason for the lack of a useful fluorescence signal. The latter will be additionally diminished by the strongly absorbing magnetite. On the other hand, an excess of dye molecules bound to the surface can lead to almost complete absence of any fluorescent signal due to self-quenching. This explanation, however, does not seem very probable, not only because a large number of amino groups on the surface does not agree with the recorded zeta potential curve, but also because the relative ratios of dye and particles were varied within a wide range upon coupling. Poor stability of the dye or its link to the particle also should be unlikely because of the stability of the amide bond. Basic hydrolysis of xanthene dyes only occurs at pH values higher than the one of the purification medium. The environment used for immobilization might be unfavourable, but cross-linked acrylate matrices have already been successfully used for the immobilization of pH sensitive xanthenes fluorophores [64]. Finally, an unfortunate arrangement of the amino groups, involving block formation, is possible. If amino groups are very close to each other, self-quenching can occur even if little amino groups or dye molecules are present. That is in agreement with the tendency to form polymer areas of high AFMO-concentration and AFMO blocks (3.3.2.1). In case of a large excess in amino groups, quenching may also be caused by photoinduced electron transfer.

Coupling of amino-functionalized particles with carboxy-functional dyes was not successful. It was concluded that employment of different material (bulk component and/or AFMO) is most promising for the future. An alternative is the preparation of polymerizable dyes and direct integration upon polymerization, without a separate coupling step.

4 Conclusion and Future Prospects

The rhodamines functionalized with two piperazinyl groups show excellent pH sensitivity in the physiological pH range, together with high brightness and moderate long-wave excitability (~530nm). Therefore, they are in principle well suited for applications in solution such as intracellular measurement or microscopy. Unfortunately, immobilization in hydrogel layers turned out to be problematic because the dyes are subject to lactonization in the polymeric matrix. Esterification of the 2'-carboxy group, which prevents lactonization, resulted in loss of sensitivity due to double alkylation of the amino group responsible for PET. Rhodamines carrying only one piperazinyl function are subject to the same issues but show significantly lower sensitivity. The synthetic route towards a PET rhodamine suitable for immobilization is thus complicated and was decided not to be worth the effort since rhodamines are not easily accessible to extension of the chromophore for the preparation of more long-wave excitable dyes anyway.

Bis[4-(dibutylamino)-2-hydroxyphenyl]squaraine is a long-wave excitable (640nm) dye with excellent brightness and sensitivity in an elevated pH range (pH~9). Indeed, it did not show any sensitivity in a useful pH range when incorporated into several immobilization matrices for pH indicators. Furthermore, it suffers from severe photobleaching. In spite of its attractive spectral properties, those issues render it useless for application in pH sensing.

Cl-DMPBI, a perylene bisimide tetrachlorinated in the bay region and carrying two morpholino groups responsible for PET was found to be highly acid-base sensitive but suffers from severe leaching from hydrogel layers. If chlorine atoms are substituted with aryloxy groups, the excitation maximum is red-shifted (from ~520 ~580nm) but acid-base sensitivity is significantly decreased and only present in polar media. Those dyes show luminescence enhancement by a factor of 3-4 which is still useful. Unfortunately, they are not applicable in hydrogel layers due to aggregation issues. The preparation of an asymmetric tertachlorinated bisimide with one bulky substituent and one morpholino group was possible with a surprisingly simple approach. That dye shows good sensitivity when immobilized, though pK_A' is a little low (5,65) for most applications.

For the future, replacement of the morpholino group with another amino function seems promising as it should increase pK_A' and may also enhance sensitivity. The most obvious route towards more long-wave excitable pH-sensitive perylenes is the substitution of chlorine with aryloxy, though the sensitivity of such a dye yet is to be investigated. Alternatives lead to extended chromophores such as terrylenes [135] and perylene bisamidines [136]. Those chromophores are less easily accessible, but may provide a route towards NIR pH indicators.

Regarding magnetic particles, it has to be concluded that the preparation of magnetic pH nano-sensors is difficult or impossible with the material investigated. Variation of the employed monomers appears to be most promising here. On the other hand, preparation of polymerizable dyes is an interesting alternative. In that way, the dye could be incorporated upon copolymerization, without a separate coupling step. Also, the introduction of amino-functionalized monomers in the acrylate shell, which were found to cause troubles, is avoided.

5 References

[1] Valeur, B. Molecular Fluorescence: Principles and Applications. Wiley-VCH Verlag GmbH (2001).

[2] Bissell, R.A. et al. Molecular fluorescent signalling with 'fluor-spacer-receptor' systems: approaches to sensing and switching devices via supramolecular photophysics. *Chem. Soc. Rev.* **21**, 187-195(1992).

[3] Amao, Y. Probes and Polymers for Optical Sensing of Oxygen. *Microchimica Acta* **143**, 1-12(2003).

[4] Borisov, S.M., Nuss, G. & Klimant, I. Red Light-Excitable Oxygen Sensing Materials Based on Platinum(II) and Palladium(II) Benzoporphyrins. *Analytical Chemistry* **80**, 9435-9442(2008).

[5] Zenkl, G., Mayr, T. & Klimant, I. Sugar-Responsive Fluorescent Nanospheres. *Macromolecular Bioscience* **8**, 146-152(2008).

[6] Wu, P. & Brand L. Orientation Factor in Steady-State and Time-Resolved Resonance Energy Transfer Measurements. *Biochemistry* **31**, 7939-7947(1992).

[7] Mayr, T. et al. Light Harvesting as a Simple and Versatile Way to Enhance Brightness of Luminescent Sensors. *Analytical Chemistry* **81**, 6541-6545(2009).

[8] Kim, G. et al. The detection of platelet derived growth factor using decoupling of quencher-oligonucleotide from aptamer/quantum dot bioconjugates. *Nanotechnology* **20**, 175-179(2009).

[9] Webber, S.E. Photon-Harvesting Polymers. *Chem. Rev.* **90**, 1469-1482 (1990).

[10] Wu, P.G. & Brand, L. Resonance Energy Transfer: Methods and Applications. *Analytical Biochemistry* **218**, 1-13(1994).

[11] Levin M.D., Kaszynski P. & Michl J. Photochemical synthesis of bicyclo[1.1.1]pentane-1,3-dicarboxylic acid. *Organic Syntheses* **77** (2000).

[12] Kim, S.H., Natarajan, S. & Liu, G. Photochemical synthesis of oligothiophene thin films and nano-patterns in condensed multilayer films of 2,5-diiodothiophene -Effects of surface chemistry of substrates. *Catalysis Today* **123**, 104-112(2007).

[13] Dong, S. & Zhou, S. Photochemical synthesis of colloidal gold nanoparticles. Materials *Science and Engineering: B* **140**, 153-159(2007).

[14] Lee, S. & Okura, I. Photostable Optical Oxygen Sensing Material: Platinum Tetrakis(pentafluorophenyl)porphyrin Immobilized in Polystyrene. *Anal. Commun*. **34**, 185-188(1997).

[15] Suppan, P. Invited review solvatochromic shifts: The influence of the medium on the energy of electronic states. *Journal of Photochemistry and Photobiology A: Chemistry* **50**, 293-330(1990).

[16] Terenziani, F. et al. Charge Instability in Quadrupolar Chromophores: Symmetry Breaking and Solvatochromism. *Journal of the American Chemical Society* **128**, 15742-15755(2006).

[17] Prochazka, K. & Limpouchova Z. Time-resolved fluorimetry and its application in the study of dynamic processes, conformation changes and associations in polymer systems. *Chemicke Listy* **89**, 288-301(1995).

[18] Resch, U., Rurack K. & Senoner, M. Time-resolved fluorometry in the water analysis *Nachrichten aus Chemie, Technik und Laboratorium* **42**, 504-506(1994).

[19] Mayr, T. et al. Dual lifetime referenced optical sensor membrane for the determination of copper(II) ions. *Analytica Chimica Acta* **462**, 1-10(2002).

[20] Liebsch, G. et al. Fluorescent Imaging of pH with Optical Sensors Using Time Domain Dual Lifetime Referencing. *Analytical Chemistry* **73**, 4354-4363(2001).

[21] Gründler, P. Chemische Sensoren. Eine Einführung für Naturwissenschaftler und Ingeneure. Springer Verlag (2004).

[22] Chemical Sensors. Definitions and classification. *Pure and applied chemistry* **63,** 1247-1250 (1991).

[23] Dudak, F.C. & Boyaci I.H. Rapid and label-free bacteria detection by surface plasmon resonance (SPR) biosensors. *Biotechnology Journal* **4**, 1003-1011(2009).

[24] Arain, S. et. al. Characterization of microtiterplates with integrated optical sensors for oxygen and pH, and their applications to enzyme activity screening, respirometry, and toxicological assays. *Sensors and Actuators B: Chemical* **113**, 639-648(2006).

[25] Schouest, K., Zitova, A., Spillane, C. & Papkovsky, D. B. Toxicological assessment of chemicals using Caenorhabditis elegans and optical oxygen respirometry. *Environmental Toxicology and Chemistry* **28**, 791-799(2009).

[26] Mills, A. Oxygen indicators and intelligent inks for packaging food. *Chem. Soc. Rev.* **34**, 1003-1011(2005).

[27] Bizzarri, A. et al. Continuous oxygen monitoring in subcutaneous adipose tissue using microdialysis. *Analytica Chimica Acta* **573**, 48-56(2006).

[28] Roy, T.W. & Bhagwat, A.S. Kinetic studies of Escherichia coli AlkB using a new fluorescence-based assay for DNA demethylation. *Nucl. Acids Res.* **35**, 147(2007).

[29] Hamilton, N. Quantification and its Applications in Fluorescent Microscopy Imaging. *Traffic* **10**, 951-961(2009).

[30] Stahl, H.et al. Time-resolved pH imaging in marine sediments with a luminescent planar optode. *Limnology and Oceanography: Methods* **4**, 336-345(2006).

[31] Acosta, M.A. et al. Fluorescent microparticles for sensing cell microenvironment oxygen levels within 3D scaffolds. *Biomaterials* **30**, 3068-3074(2009).

[32] Rosenauer, M. & Vellekoop, M.J. 3D fluidic lens shaping-A multiconvex hydrodynamically adjustable optofluidic microlens. *Lab Chip* **9**, 1040-1042(2009).

[33] Fang, H., Mighri, F. & Ajji, A. Miscibility characterization of SMA/SAN and SMA/PMMA blends by differential scanning calorimetry and fluorescence techniques. *Journal of Applied Polymer Science* **105**, 2955-2962(2007).

[34] Wilschut, K. et al. Fluorescencein situ hybridization to monitor the intracellular location and accessibility of plasmid DNA delivered by cationic polymer-based gene carriers. *European Journal of Pharmaceutics and Biopharmaceutics* **72**, 391-396(2009).

[35] Lin, C. & Zhao, J. Nile red probing for sphere-to-rod-to-wormlike micelle transition in aqueous surfactant solution. *Dyes and Pigments* **84**, 223-228(2010).

[36] Borisov, S.M. et al. Composite Material for Simultaneous and Contactless Luminescent Sensing and Imaging of Oxygen and Carbon Dioxide. *Advanced Materials* **18**, 1511-1516(2006).

[37] Lieberzeit, P. et al. Polymers imprinted with PAH mixtures—comparing fluorescence and QCM sensors. *Analytical and Bioanalytical Chemistry* **392**, 1405-1410(2008).

[38] Doubell, M.J. et al. An advanced laser-based fluorescence microstructure profiler (TurboMAP-L) for measuring bio-physical coupling in aquatic systems. *J. Plankton Res*. **31**, 1441-1452(2009).

[39] De Silva, A.P.D., Gunnlaugsson, T. & Rice, T.E. Recent evolution of luminescent photoinduced electron transfer sensors. A review. *Analyst* **121**, 1759-1762(1996).

[40] Weidgans, B.M. et al. Fluorescent pH sensors with negligible sensitivity to ionic strength. *Analyst* **129**, 645-650(2004).

[41] Borisov, S. et al. New NIR-emitting complexes of platinum(II) and palladium(II) with fluorinated benzoporphyrins. *Journal of Photochemistry and Photobiology A: Chemistry* **201**, 128-135(2009).

[43] http://www.oceanoptics.com/Products/ls450.asp; 27.12.2009

[44] Filevich, O. & Etchenique, R. 1D and 2D Temperature Imaging with a Fluorescent Ruthenium Complex. *Analytical Chemistry* **78**, 7499-7503(2006).

[45] Marazuela, M. & Moreno-Bondi, M. Fiber-optic biosensors - an overview. *Analytical and Bioanalytical Chemistry* **372**, 664-682(2002).

[46] Mayr, T. et al. A planar waveguide optical sensor employing simple light coupling. *Analyst* **134**, 1544-1547(2009).

[47] Gauglitz, G. Direct optical sensors: principles and selected applications. *Analytical and Bioanalytical Chemistry* **381**, 141-155(2005).

[48] Waich, K. u. a. Dual lifetime referenced trace ammonia sensors. *Sensors and Actuators B: Chemical* **139**, 132-138(2009).

[49] Janata J. Do optical sensors really measure pH? *Anal. Chem.* **59,** 1351-1356(1987).

[50] Janata J. Ion optodes. *Anal. Chem.* **64,** 921A-927A(1992).

[51] Borisov, S.M., Mayr, T. & Klimant, I. Poly(styrene-block-vinylpyrrolidone) Beads as a Versatile Material for Simple Fabrication of Optical Nanosensors. *Analytical Chemistry* **80**, 573-582(2008).

[52] Opitz, N. & Lübbers, D. New fluorescence photometrical techniques for simultaneous and continuous measurements of ionic strength and hydrogen ion activities. *Sensors and Actuators* **4**, 473-479(1983).

[53] Munkholm, C.& Walt, D.E. Polymer Modification of Fiber Optic Chemical Sensors as a

Method of Enhancing Fluorescence Signal for pH Measurement. *Anal. Chem.* ***58,*** 1427-1430(1986).

[54] Strömberg, N., Mattsson, E. & Hakonen, A. An imaging pH optode for cell studies based on covalent attachment of 8-hydroxypyrene-1,3,6-trisulfonate to amino cellulose acetate films. *Analytica Chimica Acta* **636**, 89-94(2009).

[55] Mohr, G. et al. Design of acidochromic dyes for facile preparation of pH sensor layers. *Analytical and Bioanalytical Chemistry* **392**, 1411-1418(2008).

[56] Bissell, R.A. et al. Luminescence and charge transfer. Part 2. Aminomethyl anthracene derivatives as fluorescent PET (photoinduced electron transfer) sensors for protons. *J. Chem. Soc., Perkin Trans*. **2** 1559-1564(1992).

[57] Daffy, L.M. et al. Arenedicarboximide Building Blocks for Fluorescent Photoinduced Electron Transfer pH Sensors Applicable with Different Media and Communication Wavelengths. *Chemistry - A European Journal* **4**, 1810-1815(1998).

[58] Kocincova, A.S. et al. Fiber-Optic Microsensors for Simultaneous Sensing of Oxygen and pH, and of Oxygen and Temperature. *Analytical Chemistry* **79**, 8486-8493(2007).

[59] Schulman, S.G. et al. Dependence of the fluorescence of immobilized 1-hydroxypyrene-3,6,8-trisulfonate on solution pH: Extension of the range of applicability of a pH fluorosensor. *Analytica Chimica Acta* **304**, 165-170(1995).

[60] Borisov, S.M., Herrod, D.L. & Klimant, I. Fluorescent poly(styrene-block-vinylpyrrolidone) nanobeads for optical sensing of pH. *Sensors and Actuators B: Chemical* **139**, 52-58(2009).

[61] Pastoriza-Munoz, E., Harrington, R.M. & Graber,M.L. Parathyroid hormone decreases HCO_3 reabsorption in the rat proximal tubule by stimulating phosphatidylinositol metabolism and inhibiting base exit. *J. Clin. Invest.* **89**, 1485-1495(1992).

[62] Graber, M. et al. Acetazolamide inhibits acidification by the turtle bladder independent of cell pH.*American Journal of Physiology* **256**, F923-F93(1989).

[63] http://www.invitrogen.com/site/us/en/home/References/Molecular-Probes-The-Handbook/pH-Indicators/Probes-Useful-at-Near-Neutral-pH.html; 11.2.2010

[64] Waich, K., Mayr, T. & Klimant, I. Fluorescence sensors for trace monitoring of dissolved ammonia. *Talanta* **77**, 66-72(2008).

[65] Aust S. et al. Melatonin Modulates Acid/Base Transport in Human Pancreatic Carcinoma Cells. *Cell Physiol Biochem* **18***,* 91-102(2006).

[66] Hermanson, G.T. Bioconjugate Techniques. Second Edition. Elsivier Inc. (2008)

[67] Whitaker, J.E., Haugland, R.P. & Prendergast, F.G. Spectral and photophysical studies of benzo[c]xanthene dyes: Dual emission pH sensors. *Analytical Biochemistry* **194**, 330-344(1991).

[68] Neurauter, G., Klimant, I. & Wolfbeis, O.S. Fiber-optic microsensor for high resolution pCO2 sensing in marine environment. *Fresenius' Journal of Analytical Chemistry* **366**, 481-487(2000).

[69] Mills, A., Lepre, A. & Wild, L. Breath-by-breath measurement of carbon dioxide using a plastic film optical sensor. *Sensors and Actuators B: Chemical* **39**, 419-425(1997).

[70] Wolfbeis, O.S., Weis. L., Leiner, M.J.P. & Ziegler, W.E. Fiber-optic Fluorosensor for Oxygen and Carbon Dioxide. *Anal Chem* **60**, 2028-2030(1988).

[71] Waich, K., Mayr, T. & Klimant, I. Microsensors for detection of ammonia at ppb-concentration levels. *Measurement Science and Technology* **18**, 3195-3201(2007).

[72] Letard, J.F., Lapouyade, R. & Rettig W. Synthesis and photophysical study of 4-(N-monoaza-15-crown-5) stilbenes forming TICT* states and their complexation with cations. *Pure and Appl. Chem.*, **65**, 1705-1712(1993).

[73] Bourson, J., Pouget, J. & Valeur, B. Ion-Responsive Fluorescent Compounds. 4. Effect of Cation Binding on the Photophysical Properties of a Coumarin Linked to Monoaza- and Diaza-Crown Ethers. *J. Phys. Chem.* **97***,* 4552-4557(1993).

[74] Bourson J. & Valeur B. Ion-Responsive Fluorescent Compounds. 2. Cation-Steered Intramolecular Charge Transfer in a Crowned Merocyanine. *J. Phys. Chem.* **93***,* 3871-3876 (1989).

[75] Lu, Y. & Paige, M. An Ensemble and Single-molecule Fluorescence Spectroscopy Investigation of Calcium Green 1, a Calcium-ion Sensor. *Journal of Fluorescence* **17**, 739-748(2007).

[76] Morf, W. et al. Design of a Calcium-Selective Optode Membrane Based on Neutral Ionophores. *Analytical Chemistry* **62**, 738-742 (1990).

[77] Urbano, E., Offenbacher, H. & Wolfbeis, O.S. Optical sensor for continuous determination of halides. *Analytical Chemistry* 56, 427-429(1984).

[78] Wang, E. & Meyerhoff, M.E. Anion selective optical sensing with metalloporphyrin-doped polymeric films. *Analytica Chimica Acta* **283**, 673-682(1993).

[79] Bacon, J.R. & Demas, J.N. Determination of Oxygen Concentrations by Luminescence Quenching of a Polymer- Immobilized Transition-Metal Complex. *Anal. Chem.*, **59,** 2780-2785(1987).

[80] Borisov, S. et al. Photophysical properties of the new phosphorescent platinum(II) and palladium(II) complexes of benzoporphyrins and chlorins. *Journal of Photochemistry and Photobiology A: Chemistry* **206**, 87-92(2009).

[81] Borisov, S.M. & Klimant, I. Ultrabright Oxygen Optodes Based on Cyclometalated Iridium(III) Coumarin Complexes. *Analytical Chemistry* **79**, 7501-7509(2007).

[82] Carraway, E.R. et al. Photophysics and photochemistry of oxygen sensors based on luminescent transition-metal complexes. *Analytical Chemistry* **63**, 337-342(1991).

[83] Borisov, S.M. & Klimant, I. Optical nanosensors-smart tools in bioanalytics. *Analyst* **133**, 1302-1307(2008).

[84] Clark, H.A. et al. Optical Nanosensors for Chemical Analysis inside Single Living Cells. 1. Fabrication, Characterization, and Methods for Intracellular Delivery of PEBBLE Sensors. *Analytical Chemistry* **71**, 4831-4836(1999).

[85] Clark, H.A. et al. Optical Nanosensors for Chemical Analysis inside Single Living Cells. 2. Sensors for pH and Calcium and the Intracellular Application of PEBBLE Sensors. Analytical Chemistry **71**, 4837-4843(1999).

[86] Buck, S.M. et al. Optochemical nanosensor PEBBLEs: photonic explorers for bioanalysis with biologically localized embedding. *Current Opinion in Chemical Biology* **8,** 540-546 (2004).

[87] Xu, H. et al. A Real-Time Ratiometric Method for the Determination of Molecular Oxygen Inside Living Cells Using Sol−Gel-Based Spherical Optical Nanosensors with Applications to Rat C6 Glioma. *Analytical Chemistry* **73**, 4124-4133(2001).

[88] Chen, J. et al. A functionalized gold nanoparticles and Rhodamine 6G based fluorescent sensor for high sensitive and selective detection of mercury(II) in environmental water samples. *Analytica Chimica Acta* **599**, 134-142(2007).

[89] Sandros, M.G., Shete, V. & Benson, D.E. Selective, reversible, reagentless maltose biosensing with core-shell semiconducting nanoparticles. *Analyst* **131**, 229-235(2006).

[90] Burns, A. et al. Core/Shell Fluorescent Silica Nanoparticles for Chemical Sensing: Towards Single-Particle Laboratories13. *Sma*ll **2**, 723-726(2006).

[91] Mistlberger, G., Chojnacki, P. & Klimant, I. Magnetic sensor particles: an optimized magnetic separator with an optical window. *Journal of Physics D: Applied Physics* **41**, 41-49(2008).

[92] Odian, G. Principles of Polymerization, 4th Edition. Wiley&Sons (2004)

[93] Elaissari, A. Coloial Polymers, Synthesis and Characterization. Marcel Dekker Inc. (2003)

[94] http://old.iupac.org/reports/1996/6812jenkins/molecules.html#1.1; 28.12.2009

[95] Mayo, F.R. & Walling, C. Copolymerization. Chemical Reviews **46**, 191-287(1950).

[96] Sun, L. et al. pH sensor based on upconverting luminescent lanthanide nanorods. *Chem. Commun.* 5000-5002(2009).

[97] http://www.malvern.com/common/downloads/campaign/MRK656-01.pdf; 8.2.2010

[98] Weller, A. Electron-Transfer and complex formation in the excited state. *Pure Appl. Chem.* **16,** 115-123(1968).

[99] De Silva A.P. et al. New fluorescent model compounds for the study of photoinduced electron transfer: the influence of a molecular electric field in the excited state. *Angewandte Chemie, International Edition in English*, **34**, 1728-1731(1995).

[100] Yuan, D., Brown, R.G. J. The effect of pH on the absorption and fluorescence properties of some 4-amino-N-alkylamino-1,8-naphthalimides. *Journal of Chemical Research, Synopses* **11**, 418-419(1994).

[101] DeSilva, A.P.D. et al. Bright molecules with sense, logic, numeracy and utility. *Org. Biomol. Chem.* **6**, 2468-2480(2008).

[102] Bissell, R.A. et al. Fluorescent PET (photoinduced electron transfer) indicators for solvent polarity with quasi-step functional response. *Tetrahedron Letters* **32**, 425-428(1991).

[103] Magri, D. et al. The Anthracen-9-ylmethyloxy Unit: An Underperforming Motif Within the Fluorescent PET (Photoinduced Electron Transfer) Sensing Framework. *Journal of Fluorescence* **15**, 769-775(2005).

[104] Ireland, J.F. & Wyatt, P.A.H. Acid-base properties of electronically excited states of organic molecules. *Adv. Phys. Org. Chem.* **12,** 131(1976).

[105] Shizuka, H., Ogiwara, T. & Kimura, E. NaCl Effect on the Excited-State Proton Dissociation Reaction of Naphthols: Water Structure in the Presence of NaCl**,** *J. Phys. Chem.,* **89**, 4302(1986).

[106] Werner, T. et al.. Novel optical pH-sensor based on a boradiaza-indacene derivative, *Fresenius J Anal Chem* **359**, 150–154(1997).

[107] Kano, K., Takenoshita, I. & Ogawa, T. Fluorescence quenching of pyrene and naphthalene in aqueous cyclodextrin solutions. Evidence of three-component complex formation. *Journal of Physical Chemistry*, **86**, 1833-1838(1982).

[108] DeSilva, A.P.D. et al. Compartmental fluorescent pH indicators with nearly complete predictability of indicator parameters; molecular engineering of pH sensors. *J. Chem. Soc., Chem. Commun.* 1054-1056(1989).

[109] Hirano, T. et al. Novel Zinc Fluorescent Probes Excitable with Visible Light for Biological Applications13. *Angewandte Chemie International Edition* **39**, 1052-1054(2000).

[110] Golchini, K. et al. Synthesis and characterization of a new fluorescent probe for measuring potassium. American Journal of Physiology **258**, F438-F443(1990).

[111] Aoki, I., Sakaki, T. & Shinkai, S. A new metal sensory system based on intramolecular fluorescence quenching on the ionophoric calix[4]arene ring. *J. Chem. Soc., Chem. Commun.* 730-732(1992).

[112] De Silva, A.P.D. & Sandanayake, K.R.A.S. Fluorescent PET (photo-induced electron transfer) sensors for alkali metal ions with improved selectivity against protons and with predictable binding constants. *J. Chem. Soc., Chem. Commun.* 1183-1185(1989).

[113] Tsien, R.Y. New calcium indicators and buffers with high selectivity against magnesium and protons: design, synthesis, and properties of prototype structures. *Biochemistry* **19**, 2396-2404(1980).

[114] DeSilva, A.P.D. & Gunaratne, H.Q.N. Fluorescent PET (photoinduced electron transfer) sensors selective for submicromolar calcium with quantitatively predictable spectral and ion-binding properties. *J. Chem. Soc., Chem. Commun.* 186-188(1990).

[115] Fabbrizzi, L. & Poggi, A. Sensors and switches from supramolecular chemistry. *Chem. Soc. Rev*. **24**, 197-202(1995).

[116] Parker, D. & Williams, J.A.G. Luminescence behaviour of cadmium, lead, zinc, copper, nickel and lanthanide complexes of octadentate macrocyclic ligands bearing naphthyl chromophores. *J. Chem. Soc., Perkin Trans.* **2** 1305-1314(1995).

[117] www.fluorophores.org; 29.12.2009

[118] Beija, M., Afonso, C.A.M. & Martinho, J.M.G. Synthesis and applications of Rhodamine derivatives as fluorescent probes. *Chem. Soc. Rev.* **38**, 2410-2433(2009).

[119] Drexhage, K.H. Fluorescence efficiency of laser dyes. *Journal of Research of the National Bureau of Standards, Section A: Physics and Chemistry* **80A**, 421-428(1976).

[120] Cosby, G.A. & Demas, J.N. Measurement of photoluminescence quantum yields. Review. *Journal of Physical Chemistry* **75**, 991-1024(1971).

[121] Bossi, M. et al. Multicolor Far-Field Fluorescence Nanoscopy through Isolated Detection of Distinct Molecular Species. *Nano Letters* **8**, 2463-2468(2008).

[122] Liu, W. et al. Compact Biocompatible Quantum Dots Functionalized for Cellular Imaging. *Journal of the American Chemical Society* **130**, 1274-1284(2008).

[123] Vogel, M. et al. Structural relaxation of rhodamine dyes with different N-substitution patterns: A study of fluorescence decay times and quantum yields. *Chemical Physics Letters* **147**, 452-460(1988).

[124] Matray, T., Hernandez, V. & Singh, S. Electrophoretic tag reagents comprising fluorescent compounds. *U.S. Pat. Appl*., 2002-0146726(2002).

[125] Ge, F. et al. New Fluorescent Labels: 4- and 7-Chlorofluorescein. *Journal of Fluorescence* **15**, 829-833(2005).

[126] Hilderbrand, S.A. & Weissleder, R. One-pot synthesis of new symmetric and asymmetric xanthene dyes. *Tetrahedron Letters* **48**, 4383-4385(2007).

[127] Streitwieser, A. Heathcock, C.H. Introduction to Organic Chemistry. Macmillan Publishing Co., Inc. (1976).

[128] Cohen, S., Lacher, J.R. & Park, J.D. Dioxocyclobutendiol. *J. Amer. Chem. Soc.* **81**, 3480 (1959).

[129] Sprenger, H.-E. & Ziegenbein, W. Cyclobutendiylium-Farbstoffe. *Angewandte Chemie* **14**, 541-546(1968).

[130] Law, K. & Bailey, F.C. Squaraine Chemistry: Synthesis, Characterization and Xerographic Properties of Bis(4-methylbenzylaminophenyl)-squaraine and Its Derivatives. *Dyes and Pigments* **9**, 85-107(1988).

[131] Law, K.Y. Squaraine Chemistry. Effects of Structural Changes on the Absorption and Multiple Fluorescence Emission of Bis[4-(dimethylamino)phenyl]squaraine and Its Derivatives. *J. Phys. Chem.* **91**, 5184-5193(1987).

[132] Champ, R.B. & Shattuch, M.D. Sensitive electrophotographic plates. *U.S. Pat. Appl.* (1974), 1974-3824099(1974).

[133] Law, K.Y. Effects of fabrication and aging on the xerographic properties of squaraine photoreceptor devices. Journal of Imaging Science **31**, 83-93(1987).

[134] Merritt, V.Y. & Hovel, H.J. Organic solar cells of hydroxy squarylium. *Appl. Phys. Lett.* **29**, 414-415(1976).

[135] Isgor, Y.G. & Akkaya, E.U. Chemosensing in deep red: A squaraine-based fluorescent chemosensor for pH. *Tetrahedron Letters* **38**, 7417-7420(1997).

[136] Kraft, A., Grimsdale, A.C. & Holmes, A.B. Electroluminescent conjugated polymers-seeing polymers in a new light. *Angew Chem Int Ed* **37,** 403-428(1998).

[137] Würthner, F. Plastic Transistors Reach Maturity for Mass Applications in Microelectronics13. *Angewandte Chemie International Edition* **40**, 1037-1039(2001).

[138] Breeze, A.J. et al. Polymer-perylene diimide heterojunction solar cells. *Appl. Phys. Lett*. **81**, 3085-3087(2002).

[139] Seybold, G. & Wagenblast, G. New perylene and violanthrone dyestuffs for fluorescent collectors. *Dyes and Pigments* **11**, 303-317(1989).

[140] Law, K.Y. Organic photoconductive materials: recent trends and developments. *Chem Rev* **93**, 449-486(1993).

[141] Reisfeld, R. & Seybold, G. Solid-state tunable lasers in the visible, based on luminescent photoresistant heterocyclic colorants. Chimia **44** 295-27(1990).

[142] O'Neil, M.P. et al. Picosecond optical switching based on biphotonic excitation of an electron donor-acceptor-donor molecule. *Science* **257**, 63-65(1992).

[143] Rademacher, A., Märkle, S. & Langhals, H. Lösliche Perylen-Fluoreszenzfarbstoffe mit hoher Photostabilität. *Chemische Berichte* **115**, 2927-2934(1982).

[144] Holtrup, F.O. et al. Terrylenimides: New NIR Fluorescent Dyes. *Chemistry - A European Journal* **3**, 219-225(1997).

[145] Quante, H., Geerts, Y. & Mullen, K. Synthesis of Soluble Perylenebisamidine Derivatives. Novel Long-Wavelength Absorbing and Fluorescent Dyes. *Chemistry of Materials* **9**, 495-500(1997).

[146] Koenemann, M, BASF AG. Halogen-containing perylene tetracarboxylic acid derivatives and the use thereof.PCT Int. Appl. (2009), WO 2009024512 A1 20090226

[147] Wang, W., Shaller, A.D. & Li, A.D.Q. Twisted Perylene Stereodimers Reveal Chiral Molecular Assembly Codes. *Journal of the American Chemical Society* **130**, 8271-8279(2008).

[148] Wurthner, F. et al. Preparation and Characterization of Regioisomerically Pure 1,7-Disubstituted Perylene Bisimide Dyes. *The Journal of Organic Chemistry* **69**, 7933-7939(2004).

[149] Fan, L., Xu, Y. & Tian, H. 1,6-Disubstituted perylene bisimides: concise synthesis and characterization as near-infrared fluorescent dyes. *Tetrahedron Letters* **46**, 4443-4447(2005).

[150] Kohl, C. et al. Towards Highly Fluorescent and Water-Soluble Perylene Dyes. *Chemistry - A European Journal* **10**, 5297-5310(2004).

[151] http://www.performancechemicals.basf.com/ev-wcms-in/internet/en_GB/function/evproducts:/document/30133188/TDS; 13.2.2010

[152] Würthner, F., Thalacker, C. & Sautter, A. Hierarchical Organization of Functional Perylene Chromophores to Mesoscopic Superstructures by Hydrogen Bonding and π-π Interactions. *Advanced Materials* **11**, 754-758(1999).

[153] Baffreau, J. et al. Fullerene C_{60}-Perylene-3,4:9,10-bis(dicarboximide) Light-Harvesting Dyads: Spacer-Length and Bay-Substituent Effects on Intramolecular Singlet and Triplet Energy Transfer. *Chemistry - A European Journal* **14**, 4974-4992(2008).

[154] Nagao, Y. et al. Synthesis of unsymmetrical perylenebis(dicarboximide) derivatives. *Chemistry Letters* **2**, 151-154(1979).

[155] Kaiser, H., Lindner, J. & Langhals, H. Synthese von nichtsymmetrisch substituierten Perylen-Fluoreszenzfarbstoffen. *Chemische Berichte* **124**, 529-535(1991).

[156] Mistlberger, G., Borisov, S.M. & Klimant, I. Enhancing performance in optical sensing with magnetic nanoparticles. *Sensors and Actuators B: Chemical* **139**, 174-180(2009).

[157] Di Pasqua, A.J. et al. Preparation of antibody-conjugated gold nanoparticles. *Materials Letters* **63**, 1876-1879(2009).

[158] Jiang, X. et al. Biotinylated Glyco-Functionalized Quantum Dots: Synthesis, Characterization, and Cytotoxicity Studies. *Bioconjugate Chemistry* **20**, 994-1001(2009).

[159] Bonanno, L.M. & DeLouise L.A. Optical detection of polyacrylamide swelling behaviour in a porous

silicon sensor. *Mater. Res. Soc. Symp. Proc.* **1133** (2009).
[160] Schröder, C. Luminescent planar single and dual optodes for time-resolved imaging of pH, pCO2 and pO2 in marine systems. Dissertation. Universität Regensburg (2006).
[161] Nudelman, R. et al. Modular Fluorescent-Labeled Siderophore Analogues. *J Med Chem* **41**, 1671-1678 (1998).
[162] Law, K.Y. Squaraine chemistry. A study of the solute-solvent complexation of squaraine in solvents by proton NMR spectroscopy. *Journal of Physical Chemistry* **93***,* 5925-5930 (1989).
[163] Du,H. et al. Photochem CAD: a computer-aided design and research tool in photochemistry. *Photochemistry and Photobiology* **68**, 141-142 (1998).
[164] http://www.sigmaaldrich.com/germany.html; 29.12.2009.
[165] http://www.piercenet.com/Objects/View.cfm?type=Page&ID=C0B555CC-0F33-4818-B09D-031E7FCF89FC; 6.2.2010
[166] Grabarek, Z. & Gergely, J. Zero-length crosslinking procedure with the use of active esters. *Analytical Biochemistry* **185**, 131-135(1990).
[167] Bille J. & Schlegel, W. Medizinische Physik 1. Grundlagen. Springer Verlag (1999).
[168] Krieger, H. Grundlagen der Strahlenphysik und des Strahlenschutzes. 1.Auflage. B.G. Teubner Verlag (2004).
[169] http://www.stephansymons.de/info/proteinnachweis.pdf; 21.10.2009.
[170] Saleh, N., Al-Soud, Y.A. & Nau, W.M. Molecular and Biomolecular Spectroscopy : Novel fluorescent pH sensor based on coumarin with piperazine and imidazole substituents. *Spectrochimica Acta Part A* **71**, 818-822(2008).
[171] De Silva, A.P.D. & Rupasinghe, R.A.D.D. A new class of fluorescent pH indicators based on photo-induced electron transfer. *J. Chem. Soc., Chem. Commun*. 1669-1670(1985).
[172] Shabarov, U.S. Organic Chemistry. Chimia, Moscow (1994).
[173] Zenkl, G. Optical glucose sensors based on synthetic receptors. Dissertation. Technische Universität Graz (2009).
[174] Dashtiev, M. et al. Clear Evidence of Fluorescence Resonance Energy Transfer in Gas-Phase Ions. *Journal of the American Society for Mass Spectrometry* **16**, 1481-1487(2005).
[175] Liu, Y. et al. Assembly and Characterization of Novel Hydrogen-Bond-Induced Nanoscale Rods. *The Journal of Organic Chemistry* **69**, 9049-9054(2004).
[176] http://evans.harvard.edu/pdf/evans_pKa_table.pdf; 19.11.2009
[177] Zhang, Y. et al. Highly soluble perylene tetracarboxylic diimides and tetrathiafulvalene-perylene tetracarboxylic diimide-tetrathiafulvalene triads. *Journal of Photochemistry and Photobiology A: Chemistry* **200**, 334-345(2008).
[178] Brandrup, J., Immergut, E.H. & Grulke E.A. Polymer Handbook, 4th Edition, John Wiley & Sons, Inc., Hoboken, New Jeresy (1999).

6 Appendix

6.1 List of Chemicals

Chemical	Abbreviation	Supplier	Purity
Tetrahydrofurane	THF	Roth	Synthesis grade
Acetone	Acetone	Roth	Synthesis grade
n-Hexane		Roth	Synthesis grade
Ethanol	EtOH	Roth	Synthesis grade
Methanol	MeOH	Roth	Synthesis grade
Methylene chloride	CH_2Cl_2	Roth	Synthesis grade
Sodium citrate dihydrate		SAFC	≥99%
1-Ethyl-3-(3-dimethyl aminopropyl) carbo-diimide hydrochloride	EDC	TCI Europe	≥98%
Poly(styrene-*co*-maleic anhydride) EF80	PSMA	Sartomere	
Trimellitic anhydride	TMA	Fluka	≥97%
Methanesuflonic acid	$MeSO_3H$	Fluka	≥99%
3-(1-Piperazinyl)phenol	PipPh	ABCR	98%
Chloroform-d	$CDCl_3$	Aldrich	99,8% D
Dimethylsulfoxide d6	DMSO-d6	ABCR	99% D
Dibutylsulfate	Bu_2SO_4	ABCR	95%
Ammonia, 25% aqueous solution	NH_3	Roth	25%
Ethyldiisopropylamine	EDIPA	Sigma-Aldrich	≥99%
Dimethylformamide (anhydrous)	DMF	Sigma-Aldrich	≥99,8%
Chloroform	$CHCl_3$	Roth	Synthesis grade
Trifluoracetic acid	CF_3COOH	Roth	≥99,9%
Sodiumchloride	NaCl	Roth	≥99,5%
Silica gel		Roth	
N,N'-Dicyclohexacarbodiimide	DCC	Fluka	99%
Propionic acid	EtCOOH	ABCR	99%
Piperazine		Aldrich	99%
N-Hydroxysuccinimide	NHS	Fluka	≥97%
1-Octadecylamine	ODA	ABCR	98%
1-Octylamine	OAM	Aldrich	99%
Rhodamine 101		Fluka	Fluorescence grade
Triethylamine	Et_3N	Riedel de Haen	99%
Ethyl acetate	EE	Roth	Synthesis grade
Sodium hydroxide	NaOH	Roth	≥99%
Hydrochloric acid (concentrated)	HCl	Roth	37%
Sulforhodamine B acid chloride		Fluka	≥95%
Sodium hydrogen carbonate	$NaHCO_3$	Fluka	≥99,7%
Acetonitrile	CH_3CN	Roth	Synthesis grade
Sodium phosphate	Na_3PO_4	Riedel de Haen	≥94%
Disodium hydrogenphosphate	Na_2HPO_4	Roth	≥99%
Disodium hydrogenphosphate	NaH_2PO_4	Roth	≥99%
Sodium carbonate	Na_2CO_3	Roth	98%
2-Morpholinoethanesulfonic acid monohyd-rate	MES	Fluka	≥99,5%
Sodium sulfate (anhydrous)	Na_2SO_4	Sigma-Aldrich	≥99%
2-(4-Dibutylamino-2-hydroxybenzoyl)benzoic acid		Aldrich	99%
n-Butyl iodide	n-BuI		99%
Potassium carbonate	K_2CO_3	Merck	p.A. grade
Dimethyl sulfoxide	DMSO	Roth	99%
m-Dibutylaminophenol		TCI Europe	95%

Squaric acid		ABCR	98%
1-Butanol	1-BuOH	ABCR	99%
Toluene	$PhCH_3$	Roth	Synthesis grade
N-Methyl-2-pyrrolidone	NMP	ABCR	99%
3,4,9,10-Tetrachloro-1,6,7,12-perylene tetracarboxylic bisanhydride	TCPBA	SYNTHON Chemicals Gmbh	
3-Morpholinopopyl-1-amine		Sigma	99%
Phenol		Roth	99,5%
4-*tert*-Butylphenol		Aldrich	99%
2,6-Diisopropylaniline		Acros	92%
Tetrabutylammoniumhydroxide, 1M in MeOH	TBAOH	Sigma-Aldrich	
2-Mercaptoethanol		Roth	99%
Cyclohexene		Acros	99%
Nile Blue		EGA Chemie	78%
Rhodamine B		Fluka	99%
Polystyrene-co-vinylpyrrolidone particles, 38% aqueous emulsion	PS/PVP	Aldrich	38%
Eudragit RL100		Degussa	
EMG 1300 magnetic particles		Ferrotec	
Acrylamide	AAM	Acros	98,5%
N-(3-Aminopropyl)methacrylamide hydro-chloride	Amine 2	Polysciences Inc.	
2-Aminoethylmethacrylate hydrochloride	Amine 1	Aldrich	
N-Hydroxysulfosuccinimide sodium salt	Sulfo-NHS	Aldrich	>99%
Sodium peroxodisulfate	KPD	Roth	99%
Sodium dodecylsulfate	SDS	Fluka	>98%
N,N' Methylenebisacrylamide	Bis	Acros	96%

6.2 List of Figures

6.3 List of Schemes

6.4 List of Tables

6.5 Abbreviations

AAM	Acrylamide
ABSF	Acid-base sensitivity factor
AFMO	Amino-functionalized monomer
AIBN	α,α'-Azoisobutyronitrile
Amine 1	2-Aminoethyl methacrylate hydrochloride
Amine 2	N-(3-Aminopropyl) methacrylamide hydrochloride
a.u.	Arbitrary units
Bis	N,N'-Methylenebisacrylamide
BPCR	N,N'-Bis-(3-azapentamethylene)-(4',5')-carboxyrhodamine
BuPCR	N,N'-Bis-(3-aza-3-butylpentamethylene)-(4',5')-carboxyrhodamine
CBF	5(6)-Carboxyfluorescein
Cl-DMPBI	1,6,7,12-Tetrachloro-N,N'-di(3-morpholinopropyl)perylene-3,4,9,10-tetracarboxylic bisimide
Cl-AMPBI	1,6,7,12-Tetrachloro-N-(2,6-diisopropylphenyl)-N'-(3-(1-morpholino)propyl) perylene-3,4,9,10-tetracarboxylic bisimide
Cl-DAPBI	1,6,7,12-Tetrachloro-N,N'-di(2,6-diisopropylphenyl)perylene-3,4,9,10-tetracarboxylic bisimide
CS	Core-shell
DCC	N,N'-Dicyclohexylcarbodiimide
DLR	Dual-lifetime referencing
DLS	Dynamic light scattering
EDC	1-Ethyl-3-(3-dimethylaminopropyl) carbodiimide)
EDIPA	Ethyldiisopropylamine
EE	Ethyl acetate
ES	Excited state
equ.	Equivalents
FITC	Fluorescein-(4,5)-isothiocyanate

FRET	Förster resonance energy transfer
GS	Ground state
HOMO	Highest occupied molecular orbital
HPTS	1-Hydroxypyrene-3,6,8-trisulfonate
IC	Internal conversion
ICT	Internal charge transfer
ISC	Intersystem crossing
IUPAC	International union of pure and applied chemistry
KPD	Potassium peroxodisulfate
LED	Light-emitting diode
LiPA	Lissamine rhodamine B-4'-piperazinyl amide
LUMO	Lowest unoccupied molecular orbital
NHS	N-Hydroxysuccinimide
M	mol l^{-1}
MA	Maleic anhydride
MES	2-(*N*-Morpholino)ethanesulfonic acid
MO	Molecular orbital
MOSePs	Magnetic optical sensor particles
NIR	Near infra-red
NMR	Nuclear magnetic resonance
OAM	Octylamine
PBA	1,6,7,12-Perylene tetracarboxylic bisanhydride
PBI	1,6,7,12-Perylene tetracarboxylic bisimide
PCT	Photoinduced charge transfer
PDI	Polydispersity index
PET	Photoinduced electron transfer
PhO-DMPBI	1,6,7,12-Tetraphenoxy-N,N'-di(3-morpholinopropyl)perylene-3,4,9,10-tetracarboxylic bisimide
PipPh	3-(1-Piperazinyl)phenol
PMT	Photomultiplier tube
PPT	Photoinduced proton transfer
PS	Polystyrene
PSMA	Polystyrene-co-maleic anhydride
PVC	Polyvinylchloride
PVP	Polyvinylpyrrolidone
QY	Quantum yield
RhODA	N,N'-Bis-(3-aza-3-butylpentamethylene)-(4',5')-octadecylaminocarboxyrhodamine
RT	Room temperature
S	Singlet
SDS	Sodium dodecylsulfate
SemiPR	N-(3-Azapentamethylene)-N'-dibutylaminorhodamine
SNAFL	Seminaphtofluorescein
SNARF	Seminaphtorhodafluor
T	Triplet
TBAOH	Tetrabutylammoniumhydroxide
tBuP-DMPBI	1,6,7,12-Tetra(4-*tert*-butylphenoxy)-N,N'-di(3-morpholinopropyl)perylene-3,4,9,10-tetracarboxylic bisimide
TCPBA	3,4,9,10-Tetrachloro-1,6,7,12-perylenebisanhydride
TLC	Thin layer chromatography
TMA	Trimellitic anhydride
TOAOH	Tetraoctylammoniumhydroxide
UV/VIS	Ultra-violet/visible
V/V	Volume/volume
w/w	Weight/weight